Adaptive Immune Responses to Vaccination Against SARS-CoV-2 in Individuals with Immune Dysregulation

Emily Clare Horner

Pembroke College, University of Cambridge

This thesis is submitted for the degree of

Doctor of Philosophy

September 2024

Declaration

This thesis is the result of my own work and includes nothing which is the outcome of work done in collaboration except as declared in the preface and specified in the text. It is not substantially the same as any work that has already been submitted, or is being concurrently submitted, for any degree, diploma or other qualification at the University of Cambridge or any other University or similar institution except as declared in the preface and specified in the text. It does not exceed the prescribed word limit for the relevant Degree Committee.

Abstract

The emergence of SARS-CoV-2 and the subsequent onset of the COVID-19 pandemic led to the rapid development of vaccines against the virus. Two of the major vaccines administered in the UK and elsewhere utilised novel mRNA technology to produce an immune response against the viral spike protein. The efficacy of these vaccines was key to control the pandemic and beyond this, vital for the protection of individuals at high risk from disease. The pace of the expeditious approval and subsequent vaccination programme led to gaps in the understanding of the mechanism of protection and the breadth of effectiveness of these vaccines. Individuals with immune dysregulation, such as those with inborn errors of immunity, cancer, obesity, and on immunomodulatory drugs, make up a large proportion of the UK population. These individuals are at increased risk from COVID-19 disease but also are more likely to respond poorly to vaccination. Vaccine efficacy in these groups is vital for the prevention of mortality, disease spread, and viral evolution.

In this thesis, the adaptive immune responses of individuals with immune dysregulation, caused by primary immunodeficiency, immune checkpoint blockade therapies, and severe obesity, to mRNA vaccination against SARS-CoV-2 were assessed. Cellular immune responses, driven by cytotoxic $CD8^+$ T cells, appeared to be robust and well maintained across disease states. Impairment of the humoral, antibody and memory B cell, responses to vaccination was seen in those with elevated levels of age associated B cells. Accelerated waning of the neutralising antibody response and consequent loss of protection was associated with immune dysfunction triggered by severe obesity.

The development of a nucleotide tagged multimer and monoclonal antibody validation system, enabled the identification of sequenced antigen specific B cells from individuals with severe obesity. In-depth analysis of the V(D)J sequences and differentiation states of these cells was therefore possible. This revealed reduced levels of class switching and B cell differentiation into memory cells, at an early timepoint after vaccination. Further, no deficit was found in the B cell receptors and antibodies themselves of individuals with severe obesity. These results were indicative of a deficiency in the early germinal centre response.

Reduced expression of the IL-6R on the immune cells of individuals with severe obesity suggested a mechanism by which germinal centre responses may be impaired. Loss of IL-6 signalling alone was sufficient in mice to cause accelerated waning and impaired class switching following mRNA vaccination. This identifies IL-6 signalling as a key mechanism of immune activation by mRNA vaccines. Targeting IL-6 signalling may improve the germinal centre response and, as such, both age associated B cells and IL-6 signalling emerge from this work as targets for the improvement of mRNA vaccine responses.

“None but those who have experienced them can conceive of the enticements of science”

- Mary Wollstonecraft Shelley, Frankenstein[1]

Acknowledgements

I would like to thank Dr James Thaventhiran for his confidence in me and introduction into the complex world of immunology. I owe thanks to all of the members of the Thaventhiran lab, past and present, for the support, assistance, and opportunities provided to me. I would like to offer particular thanks to Dr Juan Carlos Yam-Puc and Dr Nonantzin Beristain Covarrubias for their mentorship and expertise during my first clinical study. Also, to Lucy Booth for assistance with the multitude of ELISpots required for the SCORPIO study.

The clinical studies would not have been possible without the work of a plethora of research and clinical collaborators, who worked tirelessly through a global pandemic. I am incredibly grateful for the time and involvement of the doctors, nurses, and especially the participants of these studies. I would notably like to thank Dr Sara Lear, Dr Nicholas Matterson, and Dr Agatha van der Klaauw for their help, insight and organisation. In addition to the provision of countless neutralisation assays I am thankful for the contagious enthusiasm and scientific input of Dr Pehuén Pereyra Gerber. I would like to offer my gratitude to all individuals who contributed to the mouse studies completed for this work: Dr Juan Carlos Yam-Puc, Dr Sarah Spencer, Dr Maria Rust, Dr Joanna Salmon, Robert Hughes, Munetomo Takahashi, and Prof. Dr Katharina Timper. My thanks also to Ed Simmons-Rosello for the production of mRNA, Jacob Vincent for making antibodies, Dr James Roy for his mentorship in molecular biology techniques, Vitalina Chamberlain Evans for her sequencing expertise, and Dr Zhaleh Hosseini for her bioinformatic analysis.

I owe significant thanks to Sarah for her knowledge and expertise on medicine and the IL-6R, but chiefly her unwavering friendship and encouragement. I have had the pleasure of working and studying with many other inspirational women over the course of my scientific education, Lakmini Kahanawita, Rebecca Boston, Magda Ali, Kate Williamson, Maddy Ebbrell, to whom I also owe huge gratitude.

A final extra thank you to Joanna, for invaluable insights into the art of thesis writing.

I would like to thank all of my friends who have supported me throughout this process. Thank you to Mats Dijkdrent, Frederik Braun, and Sophie Müller, who formed my surrogate Pembroke family and allowed me to thrive through a first year in COVID-19 lockdown. Thank you also to Ally Kirtley, Tamás Dobai, and Sodai Lotharukpong for reminding me of my enthusiasm and love for science and research.

Finally, I would like to thank my family, my mum, dad, siblings, and grandad. A particular thank you to my mum, Tracey Horner, who has been with me every step of this journey and because of whom this has never felt like an unachievable task. During the course of my studies, I had the privilege to marry my husband, Oliver. I would like to thank him for his endless support of my academic pursuits, and the countless hours spent providing constructive criticism of my statistical analyses.

Contributors to collaborative study

The results of the first two chapters of this thesis are derived from two clinical studies which were performed in collaboration with clinicians and researchers centred in Cambridge and across the UK.

The vaccine response in immune dysregulation study was designed by James Thaventhiran, Christine Parkinson, Sara Lear, and Nicholas Matheson. Recruitment and sample collection were completed by Andrea Correa-Noguera, David Favara, Lourdes Ceron-Gutierrez, Anne Elmer, Caroline Saunders, Areti Bermperi, Sherly Jose, Nathalie Kingston, Sofia Grigoriadou, Sarah Spencer, and Emily Staples.

The SCORPIO study was designed by I. Sadaf Farooqi, James Thaventhiran, and Agatha van der Klaauw. Recruitment and clinical studies were completed by Agatha van der Klaauw, Sarah Spencer, Miriam Smith, Bensi Vergese, Elana Henning, Jacopo Scotucci, Adrian J. Park, Hannah Stark, Nathalie Kingston, Francesco Rubino, and I. Sadaf Farooqi. Computational analysis of the EAVE II cohort was conducted by Utkarsh Agrawal, Colin McCowan, Chris Robertson, and Aziz Sheikh.

Once collected samples were delivered to the MRC Toxicology Unit, I was responsible for their processing, storage, distribution, and use. I coordinated the sample processing for these studies and completed PBMC and serum extractions with the assistance of Juan Carlos Yam-Puc, Nonantzin Beristain-Covarrubias, Robert Hughes, Rebecca Boston, Magda Ali, Edward Simmons-Rosello, Maria Rust, Alexander Ferreira, Lucy Booth, Thevinya Gurugama, Lihinya Gurugama, and Harry Robson. I completed ELISpot assays for both studies with the assistance of Lucy Booth. Flow cytometric assays were completed by Juan Carlos Yam-Puc and Nonantzin Beristain-Covarrubias, with assistance from me, Robert Hughes, and Magda Ali. Live virus neutralising assays were completed by Pehuén Pereyra Gerber, Isobel Ramsay Stubbs, and Jack Smith in the Department of Medicine. Luminex assays were completed under the supervision of Rainer Doffinger, Cambridge University Hospitals NHS Foundation Trust. Roche Elecsys assays were completed by the group of Ashley Otter at the UK Health Security Agency, Porton Down. The analysis presented is my own unless otherwise stated.

Associated publications

Yam-Puc, J.C., Hosseini, Z., **Horner, E.C**. et al. Age-associated B cells predict impaired humoral immunity after COVID-19 vaccination in patients receiving immune checkpoint blockade. *Nat Commun* **14**, 3292 (2023). https://doi.org/10.1038/s41467-023-38810-0

van der Klaauw, A.A., **Horner, E.C.**, Pereyra-Gerber, P. *et al.* Accelerated waning of the humoral response to COVID-19 vaccines in obesity. *Nat Med* **29**, 1146–1154 (2023). https://doi.org/10.1038/s41591-023-02343-2

Pereyra-Gerber, P., Duncan, L.M., Greenwood, E.J.D., Marelli, S., Naamati, A., Teixeira-Silva, A., Crozier, T.W.M.,Gabaev, I., Zhan, J.R., Mulroney, T.E., **Horner, E.C.,** Doffinger, R., Willis, A.E., Thaventhiran, J.E.D., Protasio, A.V., Matheson. N.J., A protease-activatable luminescent biosensor and reporter cell line for authentic SARS-CoV-2 infection. *PLOS Pathogens* **18**(2), e1010265 (2022). https://doi.org/10.1371/journal.ppat.1010265

Mulroney, T.E., Pöyry, T., Yam-Puc, J.C., Rust, M., Harvey, R. F., Kalmar, L., **Horner, E.** et al N^1-methylpseudouridylation of mRNA causes +1 ribosomal frameshifting. *Nature* **625**, 189–194 (2024). https://doi.org/10.1038/s41586-023-06800-3

Terms and abbreviations

(s)gp130 –(soluble) glycoprotein 130
(s)IL-6R – (soluble) Interleukin 6 Receptor
ABC – Age-associated B Cell
ACE2 - Angiotensin-Converting Enzyme 2
ADAM10 - A Disintegrin And Metalloproteinase 10
ADAM17 - A Disintegrin And Metalloproteinase 17
AID – Activation-Induced Cytidine Deaminase
AIM – Activation Induced Markers
AIRE - AutoImmune Regulator
APC – Antigen Presenting Cell
APC (dye) – Allophycocyanin
aRR – adjusted Rate Ratio
ASC – Antibody Secreting Cell
BCR – B Cell Receptor
BEAM – Barcode Enabled Antigen Mapping
BMI – Body Mass Index
BNT162b2 – SARS-CoV-2 Pfizer mRNA vaccine
CD- Standard Chow Diet (mice)
CDx– Cluster of Differentiation x
CFSE - Carboxyfluorescein Succinimidyl Ester
C_H – Constant Heavy
ChAdOx1 – SARS-CoV-2 AstraZeneca adenoviral vaccine
CI – Confidence Interval
C_L – Constant Light
COI – Cut-Off Index
ConA – Concanavalin A
COVID-19 – Coronavirus disease 2019
CRP – C-Reactive Protein
CSP – Cell Surface Protein
CSR – Class Switch Recombination
CT - Cytoplasmic Domain
cT_{FH} – circulating T Follicular Helper
CTLA-4 – Cytotoxic T-Lymphocyte Associated Protein 4
CTV – Cell Trace Violet
CVID – Common Variable Immunodeficiency
DC- Dendritic Cell
DZ – Dark Zone
EDTA - Ethylenediaminetetraacetic Acid
EF – Extrafollicular
ELISpot - Enzyme-Linked Immunosorbent Spot
Fab – Fragment antigen binding
FACS - Fluorescence Activated Single Cell Sorting
FBS – Foetal Bovine Serum
Fc – Fragment crystallisation
FcRn - Neonatal Fragment Crystallizable Receptor
FDC – Follicular Dendritic Cell
FP – Fusion Peptide

GALT – Gut Associated Lymphoid Tissue
GC – Germinal Centre
GLM – Generalised Linear Model
HC – Healthy Control
HFD – High Fat Diet
HIV – Human Immunodeficiency Virus
HLA - Human Leukocyte Antigen
HP1/2 - Heptapeptide Repeat Sequences 1 and 2
HRP – Horseradish Peroxidase
HTA – Human Tissue Act
IC50 – A measure of the affinity of a protein binding interaction
ICB – Immune Checkpoint Blockade (also used to refer to study cohort in chapter 3)
IEI – Inborn Error of Immunity
IFN-γ – Interferon Gamma
Ig – Immunoglobulin
IL – Interleukin
Il6ra - Interleukin 6 Receptor, alpha (mouse)
IM – Intramuscular
IV - Intravenous
JAK/STAT pathway - Janus Kinase/Signal Transducer and Activator of Transcription pathway
K_D – Equilibrium Dissociation Constant
LIBRA-seq - Linking B cell Receptor to Antigen Specificity through sequencing
LLPC – Long Lived Plasma Cell
LNP – Lipid Nanoparticle
LRBA – Lipopolysaccharide Responsive Beige-like Anchor Protein
LZ – Light Zone
M – Membrane (referring to SARS-CoV-2 protein)
MHC – Major Histocompatibility Complex
mRNA – messenger Ribonucleic Acid
mRNA-1273 – SARS-CoV-2 Moderna mRNA vaccine
N – Nucleocapsid (referring to SARS-CoV-2 protein)
NAFLD - Non-Alcoholic Fatty Liver Disease
NFκB - Nuclear Factor kappa-light-chain-enhancer of activated B cells
NHS Ester - N-Hydroxysuccinimide Ester
NK – Natural Killer
NT50 – A measure of live virus neutralising capacity
NTD - N-Terminal Domain
NW – Normal Weight (cohort of SCORPIO study)
ONS – Office for National Statistics
PAD – Predominantly Antibody Deficiency
PBMC – Peripheral Blood Mononuclear Cells
PBS – Phosphate Buffered Saline
PCR – Polymerase Chain Reaction
PD1 - Programmed cell Death Protein 1
PE - Phycoerythrin
PEI – Polyethylenimine
PFA – Paraformaldehyde
PHA - Phytohaemagglutinin
PID – Primary Immune Deficiency (also used to refer to study cohort in chapter 3)

pSTAT3 – phosphorylated Signal Transducer and Activator of Transcription 3
RAG – Recombination-Activating Gene
RBD – Receptor Binding Domain (referring to region of SARS-CoV-2 spike protein)
RR – Rate Ratio
RT – Room Temperature (18-20°C)
RT-PCR - Reverse Transcription Polymerase Chain Reaction
S – Spike (referring to SARS-CoV-2 protein)
SAffCon - SeroAffinity and Concentration
SARS-CoV-2 - Severe Acute Respiratory Syndrome Coronavirus 2
SAT – Subcutaneous Adipose Tissue
SCORPIO - SARS-COV-2 vaccine ResPonse In Obesity (study name)
scRNA-seq – single cell RNA sequencing
SFU – Spot Forming Unit
SHM – Somatic Hyper Mutation
SID – Secondary Immune Deficiency
SNP – Single Nucleotide Polymorphism
SO – Severe Obesity (cohort of SCORPIO study)
STAT3 - Signal Transducer and Activator of Transcription 3
TBS – Tris-Buffered Saline
TCR – T Cell Receptor
T_{FH} – T Follicular Helper cell
TGF-β - Transforming Growth Factor Beta
T_H – T Helper cell
TM - Transmembrane Domain
TMB - 3,3',5,5'-Tetramethylbenzidine
TNF – Tumor Necrosis Factor
Treg – T regulatory cell
V(D)J – Variable (Diversity) Joining
V1/2/3 – Vaccine dose 1/2/3
VAT – Visceral Adipose Tissue
V_H – Variable Heavy
V_L – Variable Light
VPA – 2-propyl-pentanoic acid
WHO – World Health Organisation
WT – Wild Type

Table of contents

Declaration *2*
Abstract *3*
Acknowledgements *6*
Contributors to collaborative study *8*
Associated publications *9*
Terms and abbreviations *10*
Table of contents *13*
List of Figures *18*
List of Tables *19*
1. Introduction: the human immune system *20*
1.1. The innate immune response **20**
1.2. The adaptive immune response **21**
1.2.1. Cellular immunity 21
1.2.2. Humoral immunity 23
1.2.2.1. Class switch recombination 24
1.2.2.2. Dynamics of the germinal centre 27
1.2.2.3. Somatic hypermutation 27
1.2.2.4. Long lived plasma cells 29
1.2.2.5. Age-associated B cells 29
1.2.3. Immune memory following vaccination 30
1.3. SARS-CoV-2 and the COVID-19 pandemic **31**
1.3.1. The COVID-19 pandemic 31
1.3.2. Structure of the SARS-CoV-2 virus 32
1.3.3. COVID-19 infection and protection 33
1.3.4. SARS-CoV-2 Viral Variants 33
1.3.5. Vaccination against SARS-CoV-2 34
1.3.5.1. Adenoviral vaccination 34
1.3.5.2. mRNA vaccination 34
1.4. Aims and outlines **35**
2. Materials and methods *37*
2.1. Human clinical studies **37**
2.1.1. BNT162b2 vaccination and immune dysregulation study coordination and ethics 37
2.1.2. SCORPIO study coordination and ethics 38
2.1.3. PBMC isolation from whole blood 39
2.1.4. Separation of serum and EDTA plasma from whole blood 40
2.1.5. Thawing of frozen PBMCs 40
2.1.6. EAVEII data analysis 40
2.2. Detection of antigen specific T cell responses **41**
2.2.1. CTV cell proliferation assay 41
2.2.2. Activation induced markers (AIM) assay 42
2.2.3. IFN-γ ELISpot for SARS-CoV-2 reactive T cells 42

2.2.4. IFN-γ ELISpot for omicron variant SARS-CoV-2 reactive T cells 43
2.2.5. IFN-γ/IL-2 FluoroSpot 44

2.3. Identification of antigen specific antibodies 44
2.3.1. RBD and spike binding antibody quantification 44
2.3.2. Neutralising capacity 45
2.3.3. Neutralising capacity against omicron variant 45
2.3.4. Total spike and nucleocapsid binding antibody quantification 45

2.4. Flow cytometry 46
2.4.1. Human cells 46
2.4.1.1. Identification of proliferating T cells 46
2.4.1.2. Identification of activated T cells 46
2.4.1.3. Identification of $cT_{FH}s$ 46
2.4.1.4. Identification of RBD specific cells 46
2.4.1.5. Identification of age-associated B cells 47
2.4.1.6. Identification of spike specific cells 47
2.4.2. Murine cells 48
2.4.2.1. Identification of spike specific B cells 48
2.4.2.2. Identification of IgM B cells 48
2.4.2.3. Identification of IgG B cells 48
2.4.2.3. Identification of plasma cell subsets 48

2.5. Detection of SARS-CoV-2 infection/convalescence 49

2.6. Mammalian cell culture 50
2.6.1. Maintenance of FreeStyle™ 293-F cells 50
2.6.2. Transfection of FreeStyle™ 293-F cells 50

2.7. Protein production 51
2.7.1. Production of spike protein 51
2.7.2. PCR of the pVITRO1 plasmid 51
2.7.3. Antibody variable gene fragments 52
2.7.4. Generation of monoclonal antibodies 52
2.7.5. SDS PAGE and Coomassie staining for protein identification 53

2.8. Characterisation of antibodies 54
2.8.1. ELISA to detect human spike binding IgA, IgG, and IgM antibodies 54
2.8.2. Production of RBD probe for SAffCon assay 54
2.8.3. Fluidity One M SAffCon assay 55
2.8.4. ELISA for monoclonal antibody binding affinity 55

2.9. Production of spike multimer for single cell sequencing 56

2.10. Single cell RNA sequencing 56
2.10.1. Preparation of cells for single cell sequencing 56
2.10.2. Library preparation 56
2.10.3. Processing and analysis of single cell RNA sequencing files 57

2.11. Mouse studies 57
2.11.1. Preparation of BNT162b2 vaccine 58
2.11.2. Multiple immunisations with BNT162b2 or PBS 58
2.11.3. Humoral response in *Il6ra* knockout mice 58
2.11.4. Humoral response in mice with diet induced obesity 58
2.11.5. mRNA construct immunisation 59
2.11.6. Mouse splenocyte processing 59
2.11.7. Mouse bone marrow processing 59
2.11.8. Mouse lymph node processing 60
2.11.9. Mouse serum processing 60

2.12. Immunophenotyping of mouse samples 60

2.12.1. ELISA for murine spike binding IgG 60
2.12.2. FluoroSpot for antibody secretion 61
2.12.3. IL-6 ELISA 62
2.13. mRNA constructs 62
2.13.1. Production of mRNA IL-6R constructs 62
2.13.2. Western blot validation of construct expression 63
2.14. Analysis and statistics 63
3. Antigen specific T cells and the response to vaccination in individuals with immune dysregulation 65
3.1. Introduction: dysregulation of the immune system 65
3.1.1. Primary immune deficiencies 66
3.1.2. Iatrogenic secondary immune dysregulation 67
3.1.3. The importance of antigen specific T cells 68
3.1.4. The risk of COVID-19 in individuals with immune dysregulation 68
3.1.5. Chapter aims 69
3.2. Results 70
3.2.1. Methods to test for antigen specific T cell response 70
3.2.1.1. In vitro stimulation and flow cytometry-based assays 70
3.2.1.2. In vitro stimulation and plate-based assays - ELISpot 72
3.2.2. Cellular response to vaccination in individuals with immune dysregulation 77
3.2.3. Humoral response to vaccination in individuals with immune dysregulation 79
3.2.4. Relationship between ABCs and vaccine response 81
3.3. Discussion 83
3.3.1. Results 83
3.3.1.1. Detection of antigen specific T cells 83
3.3.1.2. Immune response to SARS-CoV-2 vaccination in individuals with immune dysregulation 84
3.3.2. Conclusions and future directions 85
4. The response to vaccination in people with severe obesity 88
4.1. Introduction: immune dysregulation in obesity 88
4.1.1. Global obesity: a pandemic 88
4.1.2. The impact of obesity on the immune system 88
4.1.3. Obesity and COVID-19 disease 90
4.1.4. The efficacy of vaccination in obesity 91
4.1.5. Confounders in Obesity Research 92
4.1.6. Chapter Aims 93
4.2. Results 93
4.2.1. Cohort recruitment and sampling 93
4.2.2. The risk of severe COVID-19 outcomes following vaccination 94
4.2.3. Breakthrough infection following third dose vaccination 95
4.2.4. Cellular response to vaccination in individuals with severe obesity 97
4.2.4.1. T cell protection against the circulating omicron variant 98
4.2.5. Humoral response to vaccination in individuals with severe obesity 100
4.2.5.1. Antigen specific antibodies 100
4.2.5.2. Neutralising activity 100
4.2.5.3. Neutralising capacity against variants 101
4.2.6. Heterogeneity in individuals with severe obesity 103
4.3. Discussion 106
4.3.1. Results 106
4.3.2. Conclusions and future directions 108

5. B cell differentiation in severe obesity 111

5.1. Introduction: protection from SARS-CoV-2 provided by circulating antibodies 111
5.1.1. Antibodies against SARS-CoV-2 antigens 111
5.1.1.1. Class switching and antibody isotypes in protection against SARS-CoV-2 111
5.1.1.2. Neutralising epitopes in SARS-CoV-2 112
5.1.2. Identification of specific cells and BCR genes in single cell sequencing 113
5.1.3. Chapter aims 114

5.2. Results 115
5.2.1. Production of the HexaPro spike protein 115
5.2.2. Isotype specific assessment of spike binding antibodies by ELISA 117
5.2.3. SAffCon assay for serum antibody avidities 119
5.2.3.1. Validation of concentrations of binding antibodies 119
5.2.3.2. Serum RBD binding avidity 119
5.2.4. Development of a spike multimer to detect specific cells in single cell sequencing 122
5.2.4.1. Multimer preparation 122
5.2.4.2. Multimer validation in mice 123
5.2.5. Single cell sequencing of enriched B cells using a spike multimer 124
5.2.5.1. Production of antibodies using the pVITRO1 system 124
5.2.5.2. Multimer validation by monoclonal antibody production 127
5.2.5.3. Confirmation of antibody binding specificity 128
5.2.5.4. B cell identification in SCORPIO participants 130
5.2.6. Differentiation states of antigen specific B cells 131
5.2.7. V(D)J sequences of antigen specific B cells 134
5.2.8. Assessment of antibody binding affinities from monoclonal antibodies 136

5.3. Discussion 138
5.3.1. Results 138
5.3.2. Conclusions and future directions 140

6. IL-6 signalling in the humoral response to mRNA vaccines 143

6.1. Introduction: IL-6 signalling in the generation of an immune response 143
6.1.1. Dynamics of IL-6 signalling 143
6.1.2. Sources, targets, and functions of IL-6 145
6.1.2.1. Germinal centre and class switch response 146
6.1.2.2. Survival of plasma cells 148
6.1.3. IL-6 in COVID-19 vaccine responses in obesity 148
6.1.3.1. IL-6 and IL-6R shedding in obesity 148
6.1.3.2. IL-6 levels in severe COVID-19 148
6.1.3.3. IL-6 signalling in response to mRNA LNP vaccines 149
6.1.4. Chapter aims 150

6.2. Results 151
6.2.1. Expression of the IL-6R receptor 151
6.2.2. *Il6ra* knockout mouse model of obesity 152
6.2.2.1. Knockout of Il6ra 152
6.2.2.2. Neutralising capacity in Il6ra knockout mice following vaccination 153
6.2.2.3. Antigen specific B cell phenotypes in Il6ra knockout mice 154
6.2.3. The assessment of LLPCs 156
6.2.3.1. A FluoroSpot assay to quantify IgA, IgM, and IgG secretion by plasma cells 156
6.2.3.2. Quantification of plasma cells in Il6ra knockout mice 160
6.2.4. IL-6 signalling as a therapeutic target 163
6.2.4.1. Validation of IL-6R mRNA constructs 163
6.2.4.2. Co-immunisation with hIL-6R in IL-6R deficient mice 164

6.3. Discussion 166
6.3.1. Results 166

6.3.1.1. Il6ra knockout mouse model and LLPCs 166
6.3.1.2. Targeting IL-6 signalling to improve vaccine responses 167
6.3.2. Conclusions and future directions 168
7. Final discussion 171
7.1. Conclusions 171
7.2. Future directions 172
8. References 175
9. Appendix 201

List of Figures

Figure 1.1. Adaptive immune cells 24
Figure 1.2. The structure of antibodies and process of CSR 26
Figure 1.3. The germinal centre 28
Figure 1.4. Age-associated B cells. 30
Figure 1.5. The structure of the SARS-CoV-2 virus and vaccines. 32
Figure 3.1. Anti-PD-1 and anti-CTLA-4 immune checkpoint blockade 67
Figure 3.2. Flow cytometry assays for the detection of T cell activation and differentiation 72
Figure 3.3. Optimisation of IFN-γ ELISpot to detect spike specific T cells after vaccination 76
Figure 3.4. T cell phenotyping in individuals with primary and secondary immune dysregulation 78
Figure 3.5. The humoral response to vaccination in individuals with immune dysregulation 80
Figure 3.6. Relationship between ABCs and vaccine responses 82
Figure 4.1. Global Obesity 89
Figure 4.2. Immune environment of adipose tissue 90
Figure 4.3. Relative risk of COVID-19 in people with obesity following vaccination 96
Figure 4.4. T cell responses to vaccination in individuals with severe obesity 99
Figure 4.5. Humoral responses to vaccination in individuals with severe obesity 102
Figure 4.6. Heterogeneity of the immune responses of individuals with severe obesity ... 105
Figure 5.1. The production of trimeric HexaPro spike protein 116
Figure 5.2. Isotypes of antibody response in individuals with severe obesity 118
Figure 5.3. RBD binding antibody concentration and avidity in severe obesity 121
Figure 5.4. Creation of a nucleotide and fluorophore tagged spike multimer for the detection of B cells 123
Figure 5.5. Detection of spike binding B cells in vaccinated mice 124
Figure 5.6. Production of recombinant monoclonal IgG1 with the pVITRO1 system 126
Figure 5.7. Preparation of B cells for single cell sequencing 127
Figure 5.8. Selection of spike binding B cells for the production of antibodies 128
Figure 5.9. Validation of methods to identify antigen specific B cells 130
Figure 5.10. Selection of representative subset of samples for single cell sequencing 131
Figure 5.11. Differentiation states of antigen specific B cells following vaccination. 133
Figure 5.12. Isotypes of spike binding B cells following vaccination 135
Figure 5.13. Affinities of antibodies derived from individuals with severe obesity 137
Figure 6.1. The dynamics of IL-6 signalling 144
Figure 6.2. Sources and impacts of IL-6 146
Figure 6.3. The impact of IL-6 signalling on the humoral immune response 147
Figure 6.4. IL-6 signalling in obesity and SARS-CoV-2 infection and vaccination 150
Figure 6.5. IL-6R expression levels of B cells in severe obesity 152
Figure 6.6. Live virus neutralising capacity of vaccinated mice in the absence of IL-6 signalling 154
Figure 6.7. Class switching of antigen specific B cells in mice in the absence of IL-6 signalling 155
Figure 6.8. Mouse IgM/IgG/IgA FluoroSpot Assay for the quantification of LLPCs in bone marrow 158
Figure 6.9. Detection of antigen specific plasma cells in bone marrow but not spleen 160
Figure 6.10. Long lived antigen specific plasma cells in the bone marrow of IL-6R deficient mice following BNT162b2 vaccination 162
Figure 6.11. Expression of mRNA constructs encoding IL-6R 164

Figure 6.12. Impact of hIL-6R construct on BNT162b2 vaccine responses in IL-6R deficient mice 165
Figure 9.1. Gating strategy for CTV-stained dividing T cells 201
Figure 9.2 Gating strategy for activated $CD4^+$ and $CD8^+$ T cells from PBMCs following spike stimulation by AIM assay 202
Figure 9.3. Gating strategy for T follicular helper cells from human PBMCs 203
Figure 9.4. Gating strategy for RBD specific B cells from human PBMCs 203
Figure 9.5. Gating strategy for age associated B cells from human PBMCs 203
Figure 9.6. Serum dilution tests of spike binding antibody isotype ELISAs 204
Figure 9.7. Gating strategy for spike specific B cells from human PBMCs 205
Figure 9.8. Gating strategy for spike biding, IgM, and IgG mouse B cells 218
Figure 9.9. Flow cytometry to quality control batches of cells prepared for single cell sequencing 219
Figure 9.10. Anti-Spike monoclonal antibody affinity ELISAs 222
Figure 9.11. Comparison of mutational counts of spike binding naïve and memory cells 222

List of Tables

Table 2.1. Characteristics of the participants of the vaccination in immune dysregulation study 37
Table 2.2. Characteristics of the participants of the SCORPIO study 39
Table 2.3. Antibodies against human cell markers used for flowcytometry 47
Table 2.4. Antibodies against murine cell markers used for flowcytometry 49
Table 3.1. Plate reader settings for the counting of spots on IFN-γ ELISPOT plates 75
Table 9.1 Thermocycler settings for gradient PCR 206
Table 9.2 Thermocycler settings for PCR amplification of pVITRO1 constant regions 206
Table 9.3 Antibodies produced from single cell sequencing data 206

1. Introduction: the human immune system

1.1. The innate immune response

The human immune system is a complex set of tissues, cells, and molecules, which form a network of protection against disease. Upon encounter with a pathogen or antigen, the immune response can broadly be split into two categories: the innate response which is fast acting and non-specific; and the adaptive response which is slower but typically more specifically targeted[2]. The innate response consists of barriers such as the skin, cytokines (cell signalling molecules), and non-specific immune cells such as macrophages, neutrophils and natural killer (NK) cells[3].

If a pathogen breaches the epithelium, it may be quickly targeted by tissue resident macrophages which can then recruit neutrophils[4]. Macrophages and neutrophils are both phagocytic and recognise pathogens by receptors which bind to surface molecules common to pathogens. Pattern recognition receptors (PRRs) bind to pathogen-associated molecular patterns (PAMPs), molecular patterns found on pathogens but not in the body[5], or non-microbial damage-associated molecular patterns (DAMPs)[6]. Upon recognition and binding the pathogen is internalised by the phagocyte and directly destroyed by a process known as phagocytosis[7].

The stimulation of membrane bound PRRs also triggers a signalling cascade within macrophages and other innate cells which leads to the secretion of inflammatory cytokines such as tumour necrosis factor (TNF), IL-6, and IL-1β, and chemokines including CXCL8[8]. In addition to the release of prostaglandins and other lipid mediators these signalling molecules lead to the development of local inflammation at the site of infection or injury. During inflammation vascular permeability changes, swelling and temperature increases and immune cells are recruited, all processes to control infection or injury[9]. The complement system is activated by an enzyme cascade upon inflammation, complement proteins can then opsonize pathogens, directly kill pathogens, and recruit further inflammatory cells[4]. NK cells are recruited to the site of inflammation by cytokines such as TNF[10], there they act to kill infected cells by recognition of MHC class I downregulation and markers of cellular stress[11]. NK cells additionally secret further inflammatory cytokines including IFN-γ.

The cytokines released during inflammation also act to stimulate components of the adaptive response including T and B cells. Phagocytic macrophages and dendritic cells (DCs) are also professional antigen presenting cells (APCs) and capture and present antigen on numerous MHC complexes on their cell surfaces[12]. These complexes are required for the activation of antigen specific T cells. Additionally, inflammation leads to the upregulation of the costimulatory molecules CD80 and CD86 on DCs, needed for the induction of the adaptive immune response.

1.2. The adaptive immune response

The adaptive response, which will be the focus of this thesis, forms in response to a specific antigen. B and T cells are the basis of this response and are able to recognise a specific antigen through their B cell receptors (BCRs) and T cell receptors (TCRs) respectively[13] (**Figure 1.1**). Circulating naïve B and T cells can bind a broad repertoire of possible antigens and upon encounter with cognate antigen, a B or T cell will differentiate and clonally expand, forming memory cells. A more rapid and robust response will then occur upon repeat antigen encounter[14]. The adaptive response evolves with each repeat antigen encounter. Adaptive responses relating to T cells are known as cellular immunity and those regarding B cells are known as humoral immunity.

1.2.1. Cellular immunity

T cells are nucleated cells with membrane bound TCRs, which are able to bind to cognate antigen. T cells arise from lymphoid progenitors which migrate from the bone marrow to the thymus, a gland found in the centre of the chest[4]. Within the thymus, T cells receive a signal via Notch1 which commits them to the T cell lineage[15]. Early double negative thymocytes differentiate into two distinct lineages α:β and λ:δ which express different forms of TCR. The β chain undergoes rearrangement and a pre-TCR is expressed on the surface of double positive α:β thymocytes which express CD4, CD8 and CD3. All mature T cells express CD3 which associates with the TCR and acts as a co-receptor for the activation of T cells[16]. Following this, cells with a productively rearranged β chain are selected for further differentiation and the α chain is rearranged[17]. Within the thymus

double positive thymocytes undergo positive selection, to select for cells with receptors able to identify major histocompatibility complex (MHC) presented antigens, and negative selection to eliminate cells which recognise self-antigens. Thymic cells expressing the transcription factor *AIRE* are able to present self-antigen to T cells, those which react to the presented antigen are eliminated[18]. Cells then stop expressing either of CD4 or CD8 and become single positive cells, further negative selection also occurs at this point[19]. Subsequently, cells leave the thymus as naïve T cells and circulate around the body, ready to encounter cognate antigen. For a T cell to recognise antigen, it must be presented on an MHC by an APC[20]. T cells which express CD8 recognise antigen presented on MHC Class I, and those which express CD4 recognise antigen presented on MHC Class II[21,22]. The binding of a TCR to cognate antigen triggers proliferation and differentiation. Upon activation, both types of T cell can produce memory cells which more rapidly activate upon repeat antigen encounter. T cells interact with innate and adaptive components of the immune response and can act directly or provide help to other immune cells depending on their subtype.

$CD8^+$ T cells are typically considered to be cytotoxic and $CD4^+$ associated more with immune regulatory roles (T helper (T_H) cells), however $CD4^+$ cells can also be cytotoxic. The expression of CD27 and apparent cell functions have been used to further subdivide human $CD8^+$ T cells, into $CD8^+$ memory ($CD27^+$) and $CD8^+$ effector ($CD27^-$) cells, only the latter of which has immediate killing ability[23]. Cytotoxic T cells act directly to kill infected or damaged self-cells. Upon recognition of antigen and co-stimulatory signals from other immune cells, cytotoxic cells release cytokines, triggering cell death. $CD4^+$ T_H cells can be arranged in multiple subsets including T_H1, T_H2, T_H9, T_H17, T follicular helper (T_{FH}), T regulatory (T_{reg}), and T follicular regulatory (T_{FR}) cells each with distinct cytokine profiles[24]. Broadly, these cells function by releasing cytokines and aiding the function of other immune cells. They also play important roles in the suppression of the immune response. The differentiation of T cells into different T cell subsets is directed by the local cytokine environment[24].

1.2.2. Humoral immunity

B cells also arise from a common lymphoid progenitor produced in the bone marrow; however they remain there as they develop. Naïve B cells express a BCR and do not require MHC presentation for antigen recognition. Instead B cells are able to bind to antigen in its native form[25]. Variation is introduced to both BCRs and TCRs by V(D)J recombination[26,27]. Multiple variable (V), diversity (D), and joining (J) gene segments are encoded by each cell and these are randomly recombined to form the region of the TCR or BCR responsible for antigen binding. Recombination-activating gene (RAG) proteins are responsible for driving this process. The variety of possible combinations provides diversity which can be further expanded by imperfect joining introducing mutations at the junctions between segments[28]. Therefore, naïve B cells can bind to a broad range of antigens and following binding, activated B cells can differentiate into memory cells or antibody secreting cells (ASCs) (plasmablasts and plasma cells). The BCR on the surface of a B cell is responsible for antigen binding and recognition. In ASCs the BCR is secreted in a soluble form as an antibody, also known as an immunoglobulin (Ig), and expression on the membrane surface is reduced. B cell differentiation following activation occurs through either a follicular or extrafollicular (EF) response. The EF response can be T cell dependent or independent and produces large quantities of short-lived antibody secreting plasmablasts in addition to some memory cells[29]. This response begins early following antigen binding and plasmablast numbers typically peak at days 4-6 following antigen encounter[30]. The follicular response, also known as the germinal centre (GC) response, is generally considered to produce more specific, longer-lived cells. The GC is an organised structure of B cells, T cells, and follicular dendritic cells (FDCs). It is responsible for the production of long-lived plasma cells (LLPCs) and additional memory B cells, these responses peak around 2 weeks after antigen encounter[30].

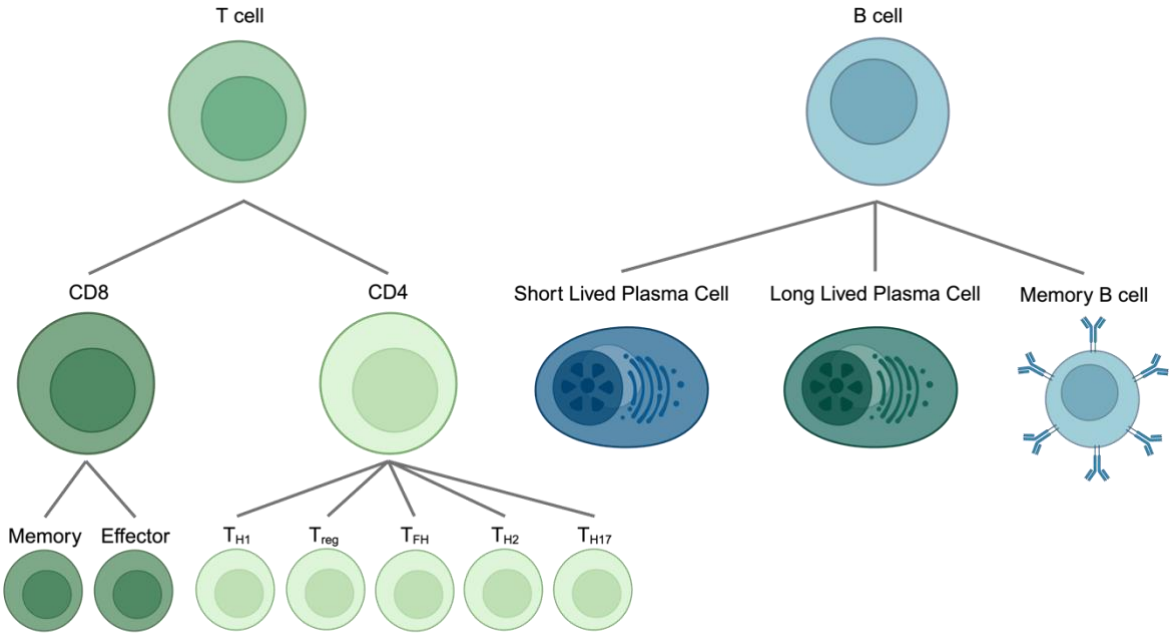

Figure 1.1. Adaptive immune cells. A non-exhaustive diagram of the organisation of T and B cell subsets. Generated using Biorender.com.

1.2.2.1. Class switch recombination

The structure of the BCR is comprised of four polypeptide chains, two heavy and two light chains, which are paired and linked by disulphide bonds. Heavy and light chains are both split into two regions: variable and constant. The variable region (V_L and V_H) shows significant variation between antibodies and is responsible for antigen binding. The constant region (C_L and C_H) is one of a defined number of different chains and can determine the function of the antibody (**Figure 1.2A**). C_L chains belong to one of two classes, kappa (κ) or lambda (λ). Roughly 2/3 antibodies in healthy individuals have κ chains and aberrant κ: λ ratios are associated with disease[31]. The C_H region determines the isotype or class of an antibody. There are more possible C_H chains: μ, γ (1/2/3/4), ε, α (1/2), and δ which comprise immunoglobulin classes IgM, IgG, IgE, IgA, and IgD respectively. The class of an antibody has an influence on its function, for instance IgM antibodies can form pentamers which allows high avidity binding and activation of the complement system (**Figure 1.2B**). Naïve B cells begin as either IgD or IgM and are considered unswitched. By a process known as class switch recombination (CSR) the isotype of a cell can switch to IgA, IgG, or IgE (class switched isotypes) (**Figure 1.2C**). A combination of signals through the CD40 receptor, IgM, and cytokine receptors are

required for the initiation of CSR. The class switched to is dependent on which cytokines are present[32], for example, interleukins, IL-4 and IL-13 are associated with switching to IgE and IgG4[33-35]. Following stimulation, recombination is mediated by activation-induced cytidine deaminase (AID) which converts cytosine to uracil, leading to base excision, mismatch repair, and end-joining recombination[36]. Class switched B cells are typically associated with the follicular GC response, rather than the EF response. However, class switch is independent of the GC, it occurs at the first B – T cell interaction following antigen encounter and is mostly complete by the time the GC is formed[37]. Additionally, CSR is supressed in the GC[37] and must occur in dividing cells[38]. Despite this, in a typical humoral response, unswitched IgM cells arise early from the EF response and later switched memory cells arise from the GC[39,40]. Therefore, CSR allows the expression of different BCR and antibody isotypes, with switching associated with more differentiated B cells.

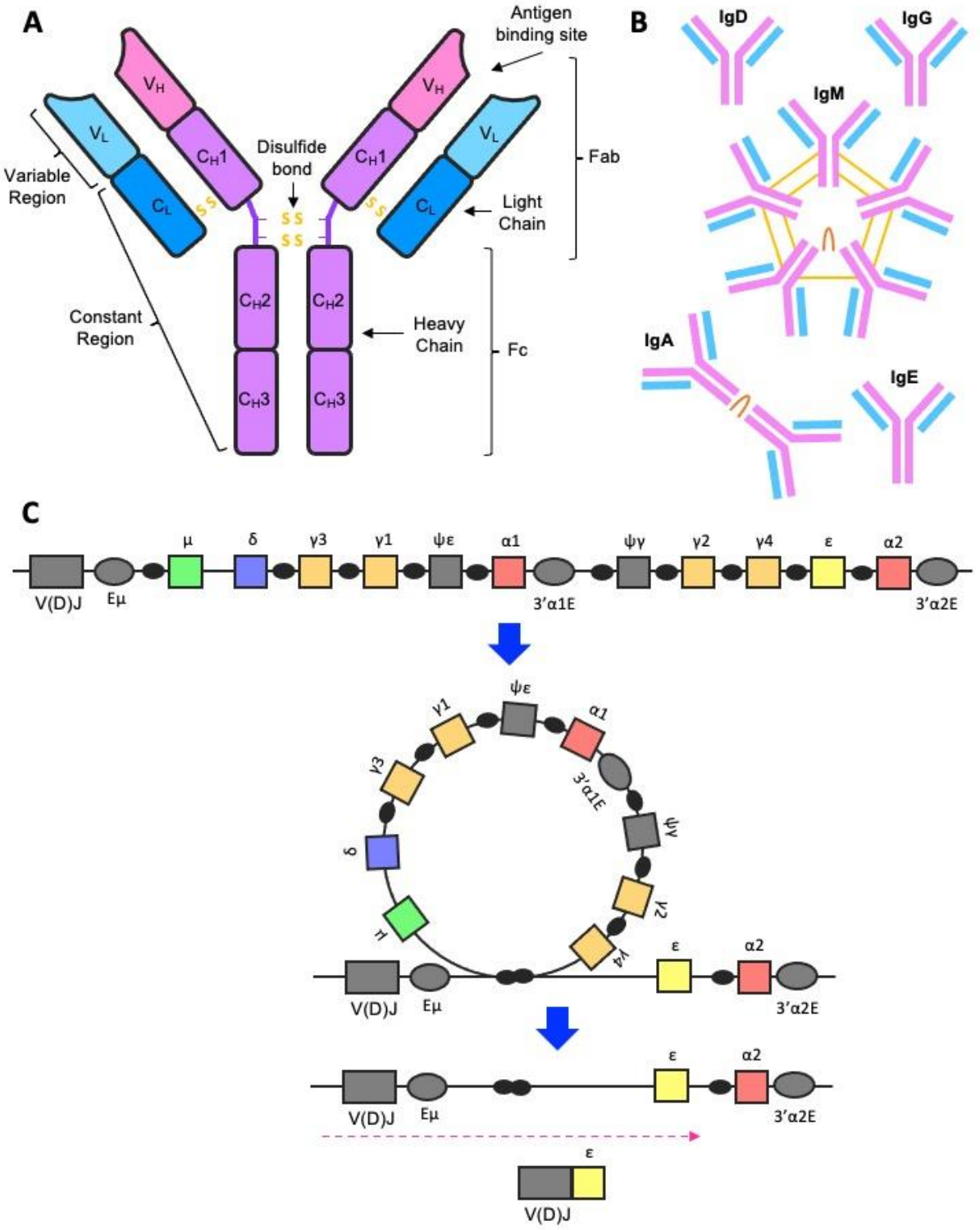

Figure 1.2. The structure of antibodies and process of CSR. A) Basic quaternary structure of an antibody. Antibodies are made up of two light chains (blue) made up of the variable (V_L) and constant (C_L) regions, and two heavy chains (pink) made up of variable (V_H) and constant (C_H1, C_H2, C_H3) regions. These chains are connected by disulfide bonds (orange) and in some isotypes the heavy chain contains a hinge region (purple). Regions are further categorised as the fragment antigen binding (Fab) region which binds antigen, and fragment crystallisation (Fc) region, which interacts with receptors and determines the isotype of the antibody. **B)** Representations of the ability of antibody isotypes to form multimers. IgD, IgE, and IgG exist as monomers, IgA can form dimers, and IgM can form pentamers. Multimers are linked by J chain (dark orange

loop) and disulfide bonds (orange). **C)** Schematic of the process of CSR. AID triggers double strand DNA breaks at switch regions (black ovals). Double strand repair leads to excision of the sequences encoding constant regions and recombination allows transcription of a sequence encoding the remaining isotype (in this case IgE). ψ – pseudogene, 3'α E – enhancer. Adapted from Stavenzer et al[36].

1.2.2.2. Dynamics of the germinal centre

High quality GC responses are important for a robust B cell response to antigen. Plasma cells accumulate at a constant rate over the early response and therefore a sustained GC can lead to a larger pool of LLPCs[41]. Establishment of a GC is dependent on the local cytokine environment and presence of other immune cells. T_{FH} cells drive the formation of GCs and produce IL-21, a potent inducer of terminal B cell differentiation[42]. In contrast, T_{FR} cells act to suppress the GC[43]. The strength of binding to antigen may influence which cells enter the GC, with high affinity cells appearing to be more likely to become plasmablasts through the EF response, with those of lower affinity entering the GC[44]. The local cytokine environment can also influence the output of the GC. Mouse GC-phenotype B cells produce increased levels of LLPCs when cultured with IL-21[45]. Upon primary antigen encounter, naïve B cells enter the GC, however upon re-encounter both naïve and memory B cells can contribute to the GC response. The isotype of memory B cells may influence whether they are likely to re-enter the GC. In one mouse model, upon secondary antigen challenge IgG1 memory cells directly differentiated into plasma cells whereas IgM memory cells restarted the GC reaction[46].

1.2.2.3. Somatic hypermutation

Affinity maturation drives the production of high affinity B and plasma cells in the GC. Mutations are introduced into the variable region of a cell's BCR by somatic hyper mutation (SHM) and cells are iteratively tested in their ability to bind to antigen presented by dendritic cells (DCs) (**Figure 1.3**). The GC is organised into two distinct regions, the dark (DZ) and light (LZ) zones. In the DZ B cells undergo SHM before migrating to the LZ where the affinities of their BCRs are tested by binding to antigen presenting FDCs with the receipt of help from T_{FH}s[47]. Dependent on antigen binding affinity, cells can either be exported as memory or plasma cells, recycled back through the GC, or destroyed. Cells migrate between the two zones to undergo iterative rounds of mutation and selection.

Those with high affinity BCRs are positively selected for, those with the highest relative affinity preferentially become LLPCs and those of moderate affinity become memory cells[47]. There are two competing theories as to why LLPCs are typically higher affinity than memory B cells. The first is that high affinity cells are selected to become LLPCs. The second, that affinity increases as affinity maturation progresses and the GC response undergoes a temporal switch from memory cell to LLPC production[48]. Despite this general pattern, LLPC selection is not limited to the highest affinity binders and plasma cells span a range of affinities, leading to a diverse LLPC population and antibody production[49].

Upon repeat antigen encounter, low affinity memory cells can re-enter a GC and undergo further SHM and affinity maturation[50,51]. However, the memory cells produced by the GC at each antigen encounter are most likely to originate from naïve cells[52]. AID is responsible for driving SHM as it converts cytosine to uracil, leading to point mutations in the genes encoding variable regions[47]. As CSR is also under the control of AID, the processes are often linked with one another. However the mechanisms each uses for the repair of cleaved ends are distinct[32] and, as mentioned, most CSR occurs prior to the GC.

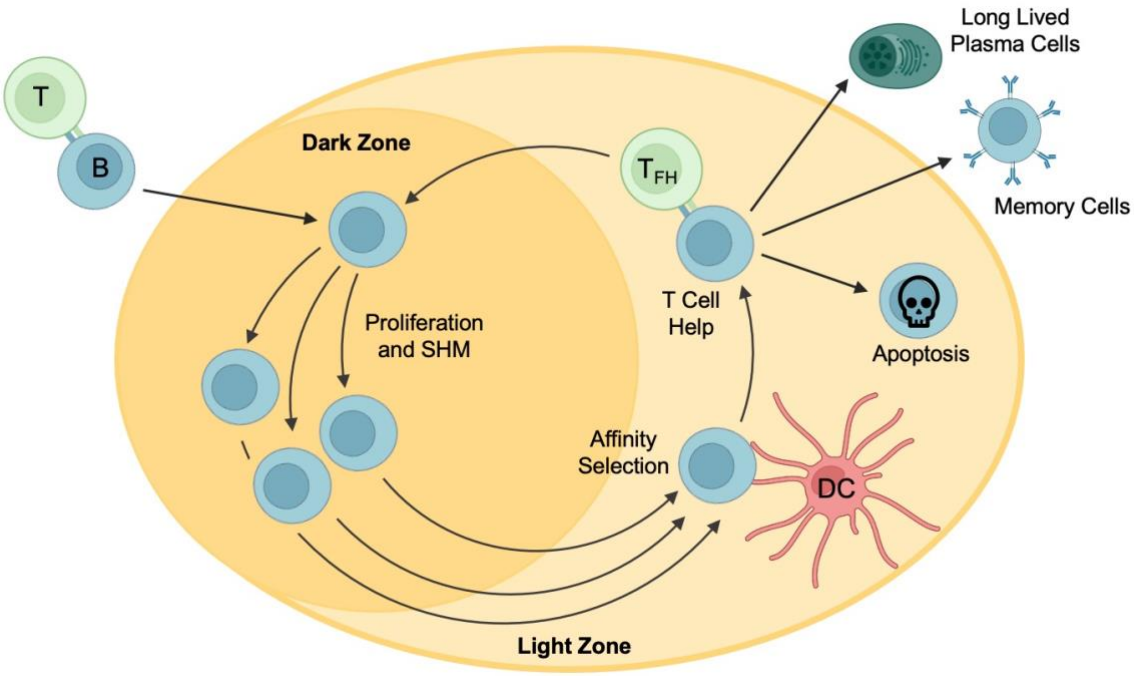

Figure 1.3. The germinal centre response. Schematic of the GC response. Following the receipt of T cell help activated B cells enter the GC and undergo proliferation and somatic hypermutation in the DZ. Mutant cells migrate into the LZ where they are tested by antigen presenting FDCs. Following interaction with T_{FH}

cells B cells are recirculated into the DZ, leave as memory B cells and plasma cells or undergo apoptosis. Created using Biorender.com.

1.2.2.4. Long lived plasma cells

LLPCs are ASCs and are responsible for sustaining circulating antibody levels[53,54]. These levels are vital for ongoing neutralisation of pathogens and protection from disease. When B cells differentiate into plasma cells, they down regulate membrane expression of the BCR and instead begin to secrete soluble antibody. Some IgM and IgA plasma cells have been seen to express membrane bound BCRs which can be functional[55] but this is not typically seen in IgG. Plasma cells have an expanded Golgi apparatus which enables them to secret 10^3 antibodies per second[56,57]. The transcriptional programs and functionality of plasma cells is determined by their isotype[38]. 80% of circulating plasma cells are IgA which are mostly made in the gut associated lymphoid tissues (GALT)[58]. After exit from the GC, plasma cells migrate to survival niches including the bone marrow, GALT, and spleen. Most human plasma cells are found in the bone marrow[59], these are typically IgG. The IgG LLPCs which reside in the bone marrow are responsible for the majority of antibody found in the serum and therefore considered the most important for the long-term protection from pathogens provided by antibodies. The survival and turnover of LLPCs within their niches is not fully understood. However, it is known that survival relies on their receipt of signals to the LLPCs themselves including CD80/86 signals from CD11c cells, IL-6, APRIL, BAFF, Tumor Necrosis Factor (TNF), and CXCL12 for trafficking[57,59].

1.2.2.5. Age-associated B cells

Age-associated B cells (ABCs) are a population of abnormal antigen experienced memory B cells (**Figure 1.4**). These cells are also known as $CD21^{low}$ cells, $CD11c^{+}$ B cells, double negative (DN) B cells and atypical B cells, and due to heterogeneity have been defined in multiple ways[60,61]. They were first identified as memory B cells expressing inhibitory receptors and with a poor response to antigen stimulation[62]. In both mice and humans these cells express reduced levels of the CD21 receptor and increased levels of CD11c and Tbet[63]. ABCs can be produced in response to external challenges in, both

mice and humans, including viral infection[64-66]. They form part of the vaccine response and evidence suggests that repeated vaccination drives them to have a more atypical phenotype [67]. However, expanded levels of circulating ABCs are seen in people with autoimmune diseases, obesity, inborn errors of immunity (IEIs), and the elderly[60,68-70]. There is evidence that high levels of ABCs may impair the B cell response through the inhibition of affinity maturation and early B cell development[60,68,71]. The primary function of ABCs is therefore unclear and may vary based on immune context.

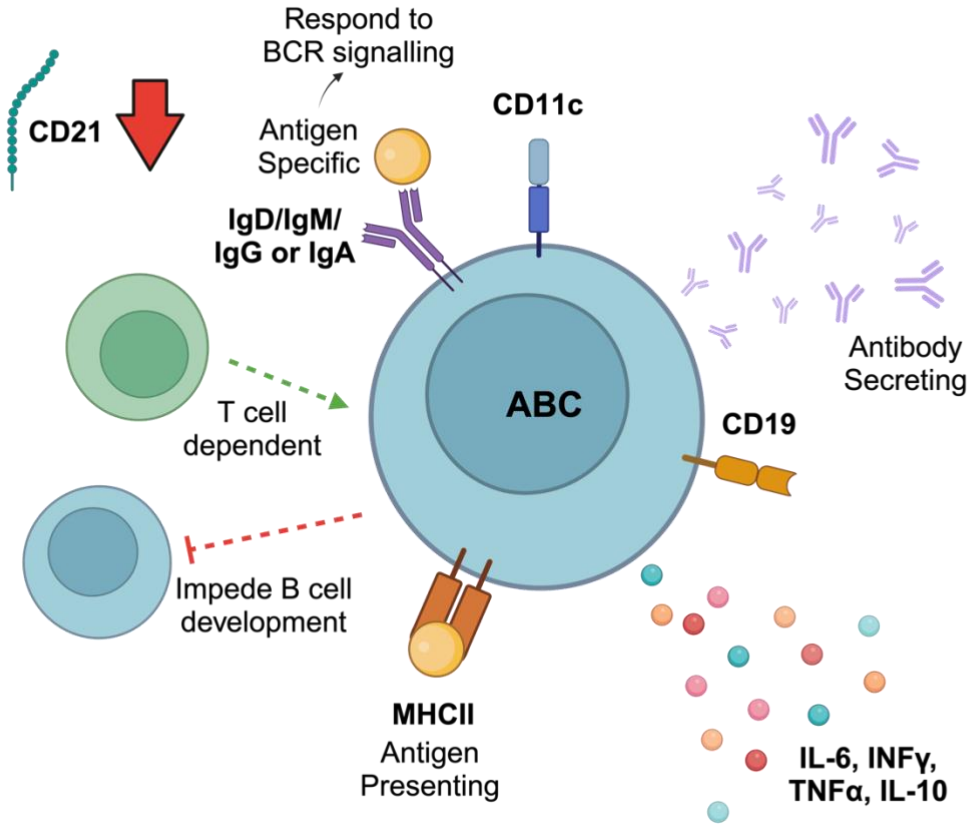

Figure 1.4. Age-associated B cells. Diagram of the features of an ABC. ABCs express CD11c, CD19, MHCII, and a BCR, and down regulate CD21 expression. ABCs can be antigen presenting and antigen specific, responding to BCR stimulation. ABC development is T cell dependent and differentiated ABCs can impair the development of B cells. ABCs secrete cytokines including IL-6, IL-10, IFN-γ, and TNF, and can become antibody secreting. Created using Biorender.com.

1.2.3. Immune memory following vaccination

Vaccination harnesses the adaptive immune response to provide protection against pathogenic infection. The main purpose of vaccination is to form an immune memory to

an antigen of a pathogen enabling quick and efficient response to encounter of the pathogen itself. Vaccines are comprised of two main components: an antigen, and an adjuvant. The adjuvant acts to stimulate the immune system to form a response against the antigen. The antigen is a molecule found on or in the pathogen which can be recognised by immune cells. The innate immune response forms the initial response to vaccination and activates elements of adaptive immunity similarly to in the response to a pathogen. There are many forms of vaccines and vaccine type may determine the kind of immune memory produced. Historically vaccines were either, live attenuated virus, inactivated (dead) virus, or protein + adjuvant[72]. Protein vaccination is associated with higher peak antibody titres which then subsequently decay much faster than those elicited by live attenuated vaccination[73]. Recent developments in vaccine technology have introduced the potential for messenger RNA (mRNA) vaccines. These involve the introduction of a portion of modified mRNA encoding a protein found on the pathogen, without the need for the production and introduction of the protein itself. The relative success of vaccination can be measured by the identification of antigen specific circulating memory B and T cells, in addition to circulating antibody levels.

1.3. SARS-CoV-2 and the COVID-19 pandemic

1.3.1. The COVID-19 pandemic

Coronavirus disease 2019 (COVID-19) was first reported as a novel pneumonia in Wuhan in 2019. Following this, the severe acute respiratory syndrome coronavirus 2 (SARS-CoV-2) rapidly spread across the world and a pandemic was declared four months after its emergence. The virus is part of a family of coronaviruses, which includes SARS-CoV-1 and MERS-CoV[74]. The onset of the pandemic led to the implementation of lock downs and measures to prevent the spread of disease. Despite this, a total of over 200,000 deaths **involving** COVID-19 were reported in weekly reporting data by the Office for National Statistics (ONS) between March 2020 and March 2023[75]. SARS-CoV-2 remains prevalent despite the lifting of these measures and continues to be a challenge for many people.

1.3.2. Structure of the SARS-CoV-2 virus

The SARS-CoV-2 virus, responsible for the COVID-19 pandemic, is a +ssRNA coronavirus (**Figure 1.5A**). The virus comprises of a single stranded RNA genome with bound nucleocapsid (N) protein, encased within a membrane. The virus has two key external proteins, the membrane (M) protein and the spike (S) protein. The S protein is responsible for entry of the virus into host cells. It does so by binding its receptor binding domain (RBD) to the angiotensin-converting enzyme 2 (ACE2) on the surface of human cells, leading to membrane fusion[76]. Once within the host cell the viral RNA is released into the cytoplasm and is replicated and translated into protein by host polymerases and ribosomes. The produced proteins can then be assembled into virus particles, and these can leave the host cell to infect others. The S protein on the surface of the virus is split into two parts, the S1 and S2 regions. The S1 region contains the N-terminal domain (NTD) and RBD, whereas the S2 region contains the fusion peptide (FP), heptapeptide repeat sequences 1 and 2 (HP1/HP2), transmembrane domain (TM) and cytoplasm domain (CT)[77] (**Figure 1.5B**).

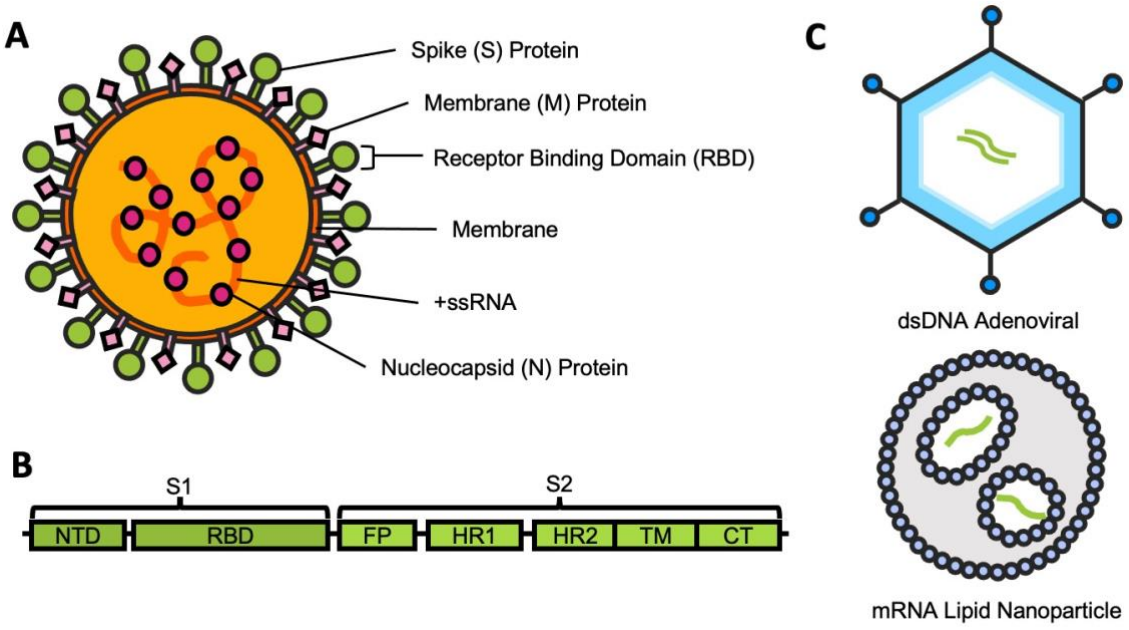

Figure 1.5. The structure of the SARS-CoV-2 virus and vaccines. A) Annotated structure of the SARS-CoV-2 virus. SARS-CoV-2 has a + single stranded RNA genome (ssRNA) and nucleocapsid (N) proteins encapsulated within a membrane. Membrane (M) and Spike (S) proteins are bound to the membrane surface. The receptor binding domain (RBD) portion of the spike protein is responsible for cell binding and entry. **B)** The SARS-CoV-2 spike protein. The S1 subunit contains the N-terminal domain (NTD) and RBD, and the S2 subunit contains the fusion peptide (FP), heptapeptide repeat sequences 1 and 2 (HP1/HP2),

transmembrane domain (TM) and cytoplasm domain (CT). Adapted from Huang et al, 2020[77]. **C)** Illustration of the basic structure of the two main forms of vaccine used against SARS-CoV-2. dsDNA adenoviral **(top)** is made up of dsDNA (green) contained within an inactivated adenovirus (blue). mRNA-LNP **(bottom**) contains mRNA (green) encapsulated in a LNP (blue).

1.3.3. COVID-19 infection and protection

Infection with SARS-CoV-2 typically leads to respiratory symptoms. Disease severity can range from asymptomatic infection to, in some cases, requiring hospitalisation and ultimately causing death. From as early as one week after infection, IgM and IgG antibodies can be detected against the N and S proteins[78]. Mild infection leads to the development of S protein specific LLPCs, which alongside their antibodies can be detected up to 8 months after recovery[79]. In asymptomatic infections, the T cell response is seen to be less than in symptomatic[80].Convalescence from COVID-19 has a protective effect against re-infection observed up to 7 months after infection[81].

1.3.4. SARS-CoV-2 Viral Variants

The COVID-19 pandemic has been defined by waves of viral variants. Many of these variants contain mutations impacting the structure of the S protein, enabling escape from neutralising antibodies[82,83]. The pandemic began in 2019 with the wild type (WT) "Wuhan-1" strain of the virus. Confirmed infections during the initial wave in the UK were low, in part due to strict lockdown regulations, however there were significant numbers of disease associated deaths[84]. In September 2020 the alpha variant (lineage B.1.1.7) was identified in the UK, this variant had mutations associated with an increased ability to evade the host immune response[85,86]. The alpha variant accounted for more infections than the initial wave and a high number of deaths[87]. Subsequent waves led to far fewer deaths than each of the first defined waves in the UK, largely because of the roll out of vaccines in early 2021. The delta variant (B.1.617.2) became the dominant variant in the UK in May 2021 and lead to a sustained wave of infections before the emergence of the omicron variant (B.1.1.529) in November 2021. Both the delta and omicron variants were able to evade the immune protection, including neutralising antibodies, provided by vaccination[88,89]. The omicron variant caused two large waves of infections in the UK, the

second in March 2022 was dominated by the omicron BA.2 subvariant. A further wave of infections were driven by the BA.4 and BA.5 subvariants in the UK in June 2022[90]. Each of these waves were associated with increases in COVID-19 related deaths however these did not reach the peaks seen at the beginning of the pandemic. The WHO continues to monitor variants of interest and SARS-CoV-2 continues to circulate in the UK.

1.3.5. Vaccination against SARS-CoV-2

From the onset of the pandemic, there was a large effort to rapidly produce a vaccine able to provide protection against the virus. A number of different vaccines were developed and used across the globe. In the UK the Oxford-AstraZeneca ChAdOx1, Pfizer BioNTech BNT162b2, and Moderna mRNA-1273 vaccines were offered to the public through the National Health Service.

1.3.5.1. Adenoviral vaccination

The ChAdOx1 vaccine is an adenoviral vaccine, developed at the University of Oxford. The vaccine comprises of an inactivated chimpanzee adenoviral vector, containing double stranded DNA encoding the S protein of SARS-CoV-2 (**Figure 1.5C**). Clinical trials found the vaccine to be safe with 70-74% efficacy[91,92] and the vaccine was deployed in the UK in January 2021.

1.3.5.2. mRNA vaccination

The Moderna mRNA-1273 and Pfizer BioNTech BNT162b2 vaccines are both mRNA vaccines. mRNA vaccine technology is in its infancy and the mRNA vaccines against COVID-19 were the first of their kind to be made available to the general public. Both vaccines are comprised of modified mRNA, encoding the S protein, enclosed within a lipid nanoparticle (LNP) (**Figure 1.5.C**). These vaccines both rely on the inherent adjuvant activity of the LNP and mRNA construct and have no added adjuvant. Regardless, clinical trials reported 86-100% efficacy for BNT162b2[93,94] and 93-94% for mRNA-1273[95,96] and the vaccines were deployed in December 2020 and April 2021 respectively.

Despite the similarities in these vaccines, differences have been observed in the immune responses they elicit. Vaccination with mRNA-1273 leads to higher levels of anti-RBD antibodies than BNT162b2, in both SARS-CoV-2 naïve and previously infected individuals[97,98] and may provide better protection against disease[99].

The roll out of vaccines against SARS-CoV-2 played a critical role in the reduction of risk from the COVID-19 pandemic. Each of the vaccines used in the UK were successful in inducing adaptive immunity and protection from disease. This immunity is then boosted by additional antigen encounter through infection and repeat vaccination which lead to increased S specific antibody levels[100] and T cell expansion and differentiation[101,102]. Antigen specific $CD8^+$ T cell levels and neutralising antibodies are associated with protection against SARS-CoV-2 infection[103,104] and thus act as a marker of a successful vaccine response.

1.4. Aims and outlines

This project began in the September of 2020, six months on from the first COVID-19 lockdown and three months prior to the beginning of the mass COVID-19 vaccine roll out in the UK. mRNA vaccines are a novel technology and were applied alongside more traditional vaccine modalities to target the emerging SARS-CoV-2 virus. The urgency of the pandemic led vaccines to be rapidly rolled out under emergency authorisation to a large and diverse population of recipients.

In this work, I aimed to investigate, how mRNA vaccines against SARS-CoV-2, provide protection against disease. In doing so, I aimed to assess their efficacy in individuals with immune dysregulation and identify targets for their improvement. This was with the goal of identifying how individuals could best be protected from COVID-19 disease using mRNA therapeutics.

With this in mind, in this thesis I address the functionality and efficacy of SARS-CoV-2 mRNA vaccines through the following:

- In **Chapter 3** I address the vaccine responses of individuals with varying levels of immune dysregulation due to PID and immunotherapy.
- In **Chapter 4** I further address the immune responses and protection provided by vaccination in individuals with immune dysregulation due to obesity.
- In **Chapter 5** I additionally explore how the chronic inflammation of obesity alters the humoral response to mRNA vaccination.
- In **Chapter 6** I address the role of cytokine signalling, specifically IL-6, in the humoral response to mRNA vaccination in obesity and more broadly. Additionally, I explore the potential for the enhancement of signalling to improve vaccine responses.

2. Materials and methods

2.1. Human clinical studies

2.1.1. BNT162b2 vaccination and immune dysregulation study coordination and ethics

Participants were recruited from Cambridge University Hospital or St Bartholomew's Hospital based on deficiency in genes of interest or receipt of immune checkpoint blockade (ICB) therapies. Healthy controls (HCs) were recruited based on lack of known immune deficiency and other potentially confounding factors. Informed written consent was obtained from all participants and samples were collected under the NIHR National BioResource - Research Tissue Bank (NBR-RTB) ethics (REC:17/EE/0025) or under the Barts and the London Immunology Registry (REC: 11/LO/1689). Cohorts of individuals with primary immune deficiencies (PID, n = 9), on ICB (n = 19) and HCs (n = 10) (**Table 2.1**) were sampled prior to and 8-, 21-, and 105-days following vaccination with two doses of BNT162b2. Peripheral blood samples were collected by clinical staff into lithium heparin or serum separating tubes. I was responsible for the central coordination of the transport of samples from the clinic to the research lab and subsequent coordination of sample management under appropriate human tissue act (HTA) regulations.

Table 2.1. Characteristics of the participants of the vaccination in immune dysregulation study
*Treatment ended at the time of sampling

Condition	Sex	Treatment
Healthy Controls (n=10)	F (5), M (5)	N/A
CTLA-4 haploinsufficiency	F	Ig Replacement
CTLA-4 haploinsufficiency	F	Ig Replacement
LRBA compound heterozygote	F	Ig Replacement
NFKB1	M	Ig Replacement
NFKB1	F	None
NFKB1	F	Ig Replacement
NFKB1	M	None

NFKB1	M	None
NFKB2	M	Ig Replacement
Stage IIIA Oesophageal cancer	M	Ipilimumab Nivolumab
Stage IIIC Melanoma	M	Pembrolizumab
Stage IV Metastatic Melanoma	M	Pembrolizumab
Stage IV Metastatic Renal	F	Ipilimumab Nivolumab
Stage IV Metastatic Renal	M	Ipilimumab* Nivolumab
Stage IIIB Melanoma	F	Pembrolizumab
Stage IV Metastatic Melanoma	M	Pembrolizumab/ Ipilimumab Nivolumab
Stage IIIC Melanoma	M	Pembrolizumab
Stage IIIB Melanoma	F	Pembrolizumab
Stage IV Metastatic Melanoma	M	Ipilimumab Nivolumab
Stage IV Metastatic Melanoma	M	Pembrolizumab
Stage IV Metastatic Melanoma	M	Pembrolizumab
Stage IV Metastatic Melanoma	M	Pembrolizumab
Stage IV Melanoma	M	Nivolumab
Stage IIIC Melanoma	M	Pembrolizumab
Stage IV Metastatic Melanoma	M	Pembrolizumab
Stage IV Melanoma	F	Nivolumab
Stage IV Metastatic Renal	M	Ipilimumab Nivolumab
Stage IV Metastatic Melanoma	F	Pembrolizumab

2.1.2. SCORPIO study coordination and ethics

SARS-COV-2 vaccine ResPonse In Obesity (SCORPIO) study participants were enrolled by the clinical team at the obesity clinic at Cambridge University Hospitals NHS Trust. Participants were recruited to the severe obesity (SO) group if they had a BMI >40 kg/m^2 or >35 kg/m^2 with obesity associated medical conditions and had previously received two doses of vaccine against COVID-19. Normal weight (NW) controls were recruited on the basis of 18.5 kg/m^2 < BMI < 25 kg/m^2. The clinical study was approved by the National Research Ethics Committee and the Health and Research Authority under the NIHR

National BioResource - Research Tissue Bank (NBR-RTB) ethics (REC:17/EE/0025). All participants gave informed written consent. All participants received a mRNA third dose vaccine against COVID-19, either BNT162b2 or mRNA1273 through the NHS. Blood samples were collected at day 0 prior to vaccination and days 8(−3)-, 28(±7)-, 105(±7)-, and 185-following vaccination. Samples were collected by clinical staff at the obesity clinic into lithium heparin or serum separating tubes. Participants were excluded from the analysis at the point of SARS-CoV-2 infection. A total of 16 NW controls and 28 individuals with SO were longitudinally sampled and included in this study (**Table 2.2**).

Table 2.2. Characteristics of the participants of the SCORPIO study
*Data missing for 3 participants

Characteristic	**NW Controls (16)**	**SO Participants (28)**
Sex	F (10), M (6)	F (20), M (8)
BMI	18-25 ($\bar{x}$=22.9)	38-67 ($\bar{x}$=47.4)
Age	38-60 ($\bar{x}$=46)	37-69 ($\bar{x}$=54)
Primary Vaccine	ChAdOx1 (10) BNT162b2 (6)	ChAdOx1 (18) BNT162b2 (10)
Booster Vaccine	mRNA1273 (2) BNT162b2 (14)	mRNA1273 (11) BNT162b2 (14)*
Hypertension	0	15
Cardiovascular Disease	0	6

2.1.3. PBMC isolation from whole blood

Peripheral blood mononuclear cells (PBMCs) were separated from whole blood by density gradient centrifugation. All blood processing was completed under sterile conditions in a category 2 tissue culture. Blood was diluted with an equal volume of sterile phosphate buffered saline (PBS) and layered onto 15mL of Histopaque®-1077 (Sigma) or Lymphoprep™ (Stem Cell) in 50mL falcon tube. Samples were spun at 800xg for 20 minutes at the lowest acceleration setting with the brake turned off. The lymphocyte layer was slowly collected with a Pasteur pipette and supplemented with separation buffer (Sterile PBS, 1% (v/v) foetal bovine serum (FBS), 2mM EDTA). Cells were washed twice (400xg, 4°C, 10 mins) with separation buffer before counting and

resuspension in FBS. An equal volume of freezing media (RPMI, 20% (v/v) DMSO, 40% (v/v) FCS) was added dropwise to the cell suspension. Cells were transferred to cryovials in 1mL aliquots and frozen in a Mr. Frosty™ Freezing Container (Thermo Scientific) in a -80°C freezer. Once fully frozen cells were transferred to liquid nitrogen storage until further use. *I completed sample processing with the assistance of Dr Juan Carlos Yam-Puc, Dr Nonantzin Baristain-Covarrubias, Robert Hughes, Rebecca Boston, Magda Ali, Edward Simmons-Rosello, Dr Maria Rust, Alexander Ferreira, Lucy Booth, Thevinya Gurugama, Lihinya Gurugama, and Harry Robson*.

2.1.4. Separation of serum and EDTA plasma from whole blood

Serum separating tubes were allowed to clot for at least one hour. Tubes were centrifuged at 1600xg, for 10 minutes at room temperature (RT). Serum or plasma was removed from the blood cell pellet and aliquoted into cryovials which were stored at -80°C until use.

2.1.5. Thawing of frozen PBMCs

Cryopreserved PBMCs were thawed in a water bath at 37°C then transferred into a falcon tube. Cryovials were rinsed with 1mL of defrosting media (culture media containing 0.01% (v/v) Benzoase Nuclease (Merck)) which was added dropwise into the sample. An additional 2mL of defrosting media was added dropwise and then the sample was gently mixed for 1 minute. A following 2mL of defrosting media was added and mixing repeated. Finally, 5mL of defrosting media was added. Cells were pelleted by centrifugation at 300xg, for 10 minutes at RT and then resuspended in culture media for further use.

2.1.6. EAVEII data analysis

Real time health care data from over 5 million individuals in Scotland was used for analysis by the EAVEII study[105]. Ethical approval was granted by the National Research Ethics Service Committee, Southeast Scotland 02 and approval for data linkage was granted by the Public Benefit and Privacy Panel for Health and Social Care. Individuals ≥18 years old, who had received two doses of vaccine against COVID-19 were included

in this analysis. They were stratified into groups based on based on the last recorded BMI measurement on their primary care record or where there was none, imputed BMI using ordinary least squares regression. Normal weight 18.5–24.9 kg/m^2, Obesity 30–39.9 kg/m^2, Severe Obesity ≥40 kg/m^2. Outcomes after vaccination were assessed from day 14 after the administration of the primary vaccine schedule. Severe COVID-19 was defined as either hospital admission within 14 days of a positive RT-PCR test, admission with COVID-19 as a reason, or a positive RT-PCR test during admission. Death due to COVID-19 was defined as death within 28 days of a positive RT-PCR test or where COVID-19 was listed as a primary reason for death. Both death and severe COVID-19 were considered under the umbrella of severe outcomes. The frequency and rate of severe outcomes were calculated for each group and generalized linear models (GLMs) assuming a Poisson distribution with person-time as an offset representing the time at risk were used to derive rate ratios (RRs) with 95% confidence intervals (CIs). Adjusted (a)RRs accounted for confounders including sex, age, comorbidities, time since vaccination, time between vaccine doses, deprivation, previous infection, and date. R (version 3.6.1) was used to carry out all statistical analyses. *This analysis was completed in full by Dr Utkarsh Agrawal, Prof Colin McCowan, Prof Chris Robertson, and Prof. Sir Aziz Sheikh.*

2.2. Detection of antigen specific T cell responses

2.2.1. CTV cell proliferation assay

Cells were rested after thawing for 1 hour at 37°C before washing twice more with PBS. Cells were resuspended in 1mL of PBS and stained with a specified concentration of cell trace violet (CTV) for 10 minutes in the dark at RT. 4mL (4x volume) of ice cold FBS was then immediately added to quench the reaction, and cells were washed in media. Cells were plated at 2.5 x10^5cells per well in a U bottomed 96 well plate and IL-2, IL-7, and Phytohaemagglutinin (PHA) were added to the relevant wells at final concentrations of 10ng/mL, 10ng/mL, and 2.5µg/mL respectively. Any empty wells on the plate were filled with PBS to prevent evaporation and the plate was placed in a sealed container and incubated for 4 days at 37°C. Following incubation cells were washed and transferred

into V bottomed plates. Cells were then stained for analysis by flow cytometry (**see 2.4.1**.).

2.2.2. Activation induced markers (AIM) assay

Cells were rested at 37°C for 2 hours following thawing. PBMCs were plated at $2x10^6$ cells per well in a 96 well plate. SARS-CoV-2 Peptivator S1, S+, and S peptides (Miltenyi) were pooled to form a collection of peptides which covered the entirety of the S protein. Peptide pools covering the N, M, and S proteins were added to a final concentration of 1µg/mL. Cells were plated in wells coated with OKT3 anti-CD3 as a positive control. Plates were incubated at 37°C for 24 hours to allow antigen presentation and T cell activation. Following stimulation cells were washed and stained for T cell activation markers and analysis by flow cytometry (**see 2.4.1**.).

2.2.3. IFN-γ ELISpot for SARS-CoV-2 reactive T cells

PBMCs were assayed for interferon gamma (IFN-γ) production using an Enzyme-linked immunosorbent spot assay (ELISpot) Plus: Human IFN-γ (HRP) kit (Mabtech) following manufacturer's instructions, with adjustments made to align with the standard operating procedure of the Protective Immunity from T cells to Covid-19 in Health workers (PITCH) study. All steps prior to overnight incubation were performed under sterile conditions in a category 2 tissue culture facility. PBMCs were thawed into Rab0 (RPMI media containing 1% (v/v) Penicillin/Streptomycin (Sigma) and 0.01% (v/v) Benzoase Nuclease (Merck)). Cells were washed (400xg, 5 minutes, RT) and rested for 2-3 hours at 37°C in Rab10 (RPMI, 10% (v/v) Human AB Serum (Sigma), 1% (v/v) Penicillin/Streptomycin). Plates precoated with capture antibody (Mabtech, mAb 1-D1K) were washed three times (200µL per well) with sterile PBS. Plates were then blocked to prevent non-specific binding with Rab10 at 37°C for 1-2 hours. PBMCs were plated at 2 $x10^5$ live cells per well (50µL). Overlapping peptide pools (18-mers with 10 amino acid overlap, Mimotopes) covering the S1 and S2 regions of spike, membrane, or nucleocapsid SARS-CoV-2 proteins were added to triplicate wells at a final concentration of 2µg/mL (50µL). Positive controls were added in duplicate and included over lapping pools covering regions of CMV, EBV,

influenza, and Tetanus toxoid at a final concentration of 2µg/ml (CEFT; Proimmune) and Concanavalin A (Sigma). All peptide stock was resuspended in DMSO (Sigma) and DMSO to an equivalent final concentration in media was used as the negative control. Cells were incubated for 18 hours at 37°C, 5% humidity in an enclosed container to prevent evaporation. Following incubation wells were washed seven times with PBS 0.05% (v/v) Tween (Sigma). Plates were incubated for 2 hours at RT with 50µL per well of ELISpot PLUS kit biotinylated detection antibody (clone 7-B6-1) at 1µg/mL in PBS. Wash steps were repeated before addition of 50µg per well of ELISpot PLUS kit streptavidin-ALP, 1µg/mL in PBS and 1 hour incubation at RT. Wash steps were repeated and 50µL of filtered NBT/BCIP was added to each well and allowed to react for 5 minutes at RT. Colour development was stopped immediately by flushing wells with cold tap water. Wells were washed multiple times with cold water and the under drain was removed to assist in drying. Plates were allowed to fully air dry for at least 48 hours before scanning with the AID iSpot Spectrum ELISpot reader (software version 7.0, Autoimmune Diagnostika GmbH, Germany). Positive spots were automatically counted using the count settings detailed. The average spot count of DMSO negative control wells was subtracted from the test wells to account for background IFN-γ production. Spot counts were adjusted to spot forming units (SFU) per 10^6 cells for reporting and statistical analysis. The completion of ELISpot assays for the vaccination in immune dysregulation and SCORPIO studies was with the assistance of Lucy Booth. 4 plate optimisation experiment was completed with the additional help of Dr Tom Mulroney and Alexander Ferreira.

2.2.4. IFN-γ ELISpot for omicron variant SARS-CoV-2 reactive T cells

To assay for T cells specific to the S protein of the SARS-CoV-2 omicron variant peptide pools covering the S1 and S2 regions of the omicron spike (Mimotopes) were included in the ELISpot Plus: Human IFN-γ (HRP) assay. Cells were assayed in triplicate in the same way as for standard WT testing. Peptides for both WT and omicron assessments were kindly provided by the PITCH project.

2.2.5. IFN-γ/IL-2 FluoroSpot

PBMCs were assayed for IFN-γ and IL-2 using FluoroSpot^{PLUS} Human IFN-γ/IL-2 kits (Mabtech) according to manufacturer's instructions. Following thawing cells were rested for 1 hour at 37°C. Cells were plated onto pre-coated plates. Peptides covering the S, M, and N proteins of SARS-CoV-2 (Mimotopes/Miltenyi) were added in triplicate wells at a final concentration of 2µg/mL. Concanavalin A (ConA) was added as a positive control at 5µg/mL. Plates were incubated for 18 hours at 37°C. Plates were washed five times with 200µL per well of PBS. Anti-IFN-γ mAb (7-B6-1) and Anti-IL-2 mAb (MT8G10) biotin were added, and plates were incubated for 2 hours at RT. Wash steps were repeated an additional five times before a 1-hour incubation with Anti-BAM mAb, 490 and SA-550 at RT. The wash was again repeated, and plates were incubated for 15 minutes at RT with enhancer before being emptied, blotted, and allowed to dry. Plates were allowed to fully air dry for at least 48 hours before fluorescence at 510 and 570nm was read with the AID iSpot Spectrum ELISpot reader (software version 7.0, Autoimmune Diagnostika GmbH, Germany). Positive spots were automatically counted using the default count settings. The average spot count of DMSO negative control wells was subtracted from the test wells to account for background IFN-γ production. Spot counts were adjusted to SFU/10^6 cells for reporting and statistical analysis.

2.3. Identification of antigen specific antibodies

2.3.1. RBD and spike binding antibody quantification

RBD, S, and N binding IgG in serum samples was quantified by Luminex assay. Recombinant target proteins were covalently coupled to carboxylated beads (Luminex, Netherlands). Coupled beads were incubated with diluted serum (1/100, 1/1000, 1/10000) for 1 hour at RT with shaking. Beads were washed then incubated for 30 minutes with an anti-human IgG PE labelled antibody (Leinco/Biotrend). Beads were washed again, and data acquired, then analysed using Exponent Software V31 software on the Luminex analyser (Luminex/R&D Systems) and reported as mean fluorescence intensity (MFI). *Luminex assays and initial data analysis were completed by collaborators in the lab of Dr Rainer Doffinger.*

2.3.2. Neutralising capacity

Serum neutralising capacity was quantified by live virus neutralising assays. Serum samples were heat inactivated at 56°C for 30 minutes. HEK293T-ACE2-30F-PLP2 reporter cells expressing Renilla luciferase (Rluc) and SARS-CoV-2 Papain-like protease-activatable circularly permuted firefly luciferase (FFluc) were plated in a 96 well plate. WT SARS-CoV-2 virus was incubated with a three-fold dilution series of serum for 2 hours at 37°C and then applied to the cells. Following 24 hours incubation cells were lysed in Dual-Glo Luciferase Buffer (Promega) diluted 1:1 with 1% NP-40 in PBS. Infectious virus was quantified as the ratio of FFluc/Rluc activity measured using the Dual-Glo kit (Promega) according to the manufacturer's instructions in each lysate. Titration curves were plotted as FFluc/Rluc vs log (serum dilution) and analysed using the Sigmoidal, 4PL, X is log(concentration) function in GraphPad Prism, NT50 was obtained using this model. For samples with no detectable neutralising capacity an arbitrary value of 2 was assigned to the sample, for those with detectable but not quantifiable activity a value of 4 was assigned. *All live virus neutralising assays and initial analysis were completed by collaborators Dr Pehuen Pereyra Gerber, Dr Isobel Ramsay Stubbs, and Jack Smith in the lab of Dr Nicholas Matheson.*

2.3.3. Neutralising capacity against omicron variant

For the quantification of neutralising capacity against the omicron variant the omicron (lineage B.1.1.529) variant virus was used in the place of WT virus. All other steps of the neutralising assay were completed as detailed.

2.3.4. Total spike and nucleocapsid binding antibody quantification

Serum was analysed using the Roche Elecsys anti-SARS-CoV-2 electrochemiluminescence immunoassay using a Roche Cobas® e801 Immunoassay Analyzer. Results were expressed as a cut-off index (COI) calculated by the analyser software as the electrochemiluminescence signal obtained from the participant sample divided by the lot-specific cut-off value. *Roche Elecsys assays and initial analysis were*

completed by the lab of Dr Ashley Otter at the Emerging Pathogen Serology group, UK Health Security Agency.

2.4. Flow cytometry

2.4.1. Human cells

Cryopreserved cells were thawed and rested for 1 hour at 37°C, all other cells were stained straight from assay processing. Cells were washed in staining buffer (PBS, 1% (v/v) FBS, 2mM EDTA). Fc regions were blocked, and cells stained for viability by incubation for 10 minutes with FcX TrueStain and fixable Live/Dead stain. All samples were stained for a minimum of 30 minutes at 4°C with relevant cocktails of fluorescently labelled antibodies and proteins, targeting markers of interest (**Table 2.3**). Cells were fixed with 4% Paraformaldehyde (PFA). Samples were acquired with a BD LSRFortessa using FACSDIVA software (BD-Biosciences).

2.4.1.1. Identification of proliferating T cells

Proliferating T cells were defined as: singlets, live, $CD3^+$, $CTV^{int/low}$. (**Appendix A.1**).

2.4.1.2. Identification of activated T cells

Activated $CD4^+$ T cells were defined as: singlets, live, $CD3^+$, $CD4^+$, $CD8^-$ $CD137^+$, $OX40^+$

Activated $CD8^+$ T cells were defined as: singlets, live, $CD3^+$, $CD4^-$, $CD8^+$ $CD137^+$, $CD69^+$ (**Appendix A.2**).

2.4.1.3. Identification of $cT_{FH}s$

Circulating T follicular helper cells were defined as: singlets, live, $CD3^+$, $CD4^+$, $CD8^-$, $CD45RA^-$, $CXCR5^+$, $PD\text{-}1^+$ - *analysis of these cells was completed by Yam-Puc et al*[106] (**Appendix A.3**)

2.4.1.4. Identification of RBD specific cells

RBD binding B cells were defined as: singlets, live, $StreptavidinBV711^-$, $CD19^+$, $RBD\text{-}1^+$, $RBD\text{-}2^+$ - *analysis of these cells was completed by Yam-Puc et al*[106] (**Appendix A.3**)

2.4.1.5. Identification of age-associated B cells

Age-associated B cells were defined as: singlets, live, $CD3^-$, $CD19^+$, $CD21^-$, $CD11c^+$ - *analysis of these cells was completed by Yam-Puc et al*[106] (**Appendix A.3**)

2.4.1.6. Identification of spike specific cells

Spike binding B cells were defined as: singlets, live, $CD19^+$, Spike 1^+, Spike 2^+ (**Appendix C.2**)

Table 2.3. Antibodies against human cell markers used for flowcytometry

Marker	Fluorochromes	Source	Clones
CCR7	PE/ Pe-Cy7	BioLegend	G043H7
CD11c	BV421	BioLegend	Bu15
CD134 (OX40)	PE	BioLegend	Ber-ACT35
CD137	APC	BioLegend	4B4-1
CD14	PeCy7	BioLegend	M5E2
CD19	PeCy7/ BUV395	Invitrogen/ BD Biosciences	HIB19
CD21	AF700	BioLegend	Bu32
CD27	APC/Vio700/APC-Cy7	Miltenyi Biotec	M-T271
CD3	BV510/BV785	BioLegend	OKT3/ SK7
CD38	BUV737	BD Biosciences	HB7
CD4	AF700	BioLegend	OKT4/ SK3
CD45RA	BV650	BioLegend	HI100
CD69	BV421	BioLegend	FN50
CD71	BV650	BioLegend	CY1G4
CD8a	AF488	BioLegend	RPA-T8
CD85j	PerCP-Cy5.5	BioLegend	GHI/75
CXCR5	BV421	BioLegend	J252D4
FcX	N/A	BioLegend	N/A
ICOS	BV711	BioLegend	C398.4A
IgA	PE-Vio615	Miltenyi Biotec	REA1014
IgD	Pe-Cy7	Miltenyi Biotec	IgD26
IgG	PE	Miltenyi Biotec	IS11-3B2.2.3
IgM	BV785	BioLegend	MHM-88

Live/Dead	Near IR/Fixable Aqua	Invitrogen	N/A
OX40	PE	BioLegend	Ber-ACT35
PD-1	APC-Cy7	BioLegend	29F.1A12
RBD-1	AF488	In House	N/A
RBD-2	AF647	In House	N/A
Streptavidin	BV711	BioLegend	N/A
Spike 1	APC	In House	N/A
Spike 2	PE	In House	N/A

2.4.2. Murine cells

Cryopreserved mouse cells were prepared and analysed in the same way as human samples with the exception of the use of mouse specific FcX and antibodies (**Table 2.4**).

2.4.2.1. Identification of spike specific B cells

Spike binding B cells were defined as: singlets, live, $B220^+$, $CD3^-$, $CD4^-$, $CD8a^-$, $NK1.1^-$, $F4/80^-$, Spike 1^+, Spike 2^+ (**Appendix C.9**)

2.4.2.2. Identification of IgM B cells

IgM^+ B cells were defined as: singlets, live, $B220^+$, $CD3^-$, $CD4^-$, $CD8a^-$, $NK1.1^-$, $F4/80^-$, IgM^+, IgG^- (**Appendix C.9**)

2.4.2.3. Identification of IgG B cells

IgG^+ B cells were defined as: singlets, live, $B220^+$, $CD3^-$, $CD4^-$, $CD8a^-$, $NK1.1^-$, $F4/80^-$, IgM^-, IgG^+ (**Appendix C.9**)

2.4.2.3. Identification of plasma cell subsets

Plasma cells were defined as: singlets, live, $B220^-$, $CD138^+$

Plasmablasts were defined as: singlets, live, $B220^{int}$, $CD138^+$

Antibody secreting - $CD138^+TACI^+$ plasma cells were defined as: singlets, live, $CD138^+$, $TACI^+$ (**Appendix D.2**)

Table 2.4. Antibodies against murine cell markers used for flowcytometry

Marker	Fluorochromes	Source	Clones
B220	PerCP-Cy5.5/BUV737/APC-Cy7	BioLegend	RA3-6B2
CD138	BV786	BioLegend	281-2
CD19	BUV395/ PeCy7/BB700	BD Biosciences	1D3
CD3	BV510/PE-Cy7	BioLegend	17A2
CD38	BUV395	BD Biosciences	90/CD38
CD4	BV421/PE-Cy7	BioLegend	GK1.5
CD8	BV421/PE-Cy7	BioLegend	53-6.7
F4/80	PE-Cy7	BioLegend	BM8
FcX (CD16/32)	N/A	BioLegend	93
IgG1	BV421	BioLegend	RMG1-1
IgG2a	BV421	BioLegend	RMG21-62
IgG2a/2b	BV421	BD Biosciences	R3-40
IgG3	BV421	BD Biosciences	R40-82
IgM	BV421/BUV737	BD Biosciences	II/41/ RA3-6B2
Live/Dead	Fixable Aqua/Near IR	ThermoFisher	N/A
NK1.1	PE-Cy7	BioLegend	S17016D
Spike 1	APC	In House	N/A
Spike 2	PE	In House	N/A
Streptavidin	BV711	BioLegend	N/A
Sca-1	FITC	BioLegend	W18174A
TACI /CD267	PE	BioLegend	8F10
IL-6Ra (CD126)	PE-Cy7	BioLegend	D7715A7

2.5. Detection of SARS-CoV-2 infection/convalescence

Participants were determined to have experienced SARS-CoV-2 infection if they fulfilled either of the following conditions. A positive Reverse transcription polymerase chain reaction (RT-PCR) test, a response of over 50 ΔSFUs/10^6 cells in an IFN-γ ELISPOT when

stimulated with peptides covering the M and N proteins, detection of N binding IgG by Luminex assay. Individuals with evidence of infection prior to the day 21 or 28 timepoint were excluded all analyses. Where individuals experienced infection subsequent to the collection of their day 21/28 samples, samples taken after infection were disregarded.

2.6. Mammalian cell culture

2.6.1. Maintenance of FreeStyle™ 293-F cells

FreeStyle™ 293-F cells (ThermoFisher, R79007) were passaged in Freestyle 293 Expression Media (ThermoFisher) in 30mL cultures within 125mL Erlenmeyer Flasks. Approximately every two days, when cell density reached $2x10^6$ cells/mL, cells were sub-cultured into a new flask at $4x10^5$ cells/mL. Cells were cultured in a shaking incubator at 37 °C, 70% humidity, 8% CO_2, 125 rpm. Cells were discarded once they had reached passage 30. All cell culture was completed under sterile conditions in a category 2 tissue culture facility.

2.6.2. Transfection of FreeStyle™ 293-F cells

Cells were seeded at a density of $5x10^5$ cells/mL and expanded overnight to $1x10^6$ cells/mL. Unless otherwise stated, cells were transfected with 1.2 µg of filtered plasmid DNA per 10^6 cells. DNA was incubated with 1mg/mL polyethylenimine (PEI) at 1:2 (DNA:PEI) for 15 minutes at RT in one tenth of cell culture volume of Freestyle 293 Expression Media. DNA-PEI mixture was added to cells which were returned to incubation. 4 hours following addition of DNA 2-propyl-pentanoic acid (VPA) was added at a final concentration of 3.5mM to boost protein expression. Cells were cultured for 6-7 days. Conditioned media containing expressed protein was harvested by centrifugation 3,100 xg for 20 minutes and filtered with a .22um filter to remove debris.

2.7. Protein production

2.7.1. Production of spike protein

The HexaPro Plasmid was obtained via Addgene from the lab of Jason McLellan, University of Austin. HexaPro spike protein was produced as described by Schaub et al[107]. A bacterial stab was used to grow further bacteria on ampicillin selection plates, colonies were selected from these plates and grown in overnight liquid cultures. Plasmid DNA was isolated from liquid cultures using the PureLink™ HiPure Plasmid Midiprep Kit (ThermoFisher, K210004) following manufacturer's instructions. Identity of purified plasmid was confirmed by sanger sequencing by Source Bioscience (**Appendix C.3**). Sequences were aligned using SnapGene. 1.2µg/10^6 cells of HexaPro expression plasmid in PEI was transfected into 30mL or 200mL cell culture. Unless otherwise stated cells were cultured for 6-7 days before harvest. Media was harvested by centrifugation. Protein was purified from media by gravity flow affinity chromatography using PD-10 columns packed with 1mL of Ni-NTA resin. Eluted protein was concentrated to a final volume of 500µL in size exclusion chromatography buffer (2mM Tris, 750mM NaCl, 3mM NaN_3, pH8.0) using Amicon® Ultra Centrifugal Filters, MWCO 50kDa. Protein was further purified by size exclusion chromatography through a Superose 6 Increase 10/300 GL column using an AKTA Pure (Cytiva) at a flow rate of 0.5mL/minute and 0.5mL fraction collection. Fractions corresponding to distinct peaks in the protein elution trace were pooled and protein was quantified by NanoDrop™ 2000 spectrophotometer (ThermoFisher). Protein size was confirmed by SDS PAGE. Protein was concentrated to ~1mg/mL and stored at -20°C until future use.

2.7.2. PCR of the pVITRO1 plasmid

Monoclonal IgG1 antibodies were produced using a method adapted from Dodev et al[108]. The regions of the pVITRO1 (Invivogen) containing the heavy and light constant regions were amplified in two separate polymerase chain reactions (PCR). Cycle conditions were optimised by test reactions using a temperature gradient 61-75°C and PCR reaction additives (**Appendix C.4-6**). Remaining template plasmid DNA was removed from PCR products by Dpn1 digestion. 50µL reaction mixes were incubated at 37°C for 1 hour with 20 units of Dpn1 enzyme (New England Biolabs) before enzyme inactivation at 80°C for

20 minutes. PCR products were then validated by gel electrophoresis on E-Gel™ 1% agarose with SYBR™ Safe gels (Invitrogen). Bands corresponding to the desired chain length were excised from the gel and the DNA was purified using the QIAquick Gel Extraction Kit (QIAGEN) following manufacturer's instructions. Multiple excised gel bands were combined during purification to increase the final concentration of eluted DNA.

2.7.3. Antibody variable gene fragments

Variable V(D)J fragments were identified from V(D)J sequencing data (**Appendix C.7-8**). The sequences from V(D)J sequencing were analysing using the NCBI IgBLAST tool which identified the beginning of the V and end of the J fragments. Sequences were trimmed and complementary ends of 30 base pairs overlapping the pVITRO1 fragments were added. These sequences were ordered as gene fragments from Azenta GENEWIZ.

2.7.4. Generation of monoclonal antibodies

Constant and variable fragments were assembled by 4 fragment Gibson assembly using the NEB Gibson Assembly Cloning Kit (E5510S) following manufacturer's instructions. 0.25 pmol of each fragment were combined with Gibson Assembly Master Mix and incubated at 50°C for 1 hour. Assembled plasmids were transformed into NEB 5-alpha Competent *E. coli* cells by heat shock and successfully transformed bacteria were isolated by growth on hygromycin selection plates. Transformed cells were grown overnight in low salt LB containing 500µg/mL hygromycin (Invitrogen). Plasmid was isolated from liquid overnight culture using the PureLink™ HiPure Plasmid Midiprep Kit (ThermoFisher, K210004) following manufacturer's instructions and were subsequently filtered using Corning™ Costar™ Spin-X™ Centrifuge Tube Filters. Successful assembly was confirmed by sanger sequencing, covering the insertion sites and variable regions, performed by Source Bioscience (**Appendix C.3**). 36µg of plasmid DNA was transfected into 30mL culture of Freestyle 293-F cells. Cells were cultured for seven days before conditioned media was harvested by centrifugation. Conditioned media was supplemented with an equal volume of Pierce™ Protein G IgG Binding Buffer

(ThermoFisher, 21011) and passed through polyprep columns packed with 0.5mL protein G resin. Columns were washed with an additional 30mL of binding buffer. The bound antibodies were eluted with 15mL of Pierce™ IgG Elution Buffer (ThermoFisher, 21004) into 1.5mL of Tris-HCl pH 8.0. Eluted protein was concentrated, and buffer exchanged into PBS pH 7.4 using Amicon Ultra 15 MWCO50kDa spin concentrators. Protein identity was confirmed by SDS-PAGE under reducing and non-reducing conditions, before storage in PBS at -20°C until future use. *Seven of the IgM "binder" antibodies were produced following these methods by Jacob Vincent as part of a supervised undergraduate and summer project*.

2.7.5. SDS PAGE and Coomassie staining for protein identification

SDS PAGE was used to separate proteins for identification by size. Protein samples were added to 4x NuPAGE™ LDS Sample Buffer (Invitrogen) and water, to a final concentration of 1X LDS. For samples run under reducing conditions 1µL of beta mercaptoethanol (BME) was added for each 40µL of protein LDS solution. Protein solutions were boiled at 72°C for 10 minutes. 30µL of sample was loaded into each well of NuPAGE™ 4 to 12%, Bis-Tris, 1.0mm, Mini Protein Gels (ThermoFisher, NP0322BOX). 5µL of Precision Plus Protein™ All Blue Prestained Protein (Bio-Rad) ladder was loaded onto at least one well of each gel. Gels were run at 200V for 42 minutes in an XCell SureLock™ Mini-Cell tank (Invitrogen) with 1X NuPAGE™ MOPS SDS Running Buffer (Invitrogen). Gels were then rinsed with water and extracted from the gel casing using a metal spatula, gels were trimmed at the top right-hand corner notched to ensure correct orientation and then washed thrice for 5 minutes each in water. Gels were then submerged in Bio-Safe™ Coomassie Stain (Bio-Rad) and incubated for a minimum of 1 hour at RT under agitation. Coomassie stain was removed, and gels were washed once in water by submersion and incubation for a minimum of half an hour at RT or overnight at 4°C under agitation. Stained gels were imaged using a LICOR Odyssey DLx.

2.8. Characterisation of antibodies

2.8.1. ELISA to detect human spike binding IgA, IgG, and IgM antibodies

Flatbottomed 96 well plates were coated with HexaPro S protein at 500ng/mL in coating buffer (12.8mM Na_2CO_3, 73.4mM $KHCO_3$, pH9.2) by incubation at 4°C overnight. Plates were emptied and blocked with blocking buffer (PBS, 1% (w/v) BSA) for a minimum of 30 minutes at RT. Human recombinant monoclonal anti-RBD antibody standards of the relevant isotype (Bethyl Laboratories) were included on all plates. Standards were two-fold serially diluted for the calculation of a standard curve. Test serum samples were diluted to specified dilutions in blocking buffer. All test samples and standards were plated at 50µL per well at a minimum in duplicate or >1 dilution. Plates were then incubated at RT for 2 hours. Goat anti-human IgG-HRP (Southern Biotech, 2040-05), goat anti-human IgM-HRP (Southern Biotech, 2020-05), or goat anti-human IgA-HRP (Southern Biotech, 2050-05) were applied 100µL per well at 1 in 4000 dilution and incubated at RT for 1 hour. Wells were washed six times with PBS 0.5% Tween then were developed for 20 minutes with 100µL per well TMB substrate before 100µL of stop solution (1M HCl) was added. Plates were read with a Varioskan LUX plate reader at 450nm and 655nm absorbance, background at 655nm was subtracted from the 450nm for analysis. Concentrations were interpolated from a sigmoidal, 4PL or asymmetric sigmoidal 5PL standard curve plotted using the absorbance values of the monoclonal standards. Dilutions with absorbance values within the linear portion of the curve were used for interpolation. Samples above of the range of the standard curve were assigned arbitrary concentration values for analysis (IgG - 30,000 ng/mL, IgM – 60 ng/mL).

2.8.2. Production of RBD probe for SAffCon assay

100µg of SARS-CoV-2 RBD protein (ACROBiosystems) was incubated with Alexa Fluor™ 647 NHS Ester (ThermoFisher) in labelling buffer (170mM $NaHCO_3$, pH 8.3) overnight at 4C. Following incubation the protein-dye solution was desalted into 100µL fractions by passage through a desalting column with PBS. Each fraction was tested for absorbance at 280nm and 650nm to quantify protein and dye concentration. Fractions were additionally tested by fluidity for hydrodynamic radius. Fractions with a dye to protein

concentration ratio 1-1.2 and R_h 3.2-3.6 were retained and those with high protein concentration but evidence of unbound dye underwent repeat desalting. Fractions containing labelled protein were pooled and concentration was quantified by NanoDrop™ 2000 spectrophotometer (ThermoFisher).

2.8.3. Fluidity One M SAffCon assay

The Fluidity One M Fluidity SeroAffinity and Concentration (SAffCon) Assay was used to determine serum antibody quantity and affinity following manufacturer's instructions. All dilution steps were completed in protein Lo-bind tubes to minimise loss of protein. Serum samples and RBD probe were diluted in ViscoMatch buffer (PBS pH7.4, 16% (w/w) glycerol) to the final combinations 0nM/50%, 10nM/50%, 10nM/10%, 10nM/2%, 10nM/0%, 100nM/50%, 100nM/10%, 100nM/2% of probe and serum concentrations respectively. These reaction mixtures were incubated at 4°C for 1 hour. Flow buffers of 2%, 10%, and 50% serum were prepared using ViscoMatch. Probe, serum mixes were loaded in triplicate at 4µL per well onto a chip. 4µL of the corresponding flow buffer was loaded into the adjacent well. Chips were inserted into the Fluidity One M and samples were measured using custom SAffCon Assay templates. Where required or recommended by the results of the initial analysis, additional concentration combinations of probe and serum were analysed in the same way to improve result accuracy. K_D, binding site concentration, R_h, free and R_h, complex measures were generated by the Fluidity One M, these files were uploaded to the Fluidity Intelligence Platform to generate concentration (µM) and affinity measures ($-\log_{10}K_D$/M).

2.8.4. ELISA for monoclonal antibody binding affinity

ELISAs to generate binding curves for monoclonal antibodies were completed in the same way as the ELISA for human spike binding IgG. Recombinant monoclonal antibodies were diluted in blocking buffer in a three-fold dilution series from 0.014ng/mL-2430ng/mL and plated at 50µL per well. Human recombinant monoclonal anti-RBD antibody standard was included at three-fold dilution between 0.41-810ng/mL on each

plate. Plates were read with a VICTOR Nivo Multimode Microplate Reader (PerkinElmer) at 450nm and 644nm. Absorbance at 644nm was subtracted from 450nm values and all plates were normalised to the absorbance of the standard at 10ngmL. Sigmoidal 4PL curves were used to calculate IC50 values.

2.9. Production of spike multimer for single cell sequencing

Biotinylated recombinant SARS-CoV-2 Spike protein (Miltenyi, 130-127-681) was incubated at RT for 15 minutes with TotalSeq™-C0951 Streptavidin-PE, AACCTTTGCCACTGC (Biolegend, 405261) or TotalSeq™-C0956 Streptavidin-APC, GGTAACTCTGGTAGC (Biolegend, 405283) in PBS 0.5% (v/w) BSA, 2mM EDTA. Following incubation protein was directly used for cell labelling. Nucleotide tagged multimers were produced immediately prior to use to reduce variation caused by degradation in storage.

2.10. Single cell RNA sequencing

2.10.1. Preparation of cells for single cell sequencing

PBMCs were enriched for B cells using a Pan B Cell Isolation Kit (Miltenyi 130-101-638), cells were incubated with a biotin antibody cocktail before incubation with anti-biotin microbeads and loaded onto a magnetic column. Flow through was collected. A portion of the flow through was set aside for flow cytometry to validate the B cell enrichment. The remaining cells were blocked with true stain Fc block (Biolegend, 422302) before being stained with oligonucleotide tagged antibodies against CD85j, CD11c, CD21, CD27, IL-6R (Biolegend, TotalSeq), and spike multimers for 30 minutes at 4°C. Cells were washed, counted and resuspended at 1000 cells/µL before library preparation.

2.10.2. Library preparation

Cells were processed according to the Chromium Next GEM Single Cell 5' Reagent Kit v2 (Dual Index) protocol (CG000330 RevF, 10X Genomics) and loaded onto Chromium Next GEM Chip K for 5’ Gene Expression (GEX), BCR V(D)J (BCR VDJ), and Cell Surface Protein/Immune Receptor Mapping (CSP) library construction, following the manufacturer's recommendations (10x Genomics). The library was quality controlled

and quantified, and samples were sequenced on an Illumina NextSeq2000. The CSP library consisted of 6 tags (CD85j, CD11c, CD21, CD27, IL-6R, Spike 1, and Spike 2. PCR enhancement was used to increase the relative abundance of the Spike 1 and Spike 2 tags from 0.6-2% to 80-95% to improve the resolution and reduce the sequencing rounds required for the identification of spike binding cells. *Sequencing libraries were prepared by Vitalina Chamberlain Evans*.

2.10.3. Processing and analysis of single cell RNA sequencing files

Cell Ranger v7.0.1 was used to process and analyse FASTQ files. CITE-seq[109] was used to determine the surface protein expression of CD85j, CD11c, CD27, and IL-6R. Sequences were aligned to the GRCh38 genome provided by Cell Ranger. Cite-seq pipeline v.1.5.0 was used for the quantification of nucleotide tags. Data was quality controlled. The Seurat package in R was used to normalise gene expression, integration, and batch effect correction. BCR and TCR genes were removed prior to principal component analysis and unsupervised clustering to obtain more biologically meaningful clusters[110]. Non-B cell clusters were removed, and cells were re-clustered and B cell subsets assigned based on differential gene expression. In total, 230,596 B cells were identified. BCR constant regions were identified by the Dandelion pipeline and used to assign cell isotype. Dandelion was used to align BCR sequences against the IGMT database and then the SHAZAM package used to calculate the mutational count of the BCR of each cell. 1075 cells with a normalised read count for each of spike 1 and spike 2 tags >1.2 were classified as spike binding cells. SPACE was used for the prediction of epitope binding. *Processing and bioinformatic analysis of single cell sequencing data was completed by Dr Zhaleh Hossieni*.

2.11. Mouse studies

All mouse studies were licensed by the UK Home Office according to the Animals Scientific Procedures Act 1986 (License PP6047951) and approved and conducted in compliance with protocols by the University of Cambridge, University Biomedical Services Animal Welfare and Ethical Review Bodies committee. *Unless otherwise stated*

all study set up and procedures conducted on mice were completed by Dr Maria Rust, Dr Sarah Spencer, Dr Joanna Salmon, Robert Hughes or Dr Juan Carlos Jam Puc. Once mice were culled, I aided in tissue processing and subsequent assays.

2.11.1. Preparation of BNT162b2 vaccine

To make up the BNT162b2 vaccine, COMIRNATY (BioNTech Manufacturing GmbH) lyophilised vaccine was reconstituted in 675µL of 0.9% sterile sodium chloride. 50µL of this solution was used as a single dose of BNT162b2 and 25µL as a half dose.

2.11.2. Multiple immunisations with BNT162b2 or PBS

WT (C57BL/6) mice received three doses of BNT162b2 or 50µL sterile PBS via intramuscular (IM) immunisations at regular intervals. Tissue was harvested 21 days following final immunisation.

2.11.3. Humoral response in *Il6ra* knockout mice

Two studies were completed to assess the response to vaccination in homozygous knockout mice. Matched groups of WT (C57BL/6) and *Il6ra* knockout mice were used in each study. Mice were vaccinated IM with (1) a single dose of BNT162b2 into a single hind limb or (2) with two half doses into each hind limb followed by repeat doses 35 days later. A subset of mice from each study were terminated at day 21 following vaccination and spleen and cardiac blood were harvested. The remaining mice underwent saphenous bleeds at regular intervals before termination at days V1D114 and V2D103 respectively and spleen and cardiac blood collection.

2.11.4. Humoral response in mice with diet induced obesity

Mice were fed standard chow or high fat diets for 180 days and their mass monitored before the initiation of the study. Mice were vaccinated IM with BNT162b2, and saphenous bleeds were collected at days 21, 54, and 72 after vaccination. Standard or high fat diets were maintained for the duration of the study. Spleens were harvested, and

blood was collected via cardiac puncture at day 105. *The study of mice on high fat and standard chow diets was performed by the group of Professor Katharina Timper at the University of Basel. Serum and spleens were processed following a protocol provided by the Thaventhiran Lab before being frozen and shipped to the UK.*

2.11.5. mRNA construct immunisation

WT (C57BL/6) mice and *Il6ra* knockout mice were vaccinated intravenously (IV) with a single dose of BNT162b2 and a dose of encapsulated mRNA construct encoding sIL-6R, IL-6-IL-6R fusion protein, IL-6R, or an empty LNP. Spleen and cardiac blood were collected at day 21 after immunisation. Mice were subsequently excluded from analysis based on age.

2.11.6. Mouse splenocyte processing

Spleens were homogenised by the flat end of a syringe plunger, then filtered through 70µm filters and supplemented with PBS 1% (v/v) FBS, 2mM EDTA. Cells were pelleted by centrifugation at 400xg for 5 mins at 4°C. Red blood cells were lysed by resuspension of cells in 1mL of red blood cell lysis buffer and incubation at RT for 5 minutes before passage through a 40µm filter and dilution with PBS 1% (v/v) FBS, 2mM EDTA. Cells were pelleted again and resuspended in FBS, before the dropwise addition of an equal volume of freezing media (RPMI, 20% (v/v) DMSO, 40% (v/v) FBS). Cells were frozen in 1mL aliquots in Mr Frosty Freezing containers at -80°C before transfer to liquid nitrogen storage until further use.

2.11.7. Mouse bone marrow processing

Muscle and connective tissue was removed from the leg bones and the ends of the bones cut off. Bones were centrifuged at 10,000xg for 15 seconds in a microcentrifuge tube with a small hole within a tube with PBS 1% (v/v) FBS, 2mM EDTA. Red blood cells were lysed by resuspension of cells in 1mL of red blood cell lysis buffer and incubation at RT for 5 minutes before passage through a 40µm filter. Cells were washed and frozen in freezing media in 1mL aliquots in Mr Frosty Freezing containers at -80°C before transfer to liquid

nitrogen storage until further use. *All bone marrow isolation was completed by Dr Maria Rust, Dr Joanna Salmon, and Dr Juan Carlos Jam Puc.*

2.11.8. Mouse lymph node processing

Lymph nodes were ruptured by tearing with two needles. They were homogenised by the flat end of a syringe plunger, then filtered through 70µm filters and supplemented with PBS 1% (v/v) FBS, 2mM EDTA. Cells were pelleted by centrifugation at 400xg for 5 mins at 4°C. Cells were resuspended in PBS 1% (v/v) FBS, 2mM EDTA and passed through a 40µm filter. Cells were pelleted again and resuspended in FBS, before the dropwise addition of an equal volume of freezing media (RPMI, 20% (v/v) DMSO, 40% (v/v) FBS). Cells were frozen in 1mL aliquots in Mr Frosty Freezing containers at -80°C before transfer to liquid nitrogen storage until further use.

2.11.9. Mouse serum processing

Serum collection tubes were allowed to clot for a minimum of 30 minutes at RT before centrifugation at 10,000xg, 5 minutes, RT. Serum was aliquoted and frozen at -80°C until further use.

2.12. Immunophenotyping of mouse samples

2.12.1. ELISA for murine spike binding IgG

Flatbottomed 96 well plates were coated with HexaPro S protein at 500ng/mL in coating buffer (12.8mM Na_2CO_3, 73.4mM $KHCO_3$, pH 9.2) and incubated at 4°C overnight. Plates were blocked at RT for a minimum of 30 minutes with PBS, 1% (v/w) BSA blocking buffer. Serum samples were diluted 500-4500x in blocking buffer and then 50µL was plated per well in duplicates or more. An anti-S1 mouse IgG standard was twofold serially diluted 0.244 – 250ng/mL and included on every plate as a positive control. Negative control wells were blocking buffer without antibody or serum. Plates were incubated at RT for 2 hours. Following incubation plates were washed with PBS 0.05% (v/v) Tween a minimum of five times and blotted dry. Goat – anti mouse IgG HRP antibody was diluted 1 in 15,000 in blocking buffer and 50µL applied to each well. Plates were incubated for 1 hour at RT

before the washing step was repeated. 100µL per well of TMB substrate solution was added and allowed to react in the dark at RT for 10 minutes. The reaction was stopped by the addition of 100µL per well of 1M HCl. Plates were read with a Varioskan LUX plate reader at 450nm and 655nm absorbance, background at 655nm was subtracted from the 450nm for analysis.

2.12.2. FluoroSpot for antibody secretion

ASCs were quantified from murine bone marrow and spleen samples using the FluoroSpot Flex: Mouse IgM/IgG/IgA kit (Mabtech, FS-60G49R50M-1) following manufacturer's instructions. All steps prior to cell incubation were performed under sterile conditions in a cat 2 tissue culture facility. Plates were pre-wetted with 35% ethanol for 1 minute before washing 5 times with water. Wells were coated with either Anti-Ig κ λ mAbs (MT24/JC5-1) at 40µg/mL or HexaPro S protein at a variety of concentrations. Plates were incubated overnight at 4°C. Cryopreserved cells were thawed and then rested for a minimum of 1 hour at 37°C. Excess antibody and antigen was removed from the coated plate and wells were washed 5 times with PBS. Plates were blocked with 200µL/well of RPMI, 10% (v/v) FBS for a minimum of 30 minutes at RT. Cells were counted and resuspended to an appropriate concentration ($1x10^6$ – $1x10^7$ cells per mL) in RPMI, 10% (v/v) FBS before plating 100µL per well. Where only one dilution of cells was tested samples were plated in triplicate. Plates were incubated for 14-16 hours at 37°C. Cells were removed, and the plate was washed 5 times with PBS. Anti-IgM mAb (MT9A2), anti-IgG mAbs (MG1/MG2a/MTG2c/MG2b/MG3), anti-IgA mAb (MT39A) detection antibodies were diluted 1:500 in PBS and incubated at 100µL per well for 2 hours at RT. Plates were then washed 5 times with PBS and FluoroSpot enhancer added and incubated for 15 minutes at RT. Wash step was once again repeated before removal of the plate underdrain. Plates were allowed to dry for a minimum of 24 hours at RT in the dark before reading. Plates were read on an AID iSpot Spectrum ELISpot reader (software version 7.0, Autoimmune Diagnostika GmbH, Germany) with LED490, LED550 and LED640 filters. Spots were counted with default settings (Emphasis – tiny, Algorithm – C, minimum intensity - 3, minimum size – 12 (IgM)/17 (IgG)/15 (IgA), minimum gradient

0(IgM)/1(IgG)/0(IgA)) and data were analysed using Prism 10 for macIOS Version 10.1.0 (264).

2.12.3. IL-6 ELISA

IL-6 levels were quantified in the day 105 serum of mice using the Mouse IL-6 Uncoated ELISA Kit (Thermo Fisher, 88-7064) as per the manufacturer's instructions. 96 well plates were coated with anti-mouse IL-6 antibody overnight at 4°C. Wells were washed with wash buffer 3 times before plates were blocked for a minimum of 1 hour at RT. Wells were washed again, and serum was plated undiluted and at a 1 in 3 dilution alongside a twofold serial dilution (3.906-500 pg/mL) of recombinant mouse IL-6 standard, diluted in ELISA diluent. Plates were incubated at RT for two hours then washed again. Biotin conjugated anti mouse IL-6 antibody was added to the plate and incubated at RT for 1 hour. Wash steps were repeated. Plates were incubated with avidin-HRP for 30 minutes at RT. Following a final wash, plates were incubated at RT for 15 minutes with TMB solution. TMB HRP reaction was stopped with stop solution and plate absorbances were read at 450 and 570nm using a Varioskan Lux plate reader. For analysis a 5PL standard curve was plotted and concentrations were interpolated using Graph Pad Prism (v10.2.3 (347)).

2.13. mRNA constructs

2.13.1. Production of mRNA IL-6R constructs

Codon optimised constructs encoding the full-length IL-6R, sIL-6R, and a hyper IL-6R-IL-6 fusion protein were produced via *in vitro* transcription using the HiScribe® T7 mRNA Kit with CleanCap® (New England Biolabs, catalog no. E2040S) from DNA fragments. Uridine was replaced by N1-methylpseudouridine and polyadenylated tails were added. LNP complexes were formed by combining aqueous mRNA and lipid using Nanoassemblr Ignite cartridges. *mRNA constructs were designed and produced by Edward Simmons-Rosello.*

2.13.2. Western blot validation of construct expression

Encapsulated IL-6R constructs were transfected into human HEK 293T cells. Cells were cultured for 24 hours to allow protein expression before conditioned media was harvested. Splenocytes from IL-6R knockout mice, were cultured with conditioned media in the presence and absence of IL-6 (20µg/mL) for 30 minutes at 37°C. Following stimulation, cells were lysed with a lysis buffer containing LDS-NuPAGE and protease inhibitor. Lysates were nuclease treated with Pierce nuclease in 0.2M MgCl to remove nucleic acid then denatured for 10 minutes at 70°C. Lysates were run on SDS-PAGE using 4-12% Bis-Tris protein gels and MOPS buffer to separate proteins. Proteins were dry blotted with the iBlot2 onto nitrocellulose (NC) membranes. Membranes were blocked by incubation in Intercept TBS blocking buffer for 1 hour at RT under agitation. Following blocking membranes were incubated for 2 hours at RT with mouse-anti-STAT3 and rabbit-anti-phospho-STAT3 primary antibodies. Membranes were washed 3 times with PBS-Tween before incubation for 1 hour with goat anti-mouse IgG IRDye 800CW and donkey anti-rabbit IgG IRDye 680CW. Membranes were then washed 3 times with PBS-Tween and once with PBS. Membranes were imaged using the LI-COR Odyssey CLx and images were analysed using Image Studio™ software. STAT3 phosphorylation was analysed as pSTAT3 band intensity/STAT3 quantification band intensity. *This assay was conducted with the assistance of Dr Joanna Salmon and Edward Simmons Rosello.*

2.14. Analysis and statistics

Flow cytometry: All FCS files from flow cytometry experiments were analysed using FlowJo v10.7.2 (BD). Values were expressed as proportion sub population of total population or median fluorescence intensity of a labelled population.

ELISpot and FluoroSpot: Plates were read using an AID iSpot Spectrum ELISpot reader (software version 7.0, Autoimmune Diagnostika GmbH, Germany) with LED490, LED550 and LED640 filters. SFUs were auto counted using defined count settings. Background values from control unstimulated wells were subtracted from each test well and values were expressed as ΔSFU per well or per million cells.

ELISA: The absorbance of ELISA plates was read using a Varioskan Lux plate reader (Thermo Scientific) or VICTOR Nivo Multimode Microplate Reader (PerkinElmer) at 450nm and one of 655nm, 644nm, and 570nm. Background reading at the non-450nm wavelength was subtracted from the 450nm absorbance. For values reported as absorbance: absorbance of a control well of blocking buffer was subtracted before reporting. For interpolated concentrations: a 4PL or 5PL standard curve was plotted and concentrations were interpolated using Graph Pad Prism (v10.2.3 (347)). IC50 values were also calculated from 4PL curve using Graph Pad Prism (v10.2.3 (347)).

SAFFCon: Assays were analysed using Fluidity Intelligence SOFTWARE VERSION 2.3.0.

Graphs and figures: Plots were generated using Graph Pad Prism (v10.2.3 (347)) or RStudio (v2023.09.0+463). Figures were generated using Microsoft PowerPoint for Mac Version 16.88.1or Biorender.com.

Genetics: SnapGene v7.2.1. was used for the alignment of gene sequences and simulation of Gibson assemblies

3. Antigen specific T cells and the response to vaccination in individuals with immune dysregulation

In this chapter, I report the results of a study of vaccination in individuals with immune dysregulation. This study was coordinated by members of the Thaventhiran lab and conducted with the help of research and clinical collaborators. Full details of results (with some cohort differences) and collaborators of this study can be found in the published paper[106] for which I am a co-first author. I was responsible for sample processing and T cell assays in this study and contributed to the completion of flow cytometric assays alongside other lab members. Other data was generated by the analysis of samples by collaborators as detailed in the preface and methods of this thesis.

3.1. Introduction: dysregulation of the immune system

Immune dysregulation occurs when an aspect of the immune system is perturbed, leading to a breakdown in the normal functioning and regulation of immune responses. This can be caused by a number of genetic or environmental factors including, but not limited to, malnutrition, obesity, the gut microbiome, immunomodulatory drugs, and infectious disease[111-113]. Immune deficiencies represent an extreme of immune dysregulation and occur when a component of the immune system is absent or functions improperly. Primary immune deficiencies (PID) are caused by IEIs, genetic disorders impacting the genes encoding for components of the immune system[114]. Due to the network like nature of the immune system, PIDs typically have systemic immune effects not limited to the genetically altered component. Individuals with PID are at risk from infectious disease as their immune systems are not at full capacity to protect them. Immune dysregulation may lead to unexpected responses to vaccination due to atypical functioning of the immune system. It is important to understand how these individuals are protected by vaccination as they are typically at higher risk from disease than those without dysregulation. Terminology surrounding these subjects is inconsistently applied. In this thesis, I use immune dysregulation to refer to any condition in which an intrinsic or extrinsic factor has caused any level of abnormal immune functioning. This chapter therefore considers mRNA vaccination in individuals with a range of immune dysregulation caused by PID and ICB therapies.

3.1.1. Primary immune deficiencies

PIDs are characterised by recurrent infections and other symptoms related to the specific IEI. There are over 400 identified IEIs[115], which are organised into ten categories based on their phenotypes, the two categories considered for this work are: predominantly antibody deficiencies (PAD), and diseases of immune dysregulation[116]. NF-κB1 and NF-κB2 deficiencies both fall under the category of PAD. These are caused by genetic defects in the *NFKB1* and *NFKB2* genes which encode for proteins important for the regulation of the nuclear factor kappa-light-chain-enhancer of activated B cells (NF-κB) signalling cascade[117,118]. NF-κB is a transcription factor heavily involved in the regulation of innate and adaptive immune responses and pro-inflammatory signalling[119]. NF-κB1 and NF-κB2 deficiencies typically lead to reduced IgG, IgA, and IgM, and low B cell numbers and are characterised by recurrent sinopulmonary infections[116]. Loss of function in *NFKB1* is believed to be the most common cause of common variable immunodeficiency (CVID) in the European population[120], a condition associated with abnormal $CD8^+$ T cell function[121].

Diseases of immune dysregulation include cytotoxic T-lymphocyte associated protein 4 (CTLA-4) haploinsufficiency and Lipopolysaccharide responsive beige-like anchor protein (LRBA) deficiency. CTLA-4 is a co-receptor expressed on activated T-cells and when stimulated, reduces effector T cell activity, while enhancing Tregs[122]. CTLA-4 haploinsufficiency is caused by a genetic defect in *CTLA4*. LRBA deficiency is caused by homozygous mutations in the *LRBA* gene, which is believed to be involved in the regulation of CTLA-4[123]. Both conditions lead to reduced circulating levels of B and T cells and dysfunction[116].

CTLA4, *LRBA*, *NFKB1*, and *NFKB2* are all clinically important in CVID[124]. Despite differential categorisation as PAD and diseases of immune dysregulation the associated deficiencies of these genes all lead to dysfunction of the humoral immune response as seen by reduced B cell numbers. Additionally, all four conditions are associated with expansion of $CD21^{low}$ B cells [120,125-128], which has been linked to aberrant B cell responses. PIDs offer unique opportunities to study the complexity of the immune system. The loss of singular specific immune components by deficiency enables the isolation of their role within the human immune system.

3.1.2. Iatrogenic secondary immune dysregulation

Immunomodulatory drugs are used to treat many different conditions and have the potential to interact with the effects of the illness being treated[129-131]. ICB is a form of immunotherapy typically used to treat cancer. ICB targets key immunomodulatory molecules such as programmed cell death protein 1 (PD1) and CTLA-4. These molecules regulate immune cell function and blockade aims to combat T cell exhaustion and increase T cell activation against cancer cells[132,133] (**Figure 3.1**). The action of ICB therapies is not inherently immunosuppressive, however, these therapies can indiscriminately activate any T cell. ICB treatment therefore, can lead to immune related adverse events[132]. Despite success in killing cancer cells, over activation of T cells can lead to imbalances in the network of the immune response and therefore, immune dysregulation.

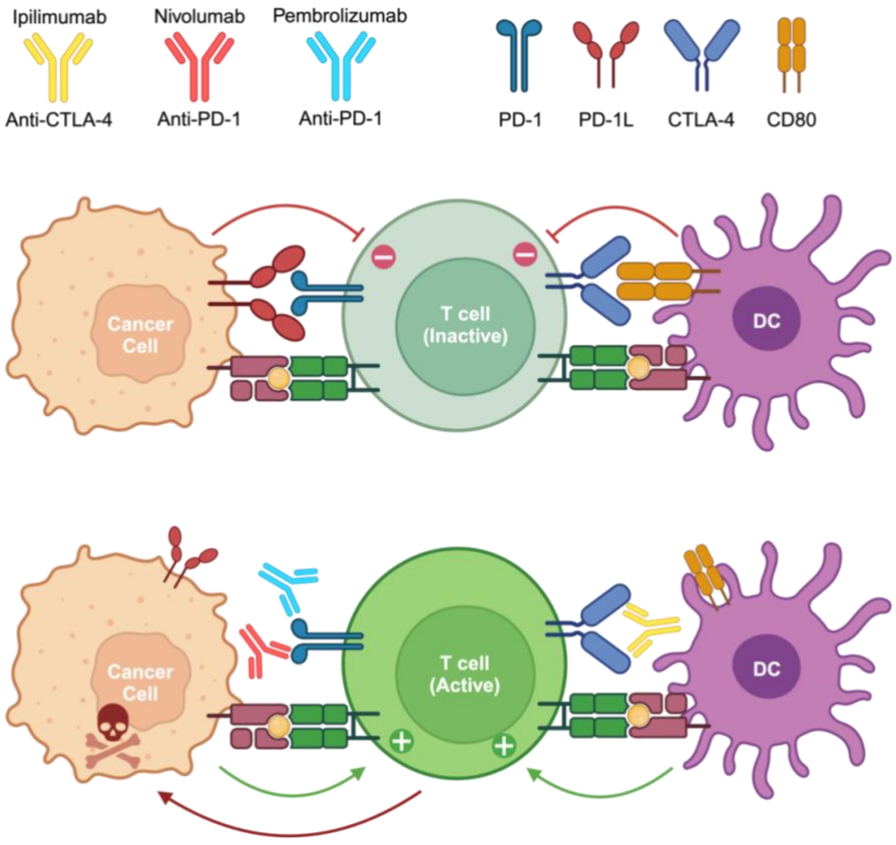

Figure 3.1. Anti-PD-1 and anti-CTLA-4 immune checkpoint blockade. A) Non-exhaustive, representative diagram of the basic function of ICB therapies. Ipilimumab is an antibody therapy which targets CTLA-4 and Nivolumab and Pembrolizumab target PD-1. In the absence of ICB therapies, tumour specific T cells can become exhausted by the receipt of inhibitory signals from tumour and other APCs through PD-1 and CTLA-4 signalling. Monoclonal antibody ICB therapeutics bind to the PD-1 or CTLA-4 receptors and prevent the

transmission of these inhibitory signals. Specific T cells can then be activated, and cytotoxic T cells kill tumour cells. Created using Biorender.com.

3.1.3. The importance of antigen specific T cells

Thereby, PIDs and ICB therapies can dysregulate T cell function. Antigen specific T cells are critical in the production of long-lived, broad protection against infection by SARS-CoV-2 and severe COVID-19 disease[134,135]. The quantification and classification of antigen specific T cells gives an indication of the extent and quality of the response to vaccination. In addition, this data gives a suggestion of the level of protection provided by immunisation[136]. There are a number of different assays which can be used to identify antigen specific T cell responses. These vary in complexity, throughput, and level of quantitation, factors which must be assessed to determine suitability for any given application. The adaptation of an assay to assess the T cell responses of individuals with PID and on ICB following vaccination would enable the determination of whether these individuals have T cell mediated protection from infection.

Assays to stimulate antigen specific T cells can be conducted on pure populations of T cells or PBMCs. PBMC samples are preferable as in addition to requiring fewer processing steps, they contain APCs. These cells can present antigen to T cells on matched MHC molecules and produce the co-stimulatory molecules required for T cell activation. This removes the need for HLA typing and the addition of costimulatory cells or molecules to culture media[137], which can be time consuming and costly due to the diversity to HLA types[138]. Accordingly, a high-throughput assay to detect human PBMC responses to SARS-CoV-2 peptides is required.

3.1.4. The risk of COVID-19 in individuals with immune dysregulation

Immune dysregulation can vary broadly in its extent, reports of its impact on the response to SARS-CoV-2 infection are heterogenous. Some individuals with IEI do not appear to have increased fatality rate from SARS-CoV-2 infection and may have lower infection incidence rate due to improved education on disease avoidance[139]. However, in multiple cases individuals with PID have been seen to be at increased risk of mortality from COVID-19[140,141]. Impaired antibody production and cell mediated immunity has been

associated with chronic infection, and prolonged viral shedding following COVID-19[142-144]. Chronic infection poses a risk to the general population in addition to the infected individual as it provides an environment for viral evolution[145].

Cancer patients are at an increased risk of severe COVID-19[146]. Receipt of ICB therapy in many cases has not appeared to impact severity of, and survival from, SARS-CoV-2 infection[147-149]. However, ICB therapies have also been seen to have an impact on diease[150]. Nevertheless, ICB treatments have mostly been continued through the pandemic. ICB has the potential to improve response to COVID-19 by non-specific boosting of the effector T cell response, however it may also increase risk of cytokine release syndrome due to increased levels of inflammation[151,152]. The efficacy of vaccination must be assessed in both groups to reduce the risks of severe outcomes and viral evolution posed by infection with SARS-CoV-2. Additionally, observations of how PID and ICB impact the response will improve understanding of how the virus and vaccine act to produce immune memory.

3.1.5. Chapter aims

Individuals with PID and cancer on ICB therapies have immune dysregulation and are at high risk from COVID-19. The protection afforded to these individuals by the COVID-19 mRNA vaccines is therefore of particular importance. T cell responses are significant for the formation of long-term immune protection against SARS-CoV-2 and both individuals with PID and on ICB have potential for T cell dysregulation. The extent of immune dysregulation in these groups is varied and subsequently a uniform response to vaccination would not be expected.

In this chapter I therefore aim to address:

- Which assays are appropriate for the rapid assessment of antigen specific T cells in human PBMC samples?
- How well do individuals with immune dysregulation due to PID and ICB treatment respond to mRNA SARS-CoV-2 vaccination?
- Which factors can predict the magnitude of response to vaccination in individuals with immune dysregulation?

3.2. Results

3.2.1. Methods to test for antigen specific T cell response

3.2.1.1. *In vitro* stimulation and flow cytometry-based assays

There are a number of flow cytometry-based assays which can be used to characterise the specific T cell response. I tested two assays to determine the feasibility of applying them to a longitudinal study of antigen specific T cell responses. Dye based proliferation assays can be used to assess the clonal expansion of T cells, triggered by exposure to a specific antigen[153]. In dye-based assays a fluorescent dye such as carboxyfluorescein succinimidyl ester (CFSE) or CTV is incorporated into the cell cytoplasm and fixed such that it is unable to leave the cell[154]. Cells are then co-incubated with an antigen and specific cells are stimulated to divide, when they do so the dye splits evenly between the two daughter cells. This enables the number of replication cycles to be tracked and activated (replicated) cells to be identified by the dilution of the fluorescence which can be detected by flow cytometry.

To determine an appropriate concentration of CTV to use, I stained cells from two healthy donors with increasing concentrations of CTV before overnight stimulation with PHA, a polyclonal T cell stimulant. I then assessed the CTV fluorescence of these cells by flowcytometry (**Figure 3.2A**). Distinct peaks could be seen in cells stained with a final concentration of 2.5μM and 5μM, but not 10μM due to the high fluorescence intensity of the undivided cells. CTV itself can be toxic to cells and lead to cell death, as such I assessed the viability of these cells. I saw a slight reduction of cell viability in unstimulated cells stained with increasing concentrations of CTV, however I did not see this same pattern in stimulated cells. Stimulation itself led to a larger decline in viability than CTV staining (**Figure 3.2B**). The cytokines IL-2 and IL-7 are known to stimulate the growth of T cells and can be added to culture media to co-stimulate cells and improve survival. I tested impact of the addition of IL-2 and IL-7 to culture media of cells stimulated with PHA was able to detect more distinct peaks of CTV fluorescence (**Figure 3.2C**). Better distinction of peaks enables more accurate determination of the number of divisions undertaken. Despite the strength of PHA stimulation, stimulated cells did not differentiate to the point that CTV levels were undetectable and fluorescence

comparable to unstained controls, therefore the incubation time and CTV concentration was suitable to detect all waves of differentiation. This CTV proliferation assay could, therefore, be applied to detect the activation and proliferation of T cells.

Having established a protocol for a dye-based proliferation assay, I was next interested in assays which could be used to directly assess activation markers on antigen specific T cells. AIM assay uses fluorescent staining of T cell markers and activation markers such as: OX40, CD137, and CD69 to detect activated T cells following PBMC stimulation with peptide pools covering a specific antigen[155,156]. This allows the identification of different T cell subsets and activation, by flow cytometry. I tested the background cross reactive SARS-CoV-2 T cells in the PBMCs of three SARS-CoV-2 naïve individuals in addition to reactivity to CD3 stimulation. A range of surface activation markers can be used in this assay. For this test activated $CD4^+$ T cells were identified as $OX40^+CD137^+$ and activated $CD8^+$ T cells as $CD69^+CD137^+$ (**Figure 3.2D**) (**Appendix A.2**). These markers were chosen to allow comparison to a published study in which this assay was previously applied to detect SARS-CoV-2 specific cells[156]. Unstimulated cells were used to determine the baseline expression of activation markers for each participant. In all three participants CD3 stimulation led to significant levels of activation in both $CD4^+$ and $CD8^+$ T cells. All participants had evidence of $CD4^+$ T cell activation above baseline against the M, N, and S SARS-CoV-2 peptide pools, however this was not consistently seen in $CD8^+$ T cells. (**Figure 3.2E**). These results agreed with other studies which show the cross reactivity of $CD4^+$ T cells against seasonal coronaviruses with SARS-CoV-2[157] and similar proportions of activated cells upon application of this assay to cells from unexposed individuals[156].

With improved optimisation either of these assays would be suitable for the detection of vaccine specific T cells in human PBMC samples. However, both require high numbers of cells, long incubation times, and lengthy manual analysis.

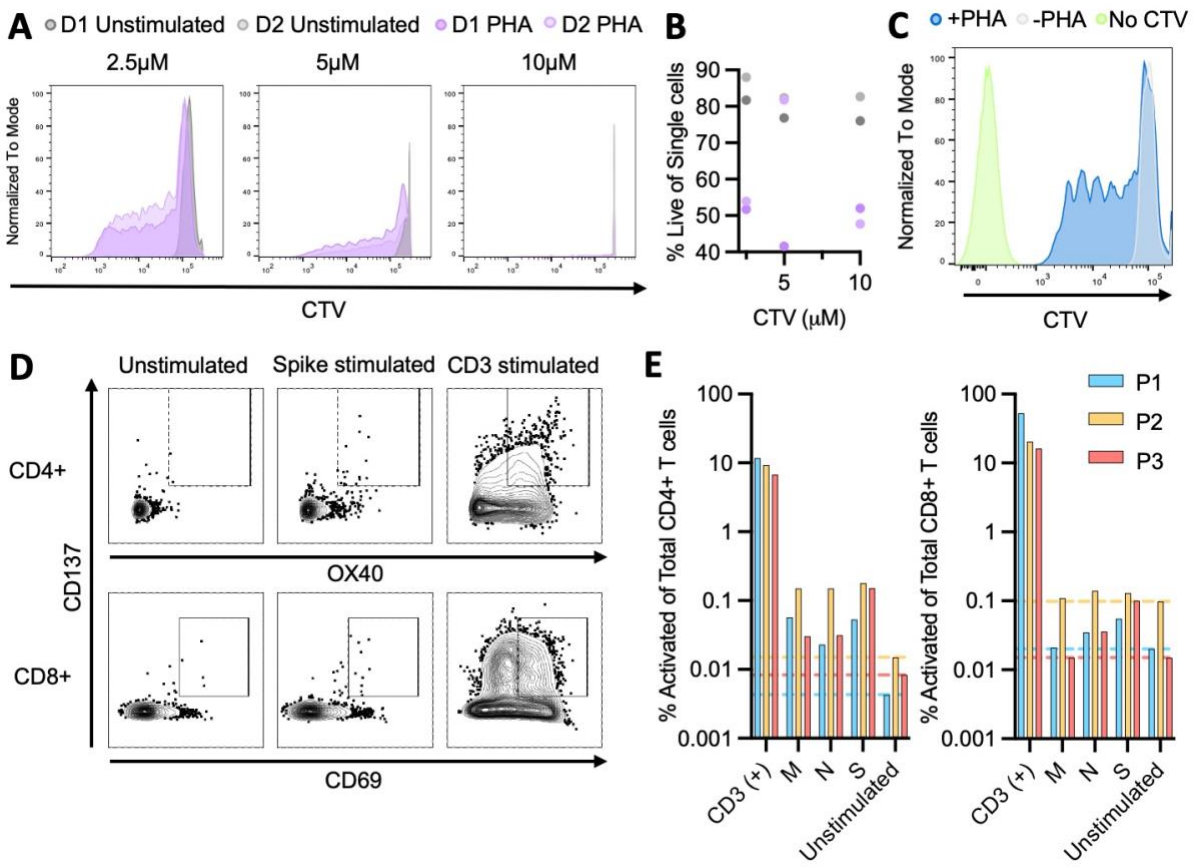

Figure 3.2. Flow cytometry assays for the detection of T cell activation and differentiation. **A)** CTV fluorescence of T cells from two donors stained with 2.5, 5, or 10μM of CTV then rested overnight (grey) or stimulated with PHA (purple). **B)** Comparison of % Live of total single cell lymphocytes following PBMC staining with increasing concentrations of CTV and rest (grey) or stimulation with PHA (purple). **C)** CTV fluorescence of T cells stimulated in the presence of IL-2 and IL-7 (dark blue) relative to unstimulated cells (grey) and unstained T cells (green). **D)** Representative plots of activated $CD4^+$ ($CD137^+OX40^+$) and $CD8^+$ ($CD137^+CD69^+$) T cells from PBMCs unstimulated or stimulated with S peptides or anti-CD3. **E)** Activation of the $CD4^+$ (left) and $CD8^+$ (right) T cells from three individuals (P1, blue. P2, orange. P3, red) following stimulation with anti-CD3, M, N, or S peptides or no stimulation. Dotted lines indicate baseline activation for each participant as measured from unstimulated samples.

3.2.1.2. *In vitro* stimulation and plate-based assays - ELISpot

ELISpot assays are plate based and measure the secretion of protein, typically cytokine or antibody, by stimulated cells[158]. To assay for specific T cells, PBMCs are incubated with antigen in a plate coated with capture antibodies for a specific cytokine marker of activation. Upon activation by antigen, cells release cytokine which is captured by these antibodies. Cells are then washed off and the captured cytokine is marked with a secondary cytokine specific detection antibody. The secondary antibody is conjugated with an enzyme and the addition of substrate leads to a reaction which forms an insoluble

precipitate. This precipitate forms spots on the membrane of the plate which indicate the prior location of a cytokine secreting cell, these spots can be counted by an ELISpot plate reader or under a microscope to quantify the activated cells. The most common cytokine used to quantify antigen specific T cells is IFN-γ which is typically released by activated $CD8^+$ T cells, however other cytokines such as IL-2 and TNF can be used[159]. The 96 well format of an ELISpot allows the measure of activity against a number of different antigens without the requirement for a high number of cells. The FluoroSpot assay follows a similar method to the ELISpot, however, it is able to detect multiple different target proteins[160]. Multiple capture antibodies and secondary antibodies conjugated to different fluorophores are used at once. Spots can be counted in the same way as in an ELISpot, the fluorophore colour indicates which of the cytokines was released by the cell in that position, as such the cells releasing one or multiple cytokines following antigen stimulation can be quantified. This assay allows IFN-γ and IL-2 to be detected in combination, providing some differentiation between activated $CD8^+$ and $CD4^+$ T cells.

I conducted a comparison of an IFN-γ ELISpot assay and an IFN-γ + IL-2 FluoroSpot using four PBMC samples from vaccinated individuals (one unknown vaccine status), five SARS-CoV-2 peptide pools, and ConA (an antigen independent T cell mitogen). With the help of lab members two ELISpots and two FluoroSpots were conducted simultaneously using the same samples and peptides to compare sensitivity and consistency between the assays. The enzymatic ELISpot was more sensitive to the release of IFN-γ than the FluoroSpot (**Figure 3.3A&B**), forming more detectable spots. However, the background in the negative control wells was also increased in this assay. Variability of replicate wells within and between plates was higher for the FluoroSpot assay and levels of detectable IL-2 spots were low. The plates contained cells from three donors with high background and a moderate response to SARS-CoV-2 peptides, and one donor with a poor response and low background. The ELISpot was best able to differentiate between these individuals (**Fig 3.3C**), despite background. I therefore selected the ELISpot assay for further experiments.

Subsequently, I conducted an optimisation of the count settings used by the plate reader to minimise the impact of the high background seen on the ELISpot plates. There are a number of spot parameters which can be set on the AID iSpot Spectrum ELISpot reader;

Intensity, Size (the diameter and area of a spot), Grade, and Emphasis. These settings can be adjusted to allow the reader to distinguish between true spots, caused by cytokine release from an activated cell, and artefacts. I assessed five different configurations (**Table 3.1**) using a test plate containing cells from six different donors, after a third dose of vaccine against SARS-CoV-2, stimulated with an S1 peptide pool and media containing DMSO. Control wells can contain positive spots due to the unstimulated release of IFN-γ by some T cells, these spots can be more numerous when the PBMCs have been taken from an individual soon after an immune reaction. Wells can also contain small spots from the transient release of IFN-γ by a cell or due to dust or other contaminants. True spots are typically larger and more rounded than background or artifacts but can be difficult to differentiate. Settings 3, 4, and 5 seemed to best exclude smaller spots, which visually appeared to be artifacts, from the count (**Fig 3.3D**). Settings 3 and 4 enabled the best distinction in SFU per well between S1 and media stimulated cells without missing positive spots in the S1 wells (**Fig 3.3E**).

The PITCH study is a collaboration between a number of universities aiming to assess the strength of the T cell response against SARS-CoV-2 after different vaccination and infection schedules. All sites in this collaboration have their own local cohorts and complete their own ELISpots, as such the assay is cross validated across sites[161]. To standardise my plate readings to those in the PITCH consortium I exchanged assay plates with the Turtle Lab, University of Liverpool. In total four plates used to assay the response of 19 vaccinated controls to SARS-CoV-2 peptides were read at both sites, using standard count setting in Liverpool and five test settings in Cambridge. The count values obtained using settings 4 and 5 were closest to those read in Liverpool (**Figure 3.3F**). However, setting 5 excluded spots which visually appeared to be true positives and setting 4 was most similar to the settings used on the Liverpool machine. Therefore, setting 4 was selected for all future use.

Table 3.1. Plate reader settings for the counting of spots on IFN-γ ELISPOT plates

Test Setting Number	Emphasis	Minimum Intensity	Minimum Size	Minimum Grade
1	Small	30	70	1
2	Small	12	22	4
3	Small	60	70	1
4	Big	60	80	1
5	Big	85	95	1

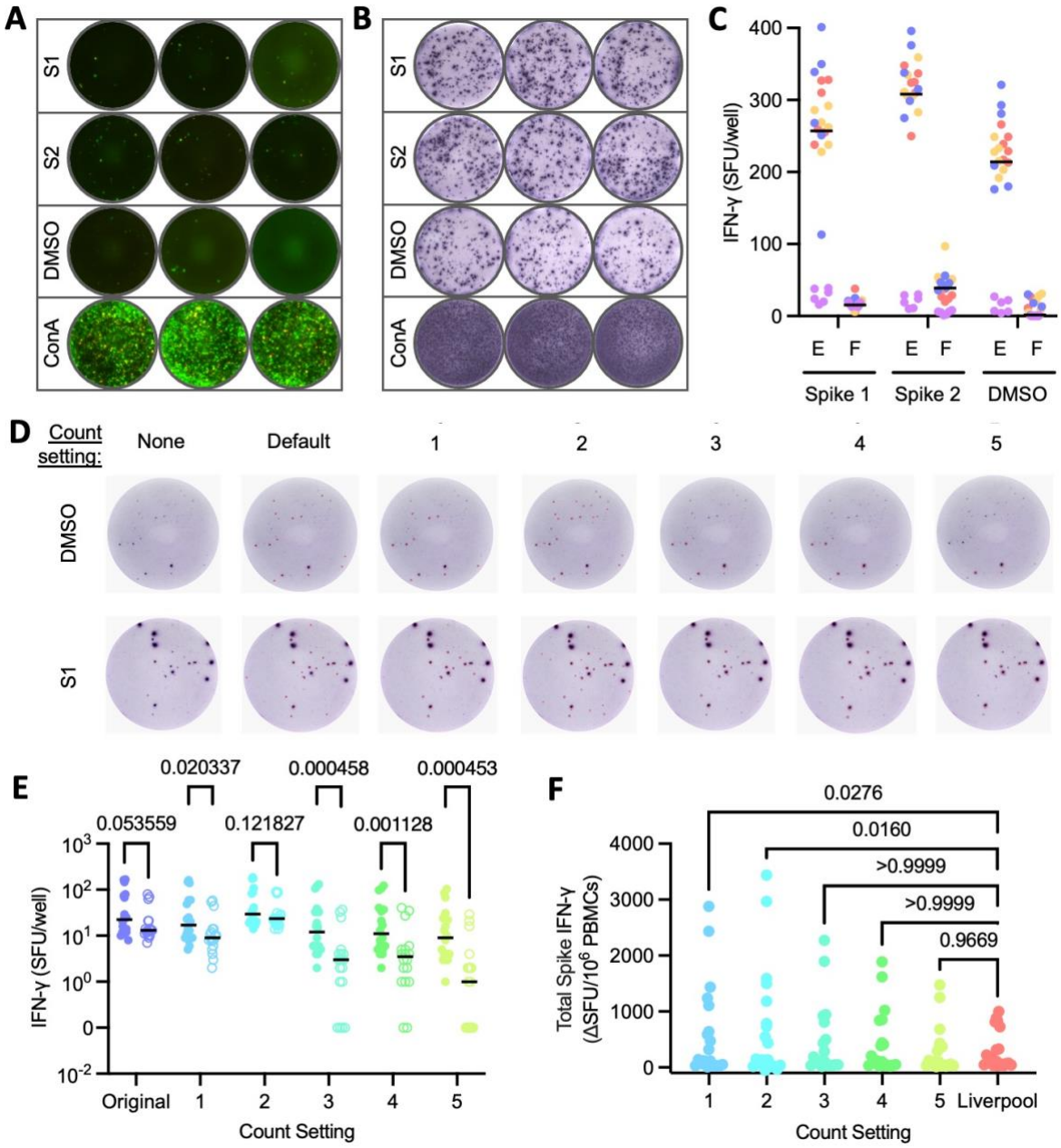

Figure 3.3. Optimisation of IFN-γ ELISpot to detect spike specific T cells after vaccination. A-B) Representative wells of a FluoroSpot **(A)** and ELISpot **(B)** plate indicating IFN-γ capture following overnight stimulation of PBMCs from a vaccinated healthy donor with S1 and S2 peptide pools. Dots in wells green (FluoroSpot) or black (ELISpot) indicate the prior location of a cell secreting IFN-γ. **C)** Comparison of the number of SFU per well detected following stimulation of cells from four donors with S1 and S2 peptide pools, or DMSO negative control on an ELISpot (E) or FluoroSpot (F) plate. Each dot represents one well, each donor is indicated by colour (pink, purple, orange, red). **D)** Representative images of the spots counted under different ELISpot count settings. Wells of PBMCs from a vaccinated individual stimulated with S1 peptides or DMSO. Counted spots are indicated by red crosses or rings. **E)** Comparison of SFUs per well following stimulation with S1 peptides (closed circles) or DMSO (open circles) of PBMCs from six vaccinated individuals. Plate counted under six different count settings. Each dot represents one well. (Multiple Mann Whitney Tests). **F)** Comparison of ΔSFU/10^6 cells of PBMCs from 19 vaccinated individuals stimulated with total S peptides when read under 5 different count settings and at a collaborative lab in Liverpool. Each dot represents the average value for one individual. (Freidman test with Dunn's multiple comparisons).

3.2.2. Cellular response to vaccination in individuals with immune dysregulation

I then applied the optimised ELISpot assay to assess the T cell responses to vaccination in individuals with immune dysregulation. Between the Thaventhiran lab and clinical collaborators, a longitudinal study was established to assess the response to vaccination in groups with immune dysregulation[106]. Samples were collected from participants at multiple timepoints around the receipt of three BNT162b2 vaccine doses (V1/2/3) against SARS-CoV-2. In total, 10 healthy controls (HC), nine individuals with PIDs affecting CTLA-4, LRBA, or NF-κB (PID), and 19 individuals on ICB therapies were included in the study (**Figure 3.4A**).

For the assessment of the antigen specific T cell response, I used the optimised IFN-γ ELISpot protocol to quantify the $CD8^+$ effector T cell response to stimulation with peptides covering the S protein encoded by the vaccine. This assay was completed using V2D105 PBMCs, in order to assess the long-term protection provided by T cells. I found no significant differences in the number of antigen specific T cells between groups (**Figure 3.4B**), however the individuals with PID or on ICB were more frequently below the limit of detection for this assay (**Figure 3.4C**). A broad range of T cell responses in the ICB cohort suggests an influence of cancer type or treatment timing on vaccine reposne[162]. Of the PID group those with the lowest responses were those with IEIs relating to NF-κB. Dysregulation in ICB and PID may influence the long-term protection provided by antigen specific $CD8^+$ T memory cells, but it appears that these cells can still be produced in response to vaccination in these cohorts.

The ELISpot assay indicated levels of antigen specific $CD8^+$ cells after vaccination, however other T cell subsets can also influence the level of protection provided by vaccination. $CD4^+$ T_{FH} cells provide help to B cells in the GC response and are important in the generation of a B cell response to vaccination. Germinal centre T_{FH} cells reside in the GCs which are typically formed in secondary lymphoid organs and so cannot be easily sampled, however circulating ($cT_{FH}s$) cells provide an alternative measure and correlate with antibody production[144,163]. Information about the impact of PIDs, cancer, and ICB therapies on T_{FH} cells is conflicting[125,164-166]. Our analysis found that neither group had significantly different proportions of cT_{FH} cells when compared to HCs. However,

interestingly, levels were significantly lower in the ICB cohort in relation to the PID group (**Figure 3.4D**). This was unexpected and suggested improved availability of T_{FH} cells to promote a GC response in individuals with PID compared to those on ICB.

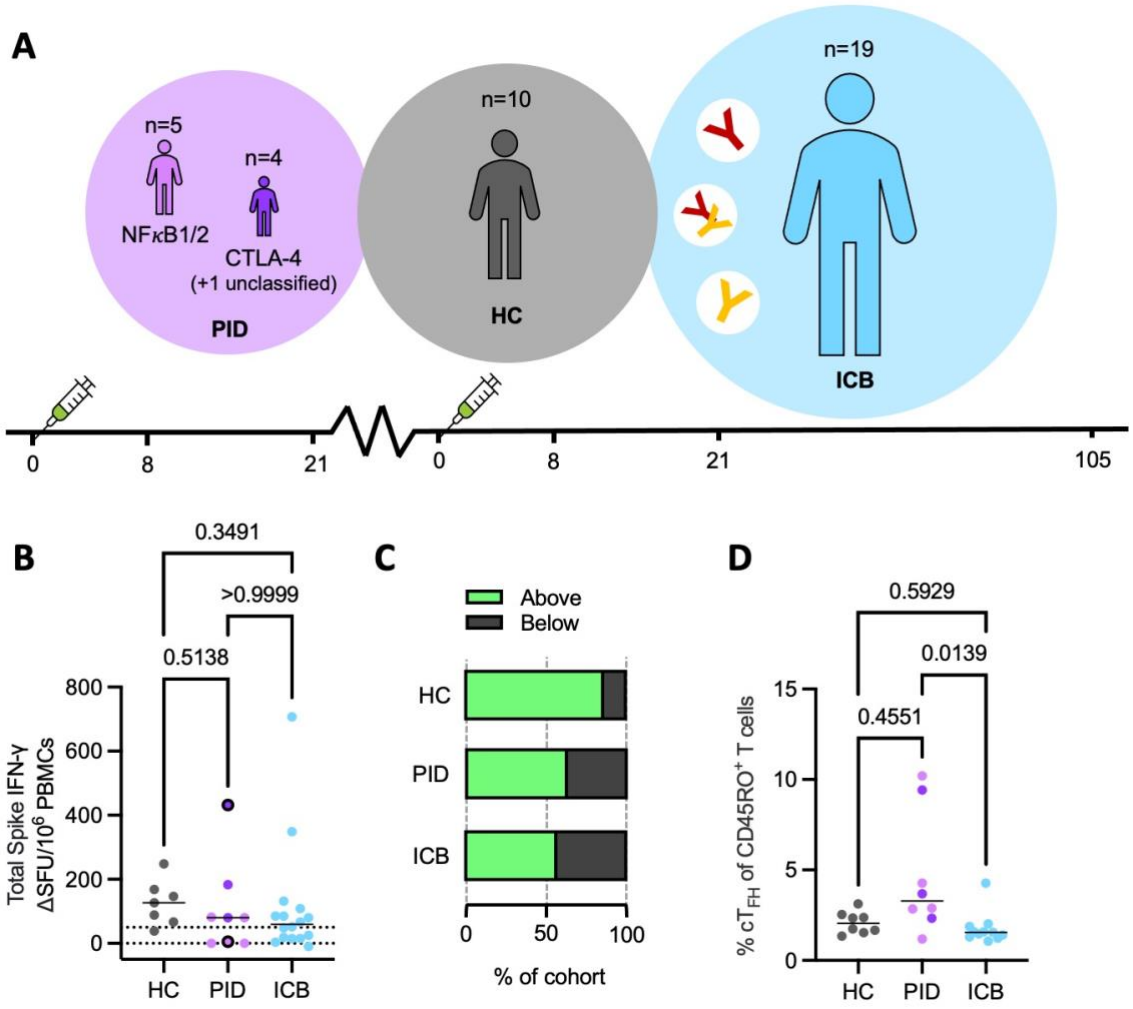

Figure 3.4. T cell phenotyping in individuals with primary and secondary immune dysregulation. A) Schematic of the timings of longitudinal vaccine study. Individuals with NF-κB1/2 deficiency (lilac) and CTLA-4 haploinsufficiency (purple) (PID), on immune checkpoint blockade (ICB – blue), and healthy controls (HC – grey) were sampled at days 0, 8, 21 after first and second vaccine and day 105 after second. Size of background circle relative to cohort size, white circles indicate ICB treatments, anti-PD1 (maroon) or anti-CTLA-4 (gold). **B)** Comparison of spike specific effector $CD8^+$ T cells as indicated by IFN-γ production at day 105 following vaccination in HCs, individuals with PID and on ICB. Dotted lines indicate 0 and Δ50 SFU/10^6 threshold for positivity, samples with high background >50 SFU/10^6 indicated with black border around point. **C)** Proportional stacked bar plot indicating the proportion of each cohort tested above (green) or below (grey) the threshold for a positive IFN-γ response to stimulation with S peptides at day 105 after 2° vaccine. **D)** Comparison of the proportion of memory T cells that are cT_{FH} cells ($CD3^+$, $CD4^+$, $CD8^-$, $CD45RA^-$, $CXCR5^+$, $PD\text{-}1^+$) at day 0 prior to vaccination in HCs, individuals with PID and on ICB. All dot plots – one dot represents a single individual. All significance values are the result of Kruskal Wallis Test with Dunn's Multiple comparisons.

3.2.3. Humoral response to vaccination in individuals with immune dysregulation

Analysis of cellular immunity did not identify any definitive deficiency in vaccine specific T cell responses and so humoral responses were then considered. While I was evaluating T cell responses, antibodies and memory B cells were assessed by the Thaventhiran lab and collaborators to evaluate the humoral response to vaccination. The EF response is expected to peak ~6 days and the GC ~14 days following antigen encounter[30], and so the V2D21 timepoint was used to capture the peak antibody response. As expected, and despite cT_{FH} cell numbers, individuals with PID had significantly reduced RBD specific IgG compared to HCs. Some individuals in the ICB group also had low levels of RBD specific IgG, however, the group was not significantly different to HCs (**Figure 3.5A**). The ranges of IgG levels in both patient groups was broad, with some individuals able to produce antibody levels similar to those seen in HCs. The proportion of B cells able to bind to the RBD was consistently lower in individuals with PID and on ICB before and after vaccination (**Figure 3.5B**), although again groups were heterogenous. This suggests reduced levels of specific memory B cell production in response to vaccination in these groups. A key correlate of protection against SARS-CoV-2 is the presence of neutralising antibodies[104], able to prevent viral entry and replication. Although RBD binding antibodies were detectable in most study participants, the location of their binding epitope or the isotype of the antibody may prevent these from being neutralising. Prior to the receipt of a second vaccine, very few participants had a quantifiable neutralising capacity (NT50) (**Figure 3.5C**). After the second dose the number of participants with detectable NT50 increased. However, significant heterogeneity in the PID and ICB groups meant that median NT50 for both groups was significantly less at days 8 and 21 than HC, despite some individuals having comparable NT50 values. The receipt of a third dose was sufficient to boost neutralising capacity to a similar level in all groups, although fewer participants were tested at this timepoint. These data suggest that the majority of individuals in all groups are able to make an initial humoral response to vaccination and produce antigen specific plasmablasts which secrete RBD binding antibodies. However, the magnitude of antibody secretion and the production of long-lived antigen specific memory cells appears to be impaired in some individuals on ICB and with PID. This may lead to a lack of long-term protection from vaccination in these individuals and inability

to maintain circulating antibody levels. Response to vaccination in both groups was incredibly heterogenous. Some individuals had no detectable RBD specific memory cells, T cell response, or NT50 after second dose (**Figure 3.5D&E**). These individuals are unlikely to be protected by vaccination from SARS-CoV-2 infection.

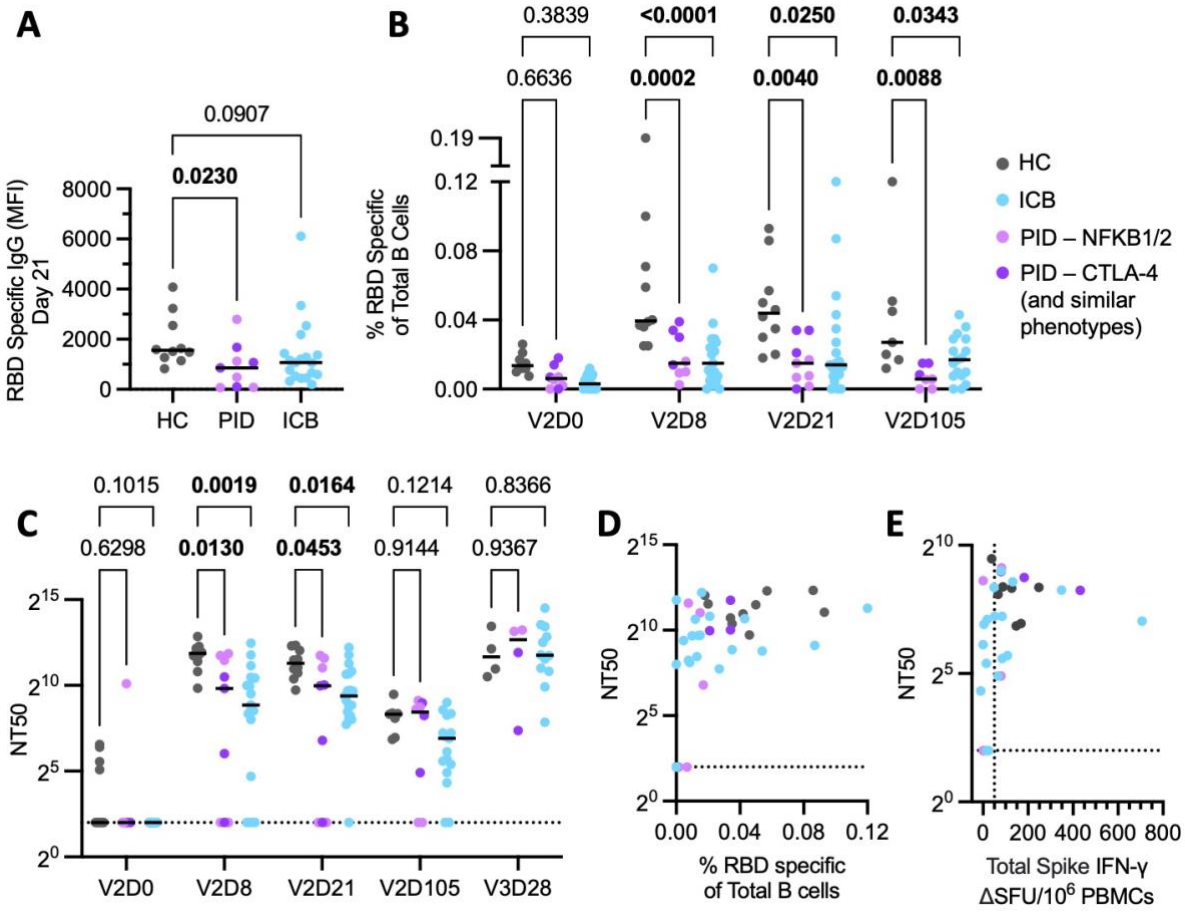

Figure 3.5. The humoral response to vaccination in individuals with immune dysregulation. A) Comparison of the levels of RBD binding IgG (median fluorescence intensity) in the serum at day 21 following two dose vaccination between participant groups (Kruskal Wallis with Dunn's Multiple Comparisons test). **B)** Comparison of the proportion of total B cells able to bind the RBD protein ($CD19^+$, RBD-1^+, RBD-2^+) at timepoints prior (V2D0) to and following (V2D8, V2D21, V2D105) vaccination with a second dose of BNT162b2 between cohort groups. (2-way ANOVA with Dunnett's multiple comparisons test). **C)** Comparison of the live virus neutralising capacity of the sera of individuals at timepoints prior (V2D0) to and following second (V2D8, V2D28, V2D105) and third (V3D28) dose vaccination between cohort groups. (Mixed-effects analysis with Dunnett's multiple comparisons test). Dotted line indicates limit of quantification, samples with detectable but unquantifiable NT50 assigned arbitrary value of 4. **D)** Scatter plot of percentage of total B cells RBD specific and NT50 at day 21 for each individual. Dotted line indicates limit of quantification for NT50. (ρ = 0.4656, P = 0.0032, Two-tailed Spearman correlation) **E)** Scatter plot of IFN-γ producing S peptide stimulated T cells and NT50 at day 105 for each individual (ρ = 0.3829, P = 0.0305, Two-tailed Spearman correlation). Dotted lines indicate limit of quantification for NT50 and threshold of positivity for T cell response. In all plots one dot indicates data from one individual at a single timepoint, from HC (grey), ICB (blue), PID – CTLA-4 (purple), and PID – NFKB (lilac) cohorts. Bars indicate median value of the group. P values <0.05 highlighted in bold.

3.2.4. Relationship between ABCs and vaccine response

Heterogeneity in the antigen specific cellular and humoral markers indicates that response to vaccination cannot be predicted simply by the presence of immune dysregulation. Biological biomarkers may aid in determining which individuals are at risk of a poor response to vaccination and improve understanding of the mechanisms behind failed responses. One potential clinical marker is $CD21^{low}$ cells or ABCs which are sometimes associated with impairment of the B cell response and are often expanded in people with PID and on ICB therapies. ABCs defined as $CD19^{+}CD11c^{+}CD21^{low/-}$ were expanded in both the PID and ICB groups before vaccination (**Figure 3.6A**). Increased levels of ABCs as a proportion of B cells had a negative relationship with the proportion of total lymphocytes that were B cells across all groups (**Figure 3.6B**). This may be reflective of ABCs comprising a larger proportion of the B cell subset when total B cell numbers are reduced or alternatively, the inhibition of B cell production by ABCs[167].

Increased proportions of ABCs prior to vaccination had a negative association with markers of the humoral and cellular response to vaccination (RBD binding B cells, S specific T cell IFN-γ production, and RBD binding IgG) (**Figure 3.6D-F**). In all instances significant negative Spearman's rank correlations were seen in both raw and log transformed data, with a linear relationship when data was log transformed (**Figure 3.6C&G-I**). Participants with the most extreme expansion of ABCs had levels over 12% of total B cells. These individuals had little to no evidence of a productive vaccine response. Increased resting levels of ABCs therefore correlate with poorer vaccine responses and expansion past a threshold may indicate inhibited response. Therefore, a threshold ABC level could be used as a marker for individuals at risk of a poor vaccine response. It is unclear the direct influence of ABCs on the immune response to vaccination. Response to vaccination may be limited by corresponding reduction of B cell numbers. Conversely, ABCs may directly impair the humoral or cellular immune responses to vaccination.

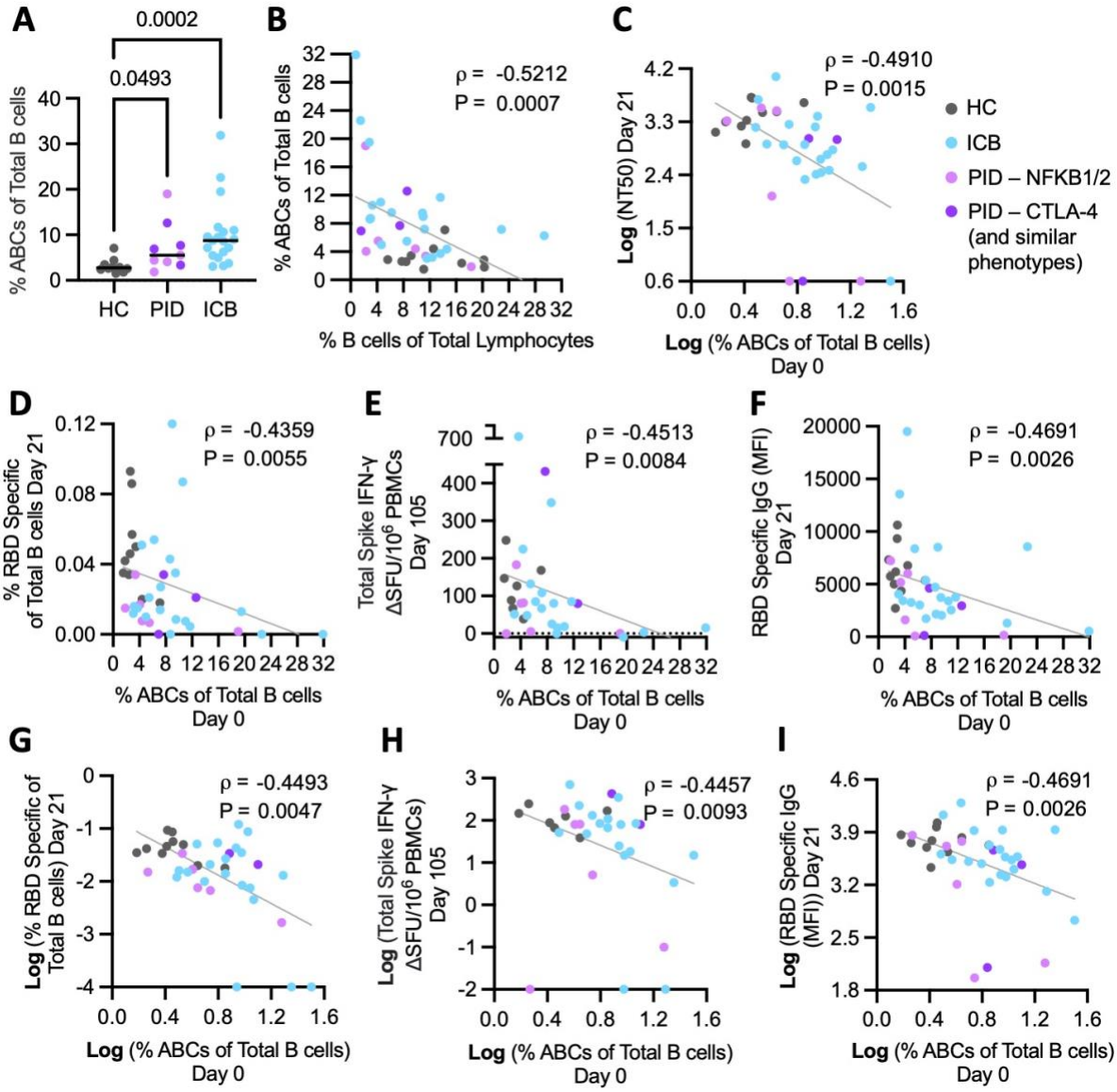

Figure 3.6. Relationship between ABCs and vaccine responses. A) Comparison of the resting levels of ABCs ($CD19^+$, $CD21^-$, $CD11c^+$) as a proportion of total B cells in cohort groups (Kruskal Wallis test with Dunn's Multiple comparisons). **B)** Relationship between ABCs as a proportion of total B cells, and B cells as a proportion of total lymphocytes at day 0 prior to vaccination. **C)** Relationship between log_{10} transformed live virus neutralising capacity at day 21 post second dose and log_{10} transformed resting levels of ABCs as a proportion of total B cells. **D-F)** Relationship between resting levels of ABCs as a proportion of total B cells and **(D)** RBD specific B cells as a proportion of total B cells at day 21 after vaccination **(E)** IFN-γ producing spike specific T cells at day 105, and **(F)** RBD specific IgG levels at day 21. **G-I)** Relationship between log_{10} transformed resting levels of ABCs as a proportion of total B cells and **(G)** log_{10} transformed RBD specific B cells as a proportion of total B cells at day 21 after vaccination **(H)** log_{10} transformed IFN-γ producing spike specific T cells at day 105, where ΔSFU was zero or less an arbitrary logged value of -2 was assigned to signify zero response, and **(I)** log_{10} transformed RBD specific IgG levels at day 21. In all plots one dot indicates data from one individual, from HC (grey), ICB (blue), PID – CTLA-4 (purple), and PID – NFKB (lilac) cohorts. Where present bars indicate median value of the group. Two-tailed Spearman correlation coefficients (ρ) and P values are shown on scatter plots, together with indicative linear regression lines.

3.3. Discussion

3.3.1. Results

3.3.1.1. Detection of antigen specific T cells

The detection of antigen specific T cells is a crucial yet complex requirement for the assessment of effective vaccine responses. To assess the production of T cells specific to the S protein encoded by the BNT162b2 mRNA vaccine a high throughput assay with low cell number requirements was needed. Following the assessment of four different flow cytometry and plate-based stimulation assays I determined that an ELISpot for IFN-γ production was best suited for the requirements of our study at the time.

The ELISpot provided the benefits of requiring low cell numbers, easy standardisation with other labs locally, worldwide use, low input time, short stimulation time, and medium throughput. Where the CTV cell proliferation assay required a long incubation time and analysis of both the CTV and AIM assays necessitated higher processing power than automated ELISpot plate readings. However, as with all assays tested, the ELISpot is not without limitations. IFN-γ is not only secreted by T cells. NK cells, T_H1, and macrophages are able to make IFN-γ and may influence ELISpot results. It should also be noted IFN-γ ELISpot assays have been seen to be less sensitive in the detection of S specific T cells following SARS-CoV-2 infection than cell proliferation assays[168]. Traditional ELISpot assays are limited to the detection of a single cytokine and the kinetics of cytokine production by activated cells is complex, cells do not all secrete cytokine at the same frequency and magnitude[169]. Although, I found that an IL-2/IFN-γ FluoroSpot was less sensitive and consistent, the additional 2-3 cytokines that could be detected using a FluoroSpot would have increased the data obtained from each sample. Given additional time and resources for set up, this would not have required any extra samples or time for assay completion. Detection of other cytokines would have provided information on T cell subsets other than IFN-γ secreting T cells.

3.3.1.2. Immune response to SARS-CoV-2 vaccination in individuals with immune dysregulation

Through the application of the IFN-γ ELISpot I found heterogeneity in the S responsive CD8+ T cells individuals with PID and on ICB after vaccination. Some participants had levels comparable to those of HCs while others had complete absence. This analysis was constrained to the single timepoint. Discrepancies in the concentration of DMSO used for the storage of cryopreserved PBMCs meant that the viability of samples processed earlier in the study were lower. This was not an issue for the humoral assays; however, the ELISpot was especially susceptible to reduced cell survival due to cytokine release upon cell death[170,171]. Nevertheless, antigen specific T cells are well maintained for up to six months in healthy controls with minimal waning[172], so the day 105 measures are likely to be representative of the T cell response. This suggests that some individuals with PID and on ICB produce few to no T cells in response to mRNA vaccination. T cell responses to SARS-Cov-2 infection have previously been reported in B cell deficiency[173-175]. My findings indicate that this is the case following vaccination in some individuals but not all. This discrepancy may be due to differences in the nature of response invoked by mRNA vaccines compared to natural infection.

We additionally found varied levels of impairment of humoral vaccine responses in our PID and ICB cohorts. Other studies have observed similar reduced antigen specific antibody levels and B cell levels following vaccination in individuals with PID[176,177]. ICB therapy may have been expected to boost humoral responses by the provision of T cell help[178-180], however lack of cT_{FH} expansion may indicate why this is not the case. All measures of humoral responses were diverse across both ICB and PID groups, ranging from levels comparable to healthy individuals to none. It is not entirely clear what dictates this range in responses. In the ICB group I found no difference between groups based on cancer stage or therapy type. However, those of the lowest response were all in later cancer stages (IV), had active disease present at the time of vaccination, and additionally were on combination anti-CTLA-4 and anti-PD-1 therapies. ICB expanded T cells can be maintained for years following treatment, however a combination of cancer type, cancer severity, treatment, and time since treatment may all contribute to vaccine response[181,182].

We identified that resting levels of ABCs negatively correlate with measures of vaccine specific immunity. Hence, they have potential as a biomarker to aid in the identification of individuals at risk of a poor vaccine response. Subsequent single cell sequencing of B cells from some study participants[106] indicated that ABCs did not differ between patient groups and represented the same population of cells. This population could be sorted into 3 distinct subsets, Classical, Anergic, and CD1c$^+$, with the Classical subset expressing genes associated with antigen processing and presentation. This suggests a functional immunological role for these ABCs. Additionally, high levels of the inhibitory Fc gamma receptor IIB (FcγRIIB) on ABCs led to increased ability to bind to immune complexes. ABCs may have an enhanced ability to clear immune complexes against antigen, reducing the length of vaccine antigen availability. Together this indicates that ABCs may be a contributing factor towards impaired vaccine responses rather than solely a marker.

3.3.2. Conclusions and future directions

In this work I adapted an ELISpot assay for the timely detection of SARS-CoV-2 S protein reactive T cells after vaccination. Through a clinical study, I and others identified heterogenous cellular and humoral responses to mRNA vaccination against SARS-CoV-2 in individuals with immune dysregulation caused by PID or ICB. ABCs were identified as a potential biomarker of, or explanation for, the variety of immune responses observed.

Although the ELISpot was the most efficient way to assess T cell responses in this study, the application of additional T cell assays would provide more detail on the role of other T cells subsets in vaccine induced immunity. Levels of antigen specific IFN-γ producing CD8$^+$ cells give an indication of whether an individual is primed to clear virally infected cells, however CD4$^+$ helper cells and other CD8$^+$ subsets are also fundamental in shaping the response to pathogen. An optimised AIM assay, cell proliferation assay, MHC tetramer staining, intracellular cytokine staining (ICS) or a combination of techniques could be applied to the remaining samples from this study[155,183]. Combining these methods with the ELISpot would provide additional information about the types of T cell responses formed following mRNA vaccination[184]. This could inform on whether T cell

responses are entirely absent in some participants or switched towards a specific subtype.

The number of people with rare inherited IEIs is very small and therefore expanding this group for further study would be difficult. On the other hand, the numbers of individuals eligible for ICB treatments for cancer is increasing[185]. Individuals with immunosuppression are classed as "at risk" from COVID-19 by the NHS[186] and as such are eligible for autumn booster vaccines. A study to investigate the immune response to larger groups of individuals on ICB therapies and potentially PID would be possible over the autumn booster campaign. This could address two questions which arise from our study. Firstly, increased cohort size would allow statistical analysis of the disease and treatment factors influencing heterogeneity in vaccine response. Importantly, this may aid in the understanding of what causes some individuals to have an entirely absent response to vaccination. Secondly, only a small number of participants had ABCs over 12% of B cells in our study. Increasing the numbers of individuals studied with ABCs over this threshold would enable confirmation of whether this is an indication of immune impairment. One caveat to this proposal is that most individuals receiving an autumn booster in 2024 or later will have already received four or more doses of vaccine and most likely will have been exposed to the virus at least once. There is evidence to suggest that the response to vaccination changes with repetitive dosing and hybrid immunity[187-189], therefore the results of such a study may not show exactly what has been observed here.

Clearance of immune complexes is one way in which ABCs may attenuate the humoral response to antigen. However, ABCs are a recently defined subset of cells and as such not much is fully understood about their function[190]. Further *in vitro* and *in vivo* experiments could provide evidence into the mechanism by which ABCs disrupt vaccine responses. For instance ABCs impair GC responses in mouse models[68], adoptive transfer of ABCs into mice prior to vaccination would enable investigation into the levels of ABCs required for vaccine impairment. The use of mice with knockout or overexpression of FcγRIIB[191] may provide further evidence as to the role this receptor plays in ABC mediated impairment of B cell responses.

ABCs are expanded in many other populations including people with obesity, autoimmune disease, and the elderly. Risk from COVID-19 disease increases with age

and severe obesity[192]. Additionally, elderly individuals have poorer immune responses to initial 2 dose courses of vaccination[193]. Future studies could also consider the role that ABC populations may play in vaccine and disease responses in these individuals. Our data suggests that ABCs should not functionally and phenotypically vary significantly between these groups and would predict a negative association between ABC levels and immune responses. ABCs emerge here as a potential therapeutic target for the improvement of vaccine responses, in addition to a useful biomarker. However, ABCs are also required for some aspects of humoral immunity[194]. Therefore, mechanistic understanding of the mode of ABC immune inhibition may enable the disentanglement of the aspects of ABC function that are negative and beneficial for the immune response. To improve the immune response in the presence of high ABC levels, the development of a targeted therapy to eliminate inhibition while maintaining anti-viral functions would be required.

Together, heterogeneity in the response to vaccination in individuals with immune dysregulation, identifies ABCs as a potential therapeutic target for the improvement of vaccine responses. Additionally, indicating the importance of improving response and protection from mRNA vaccination in some individuals.

4. The response to vaccination in people with severe obesity

In this chapter I report the results of the SCORPIO study. This study was coordinated by members of the Thaventhiran and Farooqi labs and conducted with the help of research and clinical collaborators. Full details of results and collaborators of this study can be found in the published paper[195] for which I am the second author. I was responsible for sample processing and management, and T cell assays in this study with the assistance of Lucy Booth. Other data was generated by the analysis of samples by collaborators as detailed in the preface and methods of this thesis.

4.1. Introduction: immune dysregulation in obesity

4.1.1. Global obesity: a pandemic

Obesity, defined as a body mass index (BMI) of over 30kg/m^2, is increasing in prevalence across the world (**Figure 4.1**). The WHO has classified obesity as a major public health challenge with risks to both economic and social development[196]. In 2021 26% of adults in England had obesity and current trends suggest this will continue to rise. Within England, minority groups such as those from deprived backgrounds are disproportionately affected by increasing obesity levels[197]. Obesity has major economic, health and social implications[198]. These are exacerbated for those with severe obesity, defined as a BMI of over 40kg/m^2 which can lead to increased morbidity and mortality, and a significantly reduced quality of life. A number of health complications are associated with severe obesity, including type 2 diabetes, cardiovascular disease, and non-alcoholic fatty liver disease (NAFLD)[199].

4.1.2. The impact of obesity on the immune system

Obesity is a significant cause of immune dysregulation. Subcutaneous (SAT) and visceral (VAT) adipose tissue levels are increased with obesity. This increased mass of adipose tissue is strongly linked with hypertension and insulin resistance[200]. The adipocytes which make up white adipose tissue secrete a number of cytokines known as adipokines. These include adipsin[201], IL-6, TNF[202], adiponectin[203] and leptin[204] leading to increased expression and signalling in obesity. Lean adipose tissue is infiltrated with anti-inflammatory immune cells which aid in the maintenance of metabolic homeostasis,

however obesity is associated with the recruitment of pro-inflammatory macrophages[205]. With increasing levels of obesity, increasing numbers of macrophages infiltrate into the adipose tissue[200]. Macrophages can be pro-inflammatory (M1) or immunosuppressive (M2), secreting cytokines such as TNF, IL-1, IL-6, IL-12, and IL-23, or IL-10 and transforming growth factor beta (TGF-β) respectively[206].

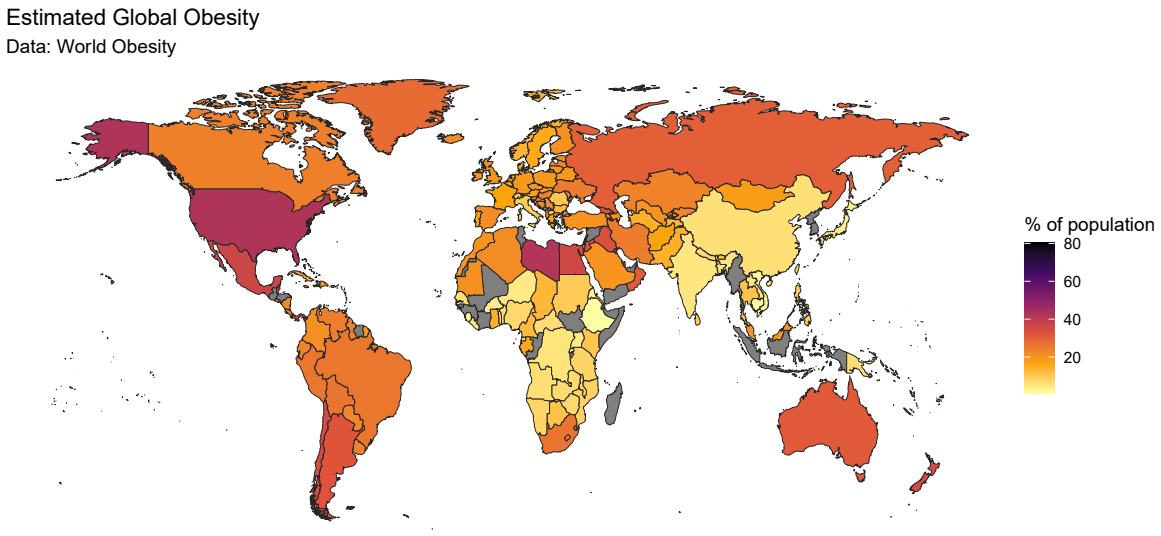

Figure 4.1. Global obesity. Estimated proportion of each country of the world's total population having obesity. Colour indicates % of total adult population classified as having obesity, grey indicates no data was available for region. Data from world obesity, global obesity observatory[207], map generated using R studio.

Accumulation of adipose tissue can lead to local metabolic dysfunction. This is believed to be a result of the development of hypoxia as adipose tissue expands, and subsequent inflammatory chemokine secretion by hypertrophic adipocytes[191,208,209]. Metabolically dysfunctional adipose tissue has increased levels of inflammation, M1 activated macrophages, and $CD8^+$ T cells, and is further associated with the adverse immunological impacts of obesity[200] (**Figure 4.2**). Chronic inflammation in obesity, then leads to systemic immune dysfunction, and it has been suggested that obesity leads to accelerated aging of the immunesystem[210,211].

In humans, increasing BMI can lead to reduced production of IFN-γ and TNF by $CD8^+$ T cells in the bone marrow in addition to increased frequencies of B cells and reduced levels of memory T cells[212]. Immune dysregulation caused by obesity can, however, be overcome to a certain extent by weight loss. Studies have shown that lymphocyte

markers can be returned to normal after weight loss following gastric banding, however not all other immune markers return to a normal level[213]. Diet induced obesity in mice leads to reduced memory T cell function and ability to respond to DC antigen presentation against influenza[214]. Additionally, obesity leads to changes in the metabolic phenotype of memory T cells in mice, which are not reversed upon weight loss[215]. Differences are also seen in B cells, which undergo metabolic reprogramming to adapt to the hostile inflammatory environment of obesity[210].

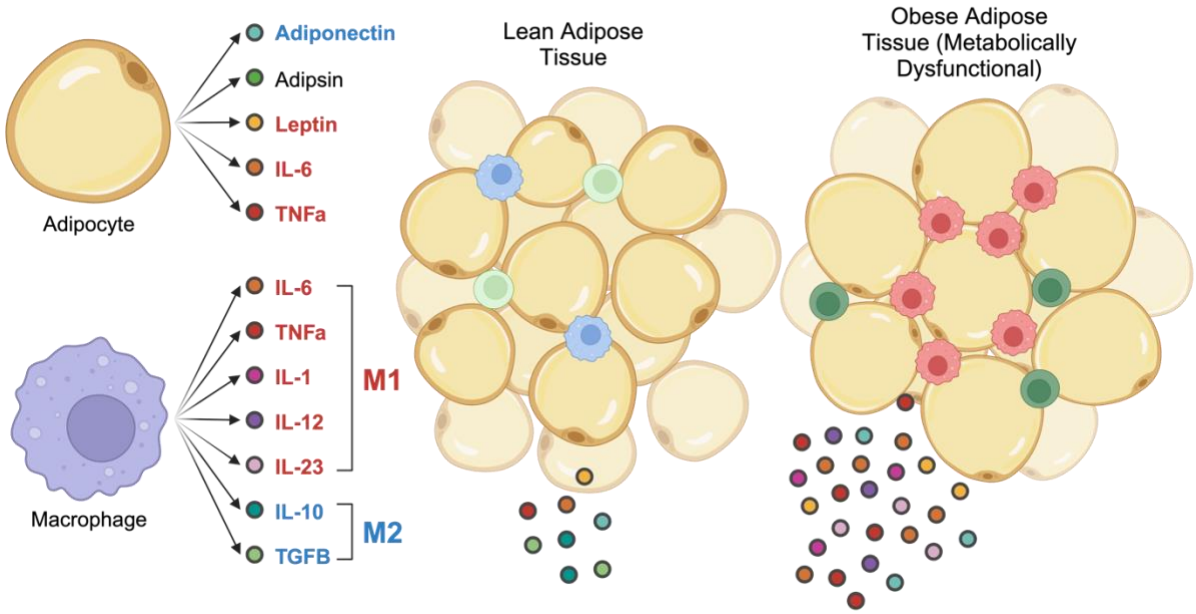

Figure 4.2. Immune environment of adipose tissue. Schematic of the white adipose tissue of a lean individual and individual with obesity and metabolic dysfunction (not to scale). Adipocytes and macrophages are the most common cells in the adipose tissue, and both secret a range of cytokines. M1 macrophages (red) secrete mostly pro-inflammatory cytokines (red text), whereas M2 (blue) secrete anti-inflammatory cytokines (blue text). Lean adipose tissue is mostly populated by M2 macrophages and $CD4^+$ T cells (pale green), and cytokine secretion is not inflammatory. Metabolically dysfunctional obese adipose tissue is made up of larger adipose tissue and infiltrated by M1 macrophages and $CD8^+$ T cells. This environment is inflammatory with large scale secretion of pro-inflammatory cytokines. Generated using Biorender.com

4.1.3. Obesity and COVID-19 disease

Immune impairment leads individuals with obesity to be at increased risk from COVID-19. Obesity, severe obesity and increasing BMI have been associated with increased risk of severe disease[216], requirement for ventilation[217], and death[218,219]. Early in the pandemic patients in one New York emergency department with BMIs 30-34 and >35 were 2x and 2.2x more likely to require acute care admission and 1.8x and 3.6x more likely to require

critical care admission respectively[220]. Individuals with obesity and SARS-CoV-2 infection have decreased inflammatory responses in the lung[221] compared to those of normal weight. There is a negative correlation between BMI and the levels of S protein binding IgG in the serum during and following infection[222]. Together this is indicative of a poorer immune response to SARS-CoV-2 infection in individuals with obesity.

In addition to increased acute risk from SARS-CoV-2 infection, higher BMI has also been associated with a risk of Post-Acute Sequelae of SARS-CoV-2 infection[223]. This is also known as long COVID and causes ongoing symptoms and disease in individuals following SARS-CoV-2 infection. Individuals with obesity require additional attention in the prevention of SARS-CoV-2 infection due to these increased, short and long-term, risks from disease.

4.1.4. The efficacy of vaccination in obesity

Vaccination is fundamental for protection against COVID-19 yet, as demonstrated in the previous chapter, is not always successful in triggering an appropriate adaptive response in those with immune dysregulation. The systemic changes to the immune response seen in people with obesity would be expected to also impact the efficacy of immunisation in these individuals. Response to vaccination against viral pathogens appears to vary in people with obesity dependent on the vaccine. Increased BMI is associated with lower antibody titres after vaccination against rabies[224], hepatitis B[225,226], and tetanus[227]. In contrast, individuals with obesity form a high antibody response to influenza vaccines. Influenza is an RNA virus which infects the upper respiratory tract, similar to SARS-CoV-2. Callahan et al[228] found that after a single dose but not a double dose against H1N1 influenza, adults with obesity had higher HA inhibition antibody titres than those of normal weight. Interestingly, Sheridan et al[229] also saw that an increased BMI correlated with an increased antibody titre after influenza vaccination. Although subsequently, higher BMIs correlated with a more rapid decline in antibody titre over the following 12 months. Despite seroconversion, vaccinated individuals with obesity are at an increased risk of developing influenza infection[230]. When T cells from vaccinated individuals were stimulated with live pH1N1 (influenza virus) those from individuals with obesity

expressed reduced levels of activation markers than those from normal weight[231]. Additionally, mice on a high fat diet have reduced antibody levels and influenza specific $CD8^+$ effector memory T cells after vaccination than those on a regular diet[232]. Together this suggests that protection from vaccination against RNA respiratory viruses may be impaired in people with obesity, despite high initial antibody responses. However, mRNA vaccine technologies have not previously been applied to influenza vaccines and this modality could additionally influence the form of protection induced against SARS-CoV-2.

4.1.5. Confounders in Obesity Research

The proportion of a population with obesity is unlikely to be demographically representative of the total population, this must be considered when selecting a normal weight comparison group for studies of obesity. Rates of obesity vary by sex, socioeconomic status, deprivation, ethnicity, disability status, education level, and age[197,233,234]. Factors associated with obesity, such as increased age and deprivation, are in many cases also associated with impaired health and immunity[235-237]. Additionally, a number of environmental factors influence the chance of obesity but also have an immunological influence themselves. For instance, smoking is typically associated with a lower BMI and has previously been noted to mask an association between BMI and mortality[238].

Obesity has a systemic impact on the immune system and is associated with a number of comorbidities including some cancers, cardiovascular disease, type 2 diabetes, and respiratory problems[239]. Individuals with confounding comorbidities are typically excluded from studies, however, this can largely reduce the population of individuals with obesity to be studied. Significantly, obesity is associated with increased risk of type 2 diabetes[240,241]. Diabetes leads to high levels of inflammation due to excess blood glucose and individuals with diabetes are at increased risk from infection[242]. Obesity is also associated with increased incidence of cardiovascular disease due to structural impacts of excess fat and inflammation induced by adipokines[243,244]. Cardiovascular diseases[245] and type 2 diabetes[246,247] have been associated with increased risk of death from COVID-

19. Common co-morbidities may exaggerate or mask the impact of obesity in the immune response to COVID-19 disease and vaccination. Studies must therefore be controlled or adjusted for potential confounders in order to determine whether associations with BMI are independent of other factors.

4.1.6. Chapter Aims

Severe obesity represents a further mode of immune dysregulation. Protection from COVID-19 disease by successful vaccination is crucial to avoid the increased risk of severe outcomes in individuals with obesity. Immunity induced by vaccination against other viral pathogens can be impaired by obesity as may be the case in COVID-19 vaccine responses. My involvement in the collaborative SCORPIO study allowed me to investigate the impact of immune dysfunction, in obesity, on vaccination.

In this chapter I therefore address the following questions:

- Does the immune dysregulation caused by severe obesity prevent protection from infection through mRNA vaccination?
- Can individuals with severe obesity form robust cellular and humoral responses to mRNA vaccination against SARS-CoV-2?
- Does immune dysregulation in severe obesity also lead to heterogeneity in immune responses, as seen in people with PID and on ICB?

4.2. Results

4.2.1. Cohort recruitment and sampling

The SCORPIO Study was set up in collaboration between researchers in the Thaventhiran Lab at the MRC Toxicology Unit and the lab of Professor Sadaf Farooqi at the Institute of Metabolic Science. Individuals with severe obesity receiving their third dose of vaccine were recruited to this study. However, the rapid roll out of vaccines in at risk groups, including those with severe obesity[248], limited the recruitment of these individuals prior to vaccination. Participants were sampled for whole blood at timepoints prior to receiving their third dose (V3) of vaccine against SARS-CoV-2 (day 0). Then, subsequently sampled at days 8-, 28-, 105-, 185- after vaccination. Individuals were excluded from this analysis

if there was any evidence of prior infection or if they did not fit into the required BMI categories. This left 28 individuals with SO and 16 NW controls, sampled at a combination of different timepoints, who were included in the longitudinal analysis of the vaccine specific immune response.

4.2.2. The risk of severe COVID-19 outcomes following vaccination

In addition to the clinical study, computational analysis was completed by the group of Professor Sir Aziz Sheikh (University of Edinburgh) on a dataset of healthcare information from over 4 million individuals in Scotland collected through EAVEII[105]. This analysis identified that higher BMI values were associated with an increased risk of severe outcomes (hospitalisation or death) from COVID-19 after vaccination. The aRRs as a measure of risk for severe COVID-19 outcomes increased in all BMI groups with time from vaccination however, this increase was of a higher rate and magnitude in individuals with obesity and severe obesity compared to those of normal weight (**Figure 4.3A**). Indeed, when BMI was stratified into groups of 1kg/m^2 the aRRs increased from BMI groups 25kg/m^2 to 42kg/m^2. For BMIs >42kg/m^2 the aRRs fluctuated but remained higher than those for individuals of normal weight (**Figure 4.3B**). This indicated that the frequency of severe outcomes was greater after vaccination in individuals of higher BMI. Outcomes after third dose vaccination were also considered in a separate analysis, however due to the timing of the study the time periods analysed were smaller. This analysis suggested improved protection and maintenance after third dose in individuals of normal weight but not those with obesity (**Figure 4.3C**). However, differences were small, and all 95% CIs covered baseline in this analysis. CIs were much wider at the extremes of BMI, especially in the case of severe obesity, meaning there is less certainty in the calculated aRRs. This is likely reflective both of the fact that there are fewer individuals in these groups but also the broad heterogeneity in the metabolic state of individuals with severe obesity[249]. Regardless of this heterogeneity, it appears clear that increased risk from COVID-19 persists, despite vaccination, in the case of obesity.

4.2.3. Breakthrough infection following third dose vaccination

Participants in the clinical SCORPIO study who showed indications of infection with SARS-CoV-2 before the day 28 timepoint were excluded from the study. Those with evidence of infection thereafter were considered to have had breakthrough infection, an infection able to overcome the protection provided by third dose vaccination. These individuals were only excluded from subsequent sampling. I conducted a brief analysis of the participants with evidence of breakthrough infection in each group. Participants were considered to have been infected with SARS-CoV-2 if they had any of, a positive RT-PCR test, IFN-γ T cell response to N protein, or IgG antibodies against N protein. Participants who had declined to return for sampling made up a larger proportion of the SO cohort at day 105 but similar proportion at day 185 when compared to NW. A marginally larger proportion of the SO cohort were excluded by days 105 (SO = 13.6%, NW = 7.1%) and 185 (SO = 40.9%, NW = 35.7%) due to evidence of infection (**Figure 4.3D**). As a consequence of small cohort sizes and lack of data from non-returning participants a meaningful analysis of this data is not possible. Yet, breakthrough infection can evidently happen in both groups as early as 3 months following booster vaccination.

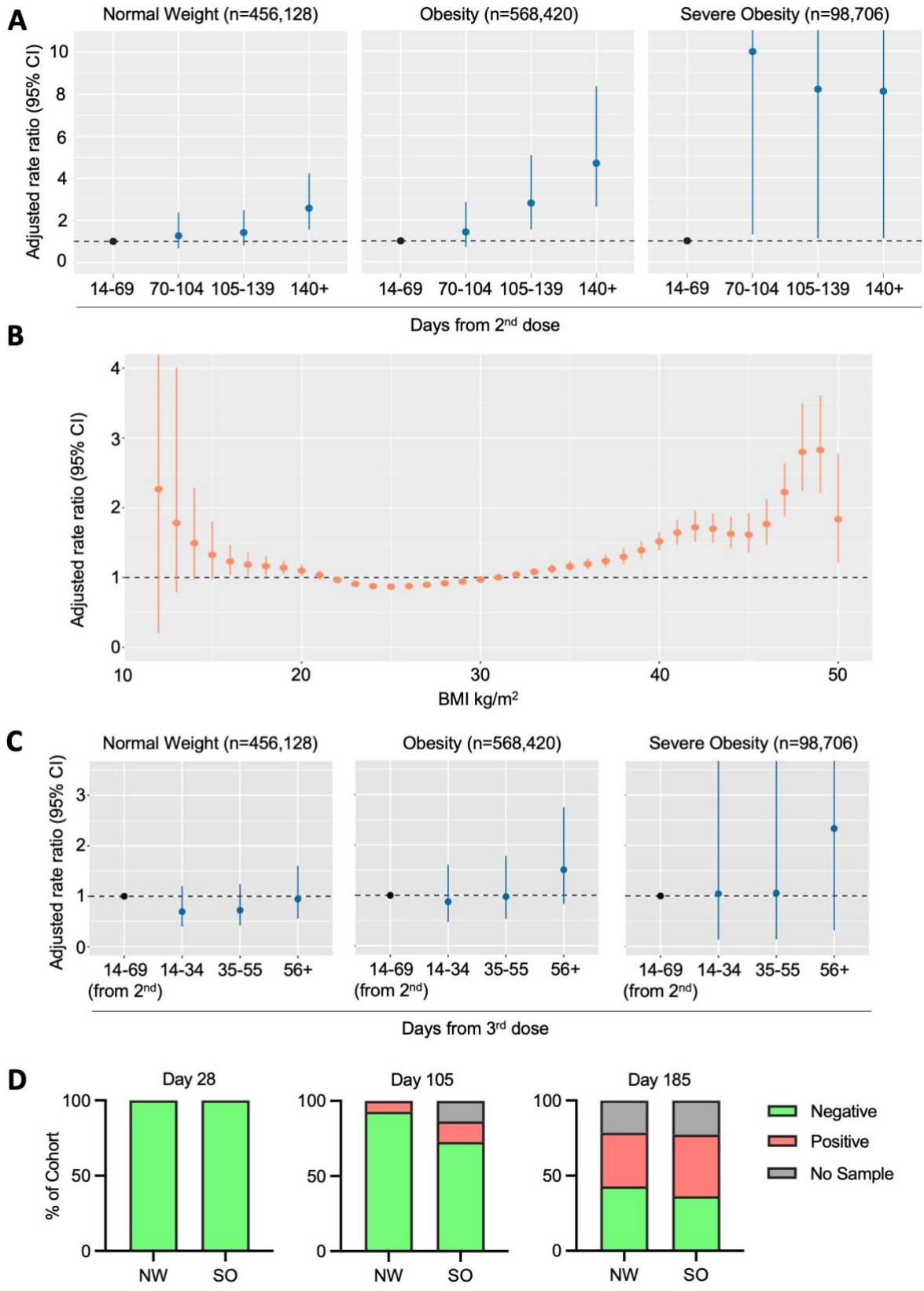

Figure 4.3. Relative risk of COVID-19 in people with obesity following vaccination. A) Mean aRRs for severe COVID-19 outcomes (hospitalization or death) at timepoints subsequent to second dose vaccination against SARS-CoV-2. Normal weight (Left), Obesity (Centre), and Severe Obesity (Right) BMI categorisation. **B)** The relationship between BMI and mean aRR of severe outcomes from COVID-19 after

second dose vaccination against SARS-CoV-2. **C)** Mean aRRs for severe COVID-19 outcomes at timepoints subsequent to third dose vaccination against SARS-CoV-2. Normal weight (Left), Obesity (Centre), and Severe Obesity (Right). **D)** Proportional bar plot of the NW and SO cohorts from the SCORPIO study indicating the proportion of each group with evidence (red) or no evidence (green) of previous SARS-CoV-2 infection, and where no sample was collected (grey). **A-C** were generated by the group of Professor Sir Aziz Sheikh and are adapted from van der Klaauw et al, 2023[195]. Error bars indicate 95% CIs, n indicates the number of individuals in each category.

4.2.4. Cellular response to vaccination in individuals with severe obesity

Specific T cell activation has previously been identified as reduced following inactivated virion vaccination against influenza in obesity[231]. Here, I wanted to determine if the same would be the case for mRNA vaccination against SASR-CoV-2. I used the ELISpot assay for IFN-γ production to assess the levels of SARS-CoV-2 antigen specific $CD8^+$ T cells induced by mRNA vaccination in SO and NW individuals.

T cell reactivity against SARS-CoV-2 M and N proteins is a marker of previous infection as these proteins are not encoded by the vaccines. As time from vaccination increased the number of individuals with detectable T cell responses against N and M increased (**Figure 4.4A**). 69% of those identified as having been infected by ELISpot were also identified by RT-PCR test, however in three cases an individual positive by RT-PCR test did not yield a positive T cell response against N and M proteins.

Prior to receipt of a third booster, 8/22 individuals with SO had S specific $CD8^+$ IFN-γ responses below the threshold of positivity (**Figure 4.4B**). In contrast proportionally fewer, only 1/16, of the NW controls fell below the threshold (P = 0.0344, Fisher's Exact test, one-sided). This is suggestive of poorer maintenance of antigen specific $CD8^+$ T cells following the initial vaccine schedule in those with SO. However, prior to and following third dose, no significant differences in S specific T cells responses were found by Multiple Mann Whitney testing (**Figure 4.4C.**). S protein specific T cells were significantly boosted by vaccination. Since T cell responses are expected to peak between 7 and 15 days following antigenic stimulation[250], V3D8 measures were considered to be representative of peak response. Both groups had a large range of specific T cell numbers at V3D8, spanning 150 to 2000 $\Delta SFU/10^6$. Some of this diversity may be due to variation in the timing of the sample collection, which was limited by participant availably. However, there may also be considerable heterogeneity in the T cell response triggered

by vaccination, regardless of BMI, as a range of values were also present at V3D28. Only one individual (from the SO group) did not make a T cell response, detectable at any time point. This participant also had lower measures for humoral response and showed evidence of SARS-CoV-2 infection between days 28 and 105, indicating a lack of sustained protection from third dose vaccination.

At days 105 and 185 there was no significant difference in S specific $CD8^+$ T cell response (**Figure 4.4D**). By V3D185 the number of participants had reduced due to infection and study drop out, leaving only 6 NW and 12 SO individuals in this comparison. This may explain why the median $\Delta SFU/10^6$ for the SO group at V3D185 (209.5) was higher than at V3D105 (186.65) as those with lower T cell levels have increased susceptibility to infection. Alternatively, $CD8^+$ memory T cell numbers have been observed to be well conserved following vaccination and may account for this. I found no difference in the percentage change in the number of S specific T cells from the peak of the response at V3D8 to V3D105 (**Figure 4.4E**). Together this suggests no significant differences in the generation or maintenance of a vaccine specific $CD8^+$ T cells following third dose vaccination in individuals with SO compared to those of NW.

4.2.4.1. T cell protection against the circulating omicron variant

At the time of this study, the main circulating variant of concern was omicron. I assayed IFN-γ production by T cells specific to the mutated spike protein of omicron in the NW cohort at timepoints V3D0-V3D28. Response against the omicron variant was less than that against the WT. However, the magnitude of this difference was small, and none fell below the limit for a positive response, indicating that T cell response was well conserved against the omicron variant. Therefore, T cells likely provide a similar level of protection against the omicron variant as the WT virus (**Figure 4.4F**).

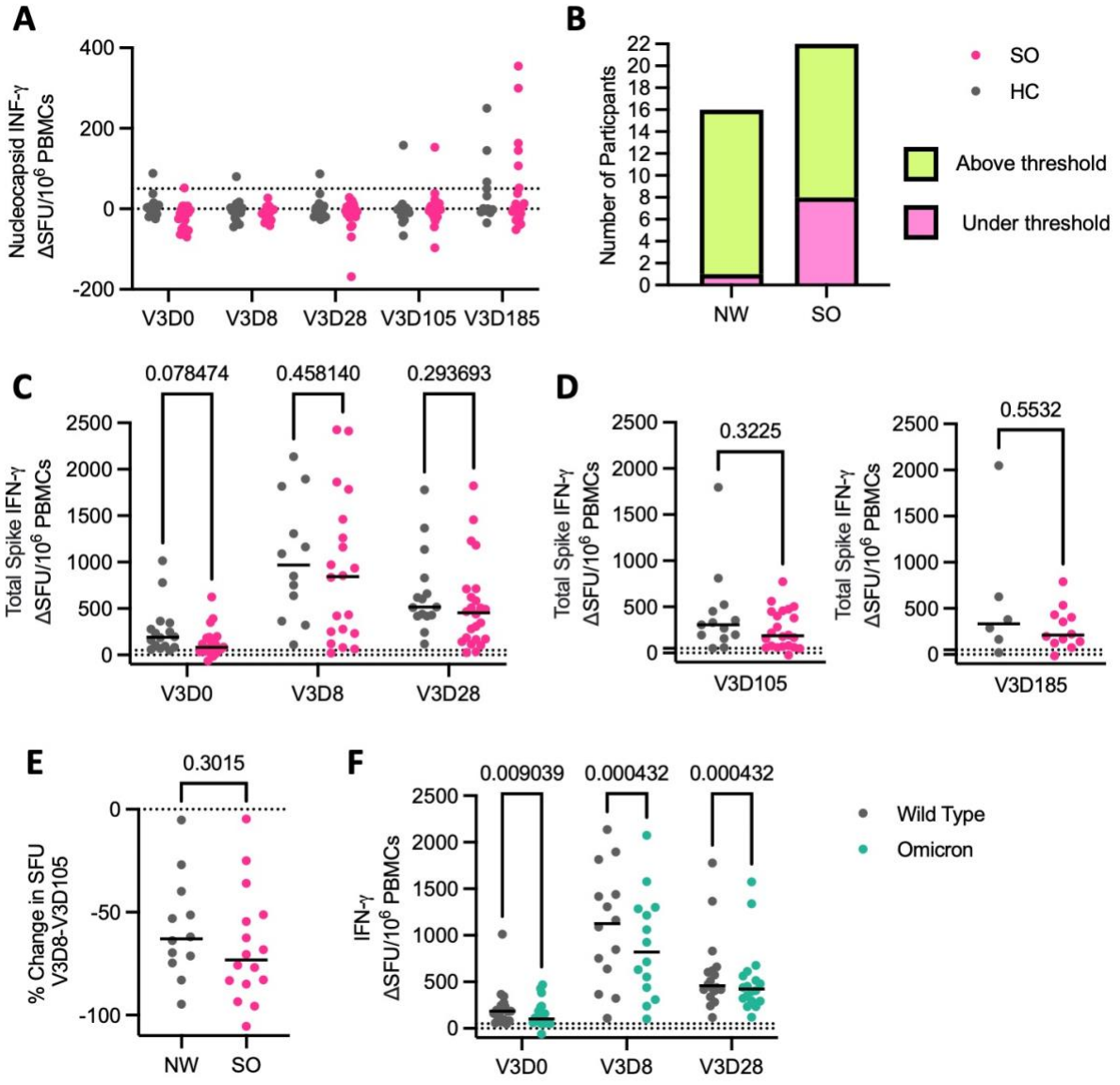

Figure 4.4. T cell responses to vaccination in individuals with severe obesity. **A)** SARS-CoV-2 membrane and nucleocapsid reactive IFN-γ producing T cells of SCORPIO participants at timepoints prior to and after third dose vaccination. **B)** The number of participants from the sampled day 0 NW and SO groups with ΔSFUs/10^6 above (green) and below (pink) the threshold of positivity for IFN-γ ELISpot following stimulation with S peptides. **C)** Comparison of spike specific $CD8^+$ T cells as indicated by IFN-γ production at days 0, 8, and 28 after third dose mRNA vaccination in PBMCs of individuals of NW and with SO (Multiple Mann Whitney Tests). **D)** Comparison of spike specific $CD8^+$ T cells as indicated by IFN-γ production at days 105 **(left)** and 185 **(right)** after third dose mRNA vaccination in PBMCs of individuals of NW and with SO (Mann Whitney Tests). **E)** Comparison of percentage change in spike specific IFN-γ SFU from day 8 to day 105 after third dose between individuals of NW and with SO. (Mann Whitney Test). **F)** Comparison of WT and omicron variant spike reactive $CD8^+$ T cells as indicated by IFN-γ ELISpot at days 0, 8, and 28 following third dose vaccination in NW control cohort (Multiple Wilcoxon matched-paired signed rank tests). For all plots each dot represents one single individual. SO + WT (Dark pink), NW + WT (grey), NW + omicron (teal) Where horizontal bars are present, these represent the median value of the group. Dotted lines indicate 0 for all plots and a threshold for positivity of Δ50 SFU/10^6 for ELISpot assay results.

4.2.5. Humoral response to vaccination in individuals with severe obesity

Obesity is also associated with diminished humoral responses to vaccination. In the absence of a clear defect in the effector T cell response, this may be responsible for the observed impairment in protection by vaccination.

4.2.5.1. Antigen specific antibodies

Prior to third dose vaccination there was no significant difference in serum RBD specific IgG levels between groups (**Figure 4.5A**). However, following third dose vaccination RBD specific IgG was boosted to higher levels in the SO group when compared to NW. Subsequently, antibody levels declined in both groups to be comparable at 105 and 185 days after vaccination (**Figure 4.5B**). Waning of RBD specific IgG levels between V3D28 and V3D105 as a proportion of day 28 levels was significantly higher in individuals with SO than NW (**Figure 4.5C**). This indicates a greater and earlier peak response followed by reduced IgG maintenance in those with SO. A similar pattern was seen in the quantification of total spike binding antibody in the serum. Total spike binding antibody in the SO group was boosted to significantly higher levels at V3D28 than those of NW and declined to comparable levels by V3D105 (**Figure 4.5D**). Together this shows that, individuals with SO rapidly produce larger quantities of vaccine specific antibody upon mRNA booster, compared to those of NW. However, these antibodies are not maintained and fall to levels more similar to that of NW controls within 3 months of vaccination.

4.2.5.2. Neutralising activity

NT50 against the WT live virus was measured at all timepoints. A larger proportion of individuals with SO compared to NW, had NT50s below the limit of quantification (NT50 = 4) prior to third dose (**Figure 4.5E**), indicating a lack of protection by neutralising antibodies. Following third dose, the NT50 of those with SO increased to comparable levels to those of NW at V3D8 and V3D28 (**Figure 4.5F**). Following day 28, neutralising capacity began to wane but did not significantly differ between groups at either V3D105 or V3D185 (**Figure 4.5G**). However, the proportional change in neutralising capacity between peak at day 28 and day 105 was significantly greater in individuals with SO. This

suggests accelerated waning of neutralising antibodies in individuals with SO when compared to NW controls (**Figure 4.5H**). The range of NT50 values of individuals with SO was much larger than that of NW controls at days 8-185, indicating a wider range of neutralising responses. Neutralising capacity continued to decline to V3D185 in both groups, suggesting that the maintenance of a circulating neutralising antibody population is poor following mRNA booster vaccination, regardless of the BMI of the vaccinated individual.

In both SO and NW groups NT50 values positively correlate with levels of RBD specific IgG in the serum (**Figure 4.5I**). However, comparison of groups suggests that for a given anti-RBD-IgG level individuals with SO have lower NT50 than NW controls. Therefore, in the immediate response to third dose anti-SARS-CoV-2 mRNA vaccination, individuals with SO seem to make more antibodies, but with a lower neutralising capacity.

4.2.5.3. Neutralising capacity against variants

The peak neutralising capacity at V3D28 was also tested against the omicron variant of the SARS-CoV-2 virus. NT50 against the omicron variant was more than an order of magnitude lower than that against WT virus in both SO and NW (**Figure 4.5J**). Similar to the results seen against the WT, NT50s against omicron were higher but not significantly in individuals with SO. NT50s against the omicron variant at the peak of the antibody response are comparable to, if not lower than, those against the WT virus at day 185. Therefore, protection against infection from the omicron variant by neutralising antibodies is poor after mRNA vaccination against the WT virus.

T cells against WT spike have been seen to have an improved ability to cross-react with SARS-CoV-2 variant spike proteins compared to antibodies[251,252]. This is reflected in the T cell and NT50 data collected in this study, as T cell responses were conserved against omicron but NT50 was not. While neutralising antibodies are associated with protection against infection T cells are associated with protection against the development of severe disease[253,254]. This may provide some explanation as to why levels of breakthrough infection in our cohorts were so high during the omicron wave of the pandemic.

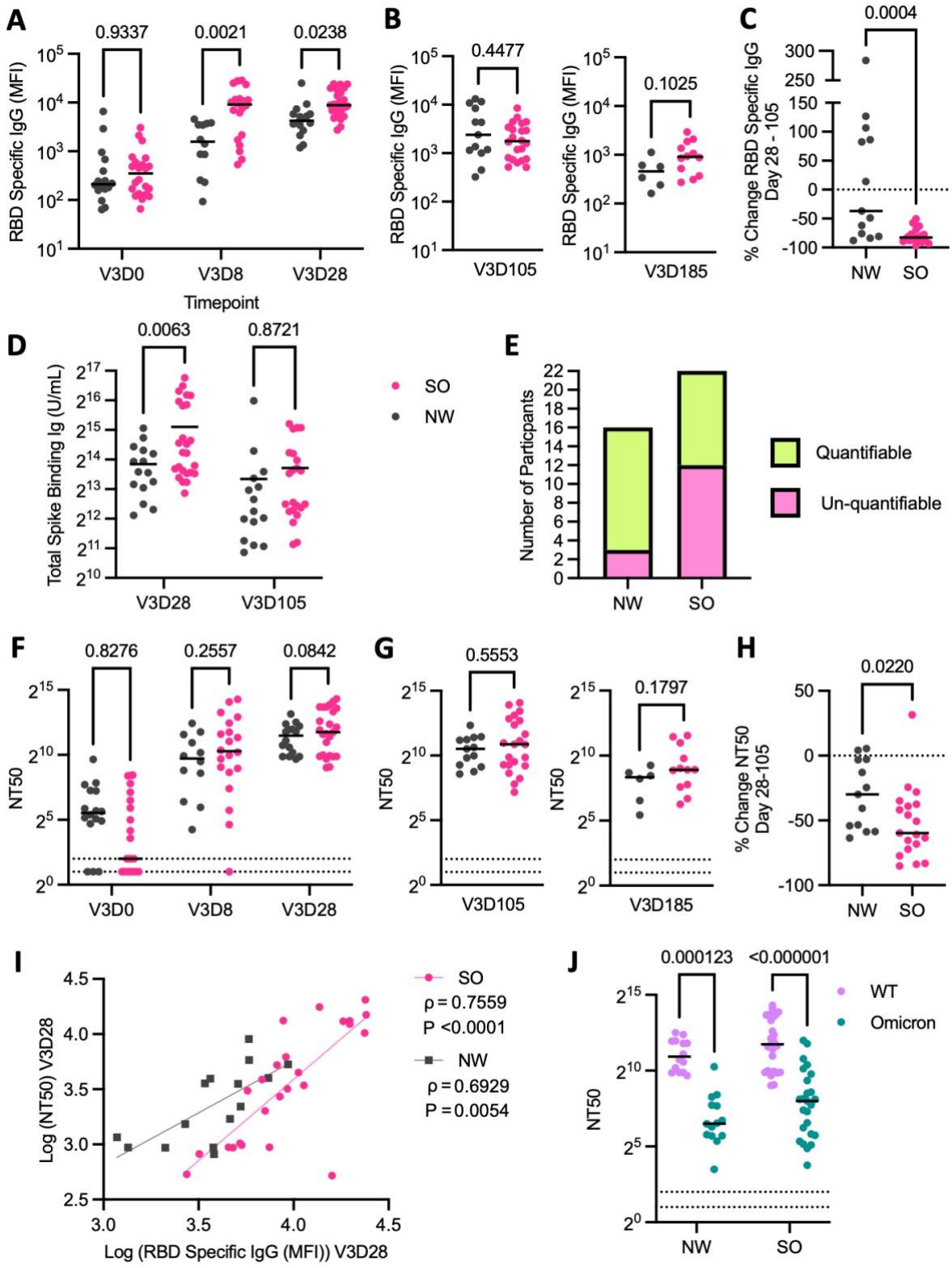

Figure 4.5. Humoral responses to vaccination in individuals with severe obesity. A) Comparison of the levels of RBD binding IgG (median fluorescence intensity) in the serum at days 0, 8, and 28 following third dose mRNA vaccination between NW and SO (Mixed-effects analysis with Sidak's multiple comparisons tests). **B)** Comparison of the levels of RBD binding IgG in the serum at days 105 **(left)** and 185 **(right)** after third dose mRNA vaccination between NW and SO (Two-tailed Mann Whitney test). **C)** Comparison of the percentage change in MFI as a measure of levels of RBD binding IgG between days 28 and 105 after third

dose mRNA vaccination between NW and SO (Two-tailed Mann Whitney test). **D)** Comparison of total spike binding antibody in the serum at days 28 and 105 after vaccination as measured by the Roche Elecsys anti-SARS-CoV-2 electrochemiluminescence immunoassay (Mixed-effects analysis with Sidak's multiple comparisons tests). **E)** Number of participants from the NW and SO groups with quantifiable (green) neutralising capacity and capacity below the limit of quantification (pink). **F)** Comparison of the live virus neutralising capacity at days 0, 8, and 28 following third dose mRNA vaccination between NW and SO (Mixed-effects analysis with Sidak's multiple comparisons tests). **G)** Comparison of the live virus neutralising capacity at days 105 **(left)** and 185 **(right)** after third dose mRNA vaccination between NW and SO (Two-tailed Mann Whitney test). **H)** Comparison of the percentage change in live virus neutralising capacity between days 28 and 105 after third dose mRNA vaccination between NW and SO (Two-tailed Mann Whitney test). **I)** Relationship between $\log_{10}$ transformed specific antibody levels and live virus neutralising capacity at day 28 following vaccination (Two-tailed Spearman correlation coefficients and indicative linear regression lines). **J)** Comparison of live virus neutralising capacity against the WT SARS-CoV-2 virus (purple) and omicron variant (teal) in individuals with SO and NW at day 28 serum after vaccination (Multiple Wilcoxon matched-pairs signed rank Tests). For all plots each dot represents one single individual. SO (dark pink), NW (grey) unless otherwise stated. Where horizontal bars are present, these represent the median value of the group.

4.2.6. Heterogeneity in individuals with severe obesity

The S specific T cell response was heterogenous in both groups however, the range of humoral responses seen in SO was much more than that in NW. As such S specific $CD8^+$ effector T cell responses positively correlated with measures of humoral response (total spike specific Ig, RDB specific IgG, and live virus neutralising capacity) in the SO group but not in the NW group (**Figure 4.6A-C**). The humoral responses of individuals with SO appear to be divided into two subgroups, those with a high peak response and those with a lower response, more comparable to NW controls (**Figure 4.6D**). A NT50 of 10,000 was set as the threshold for a high response and 8/25 day 28 SO samples fell above this threshold and were defined as high responders. The more moderate responders had NT50, RBD-IgG, and Spike-Ig measures comparable to the NW control group at day 28. The high responders had increased humoral measures but a range of T cell responses.

I assessed whether clinical or demographic data could explain distinct grouping of humoral responses in individuals with SO. First, I considered each individual's BMI, severe obesity is defined as any BMI >40kg/m^2 and therefore there is a wide range of BMIs represented in our dataset. There was no significant difference in the BMIs of the high and moderate responders (**Figure 4.6E**). Leptin is an adipokine involved in immune regulation and is elevated in obesity[255]. However, there was no significant difference in clinical leptin measures in the moderate and high responder groups, in the individuals for which this

data was available (**Figure 4.6F**). Sex can play a role in the immune response as sex chromosome genes and sex hormones can interact with the immune system[256], however neither sex was overrepresented in the high or moderate responder groups (**Figure 4.6G**). The BNT162b2 or mRNA-1273 vaccine were used for third dose vaccination, again, neither was disproportionately associated with the high responder group (**Figure 4.6H**). NW controls were more frequently vaccinated with BNT162b2, this was due to the timing of booster vaccination of at-risk groups and healthy individuals and changes in the availability of different vaccines. As both vaccines were similarly formulated and mRNA based, we did not expect to see a significant difference in the immune responses they invoked. Either the BNT162b2 mRNA vaccine or the ChAdOx1 adenoviral vaccine was used for the initial two-dose vaccine schedule for these individuals. High responders disproportionately received the ChAdOx1 vaccine as their initial vaccine course (**Figure 4.6I**). A mix of vaccine mediums may lead to a higher magnitude of immediate humoral response[257], however, a significant proportion of the NW and moderate responder groups also received the ChAdOx1 vaccine and did not experience such a high response. The impact of immunisation with a variety of vaccine types was also highlighted by the fact that only 1/8 (12.5%) of the high responders received three doses of the same vaccine (BNT162b2), despite the fact that individuals vaccinated thrice with BNT162b2 represented 35% of the total dataset at this timepoint (**Figure 4.6J**). The clinical and immunological data available following the SCORPIO study was not sufficient to explain the heterogeneity of responses to third dose vaccination in individuals with SO. As others have observed the mode of initial antigen exposure can shape subsequent responses to SARS-CoV-2 spike protein[258]. This may explain to some extent the high antibody response in certain individuals; however, it is clear there are other contributing factors yet to be determined.

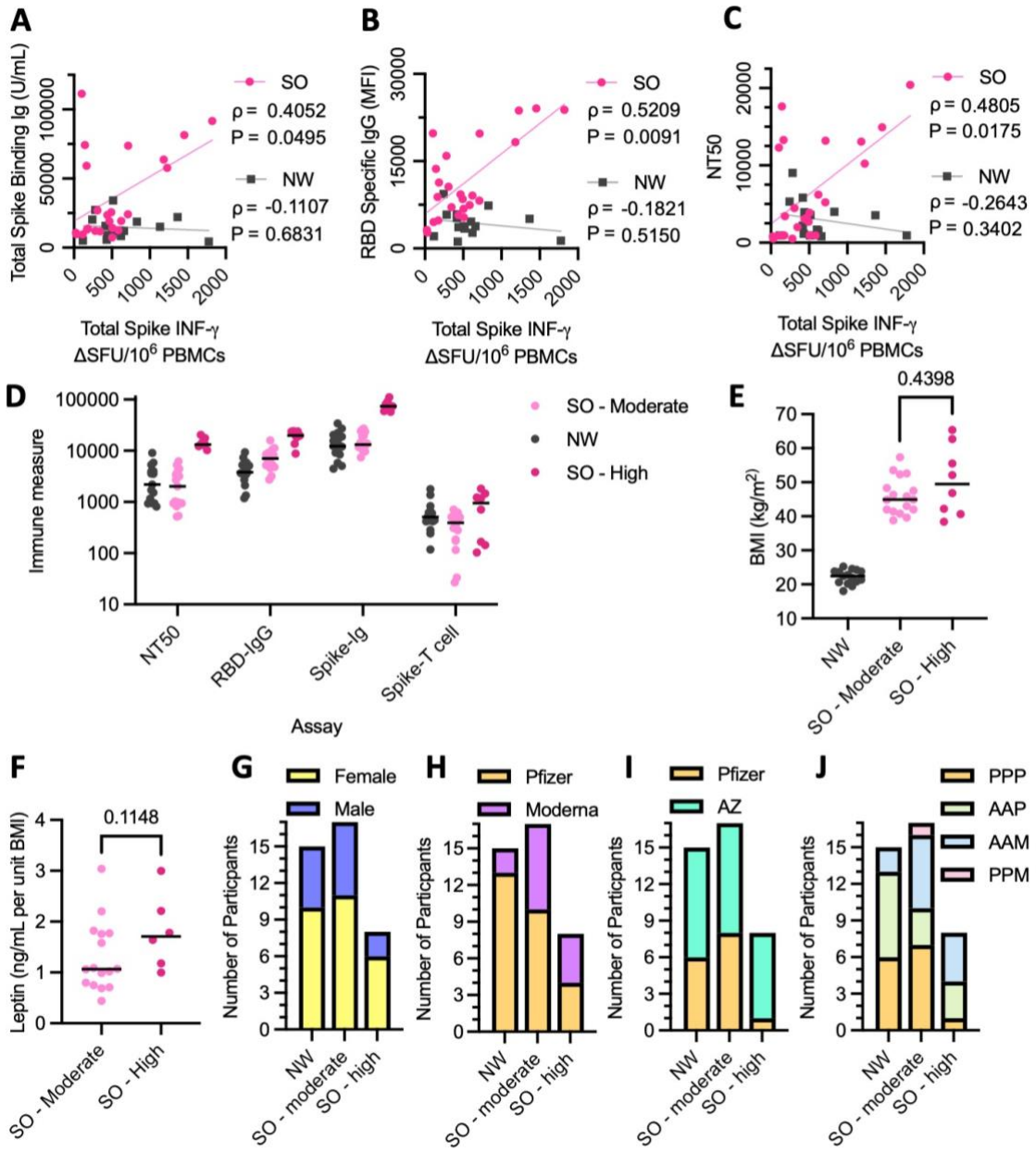

Figure 4.6. Heterogeneity of the immune responses of individuals with severe obesity. A-C) Relationship between spike specific $CD8^+$ effector T cell response and **(A)** total spike binding antibody **(B)** RBD binding IgG levels **(C)** live virus neutralising capacity, at day 28 after third dose vaccination (Two-tailed Spearman correlation coefficients and indicative linear regression lines) **D)** Comparison of immunological measures at day 28 after third dose: live virus neutralising capacity, RBD specific IgG, spike specific Ig, and spike specific T cells measured, in the NW cohort, and moderate and high responder sub groups of the SO cohort. **E)** Comparison of the BMI of moderate and high responders (Two-tailed Mann Whitney Test) and NW controls. **F)** Comparison of the serum leptin of moderate and high responders (Two-tailed Mann Whitney Test) **G-J)** Stacked bar charts of the number of individuals from each group that **(G)** are female (yellow) or male (purple) (**H)** received BNT162b2 (orange) or mRNA 1273 (lilac) as their third dose of vaccine against SARS-CoV-2. (**I)** received BNT162b2 (orange) or ChAdOx1 (aquamarine) as their first two doses of vaccine against SARS-CoV-2 **(J)** received the following combination of vaccines: Three doses of BNT162b2 (orange), two doses of ChAdOx1 then one of BNT162b2 (green), two doses of ChAdOx1 then one of mRNA1273 (blue), or two doses of BNT162b2 then one of mRNA1273 (pink). All relevant plots one dot indicates a value from a single individual. Where present horizontal bars indicate median of a group. **A-C)** NW (grey), SO (pink). **D-F)** NW (grey), moderate responder SO (pale pink) and high responder SO (dark pink).

4.3. Discussion

4.3.1. Results

The impact of immune dysregulation caused by high BMI is of increasing importance as prevalence of obesity increases globally. We identified that individuals with obesity were at increased risk from COVID-19, despite vaccination against the SARS-CoV-2 virus. Obesity is associated with a number of comorbidities including diabetes and cardiovascular disease[259]. These conditions have additionally been associated with increased risk of morbidity and mortality from SARS-CoV-2 infection[260,261]. When considering differences in infection risk it is important to recognise that many factors may confound this. Severe obesity can be debilitating and hinder mobility, therefore these individuals may be less likely to travel and mix with others, reducing their risk of infection. Comorbidities may also influence response to vaccination; however steps were taken to reduce the influence of such confounders in this study. In the clinical study, many of the NW controls were recruited from the hospital staff, by virtue of their professional environment these individuals may have higher levels of SARS-CoV-2 exposure. Conversely their specialised training and education may lead them to take more action to avoid disease than the general population. More comprehensive understanding of the failure of adaptive immunity to provide protection after vaccination will aid in the prevention of severe outcomes in this group. It is clear that those with severe obesity may require more frequent vaccination or alternative modes of disease prevention.

I found no evidence following a third dose of vaccine that antigen specific $CD8^+$ effector T cell responses were impaired in SO. This mirrors the results of previous studies including one study of 30 individuals with obesity which found no significant difference in $CD4^+$ and $CD8^+$ T cell responses up to five months after two ChAdOx1 vaccines when compared to a group of normal weight controls[262]. Together, it appears that protection provided by antigen specific effector T cells does not differ in individuals with obesity up to six months following vaccination. Although, an exhaustive analysis of T cell phenotypes was not completed and responses prior to third dose suggested some lack of maintenance in severe obesity. Subsequent analysis of humoral responses indicate that reduced protection against severe outcomes experienced in individuals with obesity is unlikely to be solely due to a deficit in T cell response. The antibody response to third

vaccination in individuals with SO peaked to higher titres than that of NW controls before waning much more rapidly. This suggests a quick initial expansion of antibody secreting plasmablasts, without the long-term maintenance of a corresponding LLPC population. As LLPCs are thought to mainly arise from the GC response, the generation of GCs may be reduced or impaired in the response to vaccination in people with obesity. Neutralising capacity did not peak at higher levels in SO but did experience similar accelerated waning. Therefore, at the peak of the antibody response, antibodies are less neutralising in SO than in NW. One explanation for this could be that the excess antibody produced at the peak of the response is non-neutralising. Neutralising antibodies have been found to arise later after initial vaccination than other, non-neutralising antibodies[136], which may be the case here. The neutralising capacities of antibodies are exerted via their Fc regions[263], these regions may differ in the antibodies made in SO. Alternatively, this observation may be a result of an impairment of affinity maturation in people with SO. Antibody affinity is also associated with neutralising capacity and therefore those that have not undergone affinity maturation are likely to be less neutralising[258,264]. LLPCs are thought to be a product of high affinity B cells late in the GC reaction, and affinity is an important factor in their subsequent survival[265]. It is possible that an impaired GC response may lead to fewer LLPCs which have a poorer chance of survival in severe obesity. Neutralising capacity is important for protection against symptomatic disease and this accelerated waning may be in part responsible for the disease breakthrough and severity seen in obesity.

In addition to the overall high initial antibody responses and increased waning seen in SO the humoral responses to vaccination in this group were incredibly heterogenous. This is similar to the pattern seen when individuals with immune dysregulation due to PID and ICB were assessed in the previous chapter. It is clear that as with these individuals, the extent of immune dysregulation caused by severe obesity can massively vary. Obesity can lead to a range of levels of metabolic dysfunction[266] which subsequently means a range of states of immune dysregulation. What is not clear, from the data available, is the reason why some individuals with SO have such high responses while others are low.

4.3.2. Conclusions and future directions

Through the collaborative SCORPIO study, I and others show that immune dysregulation in severe obesity means that individuals are at increased risk from COVID-19 disease despite vaccination. This was not due to a deficit in antigen specific T cells but instead appeared to result from an impairment in the production of a robust humoral response to vaccination. Additionally, this was not the case for all individuals with severe obesity, some were able to produce a strong cellular and humoral response to vaccination, indicating response to mRNA vaccines in this group is not homogenous.

The progression of the COVID-19 pandemic and emergence of variants of concern such as the omicron variant were significant obstacles to the SCORPIO study. Cohort sizes were initially moderate due to accelerated roll out of third dose vaccines and a small timeframe for participant recruitment. A large wave of omicron infections further reduced cohort sizes and lead to a bias towards the exclusion of individuals with poorer immune responses at later timepoints. However, evidence that the neutralising capacity against WT virus does not translate to equivalent protection against the omicron variant means that a breakthrough infection with omicron does not necessarily reflect a poor vaccine response. Therefore, within this study we were unable to identify whether accelerated waning of the antibodies in SO ultimately led them to fall below the levels of NW. A repeat longitudinal study over the autumn booster campaign, with expanded cohort sizes may enable this distinction. Additionally, the study of larger cohort of individuals with severe obesity may facilitate the identification of the factors leading to heterogeneity of response in this group. Although the proportion of the UK with obesity is increasing, those with severe obesity make up a small part of this population and often have additional comorbidities which could confound the recruitment of larger cohorts.

One potential explanation for the accelerated waning of antibody in individuals with SO may be the clearance of the antibody itself. The neonatal fragment crystallizable receptor (FcRn) is an IgG Fc receptor expressed on mammalian cells and important in the regulation of serum IgG levels. The FcRn can bind to IgG, and prevent it from undergoing lysosomal degradation, and in doing so increases the half-life of IgG antibodies[267]. FcRn expression is reduced in adipose tissue and has been previously suggested as an explanation for increased rates of IgG elimination[268,269]. As FcRn only binds to IgG an

assessment of whether other antibody isotypes also wane, by ELISA or Luminex assay, could substantiate the theory that the RBD specific IgG waning seen is FcRn dependent.

Spectral flow cytometry in the SCORPIO study suggested that individuals with SO had increased proportions of IgM^+ RBD specific memory cells and fewer class switched after vaccination[195]. This provided additional suggestion of the impairment GC responses. Sequencing and subsequent transcriptional analysis of antigen specific cells should consolidate this data and provide further detail on the phenotypes of B cells in severe obesity. This analysis could be completed on existing samples and would enable the expression of a broader range of markers to be assessed than is possible by traditional flow cytometry. A combination of B cell surface proteins such as CD19, CD20, CD24, and CD38 and transcription factors including RAG1, IRF4, and BCL-6 associated with different stages of B cell differentiation can be quantified in this way. This should detect smaller differences in the activity and functionality of antigen specific B cells between groups.

Affinity maturation typically occurs within the GC and enables the production of high affinity B cells and antibodies. ELISAs or competitive binding assays could be applied to existing SCORPIO serum samples, to determine the avidity and affinities of antibodies in these individuals. Any suggestion of reduced affinities would contribute to evidence dysfunction of the GC in SO. Additionally, poor binding affinity could contribute to more rapid clearance of antibody and ASCs demonstrating a mechanism for the observed accelerated waning. Poor binding affinity may also influence the neutralising capacities of antibodies. Furthermore, the epitopes within the S protein could impact the function of the antibodies produced. Epitope mapping could be conducted by, indirect ELISAs against short peptide fragments[270] or peptide arrays[271] with existing serum. Alternative methods such as co-crystallisation and structure solution, mutagenesis, or sequencing and computational predictive methods could also be applied[272]

Alternative methods for the protection of individuals with severe obesity from COVID-19, above alterations to vaccination must also be considered. This is especially important as one individual in our study demonstrated a complete absence of T cell response, suggesting it is unlikely further vaccination will boost protection. It is unclear what impact weight loss, especially ongoing weight loss, will have on vaccine responses and risk from

COVID-19. The clinical treatment of severe obesity with low calorie liquid diet[273], bariatric surgery[274], and increasingly glucagon-like peptide-1 receptor agonists[275] all represent different scenarios of weight loss in which response to mRNA vaccination could be investigated. This would inform whether vaccination is effective during the process of weight loss or provides a better response in those of stable weight.

In summary, this work identified increased risk from and abnormal humoral response to SARS-CoV-2 in individuals with severe obesity after vaccination, with an indication that this may be due to dysregulation of the GC response. Broader analysis of the humoral response to vaccination in these individuals may reveal a mechanistic link between chronic inflammation in obesity and the broad range of immune responses to vaccination observed in individuals with SO.

5. B cell differentiation in severe obesity

5.1. Introduction: protection from SARS-CoV-2 provided by circulating antibodies

In the previous chapter I display the abnormal antibody response to vaccination in some individuals with severe obesity. Circulating antibodies are the first line of adaptive defence against infection. There are a number of factors which influence the strength of this defence including but not limited to concentration, isotype, epitope, affinity, and avidity. In-depth analysis of the nature of the antibodies produced against an antigen can be completed by interrogating the cells which make them.

5.1.1. Antibodies against SARS-CoV-2 antigens

5.1.1.1. Class switching and antibody isotypes in protection against SARS-CoV-2

IgG isotype antibodies make up the majority of antibody found in the serum[276] and are regarded to play the most significant role in protection against pathogens. Other unswitched and switched antibody isotypes also contribute to protection following COVID-19 vaccination and infection. RBD binding IgG, IgM, and IgA have all been found to positively correlate with live virus neutralisation and the presence of a combination of all three is associated with increased neutralising capacity[277]. It has also been suggested that IgM and IgG1 make the largest contribution to neutralising capacity following infection with a small contribution coming from IgA[278]. Additionally, depletion of IgM from convalescent plasma leads to the most substantial loss of SARS-CoV-2 neutralising activity of all isotypes[279]. When clones of IgA monomers specific to SARS-CoV-2 proteins were compared to IgG equivalents they were found to be two-fold less neutralising, however IgA dimers against the same targets were 15 times more neutralising than monomers[280]. Similarly, pentameric IgM monoclonal antibodies derived from IgM immune memory cells following infection outperform identical monomeric IgG in neutralising SARS-CoV-2[281]. There is therefore significant evidence for the role of antigen specific IgM and IgA in protection against SARS-CoV-2, much of which may be due to multimeric structures enabling action not possible by monomeric IgG. Spike specific IgM

and IgA levels were seen to be much more variable between groups of individuals naïve, vaccinated, and recovered from COVID-19 when compared to IgG[282], this variation may directly contribute to heterogenous levels of protection against disease in different individuals.

5.1.1.2. Neutralising epitopes in SARS-CoV-2

There are a number of antibody binding epitopes on the SARS-CoV-2 S protein. The RBD portion of the protein is most associated with neutralisation as this is the location of ACE2 binding for viral entry to the host cell. The neutralising activity of SARS-CoV-2 antibodies positively correlates with competition with ACE2[283]. Nonetheless, neutralising epitopes can also be found on other portions of the protein. Neutralising epitopes can be found in the NTD, SH, and FP regions of the S protein, the NTD being the second most common region after the RBD[284]. Neutralising antibodies which bind the RBD or NTD prevent S binding to ACE2, whereas those targeting SH and FP typically prevent membrane fusion. Although neutralising antibodies most frequently target the RBD, the S2 region is more highly conserved and therefore those that bind to the SH and FP regions are more broadly neutralising across variants[284].

SHM can act both to broaden the neutralising antibody repertoire[285] and improve the affinities of neutralising antibodies through affinity maturation. Though, while some somatic mutations may increase antibody affinity they can simultaneously negatively impact stability, leading to the requirement for compensatory stabilising mutations[286]. IgG has the longest half-life of all antibody isotypes due to FcRn recycling[287]. However, this is subtype dependent, IgG1 and IgG3 compete for FcRn binding leading IgG3 to have a shorter half-life[288]. Antibodies can also undergo glycation and glycosylation which may further influence function and half-life[289,290]

Therefore, the functionality of S binding antibodies can vary, some may have little effect in directly preventing infection. As such antigen specific IgG readings will not tell a complete story about antibody mediated protection provided by vaccination.

5.1.2. Identification of specific cells and BCR genes in single cell sequencing

Advancements in single cell RNA sequencing (scRNA-seq) have expanded the capacity to analyse the sequences encoding BCRs. Heavy and light chains can now be paired, which was previously impossible using bulk sequencing techniques. The variable V(D)J regions of the heavy and light chains of the BCR of individual cells can also be paired with the transcriptome data from the cell of origin. This produces a comprehensive dataset from each sequenced cell involved in the immune response. Pairing this with the identification of antigen specific cells can enable the in-depth analysis of the dynamics and functionality of a humoral immune response to a specific immune challenge.

There are multiple ways to identify antigen specific cells. Broadly these can be split into two categories of methods: those which use antigen tags and those which use computer modelling to predict paratopes and epitopes based on V(D)J sequences. The method used most frequently is fluorescence staining and fluorescence activated single cell sorting (FACS). The target antigen is conjugated to a fluorescent tag and used to stain the cells of interest; the cells bound to the antigen tag can be sorted based on levels of fluorescence. This has been used in many studies with a variety of target antigens[291-293], however the need to sort individual cells can lead to low throughput and sorting may stress cells leading to transcriptional changes, low cell viability and selective cell death in vulnerable populations.

The use of nucleotide tags in protein detection can increase the number of markers or antigens it is possible to target, by eliminating the risk of spectral overlap from fluorophores. REAP-seq[294] and CITE-seq[109] are methods which conjugate nucleotide tags or oligos to antibodies enabling the detection of surface protein levels on cells in a scRNA-seq data set. mRNA and protein expression levels do not always correlate due to differential levels of transcription and translation. As such a combination of transcriptome and protein data can lead to better cell identification when considering known cell markers. In addition to this, these systems can be harnessed for the identification of specific B cells: Setliff et al[295] developed a method termed linking B cell receptor to antigen specificity through sequencing (LIBRA-seq) which used a panel of antigens labelled with different nucleotide tags to detect HIV and Influenza reactive B cells. This method still used FACS but was able to increase the throughput by using a

single fluorophore for all target antigens and unique nucleotide tags for subsequent assessment of specific antigen binding. Kramer et al[296] successfully adapted LIBRA-seq to detect SARS-CoV-2 spike specific cells for the analysis of the response to BNT162b2 vaccine. The Barcode Enabled Antigen Mapping (BEAM) protocol provided by 10X genomics follows a similar methodology to LIBRA-seq enabling the sorting of tagged B and T cells with subsequent V(D)J, BEAM, and transcriptome sequencing[297]. This protocol, however, still recommends the use of cell sorting prior to library preparation.

Computational methods for the identification of antigen specific cells minimise the cell processing requirements prior to DNA preparation. These techniques can be applied to unlabelled and unsorted cells, meaning they can also be applied to datasets retrospectively. However, these methods are predictive and remain in their infancy. The SPACE2 protocol[297] uses machine learning structure prediction to cluster antibodies expected to bind similar epitopes. Clustering of novel sequencing data with the sequences of antibodies with known binding sites, enables the prediction of binding epitopes. Methods proposed for the prediction of protein and antibody structure include IgFold[298], ImmuneBuilder[299], and AlphaFold[300] and their outputs can be used in protocols such as ClusPro-AbEMap[301] for epitope prediction. Each of these methods have been published in the past 5 years indicating rapid development in this area and large future potential for reliable computational prediction of antibody structures and binding.

5.1.3. Chapter aims

The SCORPIO study indicated a deficit in the maintenance and neutralising capacity of antibodies following mRNA vaccination in people with severe obesity. However, the study did not identify a definitive mechanistic reason for this. Further investigation into the characteristics of the antigen specific antibodies and cells in these individuals may provide evidence as to the functional root of antibody waning. I aimed to develop and apply a reliable technique for the identification of S specific B cells from vaccinated individuals collected during the SCORPIO study. The data generated by this assessment should address the diversity of antibodies produced in study participants and through their assessment I hoped to identify the factors contributing to accelerated antibody waning in obesity.

Therefore, in this chapter I address the following questions:

- Do the characteristics of secreted antibodies differ in individuals with severe obesity?
- Do the characteristics of encoded BCRs differ in individuals with severe obesity?
- How can S specific B cells be best identified in single cell sequencing datasets?
- What are the transcriptional differences between antigen specific B cells in normal weight individuals and those with severe obesity?

5.2. Results

5.2.1. Production of the HexaPro spike protein

Large quantities of trimeric S protein were required to assay samples for their S reactivity. As such, I established a system to produce batches of protein using the SARS-CoV-2 S HexaPro plasmid developed by Hsieh et al[302]. The HexaPro plasmid contains the sequence of the SARS-CoV-2 S protein with six proline substitutions, introduced to maintain the resulting protein in its membrane bound conformation (**Figure 5.1A**). Expression in human cell lines results in the production of His-tagged, modified trimeric S protein, appropriate for assaying the reactivity to the WT membrane bound protein. Protein was prepared by expression in human cell lines and purification by affinity and size exclusion chromatography (**Figure 5.1B**). To optimise culture duration for maximum protein production I confirmed that significantly more protein could be isolated following a six-day cell culture than three days (**Figure 5.1C**). Six- or seven-day incubations were used from thenceforth. To confirm that the HexaPro S produced was similar in structure to commercially available trimeric S protein products I ran SDS PAGE on reduced and non-reduced HexaPro S and trimeric S protein from AbCam (**Figure 5.1D**). Coomassie stain of the resulting gel identified no significant differences in the size of the proteins. I then used both proteins to coat either half of a 96 well flat-bottomed plate. This plate was subsequently used to quantify the levels of spike binding IgG, by ELISA, in two human serum samples, one known to have high antibody levels, the other low. A monoclonal RBD binding IgG was used to generate a standard binding curve for each protein. Both curves displayed increasing absorbance with increasing concentration of antibody, suggesting that the HexaPro S product is intact S protein. These curves were not identical,

which may have been as a result of the availability of binding sites due to protein conformation. Additionally, any presence of mono- and dimeric spike, or structural alterations may leave exposed binding sites not available in the AbCam spike. Irrespective of this, when the respective standard curves were used to interpolate the concentration of S binding IgG in the two serum samples tested, both proteins yielded similar results (**Figure 5.1E**). There was a clear distinction between the high and low antibody samples when tested with each protein. Although, the concentration values interpolated for both samples when assayed with the AbCam protein were slightly higher than the same values when using the HexaPro protein. From this validation I confirmed that the HexaPro S protein was sufficient for assaying S protein reactivity, so long as it was consistently used for all assays. This enabled the application of a number of assays for which the price of protein would have otherwise been prohibitive.

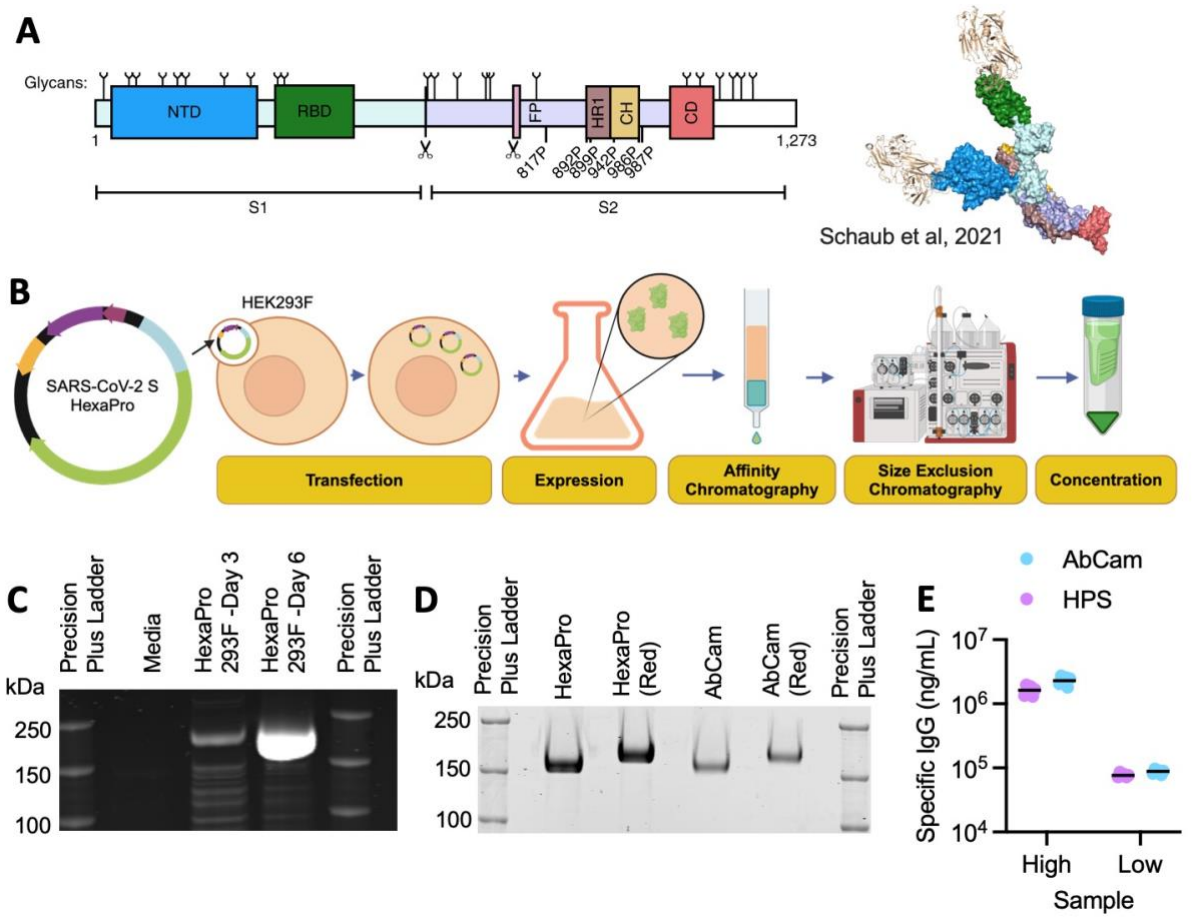

Figure 5.1. The production of trimeric HexaPro spike protein. A) Structure of the HexaPro spike protein. The location of prolines introduced to maintain the protein structure indicated by position number (**left**). Folded structure of the HexaPro spike protein with regions coloured corresponding to left panel, with two bound antibodies (gold) (**right**). Adapted from Schaub et al, 2021[107]. **B)** Schematic of the production of HexaPro Spike protein. The HexaPro plasmid is transfected into HEK293F cells and expressed for 6-7 days.

Protein is isolated from media by NiNTA affinity chromatography and purified by size exclusion chromatography. Final concentration and buffer exchange is achieved by spin concentration. **C)** Coomassie stained SDS PAGE of unconditioned media, media from transfected cells cultured for 3 days and media from cells cultured for 6 days. Band indicating the presence of HexaPro spike can be seen at 150-200kDa. **D)** Coomassie stained SDS PAGE of HexaPro spike and a commercially available AbCam trimeric spike run under reducing and non-reducing conditions. **E)** Comparison of interpolated total spike binding IgG from the serum of two donors (expected high and low concentration) as calculated from ELISAs using plates coated with HexaPro Spike (purple) and AbCam Spike (blue).

5.2.2. Isotype specific assessment of spike binding antibodies by ELISA

To determine the relative contribution of different isotypes to the S binding antibody repertoire of study participants I developed three HRP based ELISAs, one for each of IgA, IgM, and IgG. I conducted initial tests of these assays using serum from a healthy control at a number of timepoints following vaccination and infection. I then completed additional tests with day 28 serum from individuals of NW and with SO to determine the sensitivity of the assay and appropriate serum dilutions for analysis of the SCORPIO cohort (**Appendix C.1**).

I used these assays to assess the levels of S binding IgG, IgM, and IgA in the V3D28 and V3D105 serum of the participants of the SCORPIO study. I first compared the V3D28 absorbance values from my S binding IgG ELISA to the values previously obtained by Luminex assay and saw a strong positive correlation (**Figure 5.2A**). This confirmed the ability of the assay to quantify antibody levels in serum. For the IgG and IgM ELISAs concentration values were interpolated from a standard curve on each plate. However, the IgA standard did not contain sufficiently high concentrations for interpolation and absorbance values were used for cohort comparisons. The levels of S specific antibodies of all isotypes were more heterogenous in the individuals with SO. As such, a population of individuals with high levels of each isotype mean median values were higher at both timepoints for all isotypes in SO but only significantly so in IgA (**Figure 5.2B&C**). IgM has a short half-life of ~5 days and as such this timepoint may be too late to detect any significant differences in the early response[303]. Interpolated IgG concentrations correlated with Luminex assay measures (**Figure 5.2D**) with reduced strength reflecting the assignment of arbitrary values for those above the range for interpolation. The proportional change in absorbance or concentration from day 28 to 105 was higher in individuals with SO for all isotypes but again only significantly in IgA (**Figure 5.2E&F**). This

contrasts the statistically significant larger change seen in previous measures of IgG, however it has been demonstrated that although different S binding IgG serum assays show good correlation, they are not interchangeable[304]. This suggests that both the heterogeneity and impaired maintenance of the antibody response to vaccination in SO is not constrained to a single isotype. Therefore, the mechanism behind waning is unlikely to be one that exclusively targets IgG such as FcRn recycling.

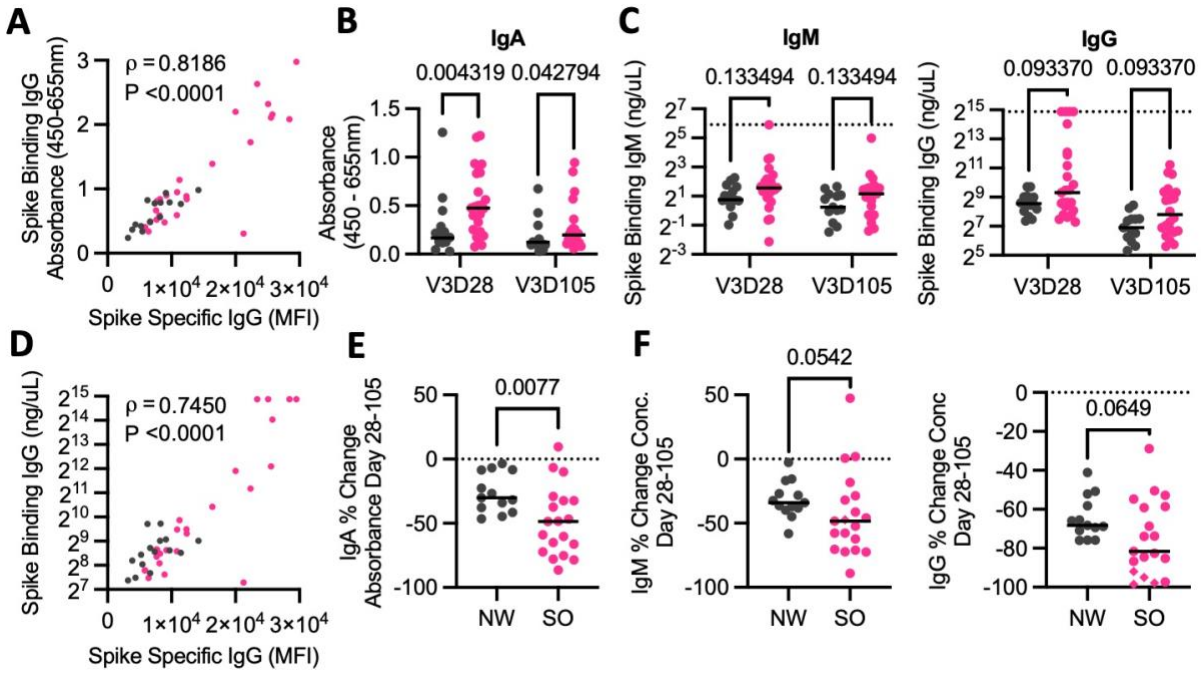

Figure 5.2. Isotypes of antibody response in individuals with severe obesity. A) Relationship between spike specific IgG at day 28 after third vaccination in individuals from the SCORPIO study as measured by Luminex assay and anti-spike indirect IgG ELISA, absorbance at 450nm. **B)** Comparison of spike specific IgA at day 28 and 105 following vaccination in NW and SO as indicated by indirect ELISA absorbance at 450nm – 655nm. **C)** Comparison of spike specific IgM (**left**) and IgG (**right**) concentrations at day 28 and 105 following vaccination in NW and SO as interpolated following indirect ELISA. **D)** Relationship between spike specific IgG at day 28 after third vaccination in individuals from the SCORPIO study as measured by Luminex assay and concentration interpolated from anti-spike indirect IgG ELISA. **E)** Comparison of % change in absorbance for spike specific indirect IgA ELISA for NW and SO individuals between day 28 and day 105 post vaccination. **F)** Comparison of % change in concentration for spike specific IgM (**left**) and IgG (**right**) interpolated from indirect ELISA for NW and SO individuals between day 28 and day 105 post vaccination. For all plots individuals from SO (pink) NW (grey) groups, a single point represents one individual. Scatter plots **(A&D)** show two-tailed Spearman correlation coefficients and indicative linear regression lines. Significance values indicate the results of **(B-C)** multiple Mann-Whitney tests or **(E-F)** Two-tailed Mann Whitney test.

5.2.3. SAffCon assay for serum antibody avidities

Most measures of antigen specific serum antibody levels are influenced by antibody affinity but do not provide a measure of it. The Fluidity One-M system uses a microfluidic diffusion chamber to determine the concentrations and binding interactions between a test sample and target (**Figure 5.3A**). The rate of diffusion of the test and target enables the calculation of both protein concentration and the affinity of binding between two proteins. The large size of the full-length spike protein is limiting in this assay due to the reduced rate of diffusion of large proteins. I instead produced a fluorescently labelled RBD protein by conjugating RBD protein to AF647 and purifying by size exclusion chromatography.

5.2.3.1. Validation of concentrations of binding antibodies

I assayed V3D28 serum samples from 20 individuals with SO and 13 individuals of NW using the SAffCon assay. Diffusion between samples is used to calculate the molar concentration of RBD binding antibody and the equilibrium dissociation constant (K_D) of the antibody-RBD complex. The Fluidity Intelligence Platform calculates and generates a cloud plot to visualise these measures for all samples and groups within an experiment. This revealed broader heterogeneity in the SO participants and less certainty in the calculated measures from this group (**Figure 5.3B**). The SAffCon assay measures total RBD binding antibody and is not isotype specific. RBD binding antibody concentrations obtained by SAffCon assay positively correlated with RBD binding IgG levels quantified by Luminex assay and total spike binding antibody quantified by Roche Elecsys assay (**Figure 5.3C&D**). The SAffCon assay, therefore, reliably calculated concentrations of RBD binding antibodies from serum. Concentration measures also confirmed the previous finding of the SCORPIO study, that total RBD binding antibody is increased in individuals with SO when compared to NW controls early after vaccination (**Figure 5.3E**).

5.2.3.2. Serum RBD binding avidity

Affinity is the strength of binding between an antibody paratope and antigen epitope. K_D is the ratio of the rate at which the antibody-antigen complex dissociates and the rate at

which antibody binds to target antigen (**Figure 5.3F**). As such a higher K_D indicates a lower affinity as rate of binding is low and dissociation is high. Avidity is a measure of overall strength of antibody-antigen interaction at all sites. Therefore, in the SAffCon assay the K_D measure gives an indication of the overall avidity in the serum.

I found that avidity was not significantly different between the two cohorts (**Figure 5.3G**) and did not correlate with antibody concentration, indicating that there was no association between the magnitude of response and strength of antibody binding (**Figure 5.3H**). The K_D measures of the individuals with obesity were calculated with wider CIs so should be stated with less certainty. However, these data suggest that differences in antibody maintenance and neutralising capacity between NW and SO are unlikely to be due to reduced antibody avidities.

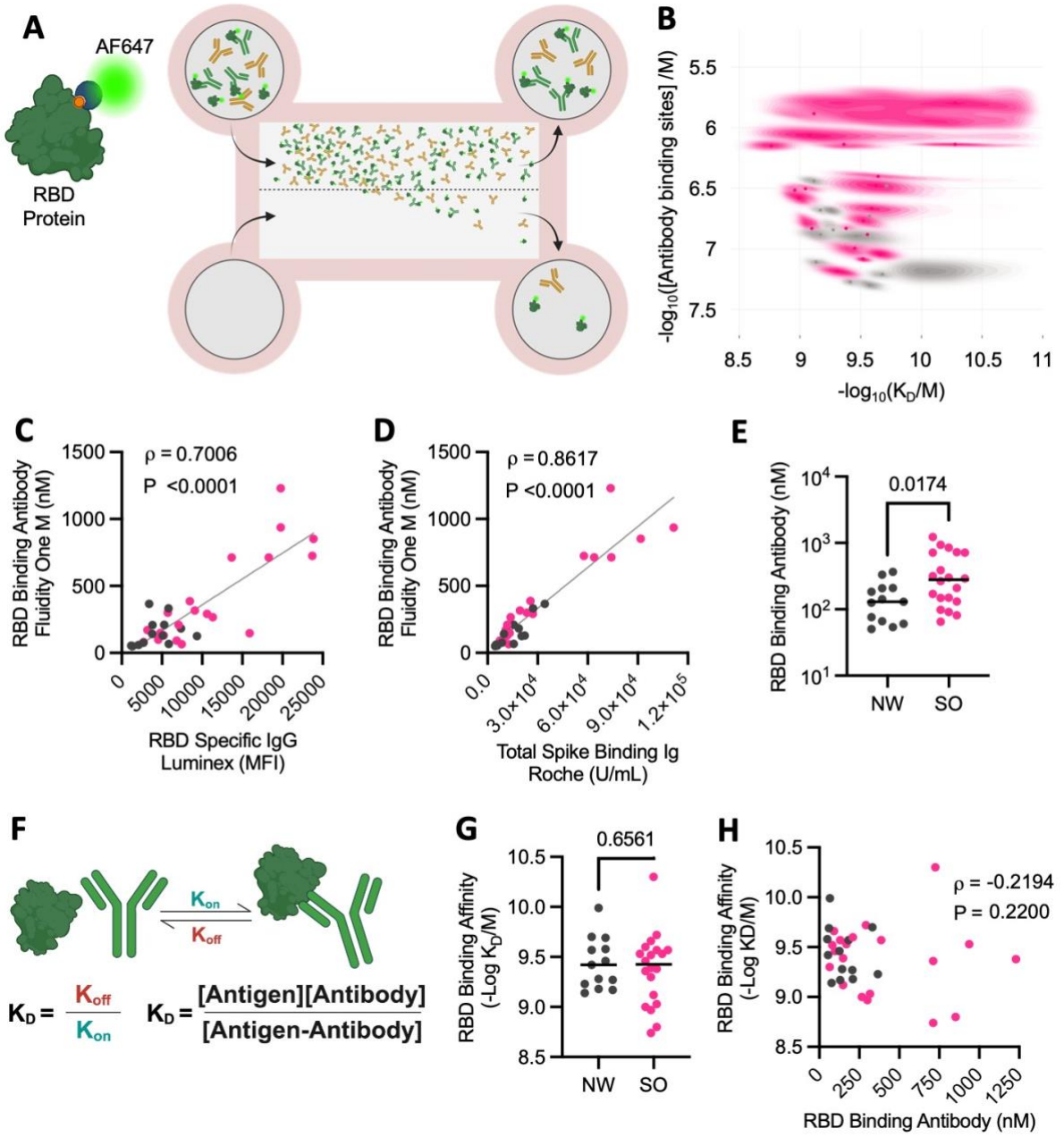

Figure 5.3. RBD binding antibody concentration and avidity in severe obesity. **A)** Schematic of the fluidity one M system. RBD protein was labelled with a fluorophore (**left**). Sample and labelled probe mixture are run in a flow cell parallel to flow buffer, diffusion of target, probe and target-probe complex across the membrane are measured at the end of the flow cell (**right**). Not to scale, created using Biorender.com. **B)** Cloud plot of measured target (RBD antibody binding sites) concentration and relative binding affinity for day 28 serum from NW (grey) and individuals with SO (pink), each cloud represents a single individual and the CIs for each measure. **C)** Relationship between concentration of total RBD antibody binding sites in serum as measured by SAffCon assay and **(C)** RBD specific IgG as measured by Luminex assay **(D)** total spike binding antibody as measured by Roche assay. Two-tailed Spearman's Correlation coefficients and indicative linear regression lines shown. **E)** Comparison of total RBD antibody binding sites (nM) at day 28 after third dose vaccination in NW and SO (Two-tailed Mann-Whitney test). **F)** Schematic of antibody antigen relationship. K_D as a measure of affinity is calculated from the ratio of the concentrations of free antibody and free antigen and the concentration of antibody-antigen complex (created using Biorender.com). **G)** Comparison of the average binding avidity ($-\log_{10}$ of K_D) of day 28 serum

in NW and SO (Two tailed Mann Whitney test). **H)** Relationship between concentration of total RBD binding antibody sites and antibody binding avidity as calculated by SAffCon assay (Two-tailed Spearman's Correlation coefficient). Points indicate data from a single individual, SO (pink), NW (grey). Where present horizontal bars indicate median of group.

5.2.4. Development of a spike multimer to detect specific cells in single cell sequencing

In the absence of any evidence of isotype or avidity differences from serum samples I turned my attention to the antigen specific cells responsible for the production of antibodies. LIBRA-seq as a method for the identification of antigen specific B cells, was initially designed to use small antigens to screen for high affinity HIV specific cells. Therefore, I adjusted this protocol to identify S binding B cells with a range of binding affinities. For this study I adapted the technique by producing two S proteins with different oligo tags. By incubating cells with these proteins directly prior to library preparation, without sorting, I was able to detect the specific binding cells based on detection of both nucleotide tags. This avoided prior single cell sorting, with the aim to reduce sample degradation.

5.2.4.1. Multimer preparation

I produced multimers by incubating biotinylated spike protein with streptavidin bound to a fluorophore (PE or APC) and nucleotide tag (AACCTTTGCCACTGC or GGTAACTCTGGTAGC) (**Figure 5.4A**). To validate the ability of these multimers to distinguish spike binding B cells I stained PBMCs from four individuals at day 8 following two dose vaccination against SARS-CoV-2. These samples had previously been assayed for RBD binding B cells and I compared the quantification of the proportion of B cells binding both RBD and S multimers by flow cytometry (**Figure 5.4B**). The four individuals selected had varying levels of response to vaccination. This was reflected in the proportion of B cells detected as binding my spike multimer, which agreed with the levels of those known to be RBD binding (**Figure 5.4C**).

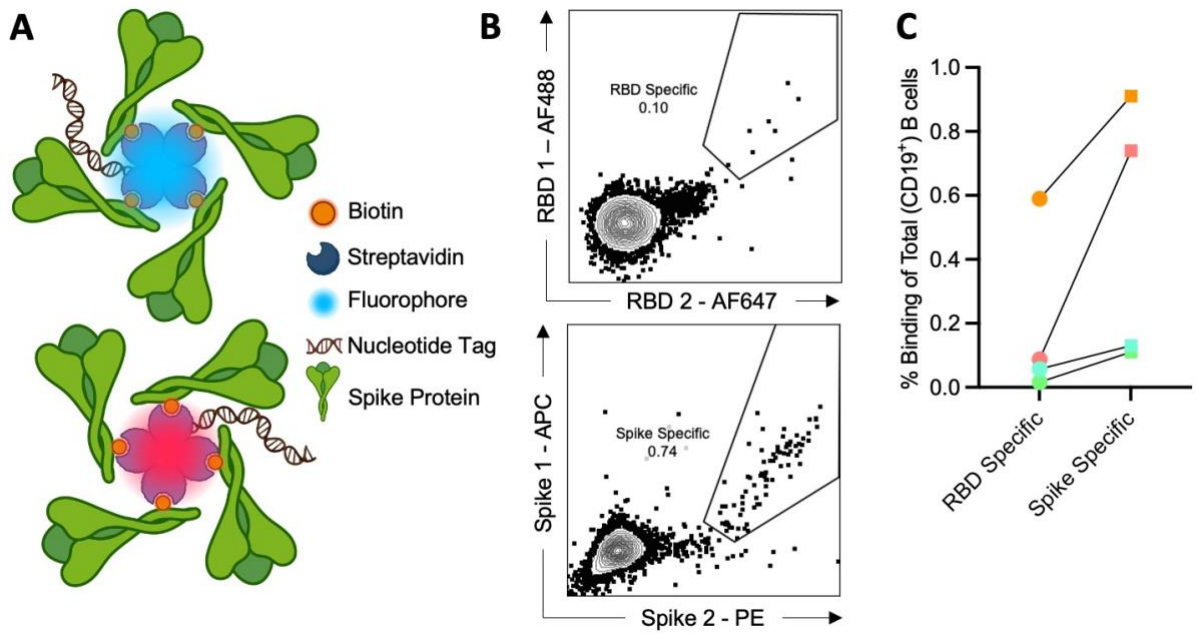

Figure 5.4. Creation of a nucleotide and fluorophore tagged spike multimer for the detection of B cells. A) Schematic of Spike Multimers. Biotinylated (orange) spike (green) protein is conjugated to streptavidin (grey) bound to a nucleotide tag (brown) and a fluorophore (PE (red) or APC (blue)). **B)** Representative plots of B cells from an individual vaccinated against SARS-CoV-2 stained with two fluorophores (AF488 and AF647) tagged RBD tetramers and the two produced spike multimers. **C)** Summary statistics of paired proportion of B cells from each of four vaccinated individuals, binding both RBD tetramers and both spike multimers. Paired samples from the same individual are indicated by colour and joining line. Flow cytometry contour plots, each point represents a single cell outlier from contour.

5.2.4.2. Multimer validation in mice

In order to avoid overuse of a limited stock of vaccinated human PBMC samples I used mouse samples for further validation of the spike multimers. Splenocytes and serum from WT mice 21 days after immunisation with three doses of BNT162b2 or PBS were used for the quantification of antigen specific IgG and B cells (**Figure 5.5A**). I quantified S binding IgG in the serum from these mice by ELISA. Mice vaccinated with BNT162b2 had much higher absorbance readings than PBS treated mice (**Figure 5.5B**) indicating vaccination was successful in triggering a specific humoral response in these animals. I then stained splenocytes from these mice with both spike multimers to detect antigen specific B cells. A distinct double positive population of S binding cells was identifiable and made up an increased proportion of total B cells in the BNT162b2 vaccinated mice compared to PBS treated (**Figure 5.5C&D**). This confirms that these multimers are able to distinguish S binding B cells from both human PBMCs and mouse splenocytes by flow cytometry. Further this establishes a simple assay in which staining of splenocytes from

these mice can used to confirm successful conjugation of each batch of multimer produced. Therefore, I continued on to test the application of my spike multimers on the detection of S binding cells in scRNAseq datasets.

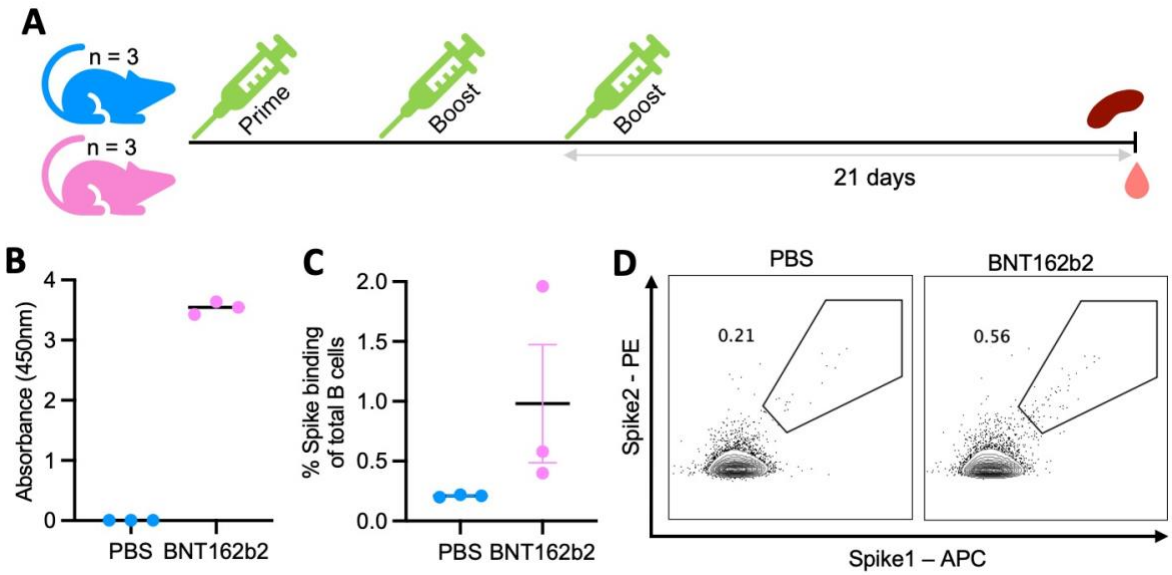

Figure 5.5. Detection of spike binding B cells in vaccinated mice. A) Schematic of the vaccination and tissue collection schedule of mice. Mice were immunised with either three doses of the BNT162b2 vaccine (pink) or three times with PBS (blue) and 21 days following the final immunisation serum and spleen were collected. In total three mice were immunised with BNT162b2 and three mice received PBS as a control group. **B)** Absorbance values at 450nm of anti-spike IgG indirect ELISA on serum from immunised mice. **C)** Comparison of the proportion of total B cells binding both spike multimers in PBS and BNT162b2 vaccinated mice. Plot shows standard error of the mean. **D)** Representative plots of spike multimer dual binding B cells from PBS and BNT162b2 immunised mice. **B-C)** each point represents data from a single mouse, horizonal bars indicate median value for group.

5.2.5. Single cell sequencing of enriched B cells using a spike multimer

5.2.5.1. Production of antibodies using the pVITRO1 system

To confirm the selection of S specific B cells from scRNAseq data, I developed a protocol for the production of monoclonal antibodies with the V(D)J regions encoded by selected cells. These antibodies could then be screened for binding to the S protein by ELISA.

I adapted a method from a published toolkit for expression of recombinant antibodies using a pVITRO1 plasmid[108] (**Figure 5.6A&B**). A pVITRO1 plasmid containing the heavy and light constant regions of the human IgG1 κ was linearised by PCR into two backbone fragments. The fragment encoding the C_L had a high GC content and therefore was more challenging to amplify by PCR. I performed an optimisation experiment using gradient

PCR to identify the best conditions for this reaction. I produced twelve different reaction mixtures using combinations of seven different length forward and reverse primers, and two PCR mix additives PCR_x enhancer and high GC enhancer. These reaction mixes were run in PCRs with an annealing temperature gradient of 61°C to 75°C (**Appendix C.4-5**). By comparing the yields of the reactions (**Figure 5.6C**) and confirming by SDS PAGE the length of the fragments produced in the highest yielding reactions (**Figure 5.6D**), I selected the best primers and optimal running conditions (annealing temperature 64°C and PCR_x enhancer additive (**Appendix C.6)**). Production of a bulk stock of C_H and C_L fragments was completed by pooling multiple PCR reactions following Dpn1 digest and gel purification (**Figure 5.6E**). Variable fragments were identified from single cell V(D)J sequencing and ordered with ends overlapping the constant fragments. These fragments were assembled into a plasmid by four fragment Gibson assembly and these plasmids were expressed in human HEK 293F suspension cells. The conditioned media from these cells was collected and the recombinant monoclonal antibody was isolated using Protein G (**Figure 5.6F**).

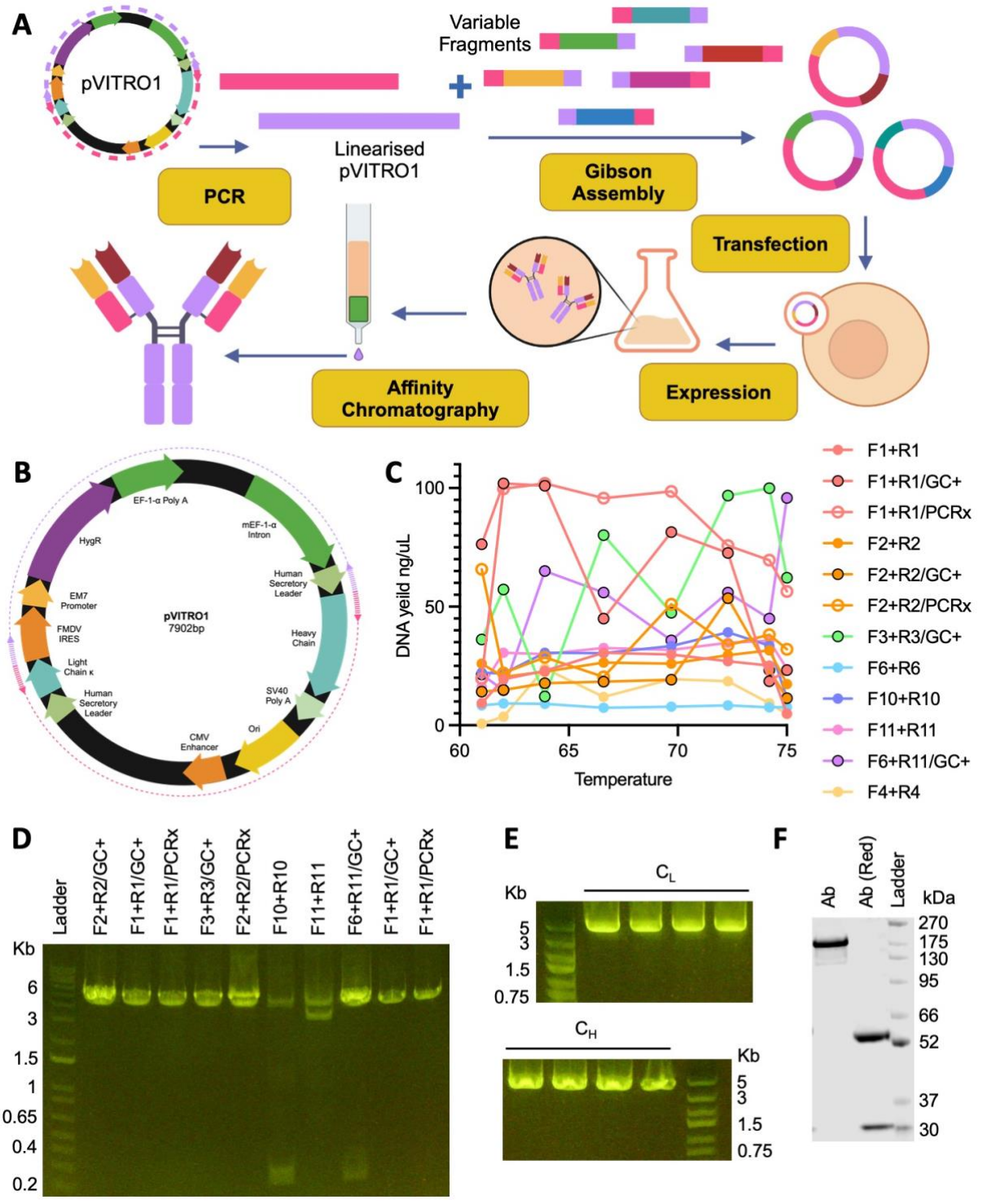

Figure 5.6. Production of recombinant monoclonal IgG1 with the pVITRO1 system. A) Schematic of the process of producing monoclonal antibodies using the pVITRO1 system. PCR is used to linearise the regions of the plasmid encoding the constant regions of IgG1. Variable fragments with overlapping ends with the pVITRO1 linearised regions are producing using sequences from single cell V(D)J sequencing. Gibson assembly is used to assemble these fragments into a plasmid which is transfected into HEK293F cells. Protein is expressed over 7 days; antibodies are extracted from the media by protein G affinity chromatography. **B)** Plasmid map of the pVITRO1 vector. PCR primer binding sites are indicated by staggered arrows and the region of PCR fragment products encompassing the heavy (pink) and light (purple) chains by dashed lines. **C)** Plot of light chain DNA yield by temperature for PCR reactions run using

twelve different reaction mixtures with different combination of primers and stabilising additives. **D)** Image of agarose gel with SYBR safe following gel electrophoresis of the PCR products from ten reaction mixes. Complete light chain can be seen at ~4kbp, other bands indicate incomplete product and primer dimers. **E)** Image of agarose gel with SYBR safe following gel electrophoresis of pVITRO1 fragments containing the heavy (**bottom**) and light (**top**) chain, amplified by PCR. **F)** Coomassie stained SDS PAGE, under reducing (Red) and non-reducing, conditions of antibody isolated from conditioned media using protein G. **A&B)** Produced using Biorender.com

5.2.5.2. Multimer validation by monoclonal antibody production

In the first instance I tested the use of the multimers in scRNAseq on B cells enriched from V3D28 samples from four individuals with SO and three of NW. I enriched samples for B cells via pan B isolation using magnetic beads. I then incubated cells with spike multimers, and nucleotide tagged antibodies targeting the B cell subset markers: IL-6R, CD21, CD11c, and CD27 immediately prior to library preparation. Microfluidic bead encapsulation and preparation of cDNA libraries for the transcriptomes, V(D)J sequences, and nucleotide tags were subsequently performed with the help of Vitalina Chamberlain Evans (**Figure 5.7**). Here the resolution of this method was enhanced by optimisation of the PCR cycle numbers enabling better discrimination of lower-level binding antigen specific B cells. Following sequencing spike binding cells were defined as those with a normalised read count for each multimer tag of >1.

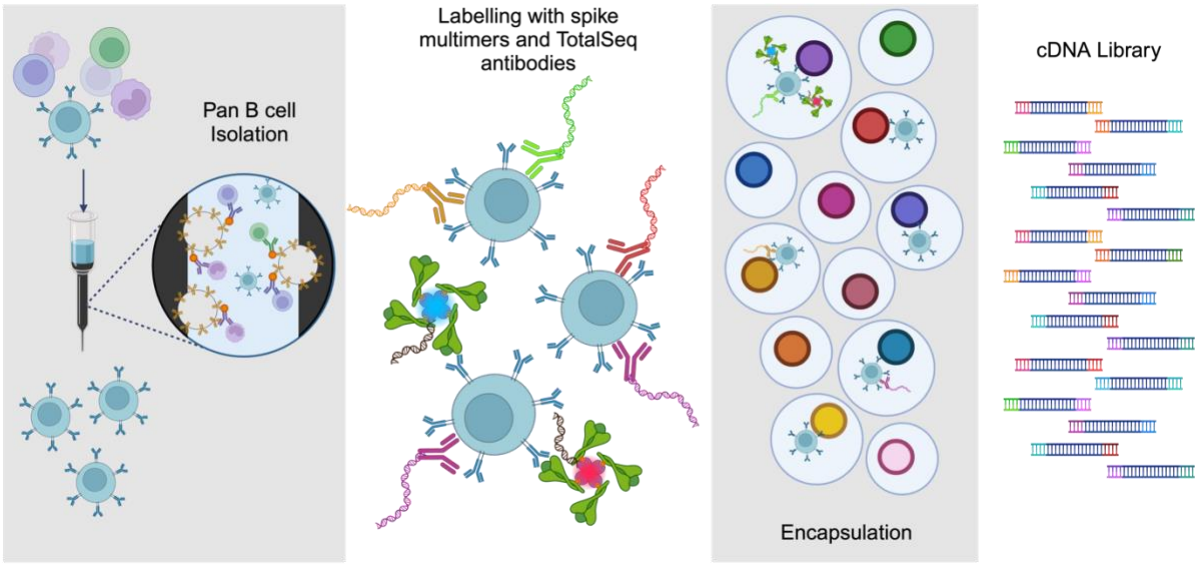

Figure 5.7. Preparation of B cells for single cell sequencing. Schematic of steps for the preparation of cells for single cell sequencing. PBMCs are enriched for B cells via magnetic bead separation. B cells are then tagged with spike multimers and TotalSeq antibodies before encapsulation and cDNA library preparation. Created using Biorender.com.

5.2.5.3. Confirmation of antibody binding specificity

I selected 20 cells for the validation of spike binding by monoclonal antibody production. Cells were selected on the basis of IgG isotype and multimer tag reads >1 (**Figure 5.8A**). Cell isotypes were identified using V(D)J sequencing data, somewhat surprisingly in this data set most specific cells with identifiable isotypes were IgM$^+$ (**Figure 5.8B**). However, a significant number were of un-identifiable isotype and required increased depth of V(D)J sequencing. Therefore, IgG$^+$ cells made up a small proportion of specific cells to select from. The 20 cells selected encompassed a range of normalised read counts 1.44-2.24 to enable an assessment of whether read count number provided informative data on BCR functionality (**Figure 5.8C**). Cells were also selected to represent all seven sampled individuals and covered the plasma, memory, and classical ABC, B cell subsets. Subsequently ten non-binding cells with a normalised read count for each multimer tag of <0.7 were randomly selected computationally with the requirement that they represented similar proportions of B cell subtypes and participants as the binding group (**Figure 5.9A**).

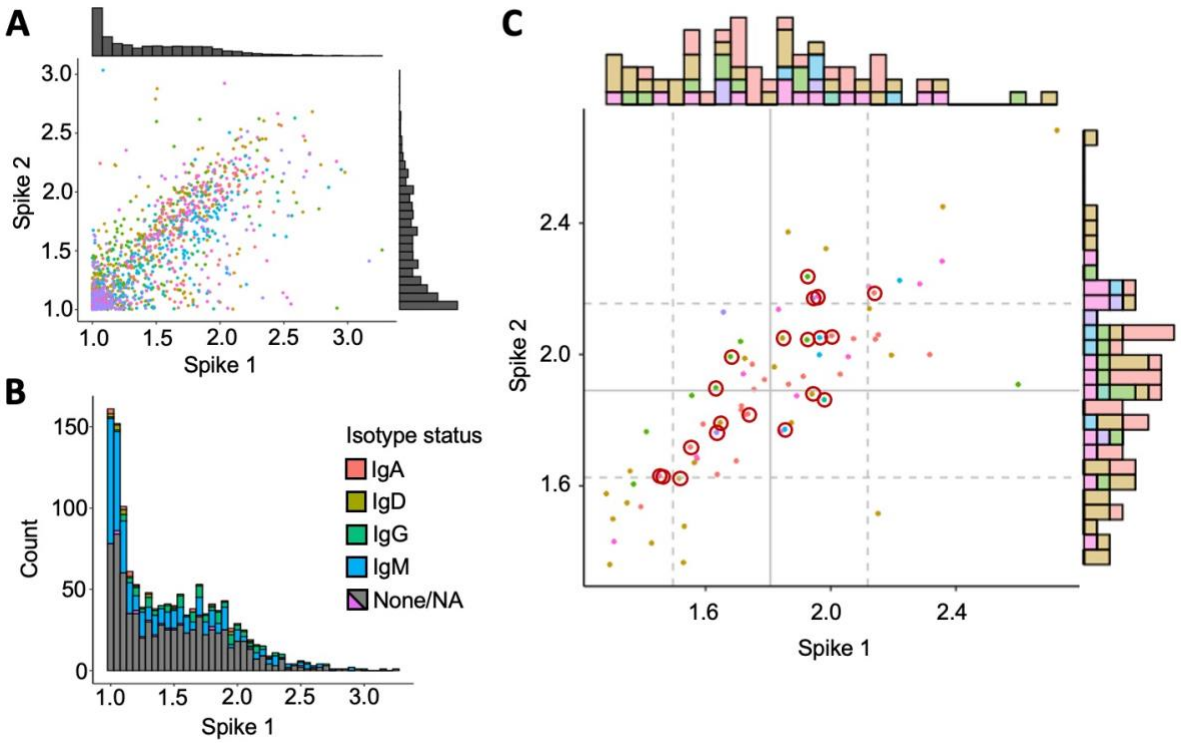

Figure 5.8. Selection of spike binding B cells for the production of antibodies. **A**) Dot and bar plot of normalised read counts of spike 1 and spike 2 multimer nucleotide tags over threshold of 1 for an initial cohort of 7 individuals. **B**) Histogram of cells above spike threshold grouped by normalised read count of spike 1 nucleotide tag, stacked bars coloured by the isotype of the cells: IgA (red), IgD (mustard), IgG

(green), IgM (blue). **C**) Dot and bar plot of normalised read counts for spike 1 and spike 2 tags in the initial cohort of seven individuals, showing IgG cells with counts >1.25 only. Cells selected for antibody cloning are circled in red. Solid lines indicate mean read count, dotted lines one standard deviation from the mean read count, for each spike multimer tag. **A+C**) One dot represents a single cell, dot colour responds to the participant of origin.

I cloned the variable BCR sequences of these cells, from V(D)J sequencing, into pVITRO1 to produce recombinant monoclonal antibodies. I then tested the ability of these monoclonal antibodies to bind to the S protein by ELISA. Antibodies produced from the sequences of non-binding cells showed very little to no ELISA reactivity however all antibodies from binding cells showed significantly higher reactivity (**Figure 5.9B**).

To compare the multimer to an alternative method of antigen specific cell detection, cells from an unlabelled dataset predicted to bind to the spike protein were identified using the SPACE program. The initial analysis identified ~15% of B cells from six individuals as spike binding. 15 cells were selected at random from these and antibodies made with their V(D)J sequences. 12/15 of these antibodies showed reactivity to the spike protein (**Figure 5.9C**) with a range of binding levels. Repeating the SPACE protocol with altered distance parameters led to a reduction in the number of cells identified. 10 of the cells previously used were still identified. Of those no longer categorised as binding only 2/5 had yielded a binding antibody. 10/10 of the cells tested from the second round were confirmed to bind spike, an improvement on the previous (**Figure 5.9C**). All three of the false positives identified in the first round of SPACE clustering were cells of unswitched isotype. Despite the improvement seen after the adjustment of the parameters, SPACE identified 5.5.% of sequenced cells as S binding which is above that which would be expected. Therefore, this analysis suggests that my tagged multimers are able to detect spike specific B cells with significant certainty, which may be above that of computational methods. However, this does not eliminate the chance that weakly binding cells may be missed or cells of isotypes other than IgG may show increased levels of off target binding.

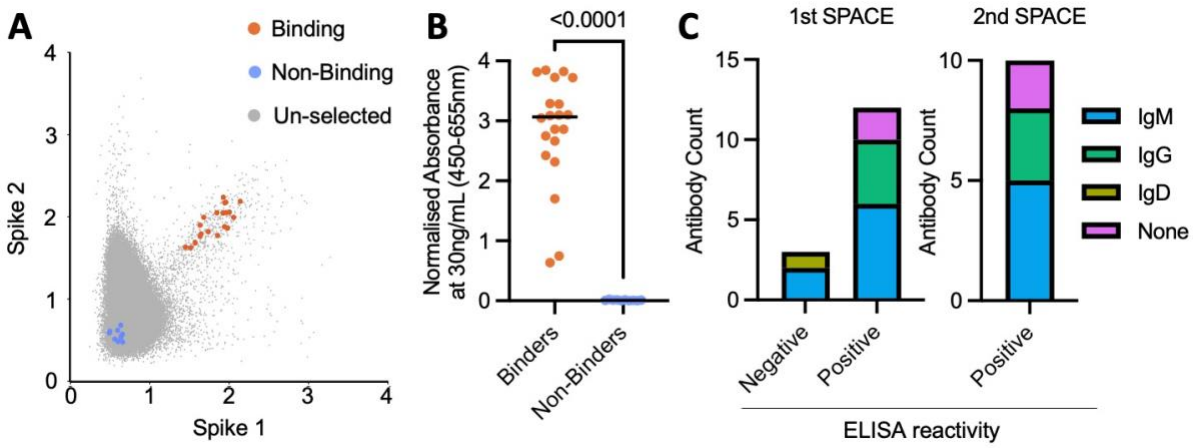

Figure 5.9. Validation of methods to identify antigen specific B cells. A) Cells selected to test spike binding (orange) and non-binding (blue) overlayed onto the normalised read counts for spike multimers for final dataset from 19 individuals after enhanced LIBRA-seq detection of spike multimer nucleotide tags and batch correction (grey). One dot indicates a single cell. **B**) Comparison of absorbance reading at 450-655nm from an indirect ELISA for spike binding of monoclonal antibodies produced using the V(D)J variable sequences of cells identified as binding or non-binding. Two-tailed Mann Whitney Test. **C)** Stacked bar plots of the number of selected cells identified as spike binding by the first and second application of SPACE, yielding antibodies with (positive) and without (negative) evidence of spike binding by indirect ELISA. Colour indicates isotype of origin cell as identified by V(D)J sequencing.

5.2.5.4. B cell identification in SCORPIO participants

A representative subset of the V3D28 samples from the SCORPIO cohort was selected for single cell sequencing with the spike multimers. 11 individuals with SO and 8 NW controls were selected based on their BMIs and neutralising capacities. The median BMIs and V3D28 neutralising capacities of the NW and SO subsets chosen for sequencing were similar to those of the total SCORPIO cohorts (**Figure 5.10A&B**). Median percentage change in neutralising capacity from day 28 to 105 was comparable in the total and subset NW cohorts (**Figure 5.10C**). However, as two of the chosen individuals with SO experienced breakthrough infection prior to day 105, the median percentage change in this subset appeared less when compared to the total SO cohort. This was not a concern as those experiencing infection likely had higher rates of waning than those protected from infection and in the absence of breakthrough would have reduced the median of the group. PBMC samples from the selected 11 individuals with SO and 8 NW controls were processed for single cell sequencing in three distinct batches (including the initial batch used for the preliminary assessment above). Prior to labelling a small proportion of the enriched B cell fraction was set aside and stained with a viability stain and anti-CD3 and

CD19 antibodies to determine viability and B cell purity after isolation. For all three batches viability was above 80% for all samples. However, B cell enrichment had varying levels of success in the second and third batches and for many samples was much lower than desired. Following sequencing, non-B cells were identified based on gene expression and excluded from subsequent analysis. As the same number of total cells were sequenced from each sample those with poor B cell purity had fewer total sequenced B cells. S binding B cells were therefore considered as a proportion of sequenced B cells to reduce the impact of inconsistent total numbers. The spike multimers were also conjugated in three batches. I confirmed successful conjugation of each batch by testing their ability to detect S binding B cells in the splenocytes BNT162b2 vaccinated mice by flow cytometry (**Appendix C.10**).

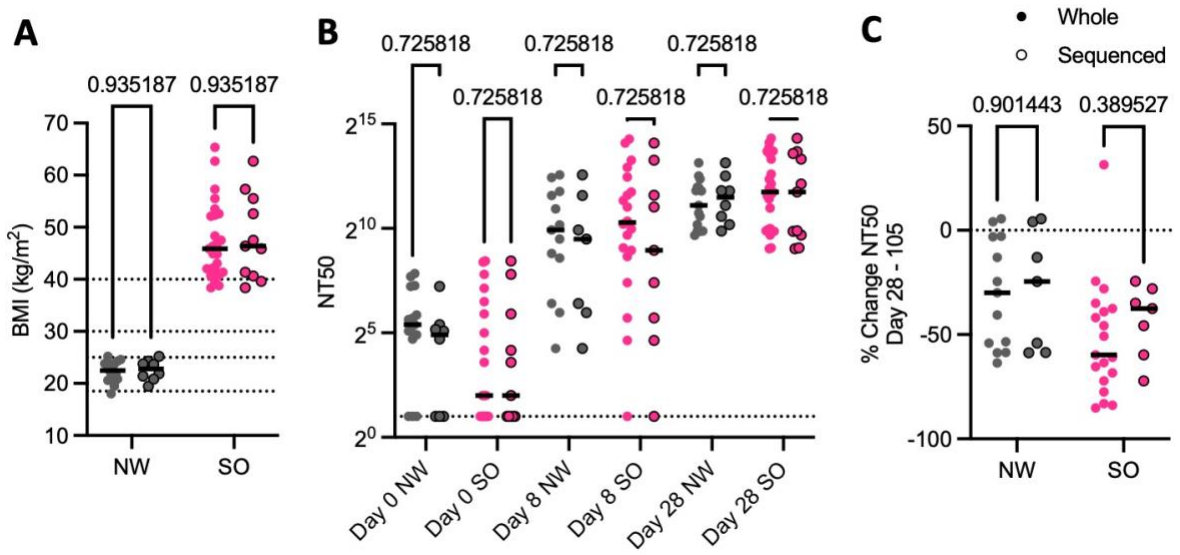

Figure 5.10. Selection of representative subset of samples for single cell sequencing. A) Comparison of BMI in the NW and SO full cohorts and subset used for sequencing. **B)** Comparison of live virus neutralising capacity at timepoints before and following third dose vaccination in the NW and SO full cohorts and subset used for sequencing. **C)** Dot plot of the percentage change in live virus neutralising capacity between day 28 and 105 following vaccination in the NW and SO full cohorts and subset used for sequencing. All plots a single point indicates one individual, horizonal bar indicates median. Points coloured by cohort, SO (pink), NW (grey), black outline indicates individual selected for sequencing. Q values indicate results of Multiple Mann-Whitney tests.

5.2.6. Differentiation states of antigen specific B cells

Non-B cells were removed from the data set based on differential gene expression and then the remaining cells underwent unsupervised clustering using transcriptome sequences. Cells were grouped into six clusters which were identified as naïve B cells, transitional B cells, memory B cells, anergic aged associated B cells, plasmablasts and

plasma cells, and atypical B cells (ABCs) (**Figure 5.11A**) based on gene expression. Cells were distributed into these six clusters at similar frequencies within the NW and SO groups (**Figure 5.11B**) and there were no significant differences in proportion of total cells in each cluster when individual samples were considered (**Figure 5.11C**). Individuals with obesity in this study therefore did not have significant expansion of ABCs. S binding B cells were identified using an updated threshold of >1.2 normalised read counts for each multimer tag, set following PCR enrichment. S binding cells were found in all B cell clusters however the subsets in which they represented the highest proportions were the atypical memory (ABC) cluster followed by the memory B cells (**Figure 5.11D&E**). There was no significant difference in the proportion of total B cells identified as S binding between the two cohorts, however, there did seem to be a tendency towards increased frequencies of S binding cells in NW individuals (**Figure 5.11F**). An increased proportion of the S binding B cells in individuals with SO belonged to the naïve cluster with no significant differences in the proportions belonging to other clusters (**Figure 5.11G**). When binding cells in each cluster were considered as a proportion of total B cells, no significant differences could be seen between groups however, in many individuals with SO S binding memory and atypical memory cells made up a lower proportion of total B cells than that seen in NW (**Figure 5.11H**). ABCs can perform some of the functions of memory cells. When atypical (ABCs) were considered together with memory cells, the resulting "memory-like" cells made up a larger proportion of the binding cells in individuals of NW when compared to SO (**Figure 5.11I**). This indicated that S binding B cells in individuals with SO are more frequently in a less differentiated naïve state which may be due to an impairment in B cell response. A negative relationship could be seen between the proportion of S binding cells that were naïve and neutralising capacity at V3D28 (**Figure 5.11J**). This suggests that bias towards a less differentiated B cell state or a lack of clonal expansion of specific cells following vaccination has a functional implication on subsequent antibody mediated protection against virus.

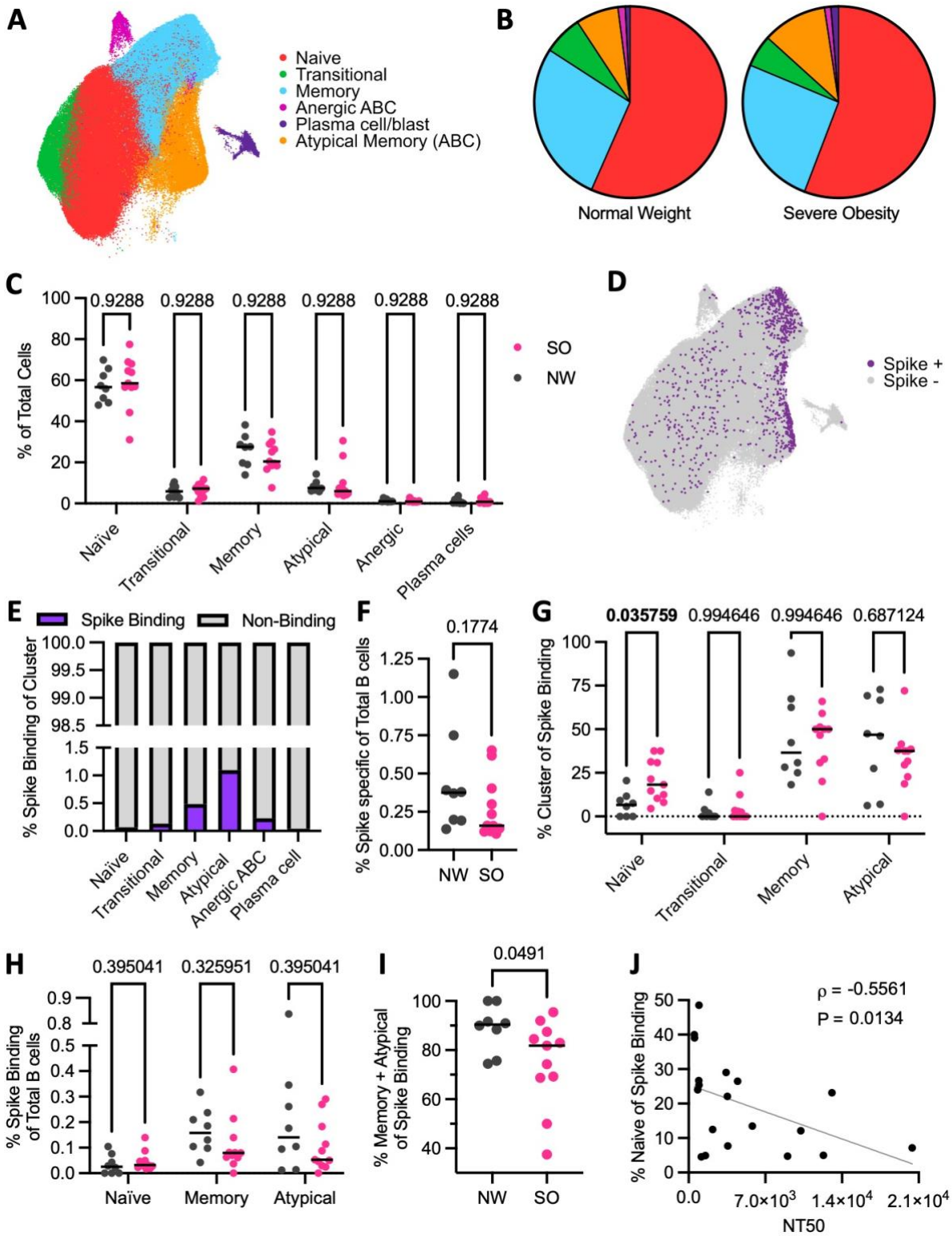

Figure 5.11. Differentiation states of antigen specific B cells following vaccination. A) UMAP of cells coloured by B cell differentiation state cluster (one dot indicates one cell). **B)** Pie charts of the proportion of total sequenced B cells assigned to each B cell cluster in cells from individuals with SO (left) and of NW (right). **C)** Comparison of the proportion of total sequenced B cells assigned to each B cell cluster for each-individual sampled in NW and SO cohorts. **D)** UMAP of cells coloured by spike binding, displaying the distribution of spike binding cells (purple) (one dot indicates one cell). **E)** Stacked bar chart of the proportion spike binding of the cells of each B cell cluster. **F)** Comparison of the proportion of total

sequenced B cells identified as spike binding by multimer from SO and NW individuals (Two-tailed Mann Whitney test). **G)** Comparison of the proportion of spike binding cells from each individual belonging to each B cell cluster in SO and NW. **H)** Comparison of the proportion of total B cells from each individuals cells identified as spike binding and naïve, memory, or atypical, in SO and NW. **I)** Comparison of the proportion of spike binding cells from each individual belonging to memory-like clusters from each individual (Two-tailed Mann Whitney test). **J)** Relationship between the proportion of spike binding cells identified as belonging to the naïve cluster and the neutralising capacity of each individual at day 28 following third dose vaccination (Two-tailed Spearman's corelation coefficient with indicative linear regression line). Unless otherwise specified all comparisons are Multiple Mann Whitney tests, and one point indicates data from a single individual. Spike binding cells shown in purple, data from NW in grey and SO in pink. UMAPs generated by Dr Zhaleh Hosseini.

5.2.7. V(D)J sequences of antigen specific B cells

Cell isotypes were determined from the V(D)J sequencing data. In keeping with increased proportions of naïve cells, an elevated proportion of spike binding cells from individuals with SO were IgM^+ and significantly reduced proportion were IgG^+ when compared to NW individuals (**Figure 5.12A**). Additionally, when other isotypes were considered, I found that spike binding B cells in individuals with SO were less class switched (IgG + IgA) and more unswitched (IgM + IgD) than those from NW (**Figure 5.12B**). Increasing BMI was associated with reduced proportions of IgG^+ S binding cells (**Figure 5.11C**) and increased proportions of binding cells that were of the unswitched isotypes IgD and IgM (**Figure 5.11D**). This was suggestive of more extreme phenotype with increasing levels of obesity. Levels of S binding IgM^+ cells appeared to negatively correlate with circulating S binding IgM in the serum at V3D28 in these individuals (**Figure 5.11E**). These IgM^+ S binding cells are therefore unlikely to be ASCs and instead represent unswitched memory and naïve cells as previously stated. Class switching from IgD or IgM to IgA, IgG, or IgE, is under the control of the AID which is the same enzyme responsible for somatic hypermutation[305]. These two processes are therefore mechanistically linked although they happen independently from one another. The BCRs of class switched IgG^+ cells typically have more mutations (a higher mutational load) than IgM^+ cells. This is in part due to the fact that IgG^+ cells are more frequently memory and plasma cells which have passed through the GC, whereas IgM^+ are mostly naïve. I therefore considered IgM^+ and IgG^+ cells independently when comparing the mutational loads in individuals with SO and of NW. As expected, mutational counts were higher in the BCRs of IgM^+ memory cells than other IgM^+ cell types. There was, however, no difference in the mutational counts in the heavy

or light chains of S binding memory or non-memory cells between individuals with SO and those of NW (**Figure 5.11F**). Surprisingly the heavy chain sequences from S binding atypical cells (ABCs) had higher mutational counts in individuals with SO, although no differences were seen in light chains or in memory cells (**Figure 5.11G**). Overall, although there may be a deficiency in class switching or differentiation in people with SO, there does not appear to be an impairment of SHM, and it is probable that affinity maturation is effectively occurring in both cohorts.

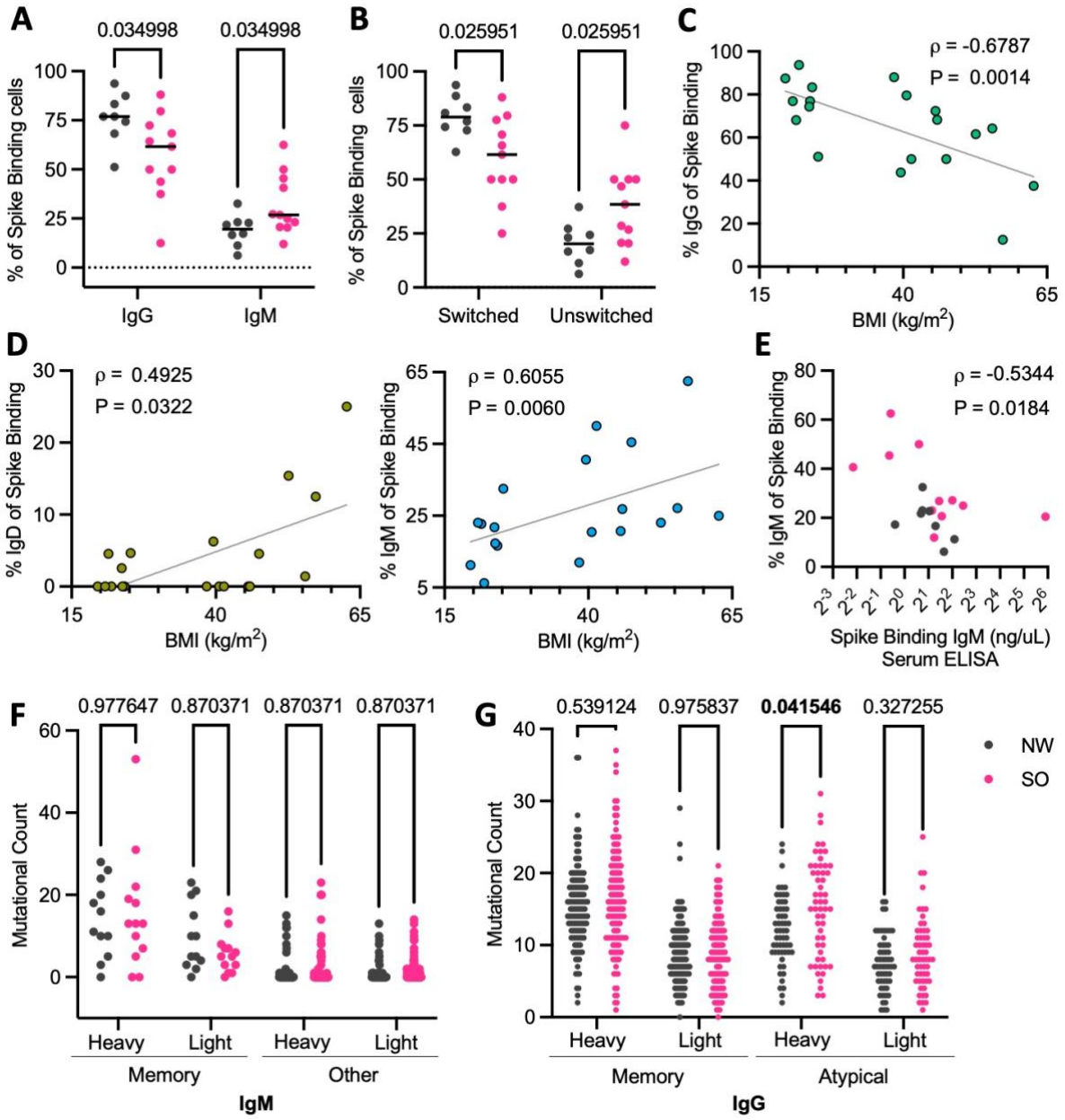

Figure 5.12. Isotypes of spike binding B cells following vaccination. A) Comparison of the of spike binding cells of IgG or IgM in NW and SO. **B)** Comparison of the of spike binding cells that are class switched or unswitched in NW and SO. **C-D)** Relationship between BMI and the proportion of spike binding cells of

(C) IgG (**D)** IgD (**left**) and IgM (**right**) isotype. Two-tailed Spearman rank correlation coefficients and indicative linear regression lines displayed. **E)** Relationship between the proportion of spike binding cells identified as IgM and the concentration in the serum of spike binding IgM at day 28. Two-tailed Spearman rank correlation coefficient **F)** Comparison of the number of mutations in the V(D)J region per cell of IgM spike binding cells from the memory cell cluster and other clusters in NW and SO. **G)** Comparison of the number of mutations in the V(D)J region per cell of IgG spike binding cells from the memory and atypical memory cell clusters in NW and SO. Multiple Mann Whitney test q values indicated on comparative plots. **A-E)** One point indicates one individual **F-G)** one point indicates one cell.

5.2.8. Assessment of antibody binding affinities from monoclonal antibodies

The production of recombinant monoclonal antibodies also allowed further assessment of the qualities of the S specific antibodies produced by individuals with SO. I optimised the anti-S IgG ELISA to capture the range of antibody concentrations which could produce a complete binding curve. I subsequently tested the antibodies from the 20 binders and 10 non-binders at a serial dilution (0.013-2430ng/mL) (**Appendix C.11**). All 20 binders produced clear binding curves, and all non-binders did not show any significant increase in absorbance with increasing concentration (**Figure 5.13A**). I calculated the IC50 as a measure of affinity from the binding curves. There was no difference in the affinities of antibodies produced from individuals with SO compared to those from individuals of NW (**Figure 5.13B**). There was also no correlation between the affinity of antibodies and the mutational counts of their heavy or light chains (**Figure 5.13C**). Similarly, no relationship was seen between affinity and the quantity of bound multimer tags as indicated by average tag normalised read count (**Figure 5.12D**). I also tested the affinity of seven antibodies produced using variable regions from IgM cells identified by the spike multimers. Only 1/7 yielded a complete binding curve similar to that seen from IgG binders, however a further 4/7 produced clear truncated right shifted curves, indicative of lower affinity binding (**Figure 5.12E**). IC50 values could only be reliably calculated for three of the IgM binder antibodies, as such arbitrary values were assigned to antibodies which: showed right shifted curves, some indication of increasing absorbance, or no significant change in absorbance across all concentrations tested. By these measures IgM binders had a range of affinities spanning from levels comparable to IgG binders and IgG monoclonal standards to comparable to the non-binders. Most frequently, however, the affinity of antibodies produced from IgM^+ binders was less than those from IgG^+ binders (**Figure 5.13F**). These data do not indicate a difference in affinity

between the antibodies or BCRs encoded by spike binding IgG⁺ cells in SO and NW. Furthermore, they confirm that those encoded by IgM⁺ cells are lower affinity than IgG⁺.

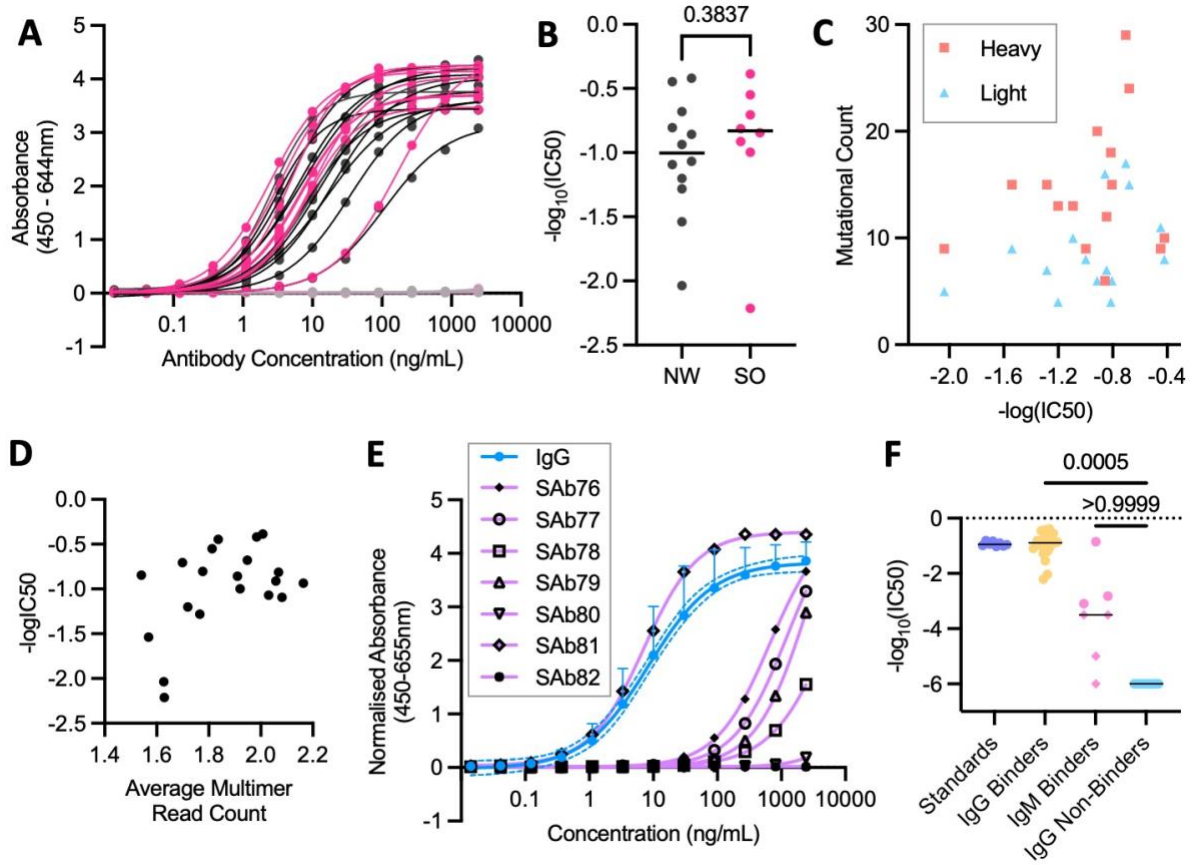

Figure 5.13. Affinities of antibodies derived from individuals with severe obesity. A) Plot of anti-spike IgG indirect ELISA absorbance against antibody concentration for antibodies produced from IgG binder cells from SO (dark pink) and NW (dark grey) and non-binder cells from SO (pale pink) and NW (pale grey). **B)** Comparison of -log10 IC50 affinity values of antibodies derived from binder cells from NW and SO (Two-tailed Mann-Whitney test). **C)** Relationship between -log10 IC50 measure of affinity against heavy (red) and light (blue) chain mutational counts of each monoclonal binder antibody. Two-tailed Spearman correlation coefficient: Heavy p=0.1458 P=0.6018, Light p=0.3781, P=0.1643. **D)** Relationship between -log10 IC50 measure of antibody affinity and average of normalised read count for spike 1 and spike 2 tags for the antibody parent cell. Two-tailed Spearman correlation coefficient: p=0.3038, P=0.1929. **E)** Plot of anti-spike IgG ELISA absorbance against antibody concentration for antibodies produced from IgM binder cells (purple) and average values for 20 antibodies produced from IgG binder cells (blue). **F)** Comparison of -log10 IC50 values of 8 anti-RBD IgG standard repeats (lilac), and antibodies derived from IgG binders (gold), IgM binders (pink), IgG non-binders (blue) (Kruskal-Wallis with multiple comparisons). Where IC50 values were not calculated arbitrary values of -3.5, -5, and -6 are indicated by diamonds. Where present bars represent median vales and curves sigmoidal 4PL, dashed lines indicate 95% CI and error bars SD.

5.3. Discussion

5.3.1. Results

There may be a number of causes for the accelerated waning of protection through S specific antibodies observed in individuals with severe obesity following mRNA vaccination. I identified no significant differences in the isotypes or relative avidity of antibodies in the serum of individuals with SO compared to NW controls. Differences in neutralising capacity and maintenance are therefore not due to the dominance of the response by one particular antibody isotype or the loss of a specific antibody isotype. This data suggested that the previously observed higher peak antibody response in individuals with SO is most likely due to a rapid expansion of ASCs irrespective of class switched status. One potential cause for this may be the low-grade inflammatory environment in obesity leading to high levels of positive feedback and a rapid inflammatory response upon vaccination. What is unclear is whether accelerated waning leads to lower avidities at later timepoints following vaccination. The testing of serum from later timepoints after vaccination may have resolved this. However, experiments by SAffCon assay were limited by issues in the supply of the required consumables.

I developed and validated two nucleotide-tagged spike multimers for the identification of antigen specific B cells in single cell sequencing. This method was able to reliably identify S binding B cells without the need for FACS and the risk of transcriptional changes triggered by prolonged antigen binding. In addition, this method appeared to be more accurate than computational techniques tested, although both modes of specific cell identification could be further optimised. The identification of antigen specific B cells enabled the in-depth analysis of the transcriptional states and V(D)J sequences of cells formed in response to vaccination.

Analysis of B cell subsets showed a clear increase in the proportion of S binding cells that were naïve and IgM^+ in individuals with SO. Reduced levels of B cell differentiation in the early response to vaccination appears to lead to impairment in the production of antigen specific memory and ABCs. Subsequently naïve cells are overrepresented in the S binding compartment in SO. Increased proportions of IgM^+ binding B cells do not correlate with IgM production and therefore do not indicate increased levels of IgM^+ ASCs. Antibodies produced from the V(D)J regions of IgM^+ were of lower affinity than

those from IgG^+ cells regardless of the V(D)J mutational count or whether the sequence was from a naïve or memory cell. Therefore IgM^+ S binding cells are either naïve or unswitched memory cells and are likely to function poorly in protecting individuals with SO from SARS-CoV-2.

Analysis of the mutational counts in the V(D)J sequences of spike binding B cells provided evidence for SHM and affinity maturation in the IgG^+ and memory B cells (**Appendix C.12**) of individuals with SO. This was further confirmed by the improved binding affinities of monoclonal antibodies produced from IgG^+ cells over those from IgM^+. The extent of affinity maturation in the S binding IgG^+ cells in SO did not differ from those of NW as measured by mutational count and monoclonal antibody binding affinity. Together, this indicates that production of affinity maturated class switched memory cells is not fully impaired in individuals with severe obesity. Therefore, previously observed perturbations in the humoral response are not due to the total absence of the GC response. Regulation of the GC reaction relies on multiple cytokines[306] which are dysregulated in obesity and inflammation. These cytokines include, IL-6, IL-10[307,308], IFN-γ[309], IL-27[310,311], and IL-2[312], and their imbalance could lead to impairment of normal GC formation or progression. GCs are difficult to assay in human samples due to the importance of their structural organisation and location within secondary lymphoid tissue. The outputs of the GC, class switched memory cells and LLPCs, can however, be more easily assessed.

The EF response can yield memory B cells and in prolonged responses affinity maturation may also occur[30]. LLPCs, however, are considered to be an output of the GC response. Reduced persistence of antibody levels following vaccination in SO suggests an impairment in LLPC production by the GC. Additionally, reduced levels of class switched antigen specific cells indicate a bias towards EF response. Plasmablasts and plasma cells downregulate expression of their external BCRs and so are not typically detectable by multimer binding. They, therefore, could not be directly assessed in this analysis and their presence must be inferred from antibody levels and evidence of EF and GC response. Memory B cells have important roles in protection against viral variants which are not shared by plasma cells[66]. Therefore, impaired GC production of class switched memory B cells will have a significant impact on protection against infection, irrespective of LLPC production.

5.3.2. Conclusions and future directions

Here I show, in individuals with severe obesity, no impairment in the isotypes or avidities of antibodies produced and encoded following mRNA vaccination. Instead, reduced levels of class switched memory cells are produced despite evidence of productive GC responses, indicating a reduction in the rate of early B cell entry into the GC.

An exhaustive analysis of serum antibodies was not completed in this study and there are additional avenues which could be explored to investigate other factors which may influence antibody clearance. Post translational modifications of antibodies could be explored. Techniques including mass spectrometry can be applied for the analysis of glycosylation of antibodies[313]. Inflammation has been seen to influence Fc-glycan profiles and therefore it is possible this influences the humoral response in obesity and other inflammatory conditions[314].

In this project I produced and assessed antibodies from 43 cells identified, by multimer stain and SPACE, as spike binding and 14 identified as non-binding. There were, however, 1075 cells identified as having high binding to the spike multimers. Production of antibodies from the sequences of all of these cells and an expanded portion of the non-binding cells, would provide a more comprehensive assessment of BCR repertoire after vaccination. Additionally, alternative methods such as surface plasmon resonance (SPR)[315] or microfluidic diffusional sizing (MDS)[316] may provide a more reliable assessment of antibody affinity. The live virus neutralising assay previously used for whole serum assessments could also be used to determine the individual neutralising capacities of each antibody made. Together, this would enable a deeper assessment of the binding and functional differences of spike specific cells produced following vaccination in people with SO and NW. Additionally, sequencing was not applied to the entirety of the SCORPIO cohort. There are 22 remaining V3D28 samples which could be sequenced and included in the existing analysis, which would more than double its size. Additionally, samples from the other timepoints could be investigated to provide data on how the phenotypes of spike binding B cells change over the course of the vaccine response. Evidence of an impairment in early B cell response means sequencing of day 8 samples could be valuable.

Nucleotide tagged antigens are useful for the detection of memory and naïve B cells membrane bound BCRs, however plasmablasts and LLPCs are unlikely to be detected as they rarely express membrane bound BCRs. Alternative methodologies such as predictive computational models or the TRAPnSeq system (which enables the detection of specific ASCs by trapping secreted antibody on the surface of cells)[317] could be used to determine whether there is a difference in the early production of LLPCs in SO. Improved computational prediction of antigen specific cells in the plasma cell cluster of the existing dataset could be combined with the production and assessment of recombinant monoclonal antibodies. This would enable affinities and neutralising capacities of produced antibodies to be assessed alongside transcriptional information from their parent cells. Therefore, the quantities and transcriptional state of antigen specific plasma cells in NW and SO could be compared. However further to this, these could be linked to the functionality of the antibodies they secrete. This could provide additional evidence to support the impairment of GC responses in obesity and would also aid in the identification of which cells are responsible for the early burst and subsequent waning of antibody produced in individuals with SO.

Plasma cells and plasmablasts have reduced BCR expression and migrate to specific niches, this means they are difficult to sample and analyse in human subjects. Therefore, identification of a good model for severe obesity, such as mice with diet induced obesity, would provide an opportunity to explore in more depth the impact of obesity on humoral responses. Additionally, mouse models would enable detailed study of GC size, numbers, structure, and functionality. This would allow vaccine studies to be completed without the need for human participant recruitment and provide flexibility in *in vivo* experimentation[318,319].

The existing scRNA-seq dataset could also be analysed further, to elucidate a mechanism by which humoral responses are dysregulated. Although initial comparison of gene expression between B cells from NW and SO did not identify any genes of interest, a focused analysis to compare gene sets involved in GC responses, antibody production, B cell differentiation, immune cell metabolism, and cytokine signalling may highlight a disparity in one of these processes relating to the immune response to vaccination.

In this chapter I have demonstrated that accelerated antibody waning in severe obesity is not due to an impairment of class switching in ASCs, or low affinity antibody binding. Additionally, S binding cells in SO are enriched for unswitched, less differentiated B cells. In the absence of definitive structural differences in the antibodies and BCRs of individuals with SO, the differentiation states of antigen specific B cells themselves emerge as a potential cause for impaired protection from vaccination.

6. IL-6 signalling in the humoral response to mRNA vaccines

6.1. Introduction: IL-6 signalling in the generation of an immune response

IL-6 is a pro-inflammatory cytokine produced by a number of immune and non-immune cells[320,321]. The pleotropic function of IL-6 signalling means that its influence can be variable depending on the microenvironment and immune stimulus. A positive feedback loop of IL-6 production in obesity has been considered to be key in the initiation of chronic inflammatory disease[322]. IL-6 signalling has been implicated in obesity induced chronic inflammation, SARS-CoV-2 infection, and response to mRNA vaccination and as such could be expected to play a key role in response to COVID-19 mRNA vaccination in people with obesity.

6.1.1. Dynamics of IL-6 signalling

IL-6 signals through the IL-6 receptor (IL-6R) and glycoprotein 130 (gp130). Upon binding to IL-6, IL-6R associates with gp130 coreceptor which homodimerizes initiating tyrosine kinase activity[323]. Signalling typically occurs via the Janus kinase/signal transducer and activator of transcription (JAK/STAT) pathway by phosphorylation and homodimerization of STAT3. However, there is evidence that other signalling pathways can be activated dependent on the mode of IL-6 signalling[324,325].

There are three ways in which IL-6 can signal through the IL-6R (**Figure 6.1**). Classical IL-6 signalling occurs when IL-6 binds to membrane bound IL-6R on the surface of leukocytes and hepatocytes, which then associates with membrane bound gp130. IL-6R expression is mostly limited to these cell types with particularly high levels of expression found in neutrophils[326] (https://www.proteinatlas.org). Trans signalling requires the binding of IL-6 to circulating soluble IL-6R (sIL-6R) which can then associate with gp130 on the surface of cells. Trans signalling allows IL-6 to signal cells which do not express the IL-6R as gp130 expression is ubiquitous across tissues[321]. The final form of signalling is cluster signalling, which also enables signalling to cells which do not express the IL-

6R. IL-6 binds to a membrane bound IL-6R on one cell and this complex then activates the gp130 subunit of a second cell causing a signalling cascade in the recipient cell.

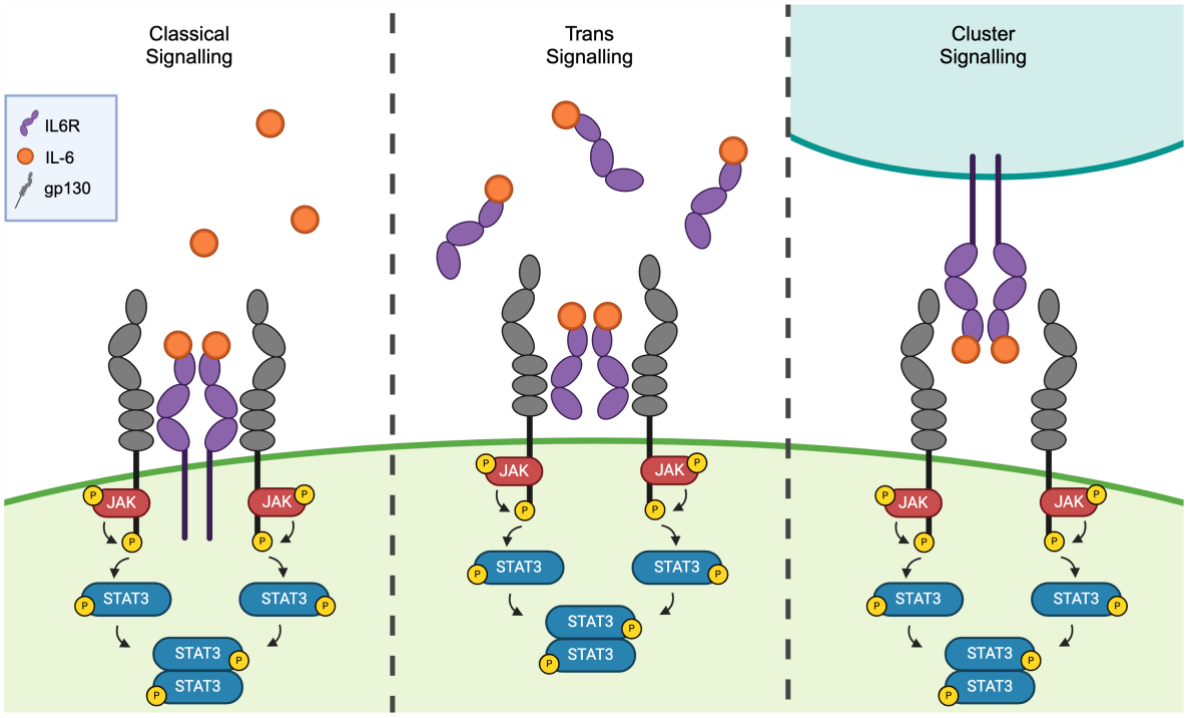

Figure 6.1. The dynamics of IL-6 signalling. Diagram of the modes of IL-6 signalling and signalling cascade. Classical signalling (**left**). IL-6 (orange) binds to membrane bound IL-6R (purple) which associates with gp130 (grey). Trans signalling (**centre**). Soluble IL-6R binds to IL-6 and then binds to membrane bound gp130. Cluster signalling (**right**). IL-6 binds to membrane bound IL-6R on the surface of a transmitting cell (teal). This complex associates with gp130 on the membrane of a receiving cell (green). In all pathways IL-6R/gp130 association leads to dimerization and phosphorylation (yellow) via JAK kinases (red) and subsequent phosphorylation and homodimerization of STAT3 (blue). Created using Biorender.com.

Although IL-6 is considered to be a pro-inflammatory cytokine, classical IL-6 signalling is generally associated with more regenerative and anti-inflammatory activities whereas trans signalling is observed to be pro-inflammatory[327]. It is uncertain why the effects of classical and trans signalling differ. The difference may be due to receptor subunit expression levels[328], gp130 is more abundantly expressed on the surface of cells than IL-6R meaning cells can receive a higher magnitude of trans signals than classical. In this way trans IL-6 signalling may also overcome negative feedback regulation. Additionally, the cell types signalled to via trans signalling are more diverse with potentially more inflammatory responses to IL-6 signalling. Finally there is some evidence that different

signalling pathways may be triggered by IL-6 signalling dependent on the form and recipient cell type[324].

The generation of sIL-6R required for trans signalling is predominantly mediated by cleavage of the membrane bound receptor from the surface of cells by A Disintegrin And Metalloproteinases 10 and 17 (ADAM10 and ADAM17) which are considered to be responsible for constitutive and induced shedding respectively[329,330]. A number of factors can induce increased shedding of IL-6R including bacterial toxins, CRP, and SNPs[331,332]. Activation of the TCR leads to shedding of the IL-6R from the surface of $CD4^+$ naïve and memory T cells[333]. Circulating DCs have been found to be a major source of the sIL-6R[334]. A small portion of the sIL-6R found in humans is also produced by alternative splicing[335], however this has not been detected in mice. Alternative splicing can also generate a soluble form of gp130 (sgp130) which can bind to sIL-6R-IL-6 complexes and neutralise them[336]. Under typical conditions serum concentration of sIL-6R and sgp130 are much higher than that of IL-6, meaning that there is little to no IL-6 signalling. However, under inflammatory conditions IL-6 levels increase to higher levels triggering signalling. Increased levels of both sIL-6R and sgp130 may therefore be associated with a higher threshold for IL-6 signalling.

6.1.2. Sources, targets, and functions of IL-6

IL-6 is produced by various cell types, immune and non-immune, including B cells, DCs, plasma cells, macrophages, adipocytes and endothelial cells. One of the most potent producers of IL-6 are plasmablasts which contributes to the onset of inflammation in the early response to infection[337]. Ubiquitous expression of gp130 means most cell types can receive signals via IL-6 signalling which has pleotropic function. IL-6 signalling has direct and indirect effects on the immune response which can be both pro- and anti-inflammatory (**Figure 6.2**). Significant roles in immune signalling include, encouraging the survival of and production of antibodies by plasma cells[338] and signalling to T cells in conjunction with other cytokines to trigger T_{FH} and T_{H17} differentiation[339]. As such levels and modes of IL-6 signalling can influence the humoral response to an immune challenge.

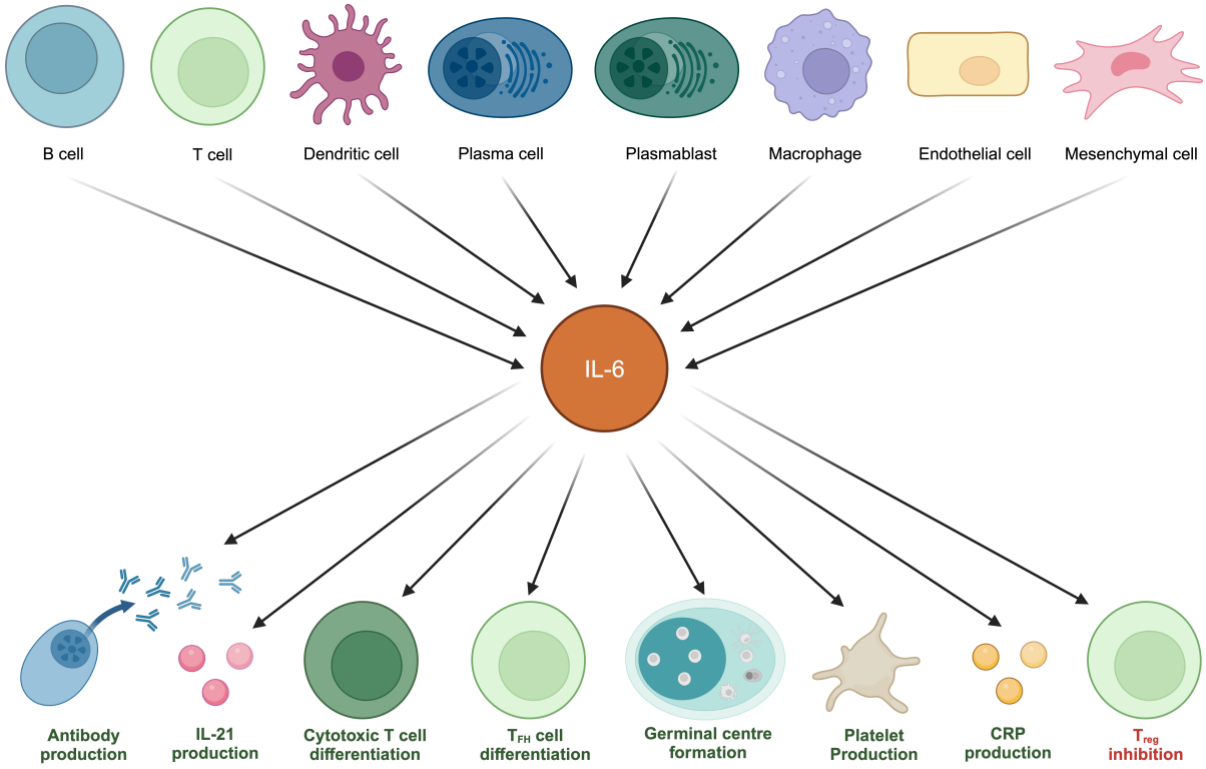

Figure 6.2. Sources and impacts of IL-6. A representative schematic of some of the cells which secrete and produce IL-6 cytokine (**top**) and the potential functional impacts of increased IL-6 signalling (**bottom**)[340]. Positive effects of IL-6 shown in dark green, negative effects shown in red. Created using Biorender.com.

6.1.2.1. Germinal centre and class switch response

IL-6 is one of a number of cytokines which function to regulate the GC response by action upon both the B cells themselves and the T_{FH} cells which provide B cell help (**Figure 6.3**). IL-6 production by cells such as FDCs can generate the formation of GCs, and in the absence of IL-6 GCs are fewer and smaller[341-343]. IL-6 signalling also plays a role in the generation of BCR diversity. The activation, reactivation, and termination of RAG enzyme activity responsible for recombination in CSR and V(D)J recombination is regulated by IL-6 levels[344,345]. Therefore, IL-6 can drive the production of class switched antibodies[341] and rates of SHM[342]. B cells only express the IL-6R in the final stages of maturation and as such are subject only to trans and cluster signalling until this point. Despite this, IL-6 signalling plays a role in the generation of plasma cells and antibodies in conjunction with and by inducing the production of other cytokines such as IL-2, IL-10[346], and IL-21[347,348]. Therefore, IL-6 deficient mice have both physically smaller GCs and reduced IgG

production with no change in IgM[349]. IL-6 signalling to B cells and plasma cells importantly enhances GCs and antibody production.

IL-6 interacts with IL-21 to induce the activation and differentiation of T_{FH} cells. B cell derived IL-6 appears to be responsible for early T_{FH} generation[350] and in the absence of IL-6 a defect in early T_{FH} cell differentiation can be seen in mice[351]. A combination of IL-6 and IL-21 deficiency in mice reduces T_{FH} differentiation and antiviral IgG production[352]. IL-6 induces the production of IL-21 by activated $CD4^+$ T cells in mice which is required for the promotion of *in vitro* antibody production[353]. In the later stages of infection IL-6 is crucial for T_{FH} responses in mice and IL-21 is not sufficient to make up for an absence of IL-6[354]. The provision of B cell help in the GC by T_{FH} cells is therefore reliant on IL-6 signalling.

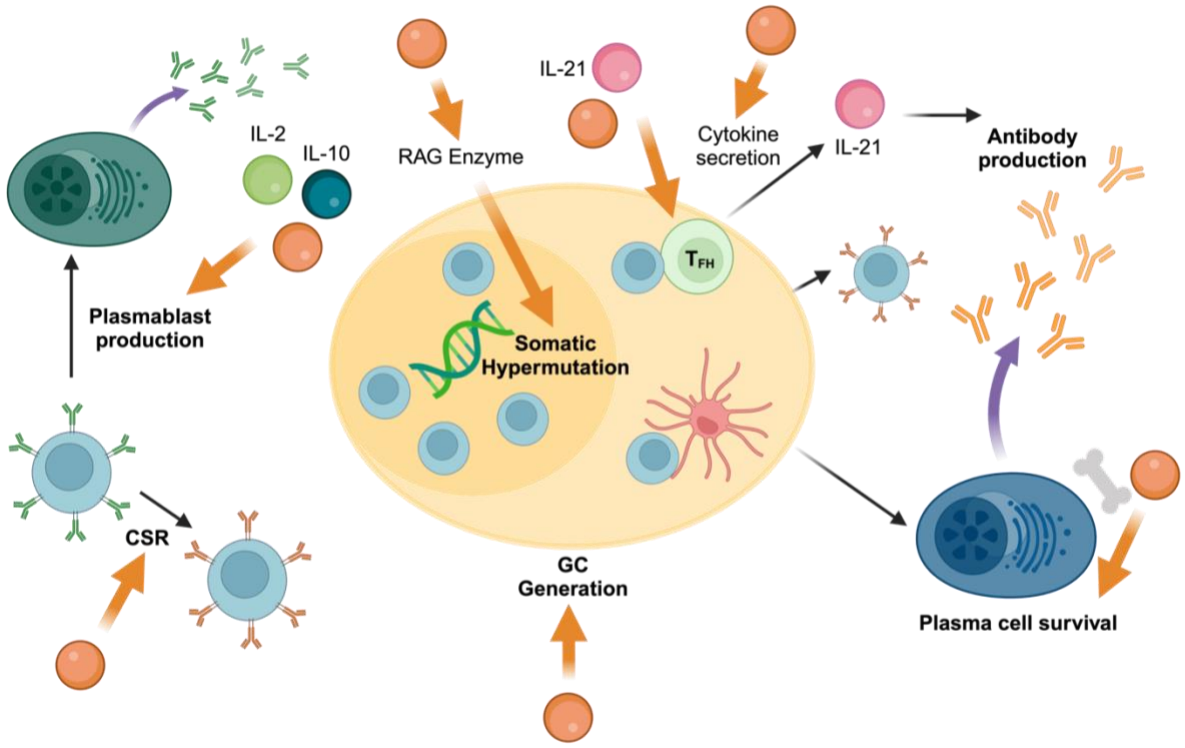

Figure 6.3. The impact of IL-6 signalling on the humoral immune response. Simplified diagram of the components of the humoral immune response. IL-6 signalling contributes to EF CSR and early plasmablast production. IL-6 signalling then encourages the formation of GCs and within the GC promotes SHM and T cell help. Subsequent to the GC IL-6 signalling provides survival signals to plasma cells which have migrated to survival niches in the bone marrow and secrete antibodies. Processes impacted by IL-6 levels indicated by orange arrows and key components of the humoral response influenced by IL-6 in bold. Created using Biorender.com.

6.1.2.2. Survival of plasma cells

The persistence of LLPCs is crucial for the continual production of antibody. IL-6 signalling induces the expression of BLIMP1, a plasma cell differentiation factor[355]. It has been observed that STAT3 activation is required for plasma cell maturation however this can also be done by IL-10 and IL-21[356]. Survival of LLPCs requires migration to a niche, typically the bone marrow for IgG cells, and the receipt of survival signals. IL-6 is one such survival signal and has been observed to be mandatory for the maintenance of human LLPCs *in vitro*[357]. The role of IL-6 on the survival and antibody secretion of plasma cells is dependent on the resident niche, with IL-6 signalling being of more importance in the blood and bone marrow compared to the lymph node[356]. IL-6 therefore has a role in the differentiation, survival, and antibody production of plasma cells, but this is variable for different plasma cell subsets.

6.1.3. IL-6 in COVID-19 vaccine responses in obesity

6.1.3.1. IL-6 and IL-6R shedding in obesity

SAT is a significant source of a large proportion of circulating IL-6[358] and so levels are increased with obesity. Not only is adipose tissue volume increased, the adipose tissue in people with obesity has higher expression levels of both IL-6 and IL-6R, with levels rising with increasing BMI[359]. Circulating sIL-6R is also increased in people with obesity[360] and positively correlates with percentage body fat in young adults[361]. High levels of sIL-6R and IL-6 will contribute to more pro-inflammatory trans signalling and therefore increases in IL-6 expression in obesity are likely immunogenic. However, the inhibition of IL-6 and IL-6R has been seen to increase weight gain in obesity, with IL-6 pathway inhibitor treatment associated with an increase in BMI[362]. Elevated IL-6 and inflammation is a symptom rather than a cause of obesity and may signal in a way to prevent further accumulation of adipose tissue.

6.1.3.2. IL-6 levels in severe COVID-19

IL-6 has also been implicated in the response to SARS-CoV-2 infection. IL-6 levels are increased in COVID-19 disease and higher in those with severe disease and negative

outcomes[363]. Anti-IL-6 therapies such as Tocilizumab are broadly associated with improved outcomes from severe cases of COVID-19[364-366]. One study found that patients treated with anti-IL-6 therapies during infection had improved neutralising antibody levels and T cell response up to 1 year after infection[367]. Severe SARS-CoV-2 infection likely leads to a large inflammatory response which is amplified by positive feedback, causing tissue damage and an ineffective adaptive immune response. Therefore, IL-6 signalling blockade would reduce inflammation in severe infections and improve specificity of the adaptive response and subsequent protection. However, IL-6 also forms part of the normal immune response to pathogenic infection and in moderate infection with lower levels of inflammation blockade may instead impair normal anti-viral response.

6.1.3.3. IL-6 signalling in response to mRNA LNP vaccines

The BNT162b2 and mRNA1273 mRNA vaccines trigger IL-6 production for the formation of an immune response in both mice and humans[368-370]. The BNT162b2 vaccine does not contain a specific adjuvant and instead relies on the inherent adjuvanticity of the LNP and mRNA itself[371]. Vaccination with BNT162b2 leads to a transient increase in IL-6 after the first and second dose[372]. In mice it has been shown that the induction of a potent T_{FH} and B cell response by LNPs relies on the induction of IL-6[373]. IL-6 induction by LNPs may however be dependent on pre-existing levels of inflamation[374]. In human immune cells mRNA vaccination induces IL-1 cytokines which in turn trigger the production of IL-6 and other proinflammatory cytokines, and this effect was amplified by certain LNP formulations[375]. The formulation of lipids making up the LNP influences the immune activation profile, and some lipid components lead to increased IL-6 production[376]. IL-6 production following vaccination with either of the mRNA COVID-19 vaccines appears to have a significant role in the formation of an adaptive immune response (**Figure 6.4**). It is possible that dysregulation of IL-6 signalling in obesity may influence the response to vaccination.

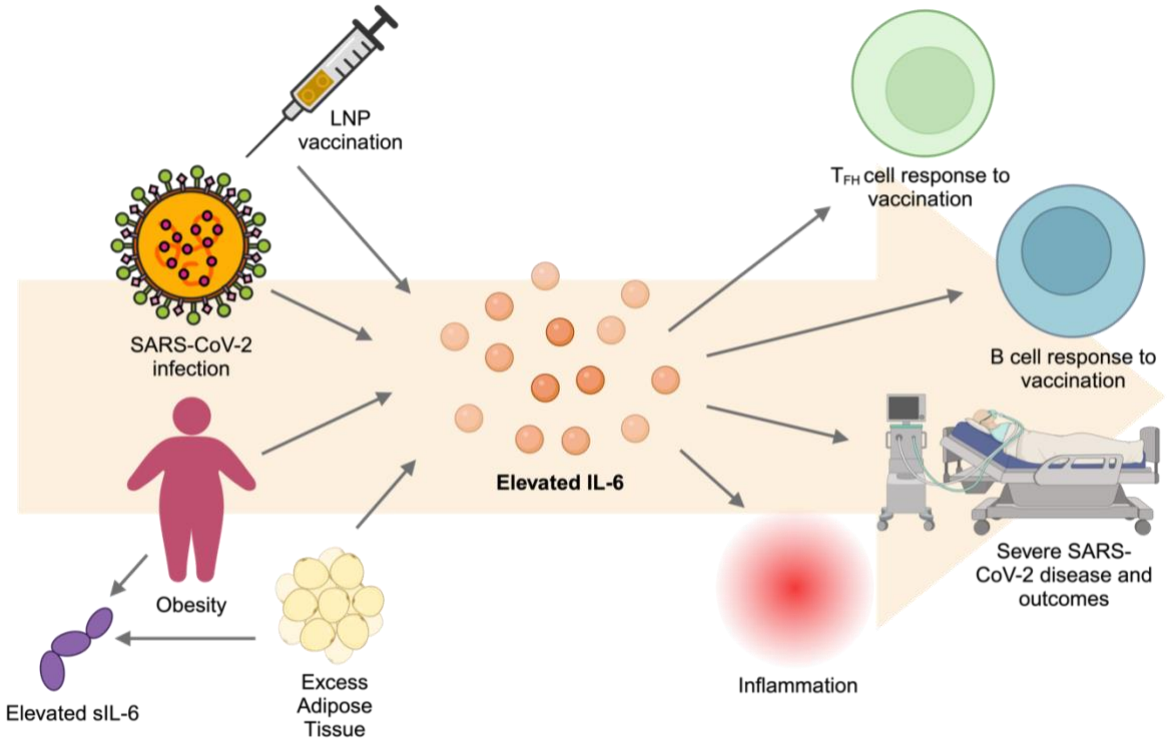

Figure 6.4. IL-6 signalling in obesity and SARS-CoV-2 infection and vaccination. Schematic of contributors to elevation of IL-6 levels: obesity, adipose tissue, LNP vaccination, SARS-CoV-2 infection, and consequences of increased IL-6 signalling: T_{FH} and B cell responses to mRNA vaccination, severe COVID-19, and increased inflammation. Created using Biorender.com.

6.1.4. Chapter aims

IL-6 signalling is dysregulated in individuals with obesity. I aimed to investigate the extent to which aberrations in IL-6 signalling may be responsible for the observed abnormal humoral responses to vaccination in people with severe obesity. This opened avenues of exploration into the possibility of targeting IL-6 signalling to improve responses to mRNA vaccination, not only in people with severe obesity but also in the general population, to increase vaccine efficacy.

The key questions I investigated in this work were:

- Using mouse models, what is the influence of a loss of IL-6 signalling on the humoral response to SARS-CoV-2 vaccination?
- Can antigen specific plasma cells be quantified from the bone marrow of mice and how does the absence of IL-6 signalling influence their numbers?
- Could boosting IL-6 signalling at the time of immunisation improve the response to COVID-19 vaccination?

6.2. Results

6.2.1. Expression of the IL-6R receptor

One potential cause for the impaired humoral responses we have observed in people with obesity may be dysfunctional IL-6 signalling. IL-6 is implicated in both obesity and B cell responses; I therefore included a nucleotide tagged antibody against IL-6R when processing cells for single cell sequencing (**Figure 6.5A-B**). Surface levels of IL-6R were reduced in S binding naïve, memory, and atypical memory B cells from individuals with SO and showed a trend for a similar pattern in transitional B cells (**Figure 6.5C**). Additionally, IL-6R levels on total plasma cells and plasmablasts were reduced in individuals with SO (**Figure 6.5D**). Flow cytometry of PBMCs from individuals with SO by Sarah Spencer also confirmed reduced IL-6R levels on circulating B cells, $CD4^+$ memory T cells, and $CD4^+$ naïve T cells. However, in the plasma cell cluster transcriptomic expression of the *IL6R* gene was increased in SO (**Figure 6.5E**). This suggests that reduced surface levels are not due to reduced gene expression but instead shedding or secretion of the receptor. The main mechanism for the production of sIL-6R is the cleavage of the membrane bound form from the surface of cells by ADAM10 and ADAM17[257]. Expression levels of *ADAM10* were significantly elevated in the plasma cells of individuals with severe obesity and levels of *ADAM17* appeared to be elevated but not significantly (**Figure 6.5F**). Together this suggests that individuals with severe obesity experience increased cleavage of the IL-6R from the surface of B cells which will subsequently reduce the magnitude of classical IL-6 signalling in these cells. This was further confirmed by Sarah Spencer's analysis that sIL-6R levels were elevated in the serum of SCORPIO participants with SO.

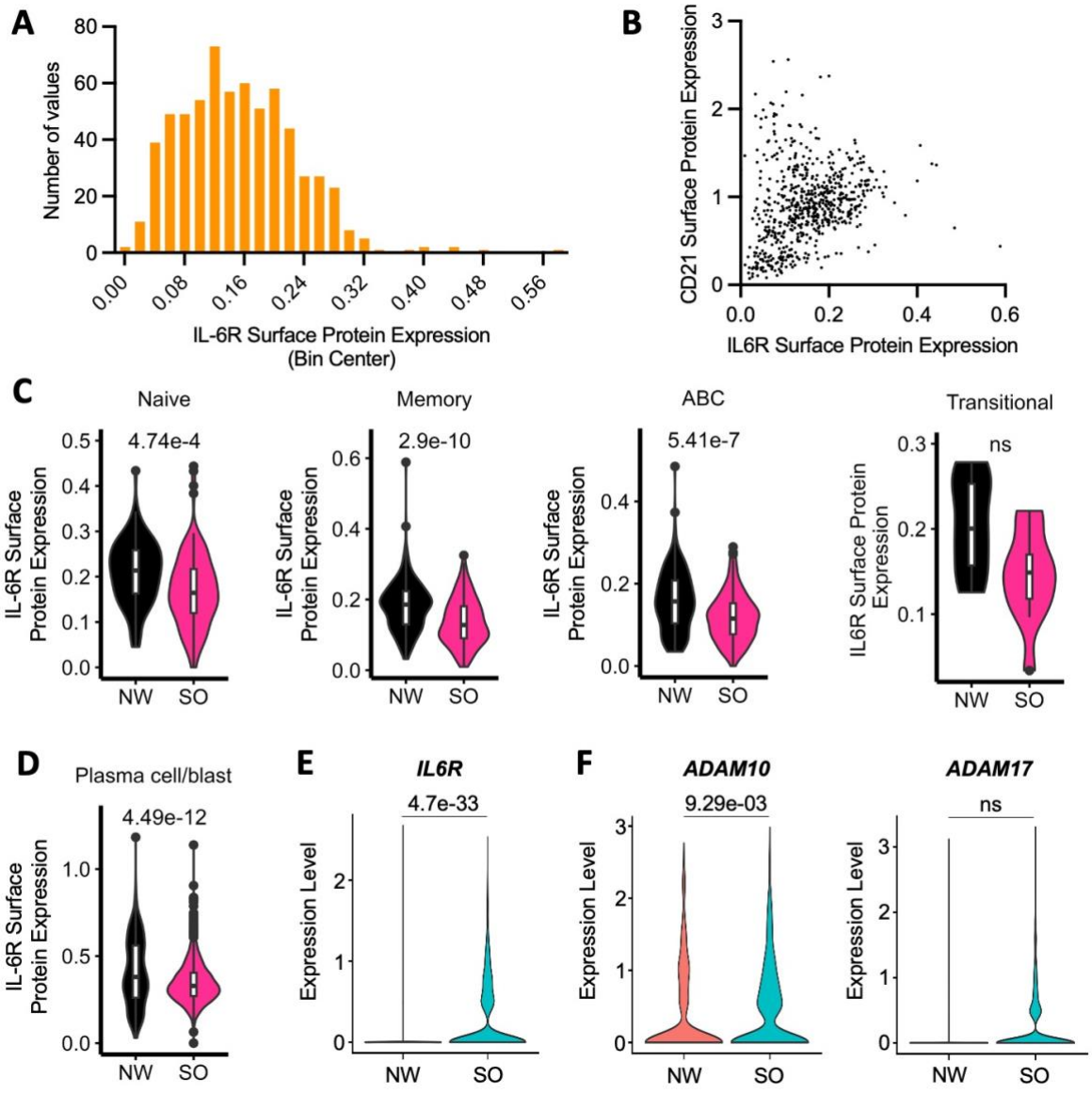

Figure 6.5. IL-6R expression levels of B cells in severe obesity. A) Frequency distribution of IL-6R surface protein expression on all spike binding B cells as determined by CITE-seq, bin width 0.02. **B)** Representative plot of CD21 and IL-6R surface protein expression on all spike binding B cells, each dot represents a single cell. **C-D)** Comparative violin plots of the IL-6R levels on the surface of **(C)** S binding Naïve, Memory, ABC, and Transitional B cells respectively and **(D)** total plasma cells and plasmablasts, of sequenced cells from individuals with SO and NW as determined by CITEseq. **E)** Comparative violin plots of *IL6R* gene expression levels in the total plasma cells from individuals with SO and NW. **F)** Comparative violin plots of the *ADAM10* (**left**) and *ADAM17* (**right**) gene expression levels in the total plasma cells from individuals with SO and NW. Plots **C-F** generated by Dr Zhaleh Hosseini. Two-tailed Mann Whitney test values displayed, ns >0.05.

6.2.2. *Il6ra* knockout mouse model of obesity

6.2.2.1. Knockout of *Il6ra*

To explore the impact of an absence of IL-6 signalling, mice with a knockout of the *Il6ra* gene were generated by single base deletion at the Wellcome Sanger Institute. I stained

cells from these mice and analysed by flow cytometry to quantify IL-6R expression and confirm receptor knockout. The splenocytes from mice homozygous (homs: -/-) and heterozygous (hets: -/+) for the *Il6ra* knockout and from WT mice indicated that receptor expression was eliminated in homs and roughly half that of WT mice in hets (**Figure 6.6C**). Therefore, mice homozygous for the mutant *Il6ra* should be unable to undergo IL-6 signalling. Two mouse studies were conducted to longitudinally assess the humoral response to BNT162b2 vaccination in these mice (**Figure 6.6A&B**).

6.2.2.2. Neutralising capacity in *Il6ra* knockout mice following vaccination

Mouse samples were assessed for live virus neutralising capacity. WT and *Il6ra* knockout mice had comparable peak responses at day 21 (**Appendix D.1.A**) however, knockout mice experienced accelerated waning in their neutralising capacity between days 21 and 79 when compared to WT mice (**Figure 6.6D**). A similar pattern of accelerated waning was also seen in a study completed on mice with high fat diet induced obesity (HFD) (**Figure 6.6E**) (**Appendix D.1.B-C**). When I tested the resting IL-6 levels of these HFD mice by ELISA they were elevated compared to mice on a standard chow diet (CD) (**Figure 6.6F**), Diet induced obesity in mice therefore leads to elevated IL-6 levels and accelerated waning of the neutralising antibody response as was also seen in severe obesity in humans. Deficiency of the IL-6R is sufficient to generate this same accelerated waning in mice.

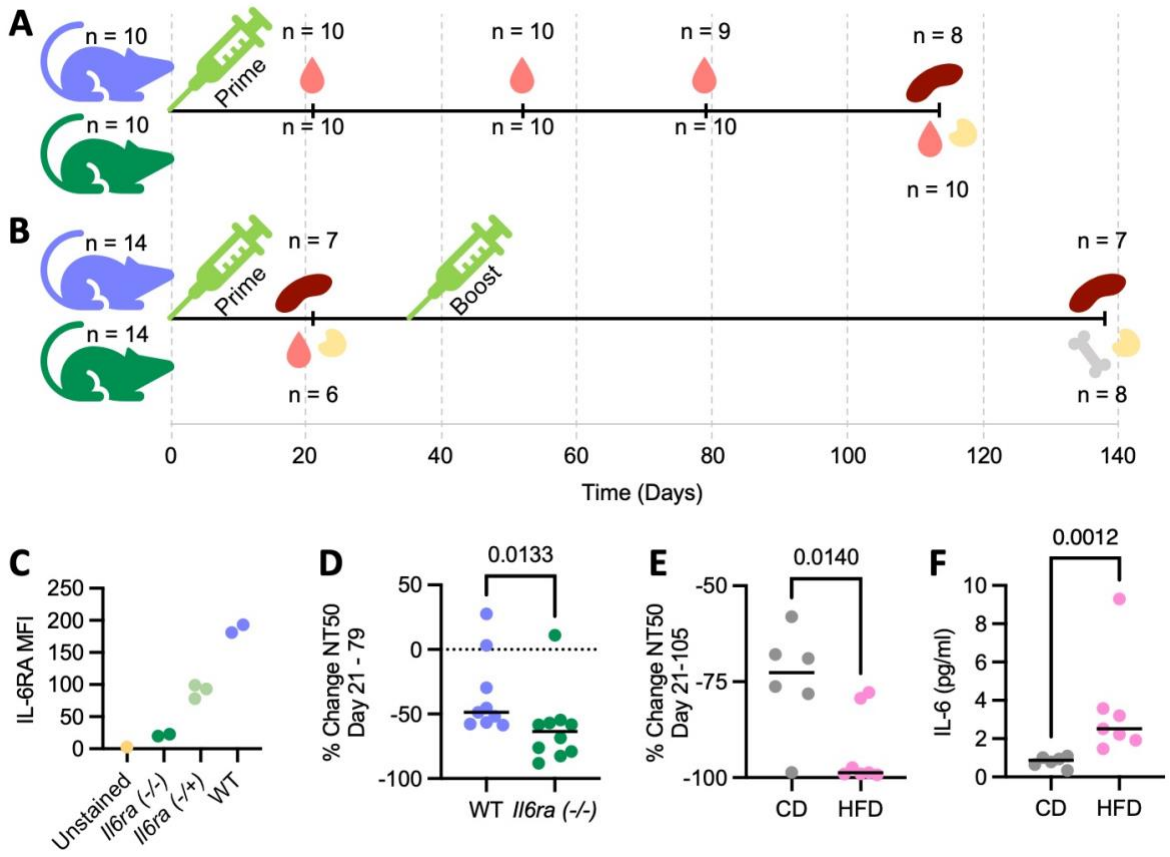

Figure 6.6. Live virus neutralising capacity of vaccinated mice in the absence of IL-6 signalling. A+B) Schematics of the timelines of studies completed to assess the response of *Il6ra* knockout (green) and WT (purple) mice to BNT162b2 vaccination. Mouse and sample numbers indicated by n. **A)** Mice were vaccinated with a single dose of BNT162b2, saphenous bleeds were collected at days 21, 52, and 79 subsequent and spleen, draining lymph node, and cardiac bleeds at day 114. **B)** Mice were vaccinated with a single dose of BNT162b2, spleen, draining lymph node, and cardiac bleeds were collected from a subset of mice at day 21. Remaining mice were boosted with a second dose of BNT162b2 at day 35 and spleen, bone marrow, and cardiac bleeds were collected at day 138. **C)** Comparison of IL-6R levels on the surface of splenocytes from homozygous *Il6ra* knockout (*Il6ra-/-*: green), heterozygous *Il6ra* knockout (*Il6ra-/+*: pale green) and WT (WT: purple) mice, median fluorescence intensity as measured by flow cytometry following staining against the IL-6RA subunit. **D)** Comparison of percentage change in live virus neutralising capacity in WT and knockout mice from day 21 to day 79 post vaccination. **E)** Comparison of percentage change in live virus neutralising capacity in mice on a standard chow diet (grey) and high fat diet (pink) from days 21 to 105 post single BNT162b2 vaccination**. F)** Comparison of resting serum IL-6 concentration measured from the serum of chow diet and high fat diet mice 105 days after vaccination. One point indicates a single mouse. Where present horizontal bars indicate median values and p values from Two-tailed Mann Whitney tests.

6.2.2.3. Antigen specific B cell phenotypes in *Il6ra* knockout mice

To interrogate the potential cause of accelerated waning I assessed the B cells from the spleen and lymph nodes of hom and WT mice collected at day 21 following vaccination. The B cells in the spleens of knockout mice were significantly more frequently IgM^+ with

indications of reduced levels of class switching to IgG (**Figure 6.7A**). Both groups had comparable levels of S binding B cells (**Figure 6.7B**). However, specific cells from knockout mice were more frequently unswitched IgM$^+$ with a trend towards reduced proportions IgG$^+$ (**Figure 6.7C**). In contrast, the B cells in the lymph nodes showed no differences in the proportions of total cells that were S binding but also no differences in the proportion of total or spike binding cells that were IgG$^+$ or IgM$^+$ (**Figure 6.7D,E&F**). The lymph node is the main site of the GC response. Here a population of double positive B cells that were neither definitively IgG$^+$ or IgM$^+$ were present that were not in the spleen, likely due to recent or ongoing CSR. The increased proportion of IgM$^+$ S binding cells in spleens of mice with *Il6ra* knockout is similar to that seen in the sequenced B cells of individuals with severe obesity. This may indicate reduced levels of CSR and B cell maturation when IL-6 signalling is impaired either by knockout or severe obesity.

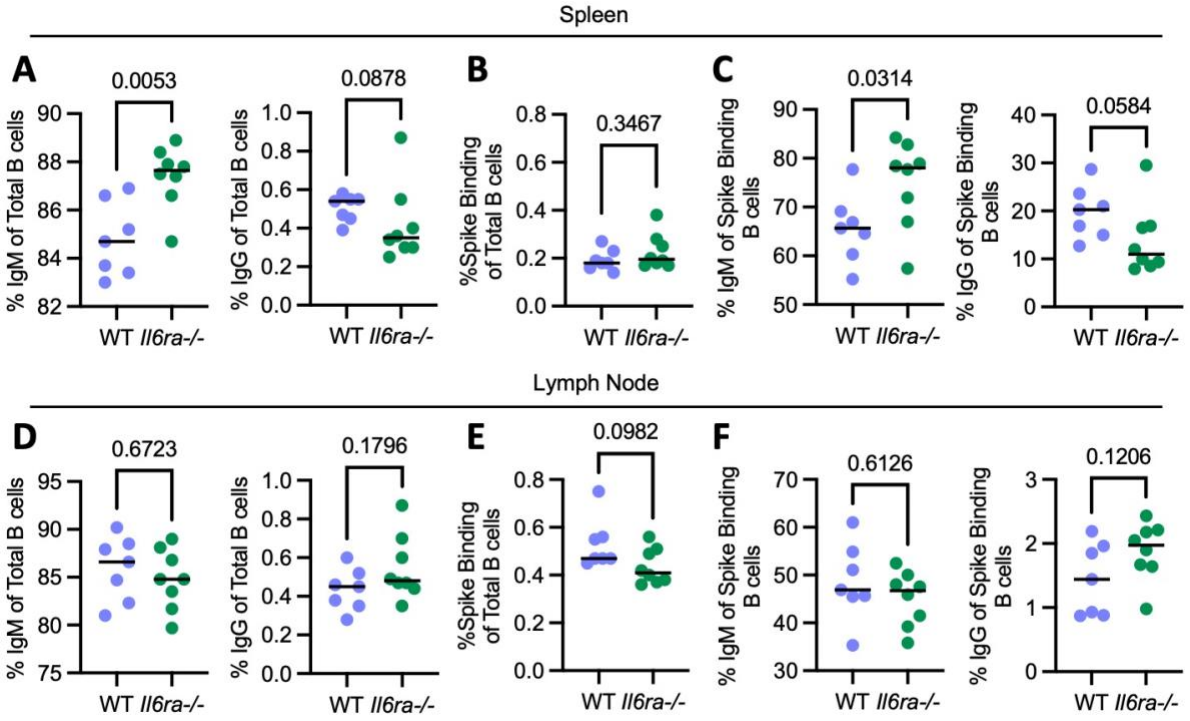

Figure 6.7. Class switching of antigen specific B cells in mice in the absence of IL-6 signalling. A-C) Comparison of B cell subsets in the spleen of *Il6ra* knockout and WT mice at day 21 after vaccination with BNT162b2. **A)** Comparison of the proportion of total B cells that are IgM$^+$ (**left**) and IgG$^+$ (**right**). **B)** Comparison of the proportion of total B cells that are spike binding. **C)** Comparison of the proportion of spike binding B cells from that are IgM$^+$ (**left**) and IgG$^+$ (**right**). **D-F)** Comparison of B cell subsets in the draining lymph node of *Il6ra* knockout and WT mice at day 21 after vaccination with BNT162b2. **D)** Comparison of the proportion of total B cells that are IgM$^+$ (**left**) and IgG$^+$ (**right**). **E)** Comparison of the proportion of total B cells that are spike binding. **F)** Comparison of the proportion of spike binding B cells that are IgM$^+$ (**left**) and IgG$^+$ (**right**). For all plots a single dot represents one mouse, horizontal bar indicates median of group, Two-tailed Mann Whitney test values displayed.

6.2.3. The assessment of LLPCs

Following the GC response LLPCs migrate to niches in the bone marrow, spleen, and gut. IgG plasma cells responsible for the majority of circulating antibody migrate to the bone marrow and persist due to the receipt of survival signals such as CXCL12, APRIL, and IL-6 signalling through the IL-6R[377]. The residence of plasma cells in the bone marrow, mean that it is incredibly challenging to assess the extent of the LLPC response and survival in human subjects without invasive sampling. In mice, bone marrow can be collected following termination from the femur bone. This enables plasma cells to be assessed at a single time point per mouse. The identification of *Il6ra* knockout mice as a model for vaccine responses in severe obesity allows further investigation of the role of the IL-6R in antibody waning and plasma cell longevity.

6.2.3.1. A FluoroSpot assay to quantify IgA, IgM, and IgG secretion by plasma cells

I tested whether a FluoroSpot assay for the detection of secreted IgA, IgG, and IgM was able to quantify LLPCs in bone marrow and spleen samples from WT and hom mice. I coated PVDF membrane 96 well plates with Fab binding total capture antibodies or HexaPro trimeric spike protein to capture total and spike binding antibodies. Mouse cells were incubated on coated plates for 14 – 16 hours, to enable time for the secretion of antibodies from plasma cells without sufficient time for memory cells to be activated and differentiate into new ASCs. Secreted antibodies were captured by the coating proteins and three secondary antibodies against the constant region of IgA, IgM, or IgG conjugated to different fluorophores were used for detection. The previous location of cells secreting antibodies of each isotype was detected as corresponding-coloured fluorescent spots on the membrane and thus quantified as SFU (**Figure 6.8.A&B**).

To begin, I assessed the ability of the FluoroSpot assay to detect S specific antibody secreting plasma cells in the bone marrow of WT mice. Bone marrow from 21 days after placebo, single BNT162b2, or multiple BNT162b2 vaccination was incubated at $5x10^5$, $2.5x10^5$, and $1.25x10^5$cells per well on plates coated with total capture and spike. Total IgG, IgM, and IgA SFU per well increased with increasing number of cells per well, with the best distinction between vaccination state being at the highest cell number,

$5x10^5$cells per well (**Figure 6.8C**). The only detectable isotype of S binding antibody was IgG, again SFU per well increased with cell number and the best distinction between groups was at $5x10^5$ cells per well (**Figure 6.8D**). All subsequent assays were therefore completed with $5x10^5$ cells per well. S specific ASCs could be definitively detected in the bone marrow of mice that had received multiple doses of BNT162b2, both as total SFU/10^6 cells and as a proportion of total captured antibody (**Figure 6.8E&F**). However, spike binding ASCs were not detected at a level significantly above that of naïve in single immunised mice. This may be due to a lack of LLPC production after a single dose of vaccine or 21 days being an insufficient length of time for plasma cells to migrate to and settle in the bone marrow. Interestingly, total numbers of ASCs of all isotypes appeared to be higher in single vaccinated and boosted mice regardless of antibody isotype (**Figure 6.8G**). Antigen exposure may be sufficient to drive increased antibody production or plasma cell survival in the bone marrow in a non-specific way.

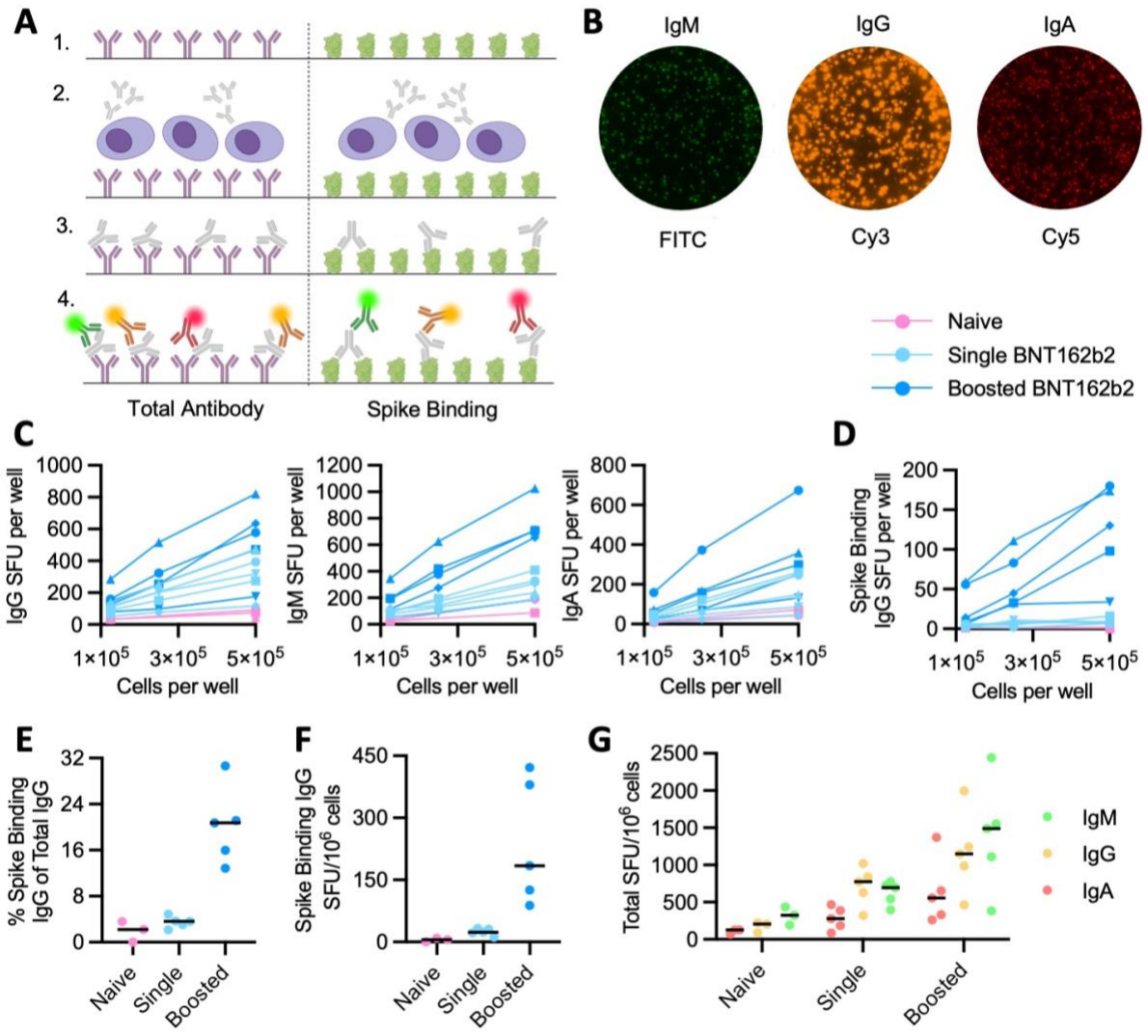

Figure 6.8. Mouse IgM/IgG/IgA FluoroSpot assay for the quantification of LLPCs in bone marrow. A) Graphical representation of the steps of a FluoroSpot to detect total antibody (left) and spike binding antibody (right) secreted by plasma cells. 1) Plate is coated with total capture antibody (purple) or trimeric spike (green), 2) Plate is incubated overnight with a sample containing plasma cells (lilac) which secret antibody without stimulation (grey), 3) Antibodies bind to total capture and spike protein and cells are removed, 4) Detection antibodies for IgM (green), IgG (yellow), IgA (red) conjugated to different fluorophores bind to the Fc regions of the captured antibodies and are detectable as spots. Created using Biorender.com. **B)** Images of representative wells of total antibody captured by secreting cells of each isotype. **C)** Plots of the relationship between total SFU counted per well and number of cells plated per well for IgG (**left**), IgM (**centre**), and IgA (**right**) production. **D)** Plot of the relationship between SFU counted per well for spike binding IgG and number of cells plated per well. **E)** Dot plot of spike specific antibody producing cells as a proportion of total antibody producing cells in each state of vaccination. **F)** Dot plot of spike binding antibody producing cells per million cells in each state of vaccination. **G)** Total ASCs of IgA, IgG, and IgM isotype from mice in each state of vaccination. For all plots a single dot represents the average value from a single mouse at given condition. **C-F**) cells from naïve mice (pink), mice vaccinated with a single dose of BNT162b2 (light blue), and mice vaccinated with multiple doses of BNT162b2 (dark blue). Horizontal bars indicate median for group.

I then completed an experiment to determine the optimal coating concentration of protein to detect spike binding ASCs. I coated plates with 10, 20, and 40µg/mL of HexaPro S protein. I again tested bone marrow cells from mice 21 days after placebo, single BNT162b2, or multiple BNT162b2 vaccination and additionally after multiple spike construct vaccination. The number of IgG SFU detected increased 10-20µg/mL and reached an upper limit before 40µg/mL of spike protein (**Figure 6.9A**). S binding IgM ASCs could not be significantly detected in any of the mouse groups and SFUs detected for IgA increased with increasing S protein concentration 10-40µg/mL for BNT162b2 boosted mice but were mostly undetectable for other groups (**Figure 6.9A**). I subsequently chose to use 25µg/mL of protein to coat plates for future experiments to balance detection of ASCs with the time needed to produce large quantities of the HexaPro S protein.

As plasma cells were more easily quantifiable in multi-dose vaccinated WT mice, I chose to assess the ASCs of twice immunised WT and *Il6ra* knockout mice at day 103 after final immunisation. To test whether two doses and 103 days provided sufficient antigen exposure and time for the generation and migration of antigen specific LLPCs, I assayed bone marrow from two WT and one hom from this timepoint. S binding IgA and IgG ASCs were detectable in all three of the test mice at levels above that of naïve mice (**Figure 6.9B**). Spike binding IgM ASCs remained undetectable in the bone marrow under all conditions despite the detection of nonspecific IgM secretion. Although IgG plasma cells migrate to the bone marrow, there is significant evidence that IgM plasma cells migrate to the spleen[378]. As such I tested splenocytes from three mice harvested at different timepoints following single or double vaccination with BNT162b2 at $1.25x10^5$, $2.5x10^5$, $5x10^5$, and $1x10^6$ cells per well. IgA, IgM, and IgG ASCs were detectable in all samples with increasing SFU per well as cell numbers increased (**Figure 6.9C**). However, there were no detectable S binding ASCs of any isotype in either of the mice, even when cells were assayed at $1x10^6$ cells per well (**Figure 6.9D**). I therefore continued to use bone marrow samples to compare LLPCs between WT and *Il6ra* knockout mice after vaccination.

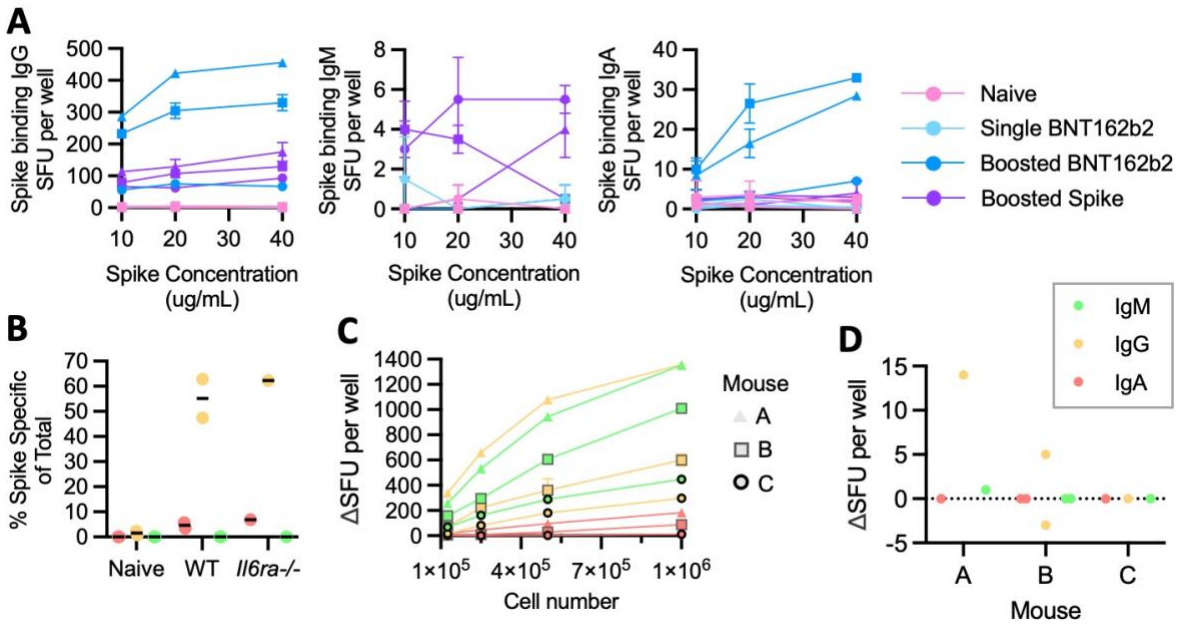

Figure 6.9. Detection of antigen specific plasma cells in bone marrow but not spleen. A) Plots of the relationship between spike specific SFU counted per well and concentration of spike protein used to coat the well for IgG (**left**), IgM (**centre**), and IgA (**right**) production. Cells from naïve mice (pink), mice vaccinated with a single dose of BNT162b2 (light blue), mice vaccinated with multiple doses of BNT162b2 (dark blue), and vaccinated with multiple doses of in-house spike mRNA construct (purple). **B)** Comparison of spike specific antibody producing cells as a proportion of total antibody producing cells for each isotype from the bone marrow of naïve mice and WT or *Il6ra* knockout mice 103 days after two doses of BNT162b2. **C)** Relationship between total antibody producing cells and total splenocytes plated per well from 3 different mice (indicated by key). **D)** Spike specific IgA, IgG, and IgM producing cells from splenocytes from each of 3 mice plated at 1 million cells per well. Dotted line indicates 0. **All plots**) a single dot represents the average value from a single mouse at given condition. **B-D)** IgA (red), IgG (orange), and IgM (green). Where present bars indicate median values.

6.2.3.2. Quantification of plasma cells in *Il6ra* knockout mice

I used the optimised FluoroSpot to quantify total and S specific LLPCs in the bone marrow of seven WT and seven *Il6ra* knockout mice collected 103 days after second dose vaccination with BNT162b2. I included bone marrow from four naïve WT mice as a negative control.

The remaining cells were stained for isotype and plasma cell markers and assessed using flow cytometry to validate the findings of the FluoroSpot. There are a number of markers used to identify plasma and ASCs in mice. I looked at three key markers, B220 which is downregulated over the course of plasma cell differentiation, and CD138 and TACI which are both upregulated. The proportion of bone marrow cells that were $B220^{-}CD138^{+}$ plasma cells was similar in WT and knockout mice (**Figure 6.10A**) however knockout mice

had reduced levels of total $B220^{int}$ $CD138^{+}$ plasmablasts when compared to WTs (**Figure 6.10B**). The proportion of total cells which were defined as antibody secreting plasma cells based on co-expression of CD138 and TACI was also comparable in WT and knockout mice although levels were elevated in both when compared to naïve mice (**Figure 6.10C&D**).

Total IgA, IgG, and IgM ASCs as measured by FluoroSpot were at similar levels in knockout and WT mice, with all isotypes being elevated in vaccinated groups compared to naïve mice (**Figure 6.10E**). A hint towards reduced levels of IgG ASCs in *Il6ra* knockout mice was present in the FluoroSpot data, and this was mirrored in the flow cytometric assessment although not significant (**Figure 6.10F**). Despite this there was no indication of any differences in IgM ASCs (**Figure 6.10G**). The FluoroSpot for total ASCs and flow cytometry assay produced comparable values for the cell count normalised levels of IgG secreting cells ($R^2 = 0.5986$, $P = 0.0002$) (**Figure 6.10H**) indicating the FluoroSpot is robust in its identification of LLPCs.

There was no difference in the levels of S binding IgG or IgA secreting cells in the bone marrow of knockout mice or WT when considered as total SFU or as a proportion of the total ASCs (**Figure 6.10I&J**). S binding IgM secreting cells were not detectable in any group and specific IgA and IgG were significantly elevated in both vaccinated mouse groups compared to in naïve mice. Surprisingly, these data indicate that although lacking the IL-6R, a key survival receptor for plasma cells, mice with knockout of the *Il6ra* have no deficiency of plasma cells in their bone marrow. Additionally, they are able to produce antigen specific plasma cells in response to vaccination which can persist for at least 100 days following antigen encounter. Furthermore, despite reduced levels of CSR in the spleen, plasma cells in the bone marrow are not significantly less class switched in mice without IL-6R.

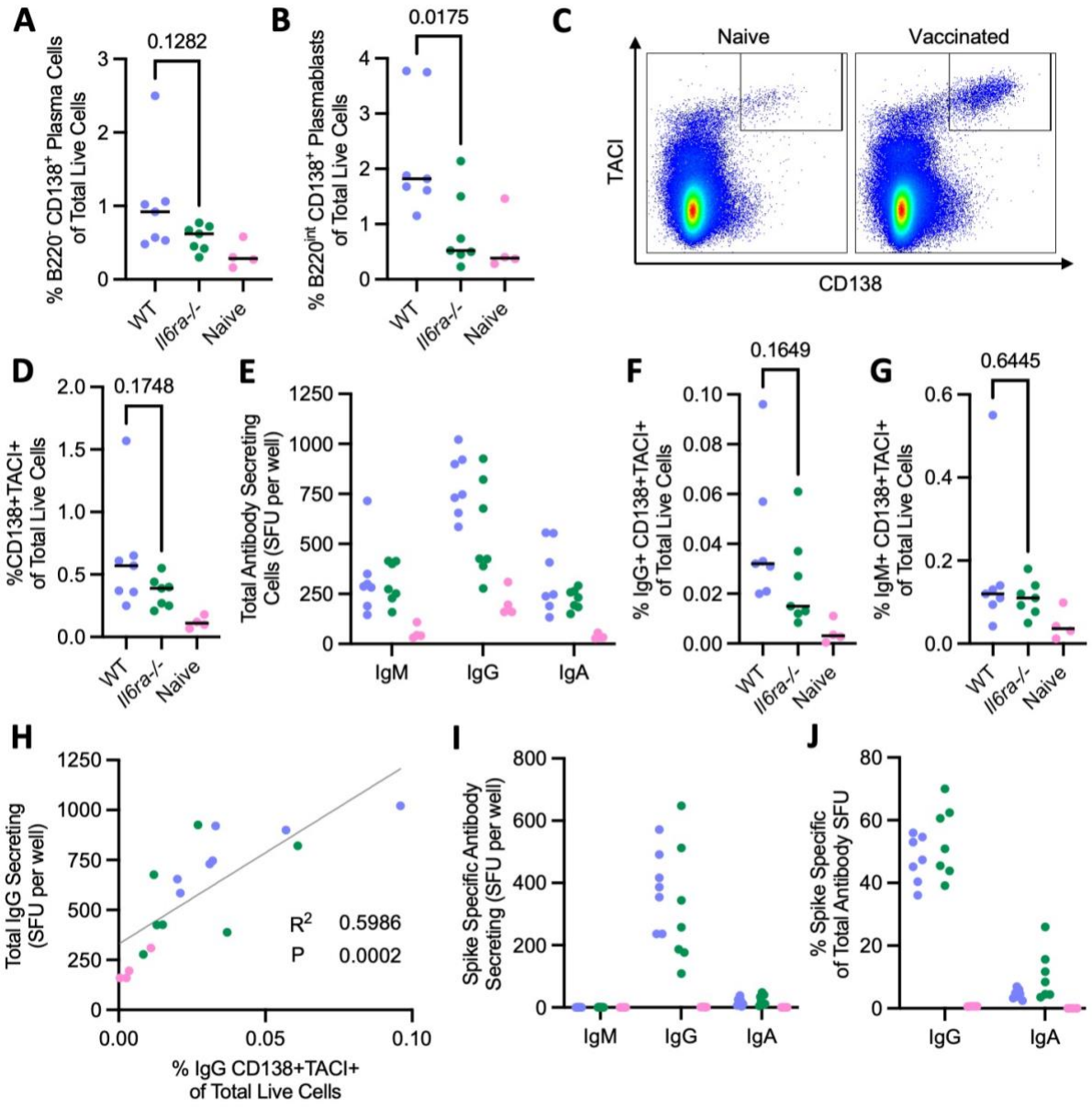

Figure 6.10. Long lived antigen specific plasma cells in the bone marrow of IL-6R deficient mice following BNT162b2 vaccination. A-B) Comparison of the proportion of total live cells which are **(A)** B220^{-}, CD138^{+} plasma cells and (**B)** B220^{int} CD138^{+} plasmablasts, in vaccinated WT and *Il6ra* knockout mice. **C)** Representative plots of TACI^{+} CD138^{+} plasma cells from the bone marrow of WT vaccinated and naïve mice. Pseudo colour – one dot represents a single cell. **D)** Comparison of the proportion of total live cells which are CD138^{+}, TACI^{+} antibody secreting plasma cells in WT and *Il6ra* knockout vaccinated mice. **E)** Total antibody secreting plasma cells in the bone marrow, as quantified by total antibody capture FluoroSpot assay, per well for each antibody isotype. **F-G)** Comparison of **(F)** IgG^{+}TACI^{+}CD138^{+} plasma cells and **(G)** IgM^{+}TACI^{+}CD138^{+} plasma cells as a percentage of total live bone marrow cells in WT and *Il6ra* knockout vaccinated mice. **H)** Relationship between total IgG secreting plasma cells as measured by FluoroSpot and percentage IgG^{+}TACI^{+}CD138^{+} of live cells as measured by flow cytometry (Simple Linear Regression). **I)** Spike binding ASCs by antibody isotype as detected by FluoroSpot. **J)** Spike binding ASCs as a proportion of total ASCs for IgG and IgA antibodies. For all plots excluding (C) one dot represents the average value for a single mouse. Comparisons between vaccinated WT (purple) and *Il6ra* knockout mice (*Il6ra-/-*: green) are with two-tailed Mann Whitney tests, unvaccinated naïve WT mice (pink) are included to indicate baseline.

6.2.4. IL-6 signalling as a therapeutic target

6.2.4.1. Validation of IL-6R mRNA constructs

Evidence that deficiency of the IL-6R leads to accelerated waning of the vaccine response in mice and potentially individuals with severe obesity identifies IL-6 signalling as a possible target for enhancing vaccine responses. One way in which this could be done is by increasing levels of the sIL-6R or introducing a fusion protein of sIL-6R and IL-6 known as Hyper IL-6 (hIL-6R)[379] at the point of vaccination. Theoretically both of these modes should increase levels of IL-6 signalling in WT mice and introduce IL-6 signalling to receptor knockout mice. To trial this, mRNA constructs encoding the membrane bound IL-6R (mIL-6R), sIL-6R and hIL-6R (**Figure 6.11A**) were designed and created in the Thaventhiran lab. To confirm the products following translation, RNA sequences encoding constructs were used to transfect HEK293T cells and the conditioned culture media applied to splenocytes from *Il6ra* knockout mice along with IL-6 (**Figure 6.11B**). Following this stimulation, I lysed these cells and completed a western blot for STAT3 and pSTAT3. STAT3 is phosphorylated upon IL-6 signalling and therefore the presence of pSTAT3 indicated that a functional IL-6R was produced and secreted following transfection with the construct. As anticipated, cells incubated with media from un-secreted mIL-6R constructs had no STAT3 phosphorylation. Those incubated with the sIL-6R construct had increased levels of pSTAT3 when stimulated with IL-6 but none in the absence of IL-6. Those incubated with the hIL-6R construct had high levels of pSTAT3 regardless of the presence of IL-6 (**Figure 6.11C&D**). This confirms the production of sIL-6R and hIL-6R upon the translation of these constructs and the ability of hIL-6R to signal independent of IL-6 availability.

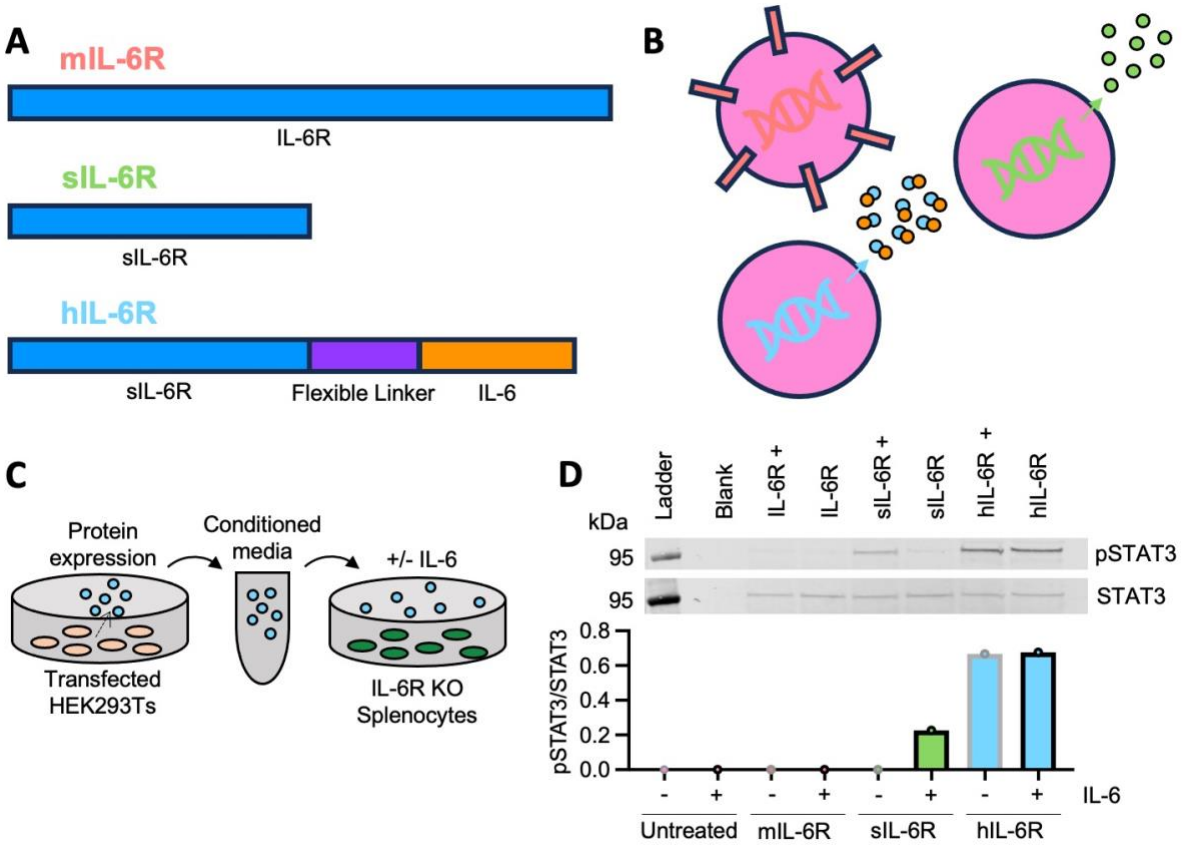

Figure 6.11. Expression of mRNA constructs encoding IL-6R. A) Diagrammatic representation of the structure of the mRNA constructs. mIL-6R encodes full length IL-6R, sIL-6R encodes truncated secreted form of IL-6R and hIL-6R encodes the truncated sIL-6R with a flexible linker (purple) joining it to IL-6 (orange) **B)** Diagram of the expected protein expression of mIL-6R (red), sIL-6R (green), and hIL-6R (blue) mRNA constructs when transfected into cells. **C**) Schematic of culture experiment to stimulate splenocytes. HEK293T cells were transfected with mRNA constructs and cultured to express them. Conditioned media was collected and layered onto *Il6ra* knockout splenocytes which were cultured in the presence and absence of IL-6. **D)** Western blot for STAT3 and pSTAT3 in *Il6ra* knockout mouse splenocytes stimulated with or without IL-6 and supernatant from cells transfected with mIL-6R, sIL-6R, or hIL-6R construct. Bar plot of the ratio of pSTAT3 band intensity to STAT3 band intensity for each condition, black outline indicates presence of IL-6 stimulation, grey indicates absence.

6.2.4.2. Co-immunisation with hIL-6R in IL-6R deficient mice

As a pilot experiment, WT and *Il6ra* knockout mice were immunised with sIL-6R, hIL-6R constructs or empty LNPs, alongside the BNT162b2 vaccine, IV. Tissues were collected at day 21 following vaccination, and I assayed the serum for spike binding IgG. Peak neutralising antibody responses following BNT162b2b vaccination in WT and knockout mice have previously been comparable. Therefore, as expected, concentrations of S binding IgG at day 21 were comparable in all mice (**Figure 6.12A**). However, significant levels of variation were seen within groups. I then stained splenocytes to investigate whether IL-6 signalling impacted the isotypes of antigen specific B cells. As hIL-6R was

confirmed to function independently of the presence of IL-6 and induced a high magnitude of signalling *in vitro*, I focused on the ability of hIL-6R to recover B cell isotypes. The proportion of total B cells that were IgM$^+$ (**Figure 6.12B**) and IgG$^+$ (**Figure 6.12C**) were comparable in *Il6ra* knockout vaccinated with an empty LNP and hIL-6R. However, the introduction of hIL-6R appeared to boost the production of IgG S binding B cells. The proportion of binding cells which were IgM$^+$ was reduced (**Figure 6.12D**) and IgG$^+$ was increased (**Figure 6.12E**). This suggests that the induction of IL-6 signalling by hIL-6R may be sufficient to recover the class switching of specific B cells early in the vaccine response.

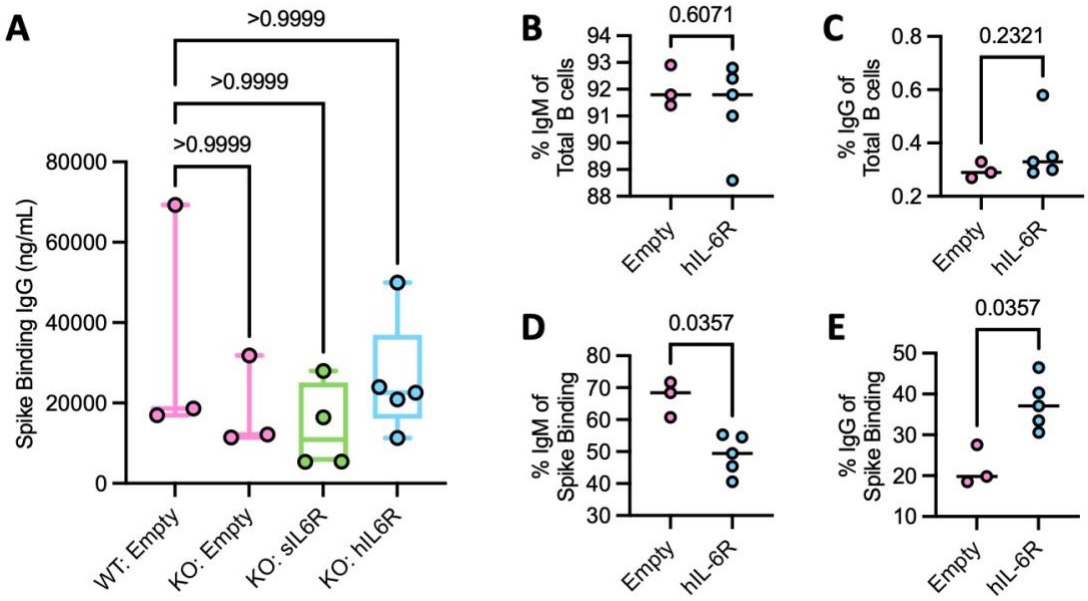

Figure 6.12. Impact of hIL-6R construct on BNT162b2 vaccine responses in IL-6R deficient mice. A) Comparison of spike binding IgG concentration 21 days after vaccination in WT mice and *Il6ra* knockout mice immunised with BNT162b2 in addition to sIL-6R construct (green), hyper IL-6 (blue) and an empty LNP (pink). **B-E**) Comparison of the splenocytes of *Il6ra* knockout mice vaccinated with empty LNP (pink) or hIL-6R (blue) in conjunction with BNT162b2 that are **(B**) IgM, and **(C)** IgG as a proportion of total B cells, (**D**) IgM and (**E**) IgG as a proportion of spike binding B cells. Where present P values are from Mann Whitney tests, horizontal bars indicate median values. Box plots indicate median, interquartile ranges and minimum and maximum values.

6.3. Discussion

6.3.1. Results

6.3.1.1. *Il6ra* knockout mouse model and LLPCs

The use of mice as a model for severe obesity enables detailed analysis of specific features and isolation of key factors of the immune response which may not be possible when considering human research subjects. In addition to previously discussed markers of humoral immunity, single cell sequencing analysis revealed that individuals with SO experience increased shedding of the IL-6R. This is a receptor expressed on the surface of immune cells and known to play a role in humoral immunity. Mice with a knockout of the gene encoding the IL-6R experience the same accelerated waning of neutralising capacity following a vaccination with BNT162b2, as seen in mice and humans with obesity. *Il6ra* knockout mice have an absence of membrane bound and sIL-6R, an extreme of the phenotype of reduced surface IL-6R expression seen in severe obesity. Therefore, these mice are useful in identifying the impact reduced IL-6R expression may have on immune responses in obesity. Normal peak and accelerated waning of the neutralising response, and reduced proportions of class switched S binding cells in *Il6ra* knockout mice mirror data previously obtained from people with severe obesity. Although mice heterozygous for the *Il6ra* knockout are phenotypically more similar to the condition in severe obesity, they do not experience the same waning. This indicates that reduced expression of the IL-6R alone is not sufficient to lead to impaired antibody maintenance, but contributes, in combination with other features of the multifactorial impact of obesity on immunity[199]. Therefore, where sampling would be invasive and costly in human participants, bone marrow from homozygous mice could be used to assess the impact of downregulated IL-6R expression on the development and survival of LLPCs.

I was able to optimise a FluoroSpot assay for the approximate quantification of LLPCs in bone marrow samples which I cross validated by flow cytometry. My assessment of the LLPCs in the bone marrow of *Il6ra* knockout and WT mice, surprisingly, revealed no significant differences in total, and antigen specific, plasma cell numbers. IL-6 is a key signalling molecule for the production and survival of LLPCs, and the production of antibodies. The presence of antigen specific LLPCs in the bone marrow of *Il6ra* knockout mice indicates that IL-6 may be redundant in these roles in mice. Furthermore, its

absence can be overcome by alternative signalling pathways to produce a normal plasma cell response[377,380,381]. From this data, there is no evidence to support that accelerated antibody waning in severe obesity is due to impaired IL-6 signalling, resulting in reduced LLPC persistence. However, unlike in other assays, due to limitations on sample availability and assay sensitivity, the FluoroSpots were conducted on twice vaccinated mice. Assessment of the neutralising capacities of these mice was unable to detect any waning up to 100 days after second dose (**Appendix D.1.D**). A booster dose of BNT162b2 therefore improves the peak response and maintenance of antibodies in both WT and *Il6ra* knockout mice and it is unclear if there is any difference in ASCs between these groups following two vaccines. LLPCs are traditionally believed to arise solely from the GC response, however some suggest that while LLPCs are not produced by the primary EF response they can be made by the secondary[377]. If accelerated waning of antibody responses is due to a deficiency in the GC response in *Il6ra* knockout mice, a second dose may overcome this and may enable LLPCs to be instead supplied by the EF response. Therefore, boosting with a second dose may cover any bias towards an EF response in these mice. I was unable to attribute accelerated waning to a deficiency of LLPC persistence, caused by the reduction of IL-6 signalling. In fact, I demonstrated that total absence of the IL-6R does not prevent LLPC production or survival in mice. Nevertheless, the waning of neutralising capacity and alterations in the IgM/IgG ratio of specific cells in *Il6ra* knockout mice indicate an impairment of the humoral vaccine response in the absence of IL-6R. One which may be mirrored in the obesity induced reductions of IL-6R expression.

6.3.1.2. Targeting IL-6 signalling to improve vaccine responses

Immune responses to vaccination in *Il6ra* knockout mice indicate the importance of IL-6 signalling in the vaccine response. Hence this shows that therapeutic repair of impaired IL-6 signalling in cases of immune dysfunction may improve antibody and B cell responses to vaccination. I have shown, in a pilot experiment, that the enhancement of IL-6 signalling with hIL-6R mRNA constructs may increase the production of class switched S specific B cells. This construct could be incorporated into the mRNA based COVID-19 vaccines and has shown some potential in improving the initial vaccine

response in *Il6ra* knockout mice. However, additional larger and longer-term studies must be completed to determine whether this recovers antibody waning. Additionally, this data only shows that the introduction of IL-6 signalling, where it was previously absent, improves class switched B cell responses and not a boosting of pre-existing levels. Mouse IL-6 is unable to stimulate the human IL-6R[382] indicating that IL-6 may have functional differences in each species. This should be taken into consideration when testing therapeutic options in mice as the impacts on vaccine responses may not be transferable.

6.3.2. Conclusions and future directions

A combination of scRNA-seq of human B cells and vaccination studies in *Il6ra* knockout mouse models, highlight a deficiency of classical IL-6 signalling in obesity and a potential contributor to the waning of antibody response in SO. Increased IL-6 signalling at the point of vaccination may improve vaccine response by encouraging class switching of specific B cells to IgG, however it is unclear if this will prevent antibody waning.

The reason for reduced levels of specific class switched memory B cells in people with SO and *Il6ra* knockout mice remains uncertain. I have been unable to rule out impaired survival of LLPCs, however have confirmed deficiency of IL-6 signalling does not prevent their production. This further demonstrates the presence of functional GCs but does not rule out a bias towards the EF response. The GC reaction is complex, and its output is dependent on the frequency, size, organisation, and throughput of the GCs themselves. Any one of these factors may contribute to the impaired production of class switched memory and antibody maintenance in severe obesity and *Il6ra* knockout. Further studies with *Il6ra* knockout mouse models will provide improved distinction of the influence of IL-6 signalling on mRNA vaccine responses. GC establishment, expansion, and dissolution occur from days 1 to 21 following antigen exposure. Future mouse vaccine studies should consider the collection of tissues over these timepoints. Flow cytometry could be used to quantify GC cells by their expression of Fas, GL-7 and other markers[383] and histopathology can be used to visualise the structure and organisation of GCs[384]. Additionally, longer term experiments should be conducted to assess vaccine responses in double vaccinated mice[385]. Although time consuming, these studies would provide a

better model for the response in humans who will have received at least a two-dose vaccine schedule, likely in addition to boosters.

The optimised FluoroSpot assay could be used to assay the LLPCs from the bone marrow of other mouse models of obesity following vaccination. It is possible that LLPCs are dysregulated in severe obesity but not due to IL-6 signalling. As such, application of this assay to other mouse models of obesity may inform on if and why this is the case. Additionally, this assay could also be adapted for the assessment of human bone marrow samples. Although bone marrow sampling is invasive, bone marrow biopsies are routinely completed for multiple clinical tests[386]. Additionally, studies have been completed using bone marrow samples collected during hip replacement surgeries[212]. It would, therefore, be possible to establish a clinical study to assess the LLPCs in the bone marrow of individuals with obesity, using FluoroSpot assessment or other plasma cell assays.

Continued assessment of the hIL-6R in mice to determine its impact on antibody waning will reveal its potential in improving the longevity of the BNT162b2 vaccine response. Following this, additional work should be undertaken to adapt the construct for human use and test it *in vitro* in human cell lines. Provided success in these steps, this technology could be developed for the improvement of vaccine responses in any group of people at risk of accelerated antibody waning. Such development should include assessments of toxicity, optimisation of dose and delivery mode, and long-term tracking of the immune response to vaccination. hIL-6R will increase IL-6 signalling to all cells through gp130, dose must be considered to avoid triggering systemic inflammation and a cytokine storm. Incorporation of the construct into an mRNA vaccine may be efficient, however there is a risk of evoking an immune response against the hIL-6R construct, which could lead to autoimmunity. Trials of repeated construct vaccination in WT mice should inform the level of risk this poses. In the case of individuals with obesity, unlike *Il6ra* knockout mice, IL-6R remains present. Membrane IL-6R levels are reduced and sIL-6R is increased, therefore the efficacy of hIL-6R constructs in mice may not translate into a benefit for humans with severe obesity. It is well acknowledged that mouse immunology is not always reflective of human immunology[387], although IL-6 signalling

appears to play similar roles in mice and humans it cannot be assumed that findings in mice will be replicated in a human system.

Although IL-6 signalling has been evidenced to contribute to the humoral response to BNT162b2, it remains unclear the significance of increased IL-6R shedding and sIL-6R levels in people with severe obesity. IL-6 signalling is generally considered to occur via the JAK-STAT3 pathway, however, there is some evidence that the Ras/Raf and the phosphoinositol-3 kinase (PI3K) – protein kinase B (PKB)/Akt pathways may also be triggered[388]. Further experiments with sIL-6R constructs may aid to elucidate the intracellular differences between classical and trans IL-6 signalling and the impact of increased trans signalling on the vaccine responses of people with obesity. Understanding of this process may open the door to alternative therapeutic methods, for example previous studies have shown that dietary changes in omega 3 fatty acids are enough to change fasting levels of sIL-6R in normal and overweight individuals[389]. Drugs to specifically target sIL-6R are commercially available and as such vaccine studies in mice reducing trans signalling with drugs and increasing with the sIL-6R construct will inform the role of sIL-6R in antibody waning.

Together with previous results, in this chapter, through analysis of sequenced human cell and IL-6R deficient vaccinated mice, I find that dysregulation of IL-6 signalling in obesity could be a key contributor to atypical humoral vaccine responses. IL-6 signalling shows potential as a target for the enhancement of class switched memory B cell responses following mRNA vaccination.

7. Final discussion

7.1. Conclusions

In this thesis I explored the efficacy and functionality of mRNA vaccination against SARS-CoV-2 in individuals with immune dysregulation, to shed light on the mechanisms important for the production of lasting protection against COVID-19 disease. To begin I worked on two clinical studies to assess immune response to mRNA vaccination in people with immune dysregulation caused by PID, ICB therapies, or severe obesity. I then developed a method for the detection and validation of spike specific cells in single cell sequencing. Using this I explored the mechanisms behind impaired maintenance of responses in obesity including B cell maturation, class switching, plasma cell survival, and IL-6 signalling.

The completion of two collaborative clinical studies revealed responses to mRNA vaccines against COVID-19 to be heterogenous across all groups vaccinated and increasingly so in groups with immune dysregulation. Induction of antigen specific T cells by mRNA vaccination was both more robust and provided broader protection than B cell and antibody production in those studied with immune dysregulation. Antigen specific antibody levels are prone to decline following vaccination, the pace and extent of which, leaves individuals with immune dysregulation without antibody mediated protection earlier than healthy controls. Levels can however be boosted in most individuals by repeat vaccination, highlighting the importance of autumn booster campaigns in at risk groups.

In these studies, we found that prior expansion of non-specific ABCs was associated with a reduced humoral response to vaccination, however vaccine induced antigen specific ABCs formed part of the normal response to vaccination. This highlights the multi-functional role of ABCs within the immune system and the importance of improved understanding of this subset.

I harnessed the production of spike protein and antibodies, in tandem with single cell sequencing to identify the impairment of class switched memory B cell production in obesity. The reduction of markers of specific B cell differentiation positively correlates

with increasing BMI and is associated with poorer antibody response. The production of mature antigen specific memory B cells and plasma cells in addition to the maintenance of antigen binding antibodies are susceptible to imbalances in the immune system and cytokine signalling. scRNA-seq of B cells identified shedding of the IL-6R as a contributor to the extent of the vaccine response in severe obesity.

I established that IL-6 signalling is an important factor in the development of class switched memory cells and long-lived antibody response to mRNA vaccination. This may go some way to explain how immune dysregulation in obesity leads to impaired maintenance of the antibody response. Deficiency of this signalling could be targeted to improve the composition of the humoral response and longevity of antibody mediated protection from SARS-CoV-2 following vaccination in at risk groups.

7.2. Future directions

The novelty of mRNA as a vaccine modality means there is much space for its optimisation and enhancement. Understanding of how mRNA vaccination invokes an immune response and protection against SARS-CoV-2, across states of immune dysregulation, gives key insights into how this may be done. Together, this could improve vaccine mediated protection against, not only SARS-CoV-2, but a variety of diseases in a range of individuals.

Cohort sizes in the clinical studies presented in this thesis were limited by the pace of vaccination in at risk groups. However, a significant proportion of the global population has now been vaccinated with mRNA vaccines against SARS-CoV-2 and the NHS currently only offers mRNA vaccines for its autumn and spring booster campaigns. There is therefore a large pool of individuals in which the long-term immunity provided by mRNA vaccination can be studied. A number of large-scale studies of mRNA vaccine immunogenicity are ongoing[390], from which data could be used to more broadly assess the factors discussed here.

The focus of this work was transferred from antigen specific T cell responses to humoral responses when it emerged that the former were less variable than humoral measures in between the groups studied. As a result, a detailed analysis of the T cell response to

mRNA vaccination was not completed. However, the extent of T cell response was not uniform within the groups studied and variation in the T cell responses of vaccinated individuals has been previously observed by others[391,392]. The application of antigen specific T cell assays discussed in this thesis may uncover deficiencies missed by the exclusive use of IFN-γ ELISpot. The storage of samples from the vaccine response in immune dysregulation and SCORPIO studies provides the opportunity for these responses to be explored further. Inducers of antigen specific T cell response will differ from those identified for B cell responses which must also be considered when developing therapeutics to enhance vaccine responses[393].

LLPCs and the organisation of the GC response, repeatedly emerge as potential contributors to the extent of antibody mediated protection after mRNA vaccination in those with immune dysregulation. Class switched memory cells and antibody levels have been used as an indicator of GC response as the human studies were limited by tissue availability. Alternative modes of sampling including of the lymph nodes via fine needle aspiration, or bone marrow biopsy, would provide more useful samples for the study of GC and plasma cells.

In broader terms, the methodologies I have adapted in this thesis could be applied further to this topic, or other studies. The application of the pVITRO1 system for the validation of the identification of antigen specific cells would be useful in the optimisation of any methodology, including those discussed here. The use of both nucleotide tagged spike multimers, as developed here, and optimised SPACE prediction could be applied to any population of B cells to identify S binding cells without the need for FACS and prolonged binding. Moreover, following successful validation by antibody production, the multimers could be further improved by the removal of the attached fluorophores and the reduction in the risk of off target binding. The ASC FluoroSpot could be applied to the assessment of antigen specific plasma cells in any tissue without the need for microfluidic antibody-plasma cell capture or sequencing and computational prediction.

ABCs and IL-6 signalling have both emerged as immune aspects to consider in vaccine responses. As it is unclear whether ABCs directly impair the immune response or are a marker of other conditions which do, further interrogation is needed before these cells

can be therapeutically targeted. Although deficiency of IL-6 signalling is evidently a contributor to poorer vaccine responses it is not sufficient to explain all impaired responses. Other cytokines such as IL-10, IL-21, and IL-27 have clearly defined roles in the initiation of GC responses and CSR. The role of these cytokines in the response to mRNA vaccination should also be studied and may reveal additional pathways to target to improve vaccine responses.

The COVID-19 pandemic remains ongoing along with the requirement for protection from SARS-CoV-2 infection in the general population. Additionally, levels of obesity, demonstrated here to increase risk from COVID-19 disease irrespective of vaccination state, are rising. The development of cytokine signalling constructs such as the hIL-6R should be explored as a mechanism to improve responses to mRNA vaccines. Improving the duration of protection provided by vaccination will reduce mortality and the frequency of booster vaccines required. mRNA constructs can be rapidly produced and incorporated into existing vaccines, indicating that in the long-term, there is the potential for mRNA vaccines to be personalised to stimulate the parts of the immune system which may be lacking in certain individuals. Applications of this work, could therefore, expand beyond the improvement of protection from SARS-CoV-2 in people with obesity. mRNA vaccine technologies are in development for the combat of multiple infectious diseases in addition to cancer and immunological diseases[394]. These therapies therefore have large future potential to correct disease and deficiency arising from immune dysfunction.

8. References

1 Shelley, M. *Frankenstein*. (Barnes & Noble, Inc, 2015).

2 Parkin, J. & Cohen, B. An overview of the immune system. *The Lancet* **357** (2001). https://doi.org/10.1016/S0140-6736(00)04904-7

3 Turvey, S. & Broide, D. Innate immunity. *Journal of Allergy and Clinical Immunology* **125** (2010). https://doi.org/10.1016/j.jaci.2009.07.016

4 Janeway, T., Walport, Shlomchik. *Immunobiology the immune system in health and disease*. 6th edn, (Garland Science Publishing, 2005).

5 Kumagai, Y. & Akira, S. Identification and functions of pattern-recognition receptors. *Journal of Allergy and Clinical Immunology* **125**, 985-992 (2010).

6 Pittman, K. & Kubes, P. Damage-associated molecular patterns control neutrophil recruitment. *Journal of innate immunity* **5**, 315-323 (2013).

7 Gordon, S. Phagocytosis: an immunobiologic process. *Immunity* **44**, 463-475 (2016).

8 Carlberg, C., Velleuer, E. & Molnár, F. in *Molecular Medicine: How Science Works* 229-252 (Springer International Publishing, 2023).

9 Chen, L. *et al.* Inflammatory responses and inflammation-associated diseases in organs. *Oncotarget* **9**, 7204 (2017).

10 Pilaro, A. M. *et al.* TNF-alpha is a principal cytokine involved in the recruitment of NK cells to liver parenchyma. *Journal of immunology (Baltimore, Md.: 1950)* **153**, 333-342 (1994).

11 Chan, C. J., Smyth, M. J. & Martinet, L. Molecular mechanisms of natural killer cell activation in response to cellular stress. *Cell Death Differ* **21**, 5-14 (2014).

12 Banchereau, J. & Steinman, R. M. Dendritic cells and the control of immunity. *Nature* **392**, 245-252 (1998).

13 Cooper, M. D. & Alder, M. N. The Evolution of Adaptive Immune Systems. *Cell* **124** (2006). https://doi.org/10.1016/j.cell.2006.02.001

14 Crotty, S. & Ahmed, R. Immunological memory in humans. *Seminars in Immunology* **16** (2004). https://doi.org/10.1016/j.smim.2004.02.008

15 Tan, J. B., Visan, I., Yuan, J. S. & Guidos, C. J. Requirement for Notch1 signals at sequential early stages of intrathymic T cell development. *Nat Immunol* **6**, 671-679 (2005).

16 Reinherz, E. L., Meuer, S. C., Fitzgerald, K. & Hussey, R. Antigen recognition by human T lymphocytes is linked to surface expression of the T3 molecular complex. *Cell* **30** (1982). https://doi.org/10.1016/0092-8674(82)90278-1

17 Godfrey, D. I., Kennedy, J., Mombaerts, P., Tonegawa, S. & Zlotnik, A. Onset of TCR-beta gene rearrangement and role of TCR-beta expression during CD3-CD4-CD8-thymocyte differentiation. *Journal of immunology (Baltimore, Md.: 1950)* **152**, 4783-4792 (1994).

18 Swat, W. *et al.* Clonal deletion of immature CD4+8+ thymocytes in suspension culture by extrathymic antigen-presenting cells. *Nature 1991 351:6322* **351** (1991). https://doi.org/10.1038/351150a0

19 Germain, R. N. T-cell development and the CD4–CD8 lineage decision. *Nature reviews immunology* **2**, 309-322 (2002).

20 ZINKERNAGEL, R. M., DOHERTY, P. C., ZINKERNAGEL, R. M. & DOHERTY, P. C. Restriction of in vitro T cell-mediated cytotoxicity in lymphocytic

choriomeningitis within a syngeneic or semiallogeneic system. *Nature 1974 248:5450* **248** (1974). https://doi.org/10.1038/248701a0
21 Meuer, S. C. *et al.* Clonal analysis of human cytotoxic T lymphocytes: T4+ and T8+ effector T cells recognize products of different major histocompatibility complex regions. *Proc Natl Acad Sci USA* **79** (1982). https://doi.org/10.1073/pnas.79.14.4395
22 Shi, Y. *et al.* Legacy of the discovery of the T-cell receptor: 40 years of shaping basic immunology and translational work to develop novel therapies. *Cellular & Molecular Immunology 2024 21:7* **21** (2024). https://doi.org/10.1038/s41423-024-01168-4
23 Mahnke, Y. D., Brodie, T. M., Sallusto, F., Roederer, M. & Lugli, E. The who's who of T-cell differentiation: Human memory T-cell subsets. *European Journal of Immunology* **43** (2013). https://doi.org/10.1002/eji.201343751
24 Luckheeram, R. V., Zhou, R., Verma, A. D. & Xia, B. CD4+T Cells: Differentiation and Functions. *Journal of Immunology Research* **2012** (2012). https://doi.org/10.1155/2012/925135
25 Heesters, B. A., Poel, C. E. v. d., Das, A. & Carroll, M. C. Antigen Presentation to B Cells. *Trends in Immunology* **37** (2016). https://doi.org/10.1016/j.it.2016.10.003
26 Christie, S. M., Fijen, C. & Rothenberg, E. V(D)J Recombination: Recent Insights in Formation of the Recombinase Complex and Recruitment of DNA Repair Machinery. *Frontiers in Cell and Developmental Biology* **10** (2022). https://doi.org/10.3389/fcell.2022.886718
27 Hozumi, N., Tonegawa, S., Hozumi, N. & Tonegawa, S. Evidence for somatic rearrangement of immunoglobulin genes coding for variable and constant regions. *Proc Natl Acad Sci USA* **73** (1976). https://doi.org/10.1073/pnas.73.10.3628
28 Chi, X., Li, Y. & Qiu, X. V(D)J recombination, somatic hypermutation and class switch recombination of immunoglobulins: mechanism and regulation. *Immunology* **160** (2020). https://doi.org/10.1111/imm.13176
29 Jenks, S. A., Cashman, K. S., Woodruff, M. C., Lee, F. E.-H. & Sanz, I. Extrafollicular responses in humans and SLE. *Immunological Reviews* **288** (2019/03/01). https://doi.org/10.1111/imr.12741
30 Elsner, R. A. & Shlomchik, M. J. Germinal Center and Extrafollicular B Cell Responses in vaccination, immunity and autoimmunity. *Immunity* **53** (2020). https://doi.org/10.1016/j.immuni.2020.11.006
31 Barandun, S., Morell, A., Skvaril, F. & Oberdorfer, A. Deficiency of kappa- or lambda-type immunoglobulins. *Blood* **47** (1976). https://doi.org/10.1182/blood.V47.1.79.79
32 Kinoshita, K. & Honjo, T. Linking class-switch recombination with somatic hypermutation. *Nature reviews. Molecular cell biology* **2** (2001). https://doi.org/10.1038/35080033
33 Lundgren, M. *et al.* Interleukin 4 induces synthesis of IgE and IgG4 in human B cells. *European Journal of Immunology* **19** (1989). https://doi.org/10.1002/eji.1830190724
34 Punnonen, J. *et al.* Interleukin 13 induces interleukin 4-independent IgG4 and IgE synthesis and CD23 expression by human B cells. *Proc Natl Acad Sci USA* **90** (1993). https://doi.org/10.1073/pnas.90.8.3730

35 Geha, R. S. *et al.* The regulation of immunoglobulin E class-switch recombination. *Nature Reviews Immunology 2003 3:9* **3** (2003). https://doi.org/10.1038/nri1181

36 Stavnezer, J. *et al.* Mechanism and Regulation of Class Switch Recombination. *Annual Review of Immunology* **26** (2008). https://doi.org/10.1146/annurev.immunol.26.021607.090248

37 Roco, J. A. *et al.* Class-Switch Recombination Occurs Infrequently in Germinal Centers. *Immunity* **51** (2019). https://doi.org/10.1016/j.immuni.2019.07.001

38 Higgins, B., McHeyzer-Williams, L. J. & McHeyzer-Williams, M. G. Programming Isotype-Specific Plasma Cell Function. *Trends in Immunology* **40** (2019). https://doi.org/10.1016/j.it.2019.01.012

39 Taylor, J. J., Pape, K. A. & Jenkins, M. K. A germinal center–independent pathway generates unswitched memory B cells early in the primary response. *Journal of Experimental Medicine* **209** (2012). https://doi.org/10.1084/jem.20111696

40 Viant, C. *et al.* Germinal center–dependent and –independent memory B cells produced throughout the immune response. *The Journal of Experimental Medicine* **218** (2021/08/08). https://doi.org/10.1084/jem.20202489

41 Robinson, M. J. *et al.* Long-lived plasma cells accumulate in the bone marrow at a constant rate from early in an immune response. *Science Immunology* **7** (2022). https://doi.org/10.1126/sciimmunol.abm8389

42 Tangye, S. G. Frontiers | Cytokine-Mediated Regulation of Plasma Cell Generation: IL-21 Takes Center Stage. *Front. Immunol.* **5** (2014). https://doi.org/10.3389/fimmu.2014.00065

43 Linterman, M. A., Hill, D. L., Linterman, M. A. & Hill, D. L. Can follicular helper T cells be targeted to improve vaccine efficacy? *F1000Research 2016 5:88* **5** (2016). https://doi.org/10.12688/f1000research.7388.1

44 Paus , D. *et al.* Antigen recognition strength regulates the choice between extrafollicular plasma cell and germinal center B cell differentiation. *Journal of Experimental Medicine* **203** (2006). https://doi.org/10.1084/jem.20060087

45 Nojima, T. *et al.* In-vitro derived germinal centre B cells differentially generate memory B or plasma cells in vivo - PubMed. *Nature Communications* **2** (2011). https://doi.org/10.1038/ncomms1475

46 Dogan, I. *et al.* Multiple layers of B cell memory with different effector functions. *Nature Immunology 2009 10:12* **10** (2009). https://doi.org/10.1038/ni.1814

47 Victora, G. D., Nussenzweig, M. C., Victora, G. D. & Nussenzweig, M. C. Germinal Centers. *Annual Review of Immunology* **40** (2022). https://doi.org/10.1146/annurev-immunol-120419-022408

48 Weisel, F. J., Zuccarino-Catania, G. V., Chikina, M. & Shlomchik, M. J. A Temporal Switch in the Germinal Center Determines Differential Output of Memory B and Plasma Cells. *Immunity* **44** (2016). https://doi.org/10.1016/j.immuni.2015.12.004

49 Sprumont, A., Rodrigues, A., McGowan, S. J., Bannard, C. & Bannard, O. Germinal centers output clonally diverse plasma cell populations expressing high- and low-affinity antibodies. *Cell* **186** (2023). https://doi.org/10.1016/j.cell.2023.10.022

50 Viant, C. *et al.* Antibody Affinity Shapes the Choice between Memory and Germinal Center B Cell Fates. *Cell* **183** (2020). https://doi.org/10.1016/j.cell.2020.09.063
51 Bende, R. J. *et al.* Germinal centers in human lymph nodes contain reactivated memory B cells - PubMed. *The Journal of experimental medicine* **204** (2007). https://doi.org/10.1084/jem.20071006
52 Mesin, L. *et al.* Restricted Clonality and Limited Germinal Center Reentry Characterize Memory B Cell Reactivation by Boosting. *Cell* **180** (2020). https://doi.org/10.1016/j.cell.2019.11.032
53 Amanna, I. J., Carlson, N. E. & Slifka, M. Duration of humoral immunity to common viral and vaccine antigens - PubMed. *The New England journal of medicine* **357** (2007). https://doi.org/10.1056/NEJMoa066092
54 Tellier, J., Nutt, S. L., Tellier, J. & Nutt, S. L. The secret to longevity, plasma cell style. *Nature Immunology 2022 23:11* **23** (2022). https://doi.org/10.1038/s41590-022-01340-w
55 Pinto, D. *et al.* A functional BCR in human IgA and IgM plasma cells. *Blood* **121**, 4110-4114 (2013). https://doi.org/10.1182/blood-2012-09-459289
56 Pioli, P. D. Frontiers | Plasma Cells, the Next Generation: Beyond Antibody Secretion. *Front. Immunol.* **10** (2019). https://doi.org/10.3389/fimmu.2019.02768
57 Khodadadi, L., Cheng, Q., Radbruch, A. & Hiepe, F. The Maintenance of Memory Plasma Cells - PubMed. *Front. Immunol.* **10** (2019). https://doi.org/10.3389/fimmu.2019.00721
58 Isho, B., Florescu, A., Wang, A. A. & Gommerman, J. L. Fantastic IgA plasma cells and where to find them. *Immunological Reviews* **303** (2021). https://doi.org/10.1111/imr.12980
59 Nutt, S. L. *et al.* The generation of antibody-secreting plasma cells. *Nature Reviews Immunology 2015 15:3* **15** (2015). https://doi.org/10.1038/nri3795
60 Cancro, M. P. Age-Associated B Cells. *Annual Review of Immunology* **38** (2020). https://doi.org/10.1146/annurev-immunol-092419-031130
61 Ma, S., Wang, C., Mao, X. & Hao, Y. Frontiers | B Cell Dysfunction Associated With Aging and Autoimmune Diseases. *Front. Immunol.* **10** (2019). https://doi.org/10.3389/fimmu.2019.00318
62 Ehrhardt , G. t. R. A. *et al.* Expression of the immunoregulatory molecule FcRH4 defines a distinctive tissue-based population of memory B cells. *Journal of Experimental Medicine* **202** (2005). https://doi.org/10.1084/jem.20050879
63 Keller, B. & Warnatz, K. T-bethighCD21low B cells: the need to unify our understanding of a distinct B cell population in health and disease. *Current Opinion in Immunology* **82** (2023). https://doi.org/10.1016/j.coi.2023.102300
64 Pape, K. A. *et al.* High-affinity memory B cells induced by SARS-CoV-2 infection produce more plasmablasts and atypical memory B cells than those primed by mRNA vaccines. *Cell Reports* **37** (2021). https://doi.org/10.1016/j.celrep.2021.109823
65 Song, W. *et al.* Development of Tbet- and CD11c-expressing B cells in a viral infection requires T follicular helper cells outside of germinal centers. *Immunity* **55** (2022). https://doi.org/10.1016/j.immuni.2022.01.002

66 Inoue, T., Kurosaki, T., Inoue, T. & Kurosaki, T. Memory B cells. *Nature Reviews Immunology 2023 24:1* **24** (2023). https://doi.org/10.1038/s41577-023-00897-3
67 Sutton, H. J. *et al.* Atypical B cells are part of an alternative lineage of B cells that participates in responses to vaccination and infection in humans. *Cell Reports* **34** (2021). https://doi.org/10.1016/j.celrep.2020.108684
68 Zhang, W. *et al.* Excessive CD11c+Tbet+ B cells promote aberrant TFH differentiation and affinity-based germinal center selection in lupus. *Proc Natl Acad Sci USA* **116** (2019). https://doi.org/10.1073/pnas.1901340116
69 Naradikian, M. S., Hao, Y. & Cancro, M. P. Age-associated B cells: key mediators of both protective and autoreactive humoral responses - PubMed. *Immunological reviews* **269** (2016). https://doi.org/10.1111/imr.12380
70 Warnatz, K. *et al.* Expansion of CD19hiCD21lo/neg B Cells in Common Variable Immunodeficiency (CVID) Patients with Autoimmune Cytopenia. *Immunobiology* **206** (2002). https://doi.org/10.1078/0171-2985-00198
71 Ratliff, M., Alter, S., Frasca, D., Blomberg, B. B. & Riley, R. L. In senescence, age-associated B cells secrete TNFα and inhibit survival of B-cell precursors*. *Aging Cell* **12** (2013). https://doi.org/10.1111/acel.12055
72 Ada, G. Vaccines and Vaccination. *N Engl J Med* **345** (2001). https://doi.org/10.1056/NEJMra011223
73 Antia, A. *et al.* Heterogeneity and longevity of antibody memory to viruses and vaccines. *PLoS Biol* **16** (2018). https://doi.org/10.1371/journal.pbio.2006601
74 Payne, S. Family Coronaviridae. *Viruses* (2017). https://doi.org/10.1016/B978-0-12-803109-4.00017-9
75 (ed The Office for National Statistics) (Office for National Statistics, 2023).
76 Jackson, C. B. *et al.* Mechanisms of SARS-CoV-2 entry into cells. *Nature Reviews Molecular Cell Biology 2021 23:1* **23** (2021). https://doi.org/10.1038/s41580-021-00418-x
77 Huang, Y., Yang, C., Xu, X.-f., Xu, W. & Liu, S.-w. Structural and functional properties of SARS-CoV-2 spike protein: potential antivirus drug development for COVID-19. *Acta Pharmacologica Sinica* **41** (2020). https://doi.org/10.1038/s41401-020-0485-4
78 Wu, H.-S. *et al.* Early detection of antibodies against various structural proteins of the SARS-associated coronavirus in SARS patients. *Journal of Biomedical Science* **11** (2004). https://doi.org/10.1007/BF02256554
79 Turner, J. S. *et al.* SARS-CoV-2 infection induces long-lived bone marrow plasma cells in humans. *Nature 2021 595:7867* **595** (2021). https://doi.org/10.1038/s41586-021-03647-4
80 Reynolds, C. J. *et al.* Discordant neutralizing antibody and T cell responses in asymptomatic and mild SARS-CoV-2 infection. *Science Immunology* **5** (2020). https://doi.org/10.1126/sciimmunol.abf3698
81 Hall, V. J. *et al.* SARS-CoV-2 infection rates of antibody-positive compared with antibody-negative health-care workers in England: a large, multicentre, prospective cohort study (SIREN). *The Lancet* **397**, 1459-1469 (2021). https://doi.org/10.1016/S0140-6736(21)00675-9
82 Alkhatib, M. *et al.* SARS-CoV-2 Variants and Their Relevant Mutational Profiles: Update Summer 2021. *Microbiology Spectrum* **9** (2021). https://doi.org/10.1128/Spectrum.01096-21

83 Choi, J. Y. & Smith, D. M. SARS-CoV-2 variants of concern. *Yonsei medical journal* **62**, 961 (2021).
84 Knock, E. S. *et al.* Key epidemiological drivers and impact of interventions in the 2020 SARS-CoV-2 epidemic in England. *Science Translational Medicine* **13**, eabg4262 (2021).
85 Flores-Vega, V. R. *et al.* SARS-CoV-2: evolution and emergence of new viral variants. *Viruses* **14**, 653 (2022).
86 Mahase, E. Covid-19: How many variants are there, and what do we know about them? *BMJ* **374** (2021). https://doi.org/10.1136/bmj.n1971
87 Carabelli, A. M. *et al.* SARS-CoV-2 variant biology: immune escape, transmission and fitness. *Nature Reviews Microbiology* **21**, 162-177 (2023).
88 Fan, Y. *et al.* SARS-CoV-2 Omicron variant: recent progress and future perspectives. *Signal Transduction and Targeted Therapy 2022 7:1* **7** (2022). https://doi.org/10.1038/s41392-022-00997-x
89 Mlcochova, P. *et al.* SARS-CoV-2 B. 1.617. 2 Delta variant replication and immune evasion. *Nature* **599**, 114-119 (2021).
90 Wise, J. Covid-19: Omicron sub variants driving new wave of infections in UK. *BMJ: British Medical Journal (Online)* **377**, o1506 (2022).
91 Falsey, A. R. *et al.* Phase 3 Safety and Efficacy of AZD1222 (ChAdOx1 nCoV-19) Covid-19 Vaccine. *N Engl J Med* **385** (2021). https://doi.org/10.1056/NEJMoa2105290
92 Voysey, M. *et al.* Safety and efficacy of the ChAdOx1 nCoV-19 vaccine (AZD1222) against SARS-CoV-2: an interim analysis of four randomised controlled trials in Brazil, South Africa, and the UK. *The Lancet* **397** (2021). https://doi.org/10.1016/S0140-6736(20)32661-1
93 Thomas, S. J. *et al.* Safety and Efficacy of the BNT162b2 mRNA Covid-19 Vaccine through 6 Months. *N Engl J Med* **385** (2021). https://doi.org/10.1056/NEJMoa2110345
94 Polack, F. P. *et al.* Safety and Efficacy of the BNT162b2 mRNA Covid-19 Vaccine. *N Engl J Med* **383** (2020). https://doi.org/10.1056/NEJMoa2034577
95 Baden, L. R. *et al.* Efficacy and Safety of the mRNA-1273 SARS-CoV-2 Vaccine. *N Engl J Med* **384** (2021). https://doi.org/10.1056/NEJMoa2035389
96 Sahly, H. M. E. *et al.* Efficacy of the mRNA-1273 SARS-CoV-2 Vaccine at Completion of Blinded Phase. *N Engl J Med* **385** (2021). https://doi.org/10.1056/NEJMoa2113017
97 Steensels, D., Pierlet, N., Penders, J., Mesotten, D. & Heylen, L. Comparison of SARS-CoV-2 Antibody Response Following Vaccination With BNT162b2 and mRNA-1273. *JAMA* **326**, 1533 (2021). https://doi.org/10.1001/jama.2021.15125
98 Al-Sadeq, D. W. *et al.* Comparison of antibody immune responses between BNT162b2 and mRNA-1273 SARS-CoV-2 vaccines in naïve and previously infected individuals - PubMed. *Journal of travel medicine* **28** (2021). https://doi.org/10.1093/jtm/taab190
99 Islam, N. *et al.* Comparative effectiveness over time of the mRNA-1273 (Moderna) vaccine and the BNT162b2 (Pfizer-BioNTech) vaccine. *Nature Communications 2022 13:1* **13** (2022). https://doi.org/10.1038/s41467-022-30059-3

100 Lombardi, A. *et al.* SARS-CoV-2 anti-spike antibody titres after vaccination with BNT162b2 in naïve and previously infected individuals. *Journal of Infection and Public Health* **14**, 1120-1122 (2021). https://doi.org/10.1016/j.jiph.2021.07.005
101 Minervina, A. A. *et al.* SARS-CoV-2 antigen exposure history shapes phenotypes and specificity of memory CD8+ T cells. *Nat Immunol* **23**, 781-790 (2022). https://doi.org/10.1038/s41590-022-01184-4
102 Liu, Y. *et al.* Robust induction of B cell and T cell responses by a third dose of inactivated SARS-CoV-2 vaccine. *Cell Discovery 2022 8:1* **8** (2022). https://doi.org/10.1038/s41421-022-00373-7
103 Scurr, M. J. *et al.* Magnitude of venous or capillary blood-derived SARS-CoV-2-specific T cell response determines COVID-19 immunity. *Nature Communications 2022 13:1* **13** (2022). https://doi.org/10.1038/s41467-022-32985-8
104 Khoury, D. S. *et al.* Neutralizing antibody levels are highly predictive of immune protection from symptomatic SARS-CoV-2 infection. *Nat Med* **27**, 1205-1211 (2021). https://doi.org/10.1038/s41591-021-01377-8
105 Simpson, C. R. *et al.* Early Pandemic Evaluation and Enhanced Surveillance of COVID-19 (EAVE II): protocol for an observational study using linked Scottish national data. *BMJ Open* **10** (2020). https://doi.org/10.1136/bmjopen-2020-039097
106 Yam-Puc, J. C. *et al.* Age-associated B cells predict impaired humoral immunity after COVID-19 vaccination in patients receiving immune checkpoint blockade. *Nature Communications* **14**, 3292 (2023). https://doi.org/10.1038/s41467-023-38810-0
107 Schaub, J. M. *et al.* Expression and characterization of SARS-CoV-2 spike proteins. *Nature Protocols 2021 16:11* **16** (2021-10-05). https://doi.org/10.1038/s41596-021-00623-0
108 Dodev, T. S. *et al.* A tool kit for rapid cloning and expression of recombinant antibodies. *Sci Rep* **4**, 5885 (2014). https://doi.org/10.1038/srep05885
109 Stoeckius, M. *et al.* Simultaneous epitope and transcriptome measurement in single cells. *Nature Methods 2017 14:9* **14** (2017). https://doi.org/10.1038/nmeth.4380
110 Sundell, T. *et al.* Single-cell RNA sequencing analyses: interference by the genes that encode the B-cell and T-cell receptors. *Briefings in Functional Genomics* **22** (2023). https://doi.org/10.1093/bfgp/elac044
111 Long, A., Kleiner, A. & Looney, R. J. Immune dysregulation. *Journal of Allergy and Clinical Immunology* **151** (2023). https://doi.org/10.1016/j.jaci.2022.11.001
112 Cao, M. *et al.* Immune dysregulation in sepsis: experiences, lessons and perspectives. *Cell Death Discovery 2023 9:1* **9** (2023). https://doi.org/10.1038/s41420-023-01766-7
113 Chinen, J. & Shearer, W. T. Secondary immunodeficiencies, including HIV infection. *The Journal of allergy and clinical immunology* **125** (2010). https://doi.org/10.1016/j.jaci.2009.08.040
114 Akalu, Y. T., Bogunovic, D., Akalu, Y. T. & Bogunovic, D. Inborn errors of immunity: an expanding universe of disease and genetic architecture. *Nature Reviews Genetics 2023 25:3* **25** (2023). https://doi.org/10.1038/s41576-023-00656-z

115 Tangye, S. G. *et al.* Human Inborn Errors of Immunity: 2019 Update on the Classification from the International Union of Immunological Societies Expert Committee. *J Clin Immunol* **40** (2020). https://doi.org/10.1007/s10875-019-00737-x
116 Tangye, S. G. *et al.* Human Inborn Errors of Immunity: 2022 Update on the Classification from the International Union of Immunological Societies Expert Committee. *Journal of Clinical Immunology 2022 42:7* **42** (2022). https://doi.org/10.1007/s10875-022-01289-3
117 Savinova, O. V., Hoffmann, A. & Ghosh, G. The Nfkb1 and Nfkb2 Proteins p105 and p100 Function as the Core of High-Molecular-Weight Heterogeneous Complexes. *Molecular cell* **34** (2009). https://doi.org/10.1016/j.molcel.2009.04.033
118 Caamaño, J. & Hunter, C. A. NF-κB Family of Transcription Factors: Central Regulators of Innate and Adaptive Immune Functions. *Clin. Microbiol. Rev.* **15** (2002). https://doi.org/10.1128/CMR.15.3.414-429.2002
119 Liu, T. *et al.* NF-κB signaling in inflammation. *Signal Transduction and Targeted Therapy 2017 2:1* **2** (2017). https://doi.org/10.1038/sigtrans.2017.23
120 Tuijnenburg, P. *et al.* Loss-of-function nuclear factor κB subunit 1 (NFKB1) variants are the most common monogenic cause of common variable immunodeficiency in Europeans. *The Journal of Allergy and Clinical Immunology* **142** (2018). https://doi.org/10.1016/j.jaci.2018.01.039
121 North, M. E., Webster, A. D. B. & Farrant, J. Primary defect in CD8+ lymphocytes in the antibody deficiency disease (common variable immunodeficiency): abnormalities in intracellular production of interferon-gamma (IFN-γ) in CD28+ ('cytotoxic') and CD28− ('suppressor') CD8+ subsets. *Clinical and Experimental Immunology* **111** (1998). https://doi.org/10.1046/j.1365-2249.1998.00479.x
122 Hossen, M. M. *et al.* Current understanding of CTLA-4: from mechanism to autoimmune diseases. *Front. Immunol.* **14** (2023). https://doi.org/10.3389/fimmu.2023.1198365
123 Kardelen, A. D. *et al.* LRBA deficiency: a rare cause of type 1 diabetes, colitis, and severe immunodeficiency. *Hormones 2020 20:2* **20** (2020). https://doi.org/10.1007/s42000-020-00257-z
124 Aggarwal, V., Banday, A. Z., Jindal, A. K., Das, J. & Raawat, A. Recent advances in elucidating the genetics of common variable immunodeficiency. *Genes & Diseases* **7** (2020). https://doi.org/10.1016/j.gendis.2019.10.002
125 Edwards, E. S. J. *et al.* Predominantly Antibody-Deficient Patients With Non-infectious Complications Have Reduced Naive B, Treg, Th17, and Tfh17 Cells. *Front. Immunol.* **10**, 2593 (2019). https://doi.org/10.3389/fimmu.2019.02593
126 Kuehn, H. S. *et al.* Immune dysregulation in human subjects with heterozygous germline mutations in CTLA4. *Science* **345** (2014). https://doi.org/10.1126/science.1255904
127 Schwab, C. *et al.* Phenotype, penetrance, and treatment of 133 cytotoxic T-lymphocyte antigen 4–insufficient subjects. *Journal of Allergy and Clinical Immunology* **142** (2018). https://doi.org/10.1016/j.jaci.2018.02.055
128 Bakhtiar, S. *et al.* Regulatory B cells in patients suffering from inborn errors of immunity with severe immune dysregulation. *Journal of Autoimmunity* **132** (2022). https://doi.org/10.1016/j.jaut.2022.102891

129 Patel, S. Y., Carbone, J. & Jolles, S. The Expanding Field of Secondary Antibody Deficiency: Causes, Diagnosis, and Management. *Front. Immunol.* **10** (2019). https://doi.org/10.3389/fimmu.2019.00033
130 Wiseman, A. C. Immunosuppressive Medications. *Clinical Journal of the American Society of Nephrology : CJASN* **11** (2016). https://doi.org/10.2215/CJN.08570814
131 Weiner, H. L. Immunosuppressive treatment in multiple sclerosis. *Journal of the Neurological Sciences* **223** (2004). https://doi.org/10.1016/j.jns.2004.04.013
132 Postow, M. A., Callahan, M. K. & Wolchok, J. D. Immune Checkpoint Blockade in Cancer Therapy. *Journal of Clinical Oncology* **33** (2015). https://doi.org/10.1200/JCO.2014.59.4358
133 Guan, Q. *et al.* Strategies to reinvigorate exhausted CD8+ T cells in tumor microenvironment. *Front. Immunol.* **14** (2023). https://doi.org/10.3389/fimmu.2023.1204363
134 Hermens, J. M. & Kesmir, C. Role of T cells in severe COVID-19 disease, protection, and long term immunity. *Immunogenetics* **75** (2023). https://doi.org/10.1007/s00251-023-01294-9
135 Kundu, R. *et al.* Cross-reactive memory T cells associate with protection against SARS-CoV-2 infection in COVID-19 contacts. *Nature Communications 2022 13:1* **13** (2022). https://doi.org/10.1038/s41467-021-27674-x
136 Kalimuddin, S. *et al.* Early T cell and binding antibody responses are associated with COVID-19 RNA vaccine efficacy onset. *Med* **2** (2021). https://doi.org/10.1016/j.medj.2021.04.003
137 Chen, L., Flies, D. B., Chen, L. & Flies, D. B. Molecular mechanisms of T cell co-stimulation and co-inhibition. *Nature Reviews Immunology 2013 13:4* **13** (2013). https://doi.org/10.1038/nri3405
138 Robnson, J., Soormally, A. R., Hayhurst, J. D. & Marsh, S. G. E. The IPD-IMGT/HLA Database – New developments in reporting HLA variation. *Human Immunology* **77** (2016). https://doi.org/10.1016/j.humimm.2016.01.020
139 Milito, C. *et al.* Clinical outcome, incidence, and SARS-CoV-2 infection-fatality rates in Italian patients with inborn errors of immunity. *The Journal of Allergy and Clinical Immunology: In Practice* **9** (2021). https://doi.org/10.1016/j.jaip.2021.04.017
140 Esenboga, S. *et al.* COVID-19 in Patients with Primary Immunodeficiency. *J Clin Immunol* **41** (2021). https://doi.org/10.1007/s10875-021-01065-9
141 Shields, A. M., Burns, S. O., Savic, S., Richter, A. G. & Consortium, U. P. C.-. COVID-19 in patients with primary and secondary immunodeficiency: The United Kingdom experience. *The Journal of Allergy and Clinical Immunology* **147** (2021). https://doi.org/10.1016/j.jaci.2020.12.620
142 Milota, T., Smetanova, J. & Bartunkova, J. Clinical Outcome of Coronavirus Disease 2019 in Patients with Primary Antibody Deficiencies. *Pathogens* **12** (2023). https://doi.org/10.3390/pathogens12010109
143 Baang, J. H. *et al.* Prolonged Severe Acute Respiratory Syndrome Coronavirus 2 Replication in an Immunocompromised Patient. *The Journal of Infectious Diseases* **223**, 23-27 (2021). https://doi.org/10.1093/infdis/jiaa666

144 Nakajima, Y. *et al.* Prolonged viral shedding of SARS-CoV-2 in an immunocompromised patient. *Journal of Infection and Chemotherapy* **27** (2021). https://doi.org/10.1016/j.jiac.2020.12.001

145 Kemp, S. A. *et al.* SARS-CoV-2 evolution during treatment of chronic infection. *Nature 2021 592:7853* **592** (2021). https://doi.org/10.1038/s41586-021-03291-y

146 Sinha, S. & Kundu, C. N. Cancer and COVID-19: Why are cancer patients more susceptible to COVID-19? *Medical Oncology (Northwood, London, England)* **38** (2021). https://doi.org/10.1007/s12032-021-01553-3

147 Tan, R. *et al.* Impact of Immune Checkpoint Inhibitors on COVID-19 Severity in Patients with Cancer. *The Oncologist* **27** (2022). https://doi.org/10.1093/oncolo/oyab083

148 Giacomo, A. M. D., Gambale, E., Monterisi, S., Valente, M. & Maio, M. SARS-COV-2 infection in patients with cancer undergoing checkpoint blockade: Clinical course and outcome. *European Journal of Cancer* **133** (2020). https://doi.org/10.1016/j.ejca.2020.04.026

149 Luo, J. *et al.* Impact of PD-1 Blockade on Severity of COVID-19 in Patients with Lung Cancers. *Cancer Discovery* **10** (2020). https://doi.org/10.1158/2159-8290.CD-20-0596

150 Robilotti, E. V. *et al.* Determinants of COVID-19 disease severity in patients with cancer. *Nature Medicine 2020 26:8* **26** (2020). https://doi.org/10.1038/s41591-020-0979-0

151 Pezeshki, P. S. & Rezaei, N. Immune checkpoint inhibition in COVID-19: risks and benefits - PubMed. *Expert opinion on biological therapy* **21** (2021). https://doi.org/10.1080/14712598.2021.1887131

152 Garassino, M. C. & Ribas, A. At the Crossroads: COVID-19 and Immune-Checkpoint Blockade for Cancer. *Cancer immunology research* **9** (2021). https://doi.org/10.1158/2326-6066.CIR-21-0008

153 Wallace, P. K. *et al.* Tracking antigen-driven responses by flow cytometry: Monitoring proliferation by dye dilution. *Cytometry Part A* **73A** (2008). https://doi.org/10.1002/cyto.a.20619

154 Tario, J. D., Soh, K. T., Wallace, P. K. & Muirhead, K. A. Monitoring Cell Proliferation by Dye Dilution: Considerations for Pane. *Flow Cytometry Protocols* (2024). https://doi.org/10.1007/978-1-0716-3738-8_9

155 Poloni, C. *et al.* Immunology & Cell Biology | ASI Journal | Wiley Online Library. *Immunology and Cell Biology* **101** (2023). https://doi.org/10.1111/imcb.12636

156 Grifoni, A. *et al.* Targets of T Cell Responses to SARS-CoV-2 Coronavirus in Humans with COVID-19 Disease and Unexposed Individuals. *Cell* **181** (2020). https://doi.org/10.1016/j.cell.2020.05.015

157 Loyal, L. *et al.* Cross-reactive CD4+ T cells enhance SARS-CoV-2 immune responses upon infection and vaccination. *Science* **374** (2021). https://doi.org/10.1126/science.abh1823

158 Kalyuzhny, A. E. Chemistry and Biology of the ELISPOT Assay. (2005). https://doi.org/10.1385/1-59259-903-6:015

159 Ranieri, E., Netti, G. S. & Gigante, M. CTL ELISPOT Assay and T Cell Detection. *Methods in Molecular Biology* (2021). https://doi.org/10.1007/978-1-0716-1507-2_5

160 Janetzki, S. *et al.* Stepping up ELISpot: Multi-Level Analysis in FluoroSpot Assays. *Cells 2014, Vol. 3, Pages 1102-1115* **3** (2014). https://doi.org/10.3390/cells3041102
161 Payne, R. P. *et al.* Immunogenicity of standard and extended dosing intervals of BNT162b2 mRNA vaccine. *Cell* **184** (2021). https://doi.org/10.1016/j.cell.2021.10.011
162 Hiam-Galvez, K. J. *et al.* Systemic immunity in cancer. *Nature Reviews Cancer 2021 21:6* **21** (2021). https://doi.org/10.1038/s41568-021-00347-z
163 Schultz, B. T. *et al.* Circulating HIV-Specific Interleukin-21+CD4+ T Cells Represent Peripheral Tfh Cells with Antigen-Dependent Helper Functions. *Immunity* **44** (2016). https://doi.org/10.1016/j.immuni.2015.12.011
164 Goubet, A.-G. *et al.* Escherichia coli–Specific CXCL13-Producing TFH Are Associated with Clinical Efficacy of Neoadjuvant PD-1 Blockade against Muscle-Invasive Bladder Cancer. *Cancer Discovery* **12** (2022). https://doi.org/10.1158/2159-8290.CD-22-0201
165 Cindy Yang, S. Y. *et al.* Pan-cancer analysis of longitudinal metastatic tumors reveals genomic alterations and immune landscape dynamics associated with pembrolizumab sensitivity. *Nature Communications 2021 12:1* **12** (2021). https://doi.org/10.1038/s41467-021-25432-7
166 Gutiérrez-Melo, N. & Baumjohann, D. T follicular helper cells in cancer. *Trends in Cancer* **9** (2023). https://doi.org/10.1016/j.trecan.2022.12.007
167 Riley, R. L., Khomtchouk, K. & Blomberg, B. B. Age-associated B cells (ABC) inhibit B lymphopoiesis and alter antibody repertoires in old age - PubMed. *Cellular immunology* **321** (2017). https://doi.org/10.1016/j.cellimm.2017.04.008
168 Ogbe, A. *et al.* T cell assays differentiate clinical and subclinical SARS-CoV-2 infections from cross-reactive antiviral responses. *Nature Communications* **12**, 2055 (2021). https://doi.org/10.1038/s41467-021-21856-3
169 Han, Q. *et al.* Multidimensional analysis of the frequencies and rates of cytokine secretion from single cells by quantitative microengraving. *Lab on a Chip* **10** (2010). https://doi.org/10.1039/B926849A
170 Place, D. E. & Kanneganti, T.-D. Cell death–mediated cytokine release and its therapeutic implications. *The Journal of Experimental Medicine* **216** (2019). https://doi.org/10.1084/jem.20181892
171 Man, S. M., Kanneganti, T.-D., Man, S. M. & Kanneganti, T.-D. Innate immune sensing of cell death in disease and therapeutics. *Nature Cell Biology 2024* (2024). https://doi.org/10.1038/s41556-024-01491-y
172 Moore, S. C. *et al.* Evolution of long-term vaccine-induced and hybrid immunity in healthcare workers after different COVID-19 vaccine regimens. *Med* **4** (2023). https://doi.org/10.1016/j.medj.2023.02.004
173 Zonozi, R. *et al.* T cell responses to SARS-CoV-2 infection and vaccination are elevated in B cell deficiency and reduce risk of severe COVID-19. *Science Translational Medicine* **15** (2023). https://doi.org/10.1126/scitranslmed.adh4529
174 Gupta, S., Su, H., Narsai, T. & Agrawal, S. SARS-CoV-2-Associated T-Cell Responses in the Presence of Humoral Immunodeficiency. *International Archives of Allergy and Immunology* **182** (2021). https://doi.org/10.1159/000514193

175 Hurme, A. *et al.* Frontiers | T cell immunity following COVID-19 vaccination in adult patients with primary antibody deficiency – a 22-month follow-up. *Front. Immunol.* **14** (2023). https://doi.org/10.3389/fimmu.2023.1146500
176 Response to Severe Acute Respiratory Syndrome Coronavirus 2 Initial Series and Additional Dose Vaccine in Patients With Predominant Antibody Deficiency - PubMed. *The journal of allergy and clinical immunology. In practice* **10** (2022). https://doi.org/10.1016/j.jaip.2022.03.017
177 Salinas, A. F. *et al.* SARS-CoV-2 Vaccine Induced Atypical Immune Responses in Antibody Defects: Everybody Does their Best. *J Clin Immunol* **41**, 1709-1722 (2021). https://doi.org/10.1007/s10875-021-01133-0
178 Shi, J. *et al.* PD-1 Controls Follicular T Helper Cell Positioning and Function - PubMed. *Immunity* **49** (2018). https://doi.org/10.1016/j.immuni.2018.06.012
179 Herati, R. S. *et al.* PD-1 directed immunotherapy alters Tfh and humoral immune responses to seasonal influenza vaccine. *Nature Immunology 2022 23:8* **23** (2022). https://doi.org/10.1038/s41590-022-01274-3
180 Wang, C. J. *et al.* CTLA-4 controls follicular helper T-cell differentiation by regulating the strength of CD28 engagement. *Proc Natl Acad Sci USA* **112** (2015). https://doi.org/10.1073/pnas.1414576112
181 Addeo, A. *et al.* Immunogenicity of SARS-CoV-2 messenger RNA vaccines in patients with cancer - PubMed. *Cancer cell* **39** (2021). https://doi.org/10.1016/j.ccell.2021.06.009
182 Pai, J. A. *et al.* Lineage tracing reveals clonal progenitors and long-term persistence of tumor-specific T cells during immune checkpoint blockade - PubMed. *Cancer cell* **41** (2023). https://doi.org/10.1016/j.ccell.2023.03.009
183 Horton, H. *et al.* Optimization and validation of an 8-color intracellular cytokine staining (ICS) assay to quantify antigen-specific T cells induced by vaccination. *Journal of Immunological Methods* **323** (2007). https://doi.org/10.1016/j.jim.2007.03.002
184 Binayke, A. *et al.* A quest for universal anti-SARS-CoV-2 T cell assay: systematic review, meta-analysis, and experimental validation. *npj Vaccines 2024 9:1* **9** (2024). https://doi.org/10.1038/s41541-023-00794-9
185 Haslam, A. & Prasad, V. Estimation of the Percentage of US Patients With Cancer Who Are Eligible for and Respond to Checkpoint Inhibitor Immunotherapy Drugs - PubMed. *JAMA network open* **2** (2019). https://doi.org/10.1001/jamanetworkopen.2019.2535
186 Agency, U. H. S. (2024).
187 Gao, B. *et al.* Repeated vaccination of inactivated SARS-CoV-2 vaccine dampens neutralizing antibodies against Omicron variants in breakthrough infection. *Cell Research 2023 33:3* **33** (2023). https://doi.org/10.1038/s41422-023-00781-8
188 Uversky, V. N. *et al.* IgG4 Antibodies Induced by Repeated Vaccination May Generate Immune Tolerance to the SARS-CoV-2 Spike Protein. *Vaccines 2023, Vol. 11, Page 991* **11** (2023). https://doi.org/10.3390/vaccines11050991
189 Pérez-Alós, L. *et al.* Previous immunity shapes immune responses to SARS-CoV-2 booster vaccination and Omicron breakthrough infection risk. *Nature Communications 2023 14:1* **14** (2023). https://doi.org/10.1038/s41467-023-41342-2

190 Hao, Y., O'Neill, P., Naradikian, M. S., Scholz, J. L. & Cancro, M. P. A B-cell subset uniquely responsive to innate stimuli accumulates in aged mice. *Blood* **118** (2011). https://doi.org/10.1182/blood-2011-01-330530
191 Espéli, M. *et al.* FcγRIIb differentially regulates pre-immune and germinal center B cell tolerance in mouse and human. *Nature Communications 2019 10:1* **10** (2019). https://doi.org/10.1038/s41467-019-09434-0
192 Booth, A. *et al.* Population risk factors for severe disease and mortality in COVID-19: A global systematic review and meta-analysis. *PLOS ONE* **16** (2021). https://doi.org/10.1371/journal.pone.0247461
193 Renia, L. *et al.* Lower vaccine-acquired immunity in the elderly population following two-dose BNT162b2 vaccination is alleviated by a third vaccine dose. *Nature Communications 2022 13:1* **13** (2022). https://doi.org/10.1038/s41467-022-32312-1
194 Rubtsova, K., Rubtsov, A. V., Dyk, L. F. v., Kappler, J. W. & Marrack, P. T-box transcription factor T-bet, a key player in a unique type of B-cell activation essential for effective viral clearance. *Proceedings of the National Academy of Sciences of the United States of America* **110** (2013). https://doi.org/10.1073/pnas.1312348110
195 van der Klaauw, A. A. *et al.* Accelerated waning of the humoral response to COVID-19 vaccines in obesity. *Nat Med* **29**, 1146-1154 (2023). https://doi.org/10.1038/s41591-023-02343-2
196 SEVENTY-FIFTH WORLD HEALTH ASSEMBLY RESOLUTIONS AND DECISIONS ANNEXES. Report No. WHA75/2022/REC/1, 81-85 (World Health Organisation, Geneva, 2022).
197 Baker, C. (House of Commons Library, 2023).
198 Blüher, M. & Blüher, M. Obesity: global epidemiology and pathogenesis. *Nature Reviews Endocrinology 2019 15:5* **15** (2019). https://doi.org/10.1038/s41574-019-0176-8
199 Shaikh, S. R. *et al.* Emerging mechanisms of obesity-associated immune dysfunction. *Nature Reviews Endocrinology 2023 20:3* **20** (2023). https://doi.org/10.1038/s41574-023-00932-2
200 Ouchi, N. *et al.* Adipokines in inflammation and metabolic disease. *Nature Reviews Immunology 2011 11:2* **11** (2011). https://doi.org/10.1038/nri2921
201 Cook, K. S. *et al.* Adipsin: a circulating serine protease homolog secreted by adipose tissue and sciatic nerve - PubMed. *Science (New York, N.Y.)* **237** (1987). https://doi.org/10.1126/science.3299705
202 Hotamisligil, G. S., Shargill, N. S. & Spiegelman, B. M. Adipose Expression of Tumor Necrosis Factor-α: Direct Role in Obesity-Linked Insulin Resistance. *Science* **259** (1993). https://doi.org/10.1126/science.7678183
203 Scherer, P. E., Williams, S., Fogliano, M., Baldini, G. & Lodish, H. F. A Novel Serum Protein Similar to C1q, Produced Exclusively in Adipocytes. *Journal of Biological Chemistry* **270** (1995). https://doi.org/10.1074/jbc.270.45.26746
204 Zhang, Y. *et al.* Positional cloning of the mouse obese gene and its human homologue. *Nature 1994 372:6505* **372** (1994). https://doi.org/10.1038/372425a0

205 Man, K. *et al.* Resident and migratory adipose immune cells control systemic metabolism and thermogenesis. *Cellular & Molecular Immunology 2021 19:3* **19** (2021). https://doi.org/10.1038/s41423-021-00804-7
206 Duque, G. A. & Descoteaux, A. Macrophage Cytokines: Involvement in Immunity and Infectious Diseases. *Front. Immunol.* **5** (2014). https://doi.org/10.3389/fimmu.2014.00491
207 Observatory, T. G. O. (World Obesity, Data.WorldObesity.org, 2024).
208 Hosogai, N. *et al.* Adipose Tissue Hypoxia in Obesity and Its Impact on Adipocytokine Dysregulation. *Diabetes* **56** (2007). https://doi.org/10.2337/db06-0911
209 Trayhurn, P. Hypoxia and Adipose Tissue Function and Dysfunction in Obesity. *Physiological Reviews* **93** (2013). https://doi.org/10.1152/physrev.00017.2012
210 Frasca, D. & Blomberg, B. B. Obesity Accelerates Age Defects in Mouse and Human B Cells. *Front. Immunol.* **11**, 2060 (2020). https://doi.org/10.3389/fimmu.2020.02060
211 Thomas, A. L. *et al.* Frontiers | Implications of Inflammatory States on Dysfunctional Immune Responses in Aging and Obesity. *Frontiers in Aging* **2** (2021). https://doi.org/10.3389/fragi.2021.732414
212 Pangrazzi, L. *et al.* The impact of body mass index on adaptive immune cells in the human bone marrow. *Immunity & Ageing 2020 17:1* **17** (2020). https://doi.org/10.1186/s12979-020-00186-w
213 Hanusch-Enserer, U. *et al.* Acute-phase response and immunological markers in morbid obese patients and patients following adjustable gastric banding. *International Journal of Obesity 2003 27:3* **27** (2003). https://doi.org/10.1038/sj.ijo.0802240
214 Karlsson, E. A., Sheridan, P. A. & Beck, M. A. Diet-induced obesity impairs the T cell memory response to influenza virus infection - PubMed. *Journal of immunology (Baltimore, Md. : 1950)* **184** (2010). https://doi.org/10.4049/jimmunol.0903220
215 Rebeles, J. *et al.* Obesity-Induced Changes in T-Cell Metabolism Are Associated With Impaired Memory T-Cell Response to Influenza and Are Not Reversed With Weight Loss. *The Journal of Infectious Diseases* **219**, 1652-1661 (2019). https://doi.org/10.1093/infdis/jiy700
216 Cai, Q. *et al.* Obesity and COVID-19 Severity in a Designated Hospital in Shenzhen, China. *Diabetes Care* **43** (2020). https://doi.org/10.2337/dc20-0576
217 Simonnet, A. *et al.* High Prevalence of Obesity in Severe Acute Respiratory Syndrome Coronavirus-2 (SARS-CoV-2) Requiring Invasive Mechanical Ventilation. *Obesity (Silver Spring, Md.)* **28** (2020). https://doi.org/10.1002/oby.22831
218 Williamson, E. J. *et al.* Factors associated with COVID-19-related death using OpenSAFELY. *Nature 2020 584:7821* **584** (2020). https://doi.org/10.1038/s41586-020-2521-4
219 Arulanandam, B. *et al.* Obesity and COVID-19 mortality are correlated. *Scientific Reports 2023 13:1* **13** (2023). https://doi.org/10.1038/s41598-023-33093-3
220 Lighter, J. *et al.* Obesity in Patients Younger Than 60 Years Is a Risk Factor for COVID-19 Hospital Admission. *Clinical Infectious Diseases* **71**, 896-897 (2020). https://doi.org/10.1093/cid/ciaa415

221 Guo, S. A. *et al.* Obesity Is Associated with Attenuated Tissue Immunity in COVID-19. *Am J Respir Crit Care Med* **207**, 566-576 (2023). https://doi.org/10.1164/rccm.202204-0751OC
222 Frasca, D. *et al.* Influence of obesity on serum levels of SARS-CoV-2-specific antibodies in COVID-19 patients. *PLOS ONE* **16**, e0245424 (2021). https://doi.org/10.1371/journal.pone.0245424
223 Vimercati, L. *et al.* Association between Long COVID and Overweight/Obesity. *Journal of Clinical Medicine* **10** (2021). https://doi.org/10.3390/jcm10184143
224 Banga, N., Guss, P., Banga, A. & Rosenman, K. D. Incidence and variables associated with inadequate antibody titers after pre-exposure rabies vaccination among veterinary medical students. *Vaccine* **32**, 979-983 (2014). https://doi.org/10.1016/j.vaccine.2013.12.019
225 Impaired Immunogenicity of Hepatitis B Vaccine in Obese Persons. *N Engl J Med* **314** (1986). https://doi.org/10.1056/NEJM198605223142119
226 Young, K. M., Gray, C. M. & Bekker, L.-G. Is Obesity a Risk Factor for Vaccine Non-Responsiveness? *PLoS ONE* **8**, e82779 (2013). https://doi.org/10.1371/journal.pone.0082779
227 Eliakim, A., Swindt, C., Zaldivar, F., Casali, P. & Cooper, D. M. Reduced tetanus antibody titers in overweight children. *Autoimmunity* **39**, 137-141 (2006). https://doi.org/10.1080/08916930600597326
228 Callahan, S. T. *et al.* Impact of Body Mass Index on Immunogenicity of Pandemic H1N1 Vaccine in Children and Adults. *Journal of Infectious Diseases* **210**, 1270-1274 (2014). https://doi.org/10.1093/infdis/jiu245
229 Sheridan, P. A. *et al.* Obesity is associated with impaired immune response to influenza vaccination in humans. *Int J Obes* **36**, 1072-1077 (2012). https://doi.org/10.1038/ijo.2011.208
230 Neidich, S. D. *et al.* Increased risk of influenza among vaccinated adults who are obese. *International Journal of Obesity 2017 41:9* **41** (2017). https://doi.org/10.1038/ijo.2017.131
231 Paich, H. A. *et al.* Overweight and obese adult humans have a defective cellular immune response to pandemic H1N1 Influenza a virus. *Obesity* **21** (2013). https://doi.org/10.1002/oby.20383
232 Park, H.-L. *et al.* Obesity-induced chronic inflammation is associated with the reduced efficacy of influenza vaccine. *Human Vaccines & Immunotherapeutics* **10** (2014). https://doi.org/10.4161/hv.28332
233 Ogden, C. L., Carroll, M. D., Kit, B. K. & Flegal, K. M. Prevalence of childhood and adult obesity in the United States, 2011-2012. *JAMA* **311**, 806-814 (2014).
234 Ogden, C. L. *et al.* Prevalence of Obesity Among Adults, by Household Income and Education — United States, 2011–2014. *MMWR Morb. Mortal. Wkly. Rep.* **66**, 1369-1373 (2017). https://doi.org/10.15585/mmwr.mm6650a1
235 Müller, L., Di Benedetto, S. & Pawelec, G. The immune system and its dysregulation with aging. *Biochemistry and cell biology of ageing: Part II clinical science*, 21-43 (2019).
236 Bertrand, A. *et al.* Impact of socioeconomic status on healthy immune responses in humans. *Immunology and Cell Biology* **102**, 618-629 (2024).
237 Noppert, G. A., Stebbins, R. C., Dowd, J. B., Hummer, R. A. & Aiello, A. E. Life course socioeconomic disadvantage and the aging immune system: findings

from the Health and Retirement Study. *The Journals of Gerontology: Series B* **76**, 1195-1205 (2021).

238 Lawlor, D. A., Hart, C. L., Hole, D. J. & Smith, G. D. Reverse causality and confounding and the associations of overweight and obesity with mortality. *Obesity* **14**, 2294-2304 (2006).

239 Apovian, C. M. Obesity: definition, comorbidities, causes, and burden. *Am J Manag Care* **22**, s176-185 (2016).

240 Abdullah, A., Peeters, A., de Courten, M. & Stoelwinder, J. The magnitude of association between overweight and obesity and the risk of diabetes: a meta-analysis of prospective cohort studies. *Diabetes research and clinical practice* **89**, 309-319 (2010).

241 Freemantle, N., Holmes, J., Hockey, A. & Kumar, S. How strong is the association between abdominal obesity and the incidence of type 2 diabetes? *International journal of clinical practice* **62**, 1391-1396 (2008).

242 Berbudi, A., Rahmadika, N., Tjahjadi, A. I. & Ruslami, R. Type 2 diabetes and its impact on the immune system. *Current diabetes reviews* **16**, 442-449 (2020).

243 Koliaki, C., Liatis, S. & Kokkinos, A. Obesity and cardiovascular disease: revisiting an old relationship. *Metabolism* **92**, 98-107 (2019).

244 Van Gaal, L. F., Mertens, I. L. & De Block, C. E. Mechanisms linking obesity with cardiovascular disease. *Nature* **444**, 875-880 (2006).

245 Mehra, M. R., Desai, S. S., Kuy, S., Henry, T. D. & Patel, A. N. Cardiovascular disease, drug therapy, and mortality in Covid-19. *N Engl J Med* **382**, e102 (2020).

246 You, J. H. *et al.* Clinical outcomes of COVID-19 patients with type 2 diabetes: a population-based study in Korea. *Endocrinology and Metabolism* **35**, 901-908 (2020).

247 Barron, E. *et al.* Associations of type 1 and type 2 diabetes with COVID-19-related mortality in England: a whole-population study. *The Lancet Diabetes & Endocrinology* **8**, 813-822 (2020).

248 Immunisation, J. C. o. V. a. JCVI statement regarding a COVID-19 booster vaccine programme for winter 2021 to 2022. (2021). <https://www.gov.uk/government/publications/jcvi-statement-september-2021-covid-19-booster-vaccine-programme-for-winter-2021-to-2022/jcvi-statement-regarding-a-covid-19-booster-vaccine-programme-for-winter-2021-to-2022#:~:text=%5Bfootnote%209%5D-,Advice,care%20homes%20for%20older%20adults>.

249 Phillips, C. M. & Phillips, C. M. Metabolically healthy obesity: Definitions, determinants and clinical implications. *Reviews in Endocrine and Metabolic Disorders 2013 14:3* **14** (2013). https://doi.org/10.1007/s11154-013-9252-x

250 Pennock, N. D. *et al.* T cell responses: naïve to memory and everything in between. *Advances in Physiology Education* **37** (2013). https://doi.org/10.1152/advan.00066.2013

251 Keeton, R. *et al.* T cell responses to SARS-CoV-2 spike cross-recognize Omicron. *Nature 2022 603:7901* **603** (2022). https://doi.org/10.1038/s41586-022-04460-3

252 Liu, J. *et al.* Vaccines elicit highly conserved cellular immunity to SARS-CoV-2 Omicron. *Nature 2022 603:7901* **603** (2022). https://doi.org/10.1038/s41586-022-04465-y

253 Tan, A. T. *et al.* Early induction of functional SARS-CoV-2-specific T cells associates with rapid viral clearance and mild disease in COVID-19 patients. *Cell Reports* **34** (2021). https://doi.org/10.1016/j.celrep.2021.108728
254 Moderbacher, C. R. *et al.* Antigen-Specific Adaptive Immunity to SARS-CoV-2 in Acute COVID-19 and Associations with Age and Disease Severity. *Cell* **183** (2020). https://doi.org/10.1016/j.cell.2020.09.038
255 Abella, V. *et al.* Leptin in the interplay of inflammation, metabolism and immune system disorders. *Nature Reviews Rheumatology 2017 13:2* **13** (2017). https://doi.org/10.1038/nrrheum.2016.209
256 Klein, S. L., Flanagan, K. L., Klein, S. L. & Flanagan, K. L. Sex differences in immune responses. *Nature Reviews Immunology 2016 16:10* **16** (2016). https://doi.org/10.1038/nri.2016.90
257 Nuñez, N. G. *et al.* High-dimensional analysis of 16 SARS-CoV-2 vaccine combinations reveals lymphocyte signatures correlating with immunogenicity. *Nat Immunol* **24**, 941-954 (2023). https://doi.org/10.1038/s41590-023-01499-w
258 Bellusci, L. *et al.* Antibody affinity and cross-variant neutralization of SARS-CoV-2 Omicron BA.1, BA.2 and BA.3 following third mRNA vaccination. *Nature Communications 2022 13:1* **13** (2022). https://doi.org/10.1038/s41467-022-32298-w
259 Fruh, S. M. Obesity: Risk factors, complications, and strategies for sustainable long-term weight management. *Journal of the American Association of Nurse Practitioners* **29** (2017). https://doi.org/10.1002/2327-6924.12510
260 Bode, B. *et al.* Glycemic Characteristics and Clinical Outcomes of COVID-19 Patients Hospitalized in the United States. *Journal of Diabetes Science and Technology* **14** (2020). https://doi.org/10.1177/1932296820924469
261 Mauer, N. *et al.* The First 110,593 COVID-19 Patients Hospitalised in Lombardy: A Regionwide Analysis of Case Characteristics, Risk Factors and Clinical Outcomes. *International Journal of Public Health* **67** (2022). https://doi.org/10.3389/ijph.2022.1604427
262 Kelly, N. E. W. *et al.* Antigen specific T cells in people with obesity at five months following ChAdOx1 COVID-19 vaccination. *International Journal of Obesity 2022 47:1* **47** (2022). https://doi.org/10.1038/s41366-022-01235-8
263 Abebe, E. C. & Dejenie, T. A. Protective roles and protective mechanisms of neutralizing antibodies against SARS-CoV-2 infection and their potential clinical implications. *Front. Immunol.* **14** (2023). https://doi.org/10.3389/fimmu.2023.1055457
264 Little, S. F., Leppla, S. H. & Friedlander, A. M. Production and characterization of monoclonal antibodies against the lethal factor component of Bacillus anthracis lethal toxin. *Infection and Immunity* **58** (1990). https://doi.org/10.1128/iai.58.6.1606-1613.1990
265 McDougal, C. E. & Pepper, M. Immunology & Cell Biology | ASI Journal | Wiley Online Library. *Immunology and Cell Biology* **102** (2024). https://doi.org/10.1111/imcb.12770
266 Smith, G. I., Mittendorfer, B. & Klein, S. Metabolically healthy obesity: facts and fantasies. *The Journal of Clinical Investigation* **129** (2019). https://doi.org/10.1172/JCI129186

267 Ward, E. S., Zhou, J., Ghetie, V. & Ober, R. J. Evidence to support the cellular mechanism involved in serum IgG homeostasis in humans. *International Immunology* **15** (2003). https://doi.org/10.1093/intimm/dxg018
268 Hodkinson, J. P. Considerations for dosing immunoglobulin in obese patients. *Clinical & Experimental Immunology* **188** (2017). https://doi.org/10.1111/cei.12955
269 Gao, X. *et al.* Mechanisms of Obesity-Induced Changes in Pharmacokinetics of IgG in Rats. *Pharmaceutical Research 2023 40:5* **40** (2023). https://doi.org/10.1007/s11095-023-03496-y
270 Geysen, H. M., Meloen, R. H. & Barteling, S. J. Use of peptide synthesis to probe viral antigens for epitopes to a resolution of a single amino acid. *Proc Natl Acad Sci USA* **81** (1984). https://doi.org/10.1073/pnas.81.13.3998
271 Hansen, L. B., Buus, S. & Schafer-Nielsen, C. Identification and Mapping of Linear Antibody Epitopes in Human Serum Albumin Using High-Density Peptide Arrays. *PLOS ONE* **8** (2013). https://doi.org/10.1371/journal.pone.0068902
272 Nilvebrant, J. & Rockberg, J. An Introduction to Epitope Mapping. *Methods in Molecular Biology* (2018). https://doi.org/10.1007/978-1-4939-7841-0_1
273 Lean, M. *et al.* Feasibility and indicative results from a 12-month low-energy liquid diet treatment and maintenance programme for severe obesity. *British Journal of General Practice* **63** (2013). https://doi.org/10.3399/bjgp13X663073
274 Maciejewski, M. L. *et al.* Bariatric Surgery and Long-term Weight Loss Durability. *JAMA Surgery* **151** (2016). https://doi.org/10.1001/jamasurg.2016.2317
275 Vilsbøll, T., Christensen, M., Junker, A. E., Knop, F. K. & Gluud, L. L. Effects of glucagon-like peptide-1 receptor agonists on weight loss: systematic review and meta-analyses of randomised controlled trials. *BMJ* **344** (2012). https://doi.org/10.1136/bmj.d7771
276 Harry W Schroeder, J. & Cavacini, L. Structure and Function of Immunoglobulins. *The Journal of allergy and clinical immunology* **125** (2010). https://doi.org/10.1016/j.jaci.2009.09.046
277 Noval, M. G. *et al.* Antibody isotype diversity against SARS-CoV-2 is associated with differential serum neutralization capacities. *Scientific Reports 2021 11:1* **11** (2021). https://doi.org/10.1038/s41598-021-84913-3
278 Klingler, J. *et al.* Role of Immunoglobulin M and A Antibodies in the Neutralization of Severe Acute Respiratory Syndrome Coronavirus 2 - PubMed. *The Journal of infectious diseases* **223** (2021). https://doi.org/10.1093/infdis/jiaa784
279 Gasser, R. *et al.* Major role of IgM in the neutralizing activity of convalescent plasma against SARS-CoV-2. *Cell Reports* **34**, 108790 (2021). https://doi.org/10.1016/j.celrep.2021.108790
280 Wang, Z. *et al.* Enhanced SARS-CoV-2 neutralization by dimeric IgA. *Science Translational Medicine* **13** (2021). https://doi.org/10.1126/scitranslmed.abf1555
281 Hale, M. *et al.* IgM antibodies derived from memory B cells are potent cross-variant neutralizers of SARS-CoV-2. *Journal of Experimental Medicine* **219** (2022/09/05). https://doi.org/10.1084/jem.20220849
282 Tarkowski, M. *et al.* Anti-SARS-CoV-2 Immunoglobulin Isotypes, and Neutralization Activity Against Viral Variants, According to BNT162b2-Vaccination and Infection History. *Front. Immunol.* **12** (2021). https://doi.org/10.3389/fimmu.2021.793191

283 Ju, B. *et al.* Human neutralizing antibodies elicited by SARS-CoV-2 infection. *Nature 2020 584:7819* **584** (2020). https://doi.org/10.1038/s41586-020-2380-z
284 Chen, Y. *et al.* Broadly neutralizing antibodies to SARS-CoV-2 and other human coronaviruses. *Nat Rev Immunol* **23** (2023). https://doi.org/10.1038/s41577-022-00784-3
285 Korenkov, M. *et al.* Somatic hypermutation introduces bystander mutations that prepare SARS-CoV-2 antibodies for emerging variants - PubMed. *Immunity* **56** (2023). https://doi.org/10.1016/j.immuni.2023.11.004
286 Julian, M. C., Li, L., Garde, S., Wilen, R. & Tessier, P. M. Efficient affinity maturation of antibody variable domains requires co-selection of compensatory mutations to maintain thermodynamic stability. *Sci Rep* **7** (2017). https://doi.org/10.1038/srep45259
287 ISRAEL, E. J., WILSKER, D. F., HAYES, K. C., SCHOENFELD, D. & SIMISTER, N. E. Increased clearance of IgG in mice that lack β2-microglobulin: possible protective role of FcRn. *Immunology* **89** (1996). https://doi.org/10.1046/j.1365-2567.1996.d01-775.x
288 Stapleton, N. M. *et al.* Competition for FcRn-mediated transport gives rise to short half-life of human IgG3 and offers therapeutic potential. *Nature Communications 2011 2:1* **2** (2011). https://doi.org/10.1038/ncomms1608
289 Goetze, A. M., Liu, Y. D., Arroll, T., Chu, L. & Flynn, G. C. Rates and impact of human antibody glycation in vivo. *Glycobiology* **22** (2012). https://doi.org/10.1093/glycob/cwr141
290 Vattepu, R., Sneed, S. L. & Anthony, R. M. Sialylation as an Important Regulator of Antibody Function. *Front. Immunol.* **13** (2022). https://doi.org/10.3389/fimmu.2022.818736
291 Goldstein, L. D. *et al.* Massively parallel single-cell B-cell receptor sequencing enables rapid discovery of diverse antigen-reactive antibodies. *Communications Biology 2019 2:1* **2** (2019). https://doi.org/10.1038/s42003-019-0551-y
292 Schaefer-Babajew, D. *et al.* Antibody feedback regulates immune memory after SARS-CoV-2 mRNA vaccination. *Nature 2022 613:7945* **613** (2022). https://doi.org/10.1038/s41586-022-05609-w
293 Vakhitova, M. *et al.* A Rapid Method for Detection of Antigen-Specific B Cells. *Cells 2023, Vol. 12, Page 774* **12** (2023). https://doi.org/10.3390/cells12050774
294 Peterson, V. M. *et al.* Multiplexed quantification of proteins and transcripts in single cells. *Nature Biotechnology 2017 35:10* **35** (2017). https://doi.org/10.1038/nbt.3973
295 Setliff, I. *et al.* High-Throughput Mapping of B Cell Receptor Sequences to Antigen Specificity. *Cell* **179** (2019). https://doi.org/10.1016/j.cell.2019.11.003
296 Kramer, K. J. *et al.* Single-cell profiling of the antigen-specific response to BNT162b2 SARS-CoV-2 RNA vaccine. *Nature Communications 2022 13:1* **13** (2022). https://doi.org/10.1038/s41467-022-31142-5
297 Genomics, x. (10x Genomics, 10xgenomics.com, 2022).
298 Ruffolo, J. A. *et al.* Fast, accurate antibody structure prediction from deep learning on massive set of natural antibodies. *Nature Communications 2023 14:1* **14** (2023). https://doi.org/10.1038/s41467-023-38063-x

299 Abanades, B. *et al.* ImmuneBuilder: Deep-Learning models for predicting the structures of immune proteins. *Communications Biology 2023 6:1* **6** (2023). https://doi.org/10.1038/s42003-023-04927-7
300 Jumper, J. *et al.* Highly accurate protein structure prediction with AlphaFold. *Nature 2021 596:7873* **596** (2021). https://doi.org/10.1038/s41586-021-03819-2
301 Desta, I. T. *et al.* The ClusPro AbEMap web server for the prediction of antibody epitopes. *Nature Protocols 2023 18:6* **18** (2023). https://doi.org/10.1038/s41596-023-00826-7
302 Hsieh, C.-L. *et al.* Structure-based design of prefusion-stabilized SARS-CoV-2 spikes - PubMed. *Science (New York, N.Y.)* **369** (2020). https://doi.org/10.1126/science.abd0826
303 Stavnezer, J. Antibody Class Switching. *Advances in Immunology* **61** (1996). https://doi.org/10.1016/S0065-2776(08)60866-4
304 Perkmann, T. *et al.* Anti-Spike Protein Assays to Determine SARS-CoV-2 Antibody Levels: a Head-to-Head Comparison of Five Quantitative Assays. *Microbiology Spectrum* (2021). https://doi.org/10.1128/spectrum.00247-21
305 Muramatsu, M. *et al.* Class Switch Recombination and Hypermutation Require Activation-Induced Cytidine Deaminase (AID), a Potential RNA Editing Enzyme. *Cell* **102** (2000). https://doi.org/10.1016/S0092-8674(00)00078-7
306 Jandl, C. & King, C. Cytokines in the Germinal Center Niche. *Antibodies* **5** (2016). https://doi.org/10.3390/antib5010005
307 Esposito, K. *et al.* Association of Low Interleukin-10 Levels with the Metabolic Syndrome in Obese Women. *The Journal of Clinical Endocrinology & Metabolism* **88** (2003). https://doi.org/10.1210/jc.2002-021437
308 Acosta, J. R. *et al.* Human-Specific Function of IL-10 in Adipose Tissue Linked to Insulin Resistance. *The Journal of Clinical Endocrinology & Metabolism* **104** (2019). https://doi.org/10.1210/jc.2019-00341
309 Schmidt, F. M. *et al.* Inflammatory Cytokines in General and Central Obesity and Modulating Effects of Physical Activity. *PLoS ONE* **10** (2015). https://doi.org/10.1371/journal.pone.0121971
310 Du, M. *et al.* Interleukin-27 is positively correlated with obesity and a decrease in insulin resistance after weight loss. *Obesity Research & Clinical Practice* **18** (2024). https://doi.org/10.1016/j.orcp.2024.05.001
311 Wang, Q. *et al.* IL-27 signalling promotes adipocyte thermogenesis and energy expenditure. *Nature 2021 600:7888* **600** (2021). https://doi.org/10.1038/s41586-021-04127-5
312 Kochumon, S. *et al.* Elevated adipose tissue associated IL-2 expression in obesity correlates with metabolic inflammation and insulin resistance. *Scientific Reports 2020 10:1* **10** (2020). https://doi.org/10.1038/s41598-020-73347-y
313 Jedrzejewski, P. M. *et al.* Towards Controlling the Glycoform: A Model Framework Linking Extracellular Metabolites to Antibody Glycosylation. *International Journal of Molecular Sciences 2014, Vol. 15, Pages 4492-4522* **15** (2014). https://doi.org/10.3390/ijms15034492
314 Irvine, E. B. & Alter, G. Understanding the role of antibody glycosylation through the lens of severe viral and bacterial diseases. *Glycobiology* **30** (2020). https://doi.org/10.1093/glycob/cwaa018

315 Kikuchi, Y. *et al.* Determination of concentration and binding affinity of antibody fragments by use of surface plasmon resonance. *Journal of Bioscience and Bioengineering* **100** (2005). https://doi.org/10.1263/jbb.100.311
316 Fiedler, S. *et al.* Serological fingerprints link antiviral activity of therapeutic antibodies to affinity and concentration. *Scientific Reports 2022 12:1* **12** (2022). https://doi.org/10.1038/s41598-022-22214-z
317 Asrat, S. *et al.* TRAPnSeq allows high-throughput profiling of antigen-specific antibody-secreting cells. *Cell Reports Methods* **3** (2023). https://doi.org/10.1016/j.crmeth.2023.100522
318 Attané, C. *et al.* Human Bone Marrow Is Comprised of Adipocytes with Specific Lipid Metabolism. *Cell Reports* **30** (2020). https://doi.org/10.1016/j.celrep.2019.12.089
319 Amar, S. *et al.* Diet-induced obesity in mice causes changes in immune responses and bone loss manifested by bacterial challenge. *Proc Natl Acad Sci USA* **104** (2007). https://doi.org/10.1073/pnas.0710335105
320 Hirano, T. *et al.* Complementary DNA for a novel human interleukin (BSF-2) that induces B lymphocytes to produce immunoglobulin. *Nature 1986 324:6092* **324** (1986). https://doi.org/10.1038/324073a0
321 Kishimoto, T., Akira, S., Narazaki, M. & Taga, T. Interleukin-6 Family of Cytokines and gp130. *Blood* **86** (1995). https://doi.org/10.1182/blood.V86.4.1243.bloodjournal8641243
322 Hirano, T. IL-6 in inflammation, autoimmunity and cancer. *International Immunology* **33** (2021). https://doi.org/10.1093/intimm/dxaa078
323 Murakami, M. *et al.* IL-6-Induced Homodimerization of gp130 and Associated Activation of a Tyrosine Kinase. *Science* **260** (1993). https://doi.org/10.1126/science.8511589
324 Montgomery, A. *et al.* Overlapping and distinct biological effects of IL-6 classic and trans-signaling in vascular endothelial cells. *American Journal of Physiology-Cell Physiology* **320** (2021). https://doi.org/10.1152/ajpcell.00323.2020
325 Babon, J. J., Varghese, L. N. & Nicola, N. A. Inhibition of IL-6 family cytokines by SOCS3. *Seminars in Immunology* **26** (2014). https://doi.org/10.1016/j.smim.2013.12.004
326 Monaco, G. *et al.* RNA-Seq Signatures Normalized by mRNA Abundance Allow Absolute Deconvolution of Human Immune Cell Types - PubMed. *Cell Reports* **26** (2019). https://doi.org/10.1016/j.celrep.2019.01.041
327 Rose-John, S. *et al.* Targeting IL-6 trans-signalling: past, present and future prospects. *Nature Reviews Immunology 2023 23:10* **23** (2023-04-17). https://doi.org/10.1038/s41577-023-00856-y
328 Barmettler, S. *et al.* Response to IL-6 trans- and IL-6 classic signalling is determined by the ratio of the IL-6 receptor α to gp130 expression: fusing experimental insights and dynamic modelling - PubMed. *Cell communication and signaling : CCS* **17** (2019). https://doi.org/10.1186/s12964-019-0356-0
329 Yan, I. *et al.* ADAM17 controls IL-6 signaling by cleavage of the murine IL-6Rα from the cell surface of leukocytes during inflammatory responses. *Journal of Leukocyte Biology* **99** (2016). https://doi.org/10.1189/jlb.3A0515-207R
330 Garbers, C. *et al.* Species specificity of ADAM10 and ADAM17 proteins in interleukin-6 (IL-6) trans-signaling and novel role of ADAM10 in inducible IL-6

receptor shedding - PubMed. *The Journal of biological chemistry* **286** (2011). https://doi.org/10.1074/jbc.M111.229393
331 Scheller, J., Chalaris, A., Schmidt-Arras, D. & Rose-John, S. The pro- and anti-inflammatory properties of the cytokine interleukin-6. *Biochimica et Biophysica Acta (BBA) - Molecular Cell Research* **1813** (2011). https://doi.org/10.1016/j.bbamcr.2011.01.034
332 Jones, S. A. *et al.* C-reactive Protein: A Physiological Activator of Interleukin 6 Receptor Shedding. *The Journal of Experimental Medicine* **189** (1999). https://doi.org/10.1084/jem.189.3.599
333 Briso, E. M., Dienz, O. & Rincon, M. Cutting Edge: Soluble IL-6R Is Produced by IL-6R Ectodomain Shedding in Activated CD4 T Cells. *J Immunol* **180** (2008). https://doi.org/10.4049/jimmunol.180.11.7102
334 Yousif, A. S. *et al.* The persistence of interleukin-6 is regulated by a blood buffer system derived from dendritic cells. *Immunity* **54** (2021/02/02). https://doi.org/10.1016/j.immuni.2020.12.001
335 Lust, J. A. *et al.* Isolation of an mRNA encoding a soluble form of the human interleukin-6 receptor - PubMed. *Cytokine* **4** (1992). https://doi.org/10.1016/1043-4666(92)90043-q
336 Soluble gp130 is the natural inhibitor of soluble interleukin-6 receptor transsignaling responses - PubMed. *European journal of biochemistry* **268** (2001 Jan). https://doi.org/10.1046/j.1432-1327.2001.01867.x
337 Chavele, K.-M., Merry, E. & Ehrenstein, M. R. Cutting Edge: Circulating Plasmablasts Induce the Differentiation of Human T Follicular Helper Cells via IL-6 Production. *J Immunol* **194** (2015). https://doi.org/10.4049/jimmunol.1401190
338 Rodríguez-Bayona, B., Ramos-Amaya, A., López-Blanco, R., Campos-Caro, A. & Brieva, J. A. STAT-3 activation by differential cytokines is critical for human in vivo-generated plasma cell survival and Ig secretion - PubMed. *J Immunol* **191** (2023). https://doi.org/10.4049/jimmunol.1301559
339 Korn, T. & Hiltensperger, M. Role of IL-6 in the commitment of T cell subsets. *Cytokine* **146** (2021). https://doi.org/10.1016/j.cyto.2021.155654
340 Tanaka, T., Narazaki, M. & Kishimoto, T. IL-6 in Inflammation, Immunity, and Disease. *Cold Spring Harbor Perspectives in Biology* **6** (2014). https://doi.org/10.1101/cshperspect.a016295
341 Arkatkar, T. *et al.* B cell-derived IL-6 initiates spontaneous germinal center formation during systemic autoimmunity - PubMed. *The Journal of experimental medicine* **214** (2017). https://doi.org/10.1084/jem.20170580
342 Wu, Y. *et al.* IL-6 produced by immune complex-activated follicular dendritic cells promotes germinal center reactions, IgG responses and somatic hypermutation - PubMed. *International immunology* **21** (2009). https://doi.org/10.1093/intimm/dxp041
343 de Valle, E. *et al.* NFκB1 is essential to prevent the development of multiorgan autoimmunity by limiting IL-6 production in follicular B cells. *Journal of Experimental Medicine* **213** (2016). https://doi.org/10.1084/jem.20151182
344 Hillion, S., Dueymes, M., Youinou, P. & Jamin, C. IL-6 Contributes to the Expression of RAGs in Human Mature B Cells. *J Immunol* **179** (2007). https://doi.org/10.4049/jimmunol.179.10.6790

345 Yan, Y., Wang, Y. & Diamond, B. IL-6 contributes to an immune tolerance checkpoint in post germinal center B cells. *Journal of Autoimmunity* **38** (2012). https://doi.org/10.1016/j.jaut.2011.09.004
346 Jego, G. t., Bataille, R. g. & Pellat-Deceunynck, C. Interleukin-6 is a growth factor for nonmalignant human plasmablasts. *Blood* **97** (2001). https://doi.org/10.1182/blood.V97.6.1817
347 Diehl, S. A., Schmidlin, H., Nagasawa, M., Blom, B. & Spits, H. IL-6 triggers IL-21 production by human CD4+ T cells to drive STAT3-dependent plasma cell differentiation in B cells. *Immunology and cell biology* **90** (2012). https://doi.org/10.1038/icb.2012.17
348 Muraguchi, A. *et al.* The essential role of B cell stimulatory factor 2 (BSF-2/IL-6) for the terminal differentiation of B cells. *Journal of Experimental Medicine* **167** (1988). https://doi.org/10.1084/jem.167.2.332
349 Kopf, M., Herren, S., Wiles, M. V., Pepys, M. B. & Kosco-Vilbois, M. H. Interleukin 6 Influences Germinal Center Development and Antibody Production via a Contribution of C3 Complement Component. *The Journal of Experimental Medicine* **188** (1998). https://doi.org/10.1084/jem.188.10.1895
350 Garbers, C. *et al.* Interleukin-6: designing specific therapeutics for a complex cytokine. *Nature Reviews Drug Discovery 2018 17:6* **17** (2018). https://doi.org/10.1038/nrd.2018.45
351 Choi, Y. S., Eto, D., Yang, J. A., Lao, C. & Crotty, S. Cutting Edge: STAT1 Is Required for IL-6–Mediated Bcl6 Induction for Early Follicular Helper Cell Differentiation. *J Immunol* **190** (2013). https://doi.org/10.4049/jimmunol.1203032
352 Eto, D. *et al.* IL-21 and IL-6 Are Critical for Different Aspects of B Cell Immunity and Redundantly Induce Optimal Follicular Helper CD4 T Cell (Tfh) Differentiation. *PLOS ONE* **6** (2011). https://doi.org/10.1371/journal.pone.0017739
353 Dienz, O. *et al.* The induction of antibody production by IL-6 is indirectly mediated by IL-21 produced by CD4+ T cells - PubMed. *The Journal of experimental medicine* **206** (2009). https://doi.org/10.1084/jem.20081571
354 Harker, J. A., Lewis, G. M., Mack, L. & Zuniga, E. I. Late interleukin-6 escalates T follicular helper cell responses and controls a chronic viral infection - PubMed. *Science (New York, N.Y.)* **334** (2011). https://doi.org/10.1126/science.1208421
355 Shapiro-Shelef, M., Calame, K., Shapiro-Shelef, M. & Calame, K. Regulation of plasma-cell development. *Nature Reviews Immunology 2005 5:3* **5** (2005). https://doi.org/10.1038/nri1572
356 Rodríguez-Bayona, B., Ramos-Amaya, A., López-Blanco, R., Campos-Caro, A. & Brieva, J. A. STAT-3 Activation by Differential Cytokines Is Critical for Human In Vivo–Generated Plasma Cell Survival and Ig Secretion. *J Immunol* **191** (2023). https://doi.org/10.4049/jimmunol.1301559
357 Jourdan, M. *et al.* IL-6 supports the generation of human long-lived plasma cells in combination with either APRIL or stromal cell-soluble factors. *Leukemia 2014 28:8* **28** (2014). https://doi.org/10.1038/leu.2014.61
358 Mohamed-Ali, V. *et al.* Subcutaneous Adipose Tissue Releases Interleukin-6, But Not Tumor Necrosis Factor-α, in Vivo1. *The Journal of Clinical Endocrinology & Metabolism* **82** (1997). https://doi.org/10.1210/jcem.82.12.4450

359 Sindhu, S. *et al.* Obesity Is a Positive Modulator of IL-6R and IL-6 Expression in the Subcutaneous Adipose Tissue: Significance for Metabolic Inflammation. *PLOS ONE* **10** (2015). https://doi.org/10.1371/journal.pone.0133494

360 Kraakman, Michael J. *et al.* Blocking IL-6 trans-Signaling Prevents High-Fat Diet-Induced Adipose Tissue Macrophage Recruitment but Does Not Improve Insulin Resistance. *Cell Metabolism* **21** (2015). https://doi.org/10.1016/j.cmet.2015.02.006

361 León-Ariza, H. H., Botero-Rosas, D. A., Acero-Mondragón, E. J. & Reyes-Cruz, D. Soluble interleukin-6 receptor in young adults and its relationship with body composition and autonomic nervous system. *Physiological Reports* **7** (2019). https://doi.org/10.14814/phy2.14315

362 Patsalos, O., Dalton, B. & Himmerich, H. Effects of IL-6 Signaling Pathway Inhibition on Weight and BMI: A Systematic Review and Meta-Analysis. *International Journal of Molecular Sciences* **21** (2020). https://doi.org/10.3390/ijms21176290

363 Coomes, E. A. & Haghbayan, H. Interleukin-6 in Covid-19: A systematic review and meta-analysis - PubMed. *Reviews in medical virology* **30** (2020). https://doi.org/10.1002/rmv.2141

364 The REMAP-CAP , I. Interleukin-6 Receptor Antagonists in Critically Ill Patients with Covid-19. *N Engl J Med* **384** (2021). https://doi.org/10.1056/NEJMoa2100433

365 Angriman, F. *et al.* Interleukin-6 receptor blockade in patients with COVID-19: placing clinical trials into context. *The Lancet Respiratory Medicine* **9** (2021). https://doi.org/10.1016/S2213-2600(21)00139-9

366 Jones, S. A., Hunter, C. A., Jones, S. A. & Hunter, C. A. Is IL-6 a key cytokine target for therapy in COVID-19? *Nature Reviews Immunology 2021 21:6* **21** (2021). https://doi.org/10.1038/s41577-021-00553-8

367 Masiá, M. *et al.* Robust long-term immunity to SARS-CoV-2 in patients recovered from severe COVID-19 after interleukin-6 blockade. *eBioMedicine* **82** (2022). https://doi.org/10.1016/j.ebiom.2022.104153

368 Li, C. *et al.* Mechanisms of innate and adaptive immunity to the Pfizer-BioNTech BNT162b2 vaccine. *Nature Immunology 2022 23:4* **23** (2022). https://doi.org/10.1038/s41590-022-01163-9

369 Rosati, M. *et al.* Rapid transient and longer-lasting innate cytokine changes associated with adaptive immunity after repeated SARS-CoV-2 BNT162b2 mRNA vaccinations. *Front. Immunol.* **14** (2023). https://doi.org/10.3389/fimmu.2023.1292568

370 DiPiazza, A. T. *et al.* COVID-19 vaccine mRNA-1273 elicits a protective immune profile in mice that is not associated with vaccine-enhanced disease upon SARS-CoV-2 challenge. *Immunity* **54** (2021). https://doi.org/10.1016/j.immuni.2021.06.018

371 Lamb, Y. N. BNT162b2 mRNA COVID-19 Vaccine: First Approval - PubMed. *Drugs* **81** (2021). https://doi.org/10.1007/s40265-021-01480-7

372 Bergamaschi, C. *et al.* Systemic IL-15, IFN-γ, and IP-10/CXCL10 signature associated with effective immune response to SARS-CoV-2 in BNT162b2 mRNA vaccine recipients. *Cell Reports* **36** (2021). https://doi.org/10.1016/j.celrep.2021.109504

373 Alameh, M.-G. *et al.* Lipid nanoparticles enhance the efficacy of mRNA and protein subunit vaccines by inducing robust T follicular helper cell and humoral responses. *Immunity* **54** (2021). https://doi.org/10.1016/j.immuni.2021.11.001
374 Parhiz, H. *et al.* Added to pre-existing inflammation, mRNA-lipid nanoparticles induce inflammation exacerbation (IE). *Journal of Controlled Release* **344** (2022). https://doi.org/10.1016/j.jconrel.2021.12.027
375 Tahtinen, S. *et al.* IL-1 and IL-1ra are key regulators of the inflammatory response to RNA vaccines. *Nature Immunology 2022 23:4* **23** (2022). https://doi.org/10.1038/s41590-022-01160-y
376 Zhu, Y. *et al.* Screening for lipid nanoparticles that modulate the immune activity of helper T cells towards enhanced antitumour activity. *Nature Biomedical Engineering 2023 8:5* **8** (2023). https://doi.org/10.1038/s41551-023-01131-0
377 Nguyen, D. C. *et al.* Plasma cell survival: The intrinsic drivers, migratory signals, and extrinsic regulators. *Immunological Reviews* **303** (2021). https://doi.org/10.1111/imr.13013
378 Bohannon, C. *et al.* Long-lived antigen-induced IgM plasma cells demonstrate somatic mutations and contribute to long-term protection. *Nature Communications* **7** (2016). https://doi.org/10.1038/ncomms11826
379 Fischer, M. *et al.* A bioactive designer cytokine for human hematopoietic progenitor cell expansion. *Nature Biotechnology 1997 15:2* **15** (1997). https://doi.org/10.1038/nbt0297-142
380 Nguyen, D. C., Joyner, C. J., Sanz, I. & Lee, F. E. Factors Affecting Early Antibody Secreting Cell Maturation Into Long-Lived Plasma Cells - PubMed. *Front. Immunol.* **10** (2019). https://doi.org/10.3389/fimmu.2019.02138
381 Rasheed, M. A. U. *et al.* Interleukin-21 Is a Critical Cytokine for the Generation of Virus-Specific Long-Lived Plasma Cells. *Journal of Virology* **87** (2013). https://doi.org/10.1128/JVI.00063-13
382 Dam, M. v. *et al.* Structure-function analysis of interleukin-6 utilizing human/murine chimeric molecules. Involvement of two separate domains in receptor binding. *Journal of Biological Chemistry* **268** (1993). https://doi.org/10.1016/S0021-9258(18)82467-X
383 Shinall, S. M., Gonzalez-Fernandez, M., Noelle, R. J. & Waldschmidt, T. J. Identification of Murine Germinal Center B Cell Subsets Defined by the Expression of Surface Isotypes and Differentiation Antigens. *J Immunol* **164** (2000/06/01). https://doi.org/10.4049/jimmunol.164.11.5729
384 Silva-Cayetano, A. *et al.* Spatial dysregulation of T follicular helper cells impairs vaccine responses in aging. *Nature Immunology 2023 24:7* **24** (2023). https://doi.org/10.1038/s41590-023-01519-9
385 Nanishi, E. *et al.* mRNA booster vaccination protects aged mice against the SARS-CoV-2 Omicron variant. *Communications Biology 2022 5:1* **5** (2022). https://doi.org/10.1038/s42003-022-03765-3
386 Tomasian, A., Jennings, J. W., Tomasian, A. & Jennings, J. W. Bone marrow aspiration and biopsy: techniques and practice implications. *Skeletal Radiology 2021 51:1* **51** (2021). https://doi.org/10.1007/s00256-021-03882-w
387 Mestas, J. & Hughes, C. C. W. Of Mice and Not Men: Differences between Mouse and Human Immunology. *J Immunol* **172** (2004). https://doi.org/10.4049/jimmunol.172.5.2731

388 Kaur, S., Bansal, Y., Kumar, R. & Bansal, G. A panoramic review of IL-6: Structure, pathophysiological roles and inhibitors. *Bioorganic & Medicinal Chemistry* **28** (2020). https://doi.org/10.1016/j.bmc.2020.115327

389 Nelson, T. L. & Hickey, M. S. Acute changes in dietary omega-3 fatty acid intake lowers soluble interleukin-6 receptor in healthy adult normal weight and overweight males. *Cytokine* **26** (2004). https://doi.org/10.1016/j.cyto.2004.02.010

390 Atti, A. *et al.* Antibody correlates of protection against Delta infection after vaccination: A nested case-control within the UK-based SIREN study. *Journal of Infection* **87** (2023). https://doi.org/10.1016/j.jinf.2023.07.007

391 Angyal, A. *et al.* T-cell and antibody responses to first BNT162b2 vaccine dose in previously infected and SARS-CoV-2-naive UK health-care workers: a multicentre prospective cohort study. *The Lancet Microbe* **3** (2022). https://doi.org/10.1016/S2666-5247(21)00275-5

392 Guerrera, G. *et al.* BNT162b2 vaccination induces durable SARS-CoV-2–specific T cells with a stem cell memory phenotype. *Science Immunology* **6** (2021). https://doi.org/10.1126/sciimmunol.abl5344

393 Tai, W. *et al.* An mRNA-based T-cell-inducing antigen strengthens COVID-19 vaccine against SARS-CoV-2 variants. *Nature Communications 2023 14:1* **14** (2023). https://doi.org/10.1038/s41467-023-38751-8

394 Zhang, G. *et al.* mRNA vaccines in disease prevention and treatment. *Signal Transduction and Targeted Therapy 2023 8:1* **8** (2023). https://doi.org/10.1038/s41392-023-01579-1

9. Appendix

Appendix A. Supplementary Data for Chapter 3.

A.1 Gating strategy for the identification of proliferating T cells by CTV assay

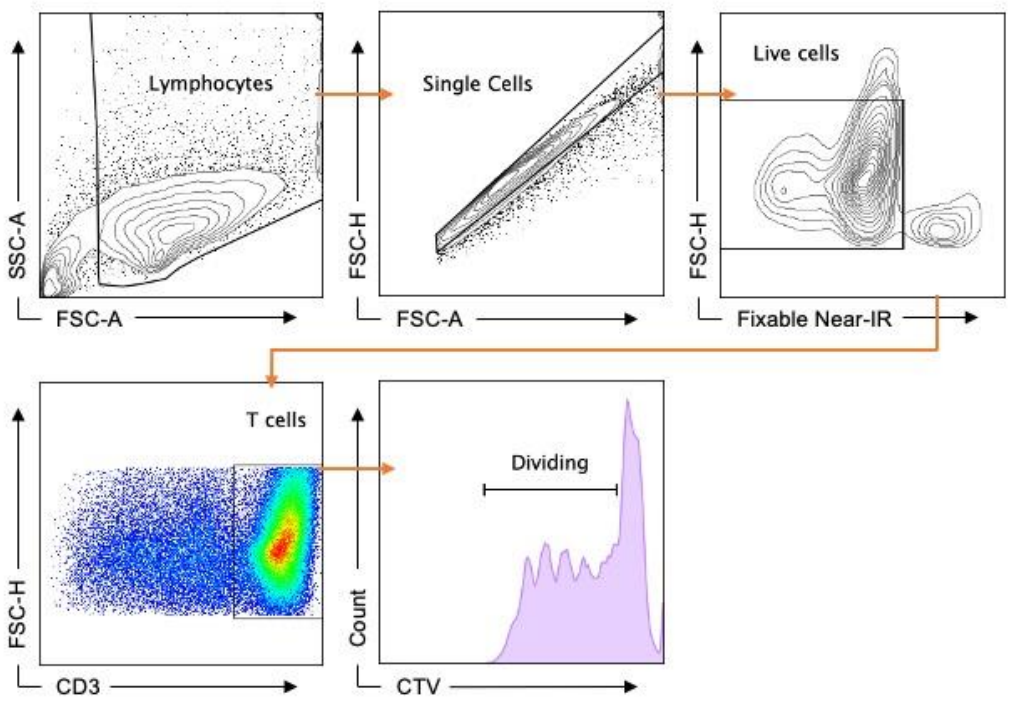

Figure 9.1. Gating strategy for CTV-stained dividing T cells. Staining displayed on PBMCs stimulated with PHA

A.2 Gating strategy for the identification of activated T cells

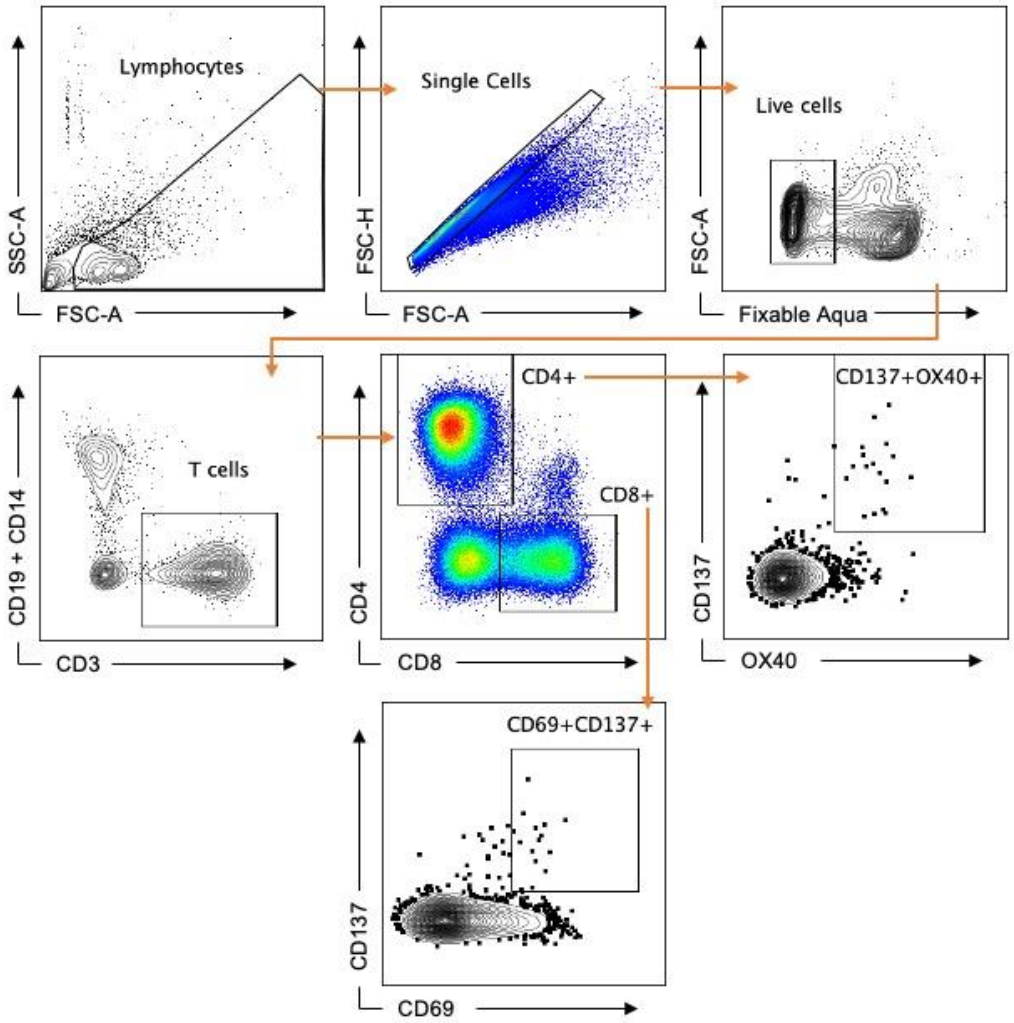

Figure 9.2 Gating strategy for activated $CD4^+$ and $CD8^+$ T cells from PBMCs following spike stimulation by AIM assay

A.3 Gating strategies for immunophenotyping of human PBMC samples in the immune dysfunction vaccination study

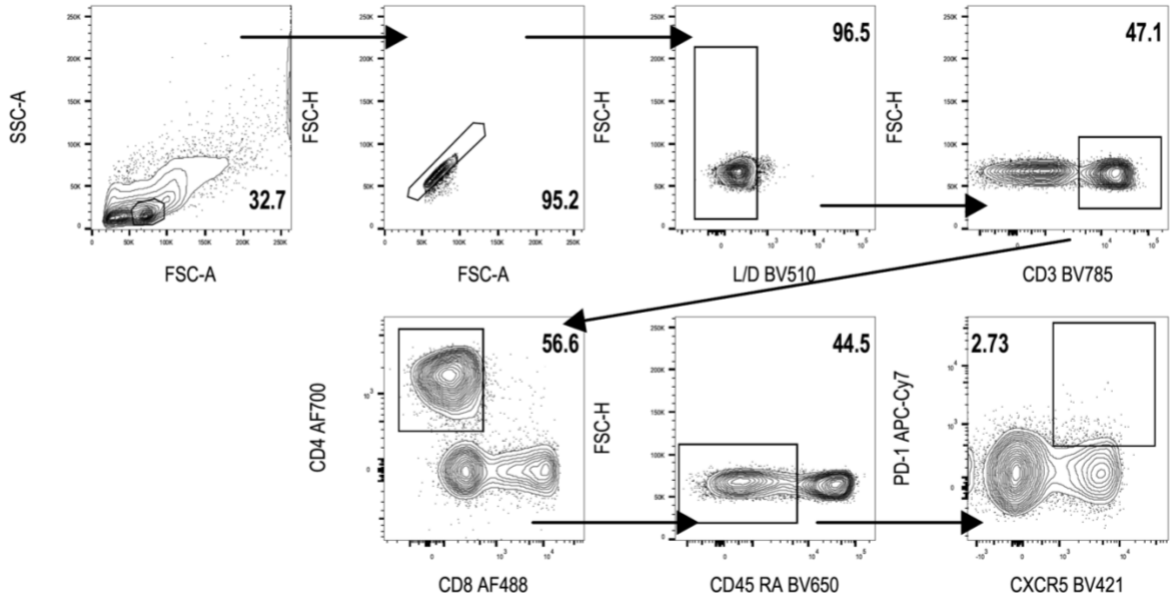

Figure 9.3. Gating strategy for T follicular helper cells from human PBMCs plots taken from Yam-Puc et al (2023)[106]

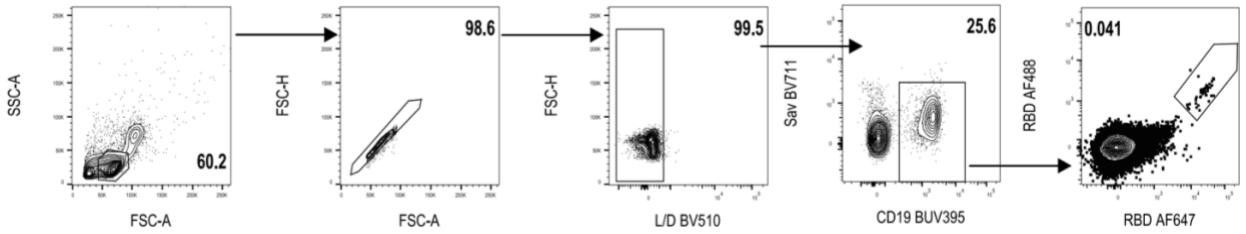

Figure 9.4. Gating strategy for RBD specific B cells from human PBMCs plots taken from Yam-Puc et al (2023)[106]

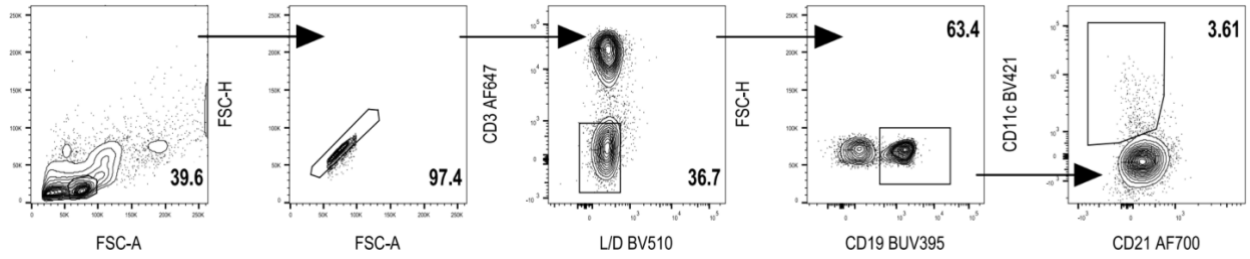

Figure 9.5. Gating strategy for age associated B cells from human PBMCs plots taken from Yam-Puc et al (2023)[106]

Appendix C. Supplementary Data for Chapter 5.

C.1 Anti-Spike ELISA of test serum dilutions for the detection of spike binding antibodies

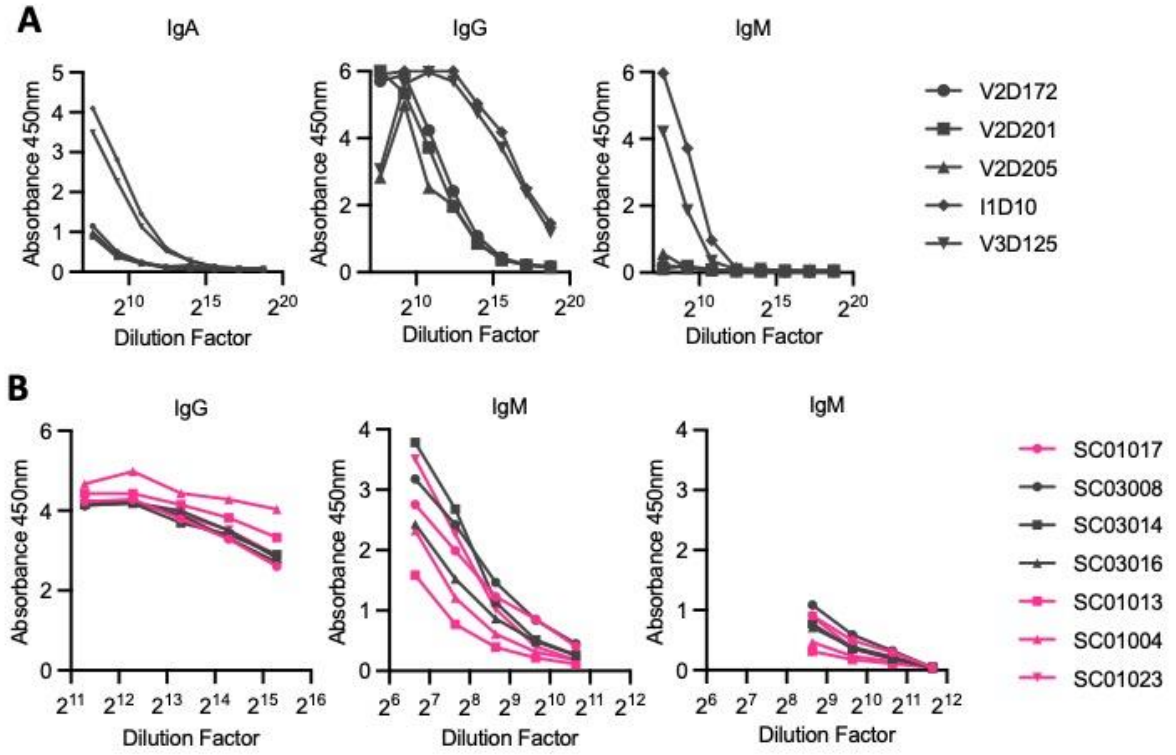

Figure 9.6. Serum dilution tests of spike binding antibody isotype ELISAs A) Absorbance reading at 450nm with increasing dilution of serum from a number of timepoints after vaccination and infection when assayed for spike specific IgA (left), IgG (centre) and IgM (right). **B)** Absorbance reading at 450nm with increasing dilution of serum from 4 SO and 3 NW individuals at day 28 following vaccination when assayed for IgG (left), IgM at high serum dilutions (centre) and IgM at low serum dilutions (right).

C.2 Gating strategy for the identification of spike binding human B cells

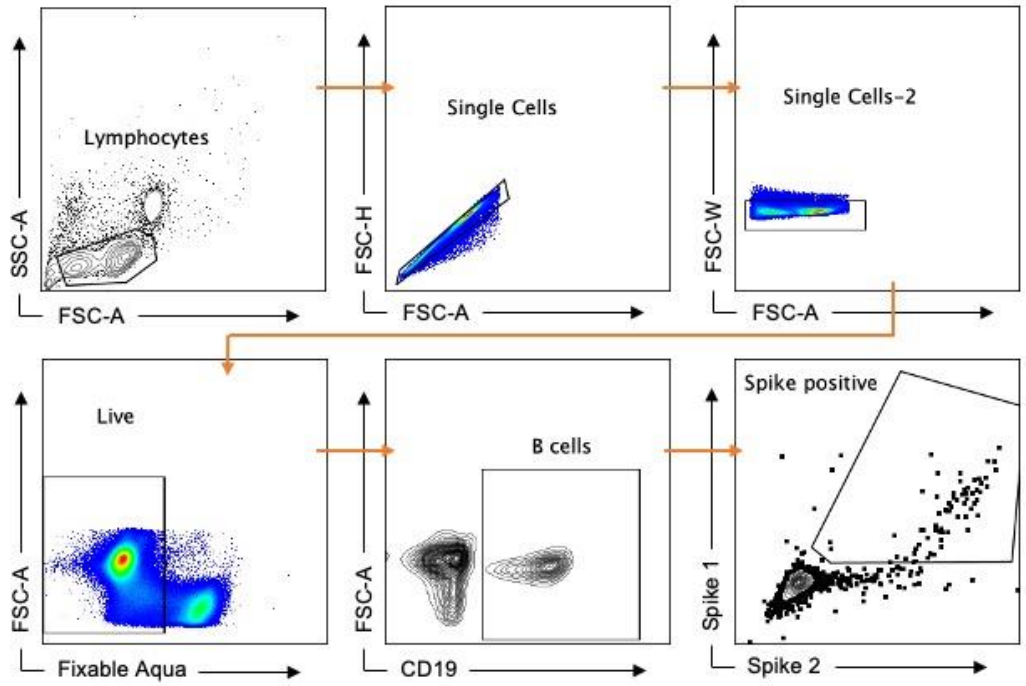

Figure 9.7. Gating strategy for spike specific B cells from human PBMCs Staining displayed on PBMCs from an individual following two doses of BNT162b2 vaccine

C.3 Primer sequences for plasmid sequencing

HexSpike_F_1	ATGTTCGTGTTCCTGGTGCTC
HexSpike_F_2	CATGTTCGTGTTCCTGGTGCTC
HPS_Sequencing_R	AATGTGCTCAGCAGTACCCA
M13R	CAGGAAACAGCTATGACC
HexSpike_R_1	CCCTGCTCGTATTTGCCGAG
Heavy_Chain_Insertion_R	TTGACCAGGCAGCCCAGG
Light_Chain_Insertion_R	AGGCAGTTCCAGATTTCAAC

C.4 Primer sequences for PCR amplification of pVITRO1 fragments

LightChain_F_1	CGAACTGTGGCTGCACCAT
LightChain_F_2	CGAACTGTGGCTGCACCATCTGTCTTCATCTTCCCGCCAT
LightChain_F_3	CGAACTGTGGCTGCACCATCTGTCTTCATCTTCCCG
LightChain_F_4	CGAACTGTGGCTGCACCATCTGTCTTCATCTTCC
LightChain_F_6	CGAACTGTGGCTGCACCATCTGTCTTCATC
LightChain_F_10	CGAACTGTGGCTGCACCATCTG
LightChain_F_11	CGAACTGTGGCTGCACCATC

LightChain_R_1	GGAGTGCGCGCCTGTG
LightChain_R_2	GGAGTGCGCGCCTGTGGCGGCCGCCACCAAGAAGAGGATC
LightChain_R_3	GGAGTGCGCGCCTGTGGCGGCCGCCACCAAGAAGAG
LightChain_R_4	GGAGTGCGCGCCTGTGGCGGCCGCCACCAAGAAG
LightChain_R_6	GGAGTGCGCGCCTGTGGCGGCCGCCACCAA
LightChain_R_10	GGAGTGCGCGCCTGTGGCGGCC
LightChain_R_11	GGAGTGCGCGCCTGTGGCGG
HeavyChain_F_1	GCCTCCACCAAGGGCCC
HeavyChain_R_1	ACCGCGGCTAGCTGGAAC

C.5 Conditions of Light Chain gradient PCR optimisation experiment

Table 9.1 Thermocycler settings for gradient PCR

Step	Temperature	Time	Cycles
Initial Denature	98°C	30 seconds	
Denature	98°C	10 seconds	X30
Annealing	61-75°C	20 seconds	
Extension	72°C	3 minutes 30 seconds	
Final Extension	72°C	10 minutes	
Hold	4°C	∞	

C.6 Conditions of PCR for Heavy and Light Chain constant regions

Table 9.2 Thermocycler settings for PCR amplification of pVITRO1 constant regions

Step	Temperature	Time	Cycles
Initial Denature	98°C	30 seconds	
Denature	98°C	10 seconds	X30
Annealing	64°C	20 seconds	
Extension	72°C	3 minutes 30 seconds	
Final Extension	72°C	10 minutes	
Hold	4°C	∞	

C.7 Monoclonal antibodies cloned from single cell V(D)J sequences

Table 9.3 Antibodies produced from single cell sequencing data
*Isotype is the isotype of the source cell V(D)J sequences were taken from – all variable regions were cloned into IgG1 antibodies

Antibody	ID Method	IDed as Spike:	Source	Cohort	Isotype*	ELISA result
SAb1	SPACE	Binding	NW1	NW	None	Positive
SAb2	SPACE	Binding	NW3	NW	IgD	Negative
SAb3	SPACE	Binding	NW3	NW	IgG	Positive
SAb4	SPACE	Binding	NW3	NW	IgM	Positive
SAb5	SPACE	Binding	NW3	NW	IgG	Positive
SAb6	SPACE	Binding	OH1	SO	IgM	Positive

SAb7	SPACE	Binding	OH1	SO	IgM	Weak
SAb8	SPACE	Binding	OH2	SO	IgG	Positive
SAb9	SPACE	Binding	OH2	SO	None	Positive
SAb10	SPACE	Binding	OL1	SO	IgM	Negative
SAb11	SPACE	Binding	OL2	SO	IgM	Negative
SAb12	SPACE	Binding	OL2	SO	IgG	Positive
SAb13	SPACE	Binding	OL2	SO	IgM	Weak
SAb14	SPACE	Binding	OL2	SO	IgM	Positive
SAb15	SPACE	Binding	OL2	SO	IgM	Positive
SAb16	Multimer	Binding	K040255E	SO	IgG	Positive
SAb17	Multimer	Binding	K036114D	SO	IgG	Positive
SAb18	Multimer	Binding	K036114D	SO	IgG	Positive
SAb19	Multimer	Binding	K036112B	SO	IgG	Positive
SAb20	Multimer	Binding	K036112B	SO	IgG	Positive
SAb21	Multimer	Binding	K040247W	SO	IgG	Positive
SAb22	Multimer	Binding	K040247W	SO	IgG	Positive
SAb23	Multimer	Binding	K040247W	SO	IgG	Positive
SAb24	Multimer	Binding	K040247W	SO	IgG	Positive
SAb25	Multimer	Binding	K034537R	NW	IgG	Positive
SAb26	Multimer	Binding	K034537R	NW	IgG	Positive
SAb27	Multimer	Binding	K034537R	NW	IgG	Positive
SAb28	Multimer	Binding	K034537R	NW	IgG	Positive
SAb29	Multimer	Binding	K034532J	NW	IgG	Positive
SAb30	Multimer	Binding	K034532J	NW	IgG	Positive
SAb31	Multimer	Binding	K034532J	NW	IgG	Positive
SAb32	Multimer	Binding	K034532J	NW	IgG	Positive
SAb33	Multimer	Binding	K034543W	NW	IgG	Positive
SAb34	Multimer	Binding	K034543W	NW	IgG	Positive
SAb35	Multimer	Binding	K034543W	NW	IgG	Positive
SAb36	Multimer	Binding	K034543W	NW	IgG	Positive
SAb41	SPACE	Non-Binding	NW3	NW	IgG	Weak
SAb42	SPACE	Non-Binding	OH1	SO	IgG	Negative
SAb49	SPACE	Non-Binding	OL2	SO	IgG	Negative
SAb51	SPACE	Non-Binding	OL2	SO	IgG	Weak
SAb53	Multimer	Non-Binding	K034543W	NW	IgG	Negative
SAb55	Multimer	Non-Binding	K034532J	NW	IgG	Negative
SAb56	Multimer	Non-Binding	K034537R	NW	IgG	Negative
SAb57	Multimer	Non-Binding	K040255E	SO	IgG	Negative
SAb67	Multimer	Non-Binding	K040247W	SO	IgG	Negative
SAb68	Multimer	Non-Binding	K040247W	SO	IgG	Negative
SAb69	Multimer	Non-Binding	K040247W	SO	IgG	Negative
SAb70	Multimer	Non-Binding	K040247W	SO	IgG	Negative
SAb71	Multimer	Non-Binding	K040247W	SO	IgG	Negative

SAb72	Multimer	Non-Binding	K040247W	SO	IgG	Negative
SAb76	Multimer	Binding	K034536N	NW	IgM	Weak
SAb77	Multimer	Binding	K034537R	NW	IgM	Weak
SAb78	Multimer	Binding	K034538Q	NW	IgM	Weak
SAb79	Multimer	Binding	K034543W	NW	IgM	Weak
SAb80	Multimer	Binding	K034551E	NW	IgM	Weak
SAb81	Multimer	Binding	K036112B	SO	IgM	Positive
SAb82	Multimer	Binding	K036114D	SO	IgM	Negative

C.8 Amino acid sequences of the variable regions of antibodies produced

SAb1H:
QVQLVESGGGVVQPGRSLRLSCAASGFTFSTYAMHWVRQAPGKGLEWVAVISYDDINKYYAD
SVKGRFTISRDNSKNTLYLQMNSLRAEDTAVYYCARSRGGSYYYGMDVWGQGTTVTVSS

SAb1L:
DIQMTQSPSSVSASVGDRVTITCRASQGISSWLAWYQQKPGKAPNLLIYGASSLESGVPSRFSG
SGSGTDFTLTISSLQPEDFATYYCQQANTFPYTFGQGTKLEMK

SAb2H:
EVQLVESGGGLVQPGGSLRLSCAASGFTFSSYDMHWVRQATGKGLEWVSAIGTAGDTYYPGS
VKGRFTISRENAKNSLYLQMNSLRAGDTAVYYCARGGITMVQGVIIPYYYYGMDVWGQGTTVTV
SS

SAb2L:
AIRITQSPSSLSASTGDRVTITCRASQGISSYLAWYQQKPGKAPKLLIYAASTLQSGVPSRFSGSG
SGTDFTLTISCLQSEDFATYYCQQYYSYPWTFGQGTKVEIK

SAb3H:
QVQLQESGPGLVKPSETLSLICTVSGGSISSYYWNWIRQTPGKGLEWIGNIYYSGSTNYNPSLQ
SRVTISVDTSKNQFSLMLSSVTAADTAVYYCAADYYDSTGYYYGMDVWGQGTTVTISS

SAb3L:
DIQMTQSPSSVSASVGDRVTITCRATQDIGNWLAWYQQKPGKAPKLLIYAASSWQSGVPSRFS
GSGSGTDFTLTISSLEPEDFAIYYCQQANSFLRTFGQGTRVEIK

SAb4H:
QVQLVESGGGVVQPGRSLRLSCAASGFTFSSYGMHWVRQAPGKGLEWVAVISYDGSNKYYA
DSVKGRFTISRDNSKNTLYLQMNSLRAEDTAVYYCAKDRSVATPYYYYGMDVWGQGTTVTVSS

SAb4L:
DIVMTQSPDSLAVSLGERATINCKSSQSVLYSSNNKNYLAWYQQKPGQPPKLLIYWASTRESGV
PDRFSGSGSGTDFTLTISSLQAEDVAVYYCQQYYSTPHTFGQGTKLEIK

SAb5H:
EVQLVESGGGLVQPGGSLRLSCVASGVTVSSNYMNWVRQAPGKGLEWVSVIYSGGSTYYADS
VKGRFTISRHNSKNTLYLQMNSLRAEDTAVYYCARDLELSGGMDVWGQGTTVTVSS

SAb5L:
IQLTQSPSSLSASVGDRVTITCRASQGISNYLAWYQQKPGKAPKLLIYAASTLQSGVSSRFSGSG
SGTDFTLTISSLQPEDFATYYCQQLNTEYQTFGQGTKLEIK

SAb6H:
QVQLVESGGGVVQPGRSLRLSCAASGFTFSSYAMHWVRQAPGKGLEWVAVISYDGSNKYYAD
SVKGRFTISRDNSKNTLYLQMNSLRAEDTAVYYCARADSGSYLYYFDYWGQGTLVTVSS

SAb6L:
QSALTQPRSVSGSPGQSVTISCTGTSSDVGGYNYVSWYQQHPGKAPKLMIYDVSKRPSGVPDR
FSGSKSGNTASLTISGLQAEDEADYYCCSYAGSYTWVFGGGTKLTVL

SAb7H:
EVQLLESGGGLVQPGGSLRLSCAASGFTFSSYAMSWVRQAPGKGLEWVSAISGSGGSTYYAD
SVKGRFTISRDNSKNTLYLQMNSLRAEDTAVYYCAKEYGMDVWGQGTTVTVSS

SAb7L:
EIVMTQSPATLSVSPGERATLSCRASQSVSSNLAWYQQKPGQAPRLLIYGASTRATGIPARFSGS
GSGTEFTLTISSLQSEDFAVYYCQQYNNWPPWTFGQGTKVEIK

SAb8H:
EVQLVESGGGLVKPGGSLRLSCAASGFTFSTYSLNWVRQAPGKGLEWVSSISSSSSFIYYADSV
KGRFTISKDNARNSLYLQMHSLRAEDTAVYYCARVRAHSFDSSGYYPDAFDIWGQGTMVTVSS

SAb8L:
EIVMTQSPATLSVSPGERATLSCRASQSVSSNLAWYQQKPGQAPRLLIYGASTRATAIPARFSGS
GSGTEFTLTISSMQSEDFAVYYCQQYYNWPPWTFGQGTKVEIK

SAb9H:
QVQVVQSGAEVKKPGSSMKVSCKASGGTLSSYGVNWVRQAPGQGLEWMGGTVPIFGTPNYA
QNFQGRVTITTDESTSTAYMELSSLRSEDTAVYYCATWGGDDAFDMWGQGTTVTVSS

SAb9L:
EIVLTQSPATLSLSPGERATLSCRASQSISTFLVWYQQKPGQAPRLLIYDASNRATGIPARFSGSG
SGTDFTLTISSLEPEDFAVYYCQRRSNWPPYTFGQGTKLEI

SAb10H:
EVQLVESGGGLIQPGGSLRLSCAASGFTVSSNYMSWVRQAPGKGLEWVSVIYSGGSTYYADSV
KGRFTISRDNSKNTLYLQMNSLRAEDTAVYYCARDTYGMDVWGQGTTVTVSS

SAb10L:
DIQMTQSPSSLSASVGDRVTITCRASQGISNYLAWYQQKPGKVPKLLIYAASTLQSGVPSRFSG
SGSGTDFTLTISSLQPEDVATYYCQKYNSAPPWTFGQGTKVEIK

SAb11H:
EVQLVESGGGLVQPGGSLRLSCAASGFTFSSYWMSWVRQAPGKGLEWVANIKQDGSEKYYV
DSVKGRFTISRDNAKNSLYLQMNSLRAEDTAVYYCARDPVTGYFDYWGQGTLVTVSS

SAb11L:
AIRMTQSPSSFSASTGDRVTITCRASQGISSYLAWYQQKPGKAPKLLIYAASTLQSGVPSRFSGS
GSGTDFTLTISCLQSEDFATYYCQQYYSYPLTFGGGTKVEIK

SAb12H:
QVQLVESGGGVVQPGRSLRLSCAASGFTFSTYAIHWVRQAPGKGLEWVALISYDGINKYYADS
VKGRFTLSRDNSKNTLYLQMNSLRADDTSVYYCARAYGGSYFGAFDIWGQGTMVTVSS

SAb12L:
EIVLTQSPGTLSLSPGERATLSCRASHSVSNNYLAWYQQKPGQAPRLLIYGASSRATGIPDRFSG
SGSGTDFTLTISRLEPEDFAVYYCQQYGNSVMYTFGQGTKLEIK

SAb13H:
EVQLVESGGGLVQPGGSLRLSCAASGFTLSSYWMSWVRQAPGKGLEWVANIKEDGTEKYYVD
SVRGRFTISRDNAKNSLYLQMNSLRAEDTALYYCARVGGSSWYFDYWGQGTLVTVSS

SAb13L:
EIVMTQSPATLSVSPGERATLSCRASQSVRSNLAWYQQKPGQAPRLLIYGASTRATGIPARFSGS
GSGTEFTLTISSLQSEDFAVYYCQQYNNWPPEDTFGQGTKLEIK

SAb14H:
QVQLVESGGGVVQPGRSLRLSCAASGFTFSSYGMHWVRQAPGKGLEWVAVISYDGSNKYYA
DSVKGRFTISRDNSKNTLYLQMNSLRAEDTAVYYCAKDRYGSYYYGMDVWGQGTTVTVSS

SAb14L:
DIQMTQSPSSLSASVGDRVTITCRASQSISSYLNWYQQKPGKAPKLLIYAASSLQSGVPSRFSGS
GSGTDFTLTISSLQPEDFATYYCQQSYSTPYTFGQGTKLEIK

SAb15H:
QVQLVESGGGVVQPGRSLRLSCAASGFTFSSYGMHWVRQAPGKGLEWVAVISYDGSNKYYA
DSVKGRFTISRDNSKNTLYLQMNSLRAEDTAVYYCAKDLNSGYLYYYYGMDVWGQGTTVTVSS

SAb15L:
SSELTQDPAVSVALGQTVRITCQGDSLRSYYASWYQQKPGQAPVLVIYGKNNRPSGIPDRFSGS
SSGNTASLTITGAQAEDEADYYCNSRDSSGNLDVVFGGGTKLTVL

SAb16H:
QVLLQESGPGLVKPSETLSLTCTVSGGSISSYYWTWIRQPPGKGLEWIGYVSNSGSTKYNPSLK
SRVTISVDTSKNQFSLKLRSVTAADTAVYYCARERDLAPRD

SAb16L:

DIVMTQSPDSLAVSLGERATINCKSSQSVLFSINNKNYLAWYQQRPGQPPKLLIYWASTRESGV
PDRFSGGGSGTDFTLTISSLQAEDVAVYYCQQYYTTPRTFGQGTKLEIK

SAb17H:
EVQLVESGGDLVQPGGSLRLSCAASGFIVNRNYMSWVRQAPGKGLEWISVIYPGGSTFYADSV
KGRFVISRDNSKNTLYLQMNSLRPNDTAVYYCARDLGTHVFDIWGQGIVVTVSS

SAb17L:
DIQLTQSPSFLSASVGDRVTITCRASQGISNYLAWYQQQSGKAPKLLIYAASTLQSGVPSRFSGS
GSGTEFTLTISSLQPEDFATYYCQQLNSYPSIFTFGPGTKVDIK

SAb18H:
QAQLVQSGPEVKKPGTSVKVSCQASGFTFSLAAVQWVRQARGQRLEWIGWSVAGSGNAYYA
QNFRERVTIRRDLSSTTAYMELRRLRSDDTAVYYCAAPYCRGGRCHDGFDIWGQGTMVTVSS

SAb18L:
EIVLTQSPDTLSLSPGERATLSCRANQSISRNYLAWYQQKPGQAPSLLIYTASSRATGIPDRFSGS
GSGTDFTLTVSRLEPEDFAVYYCQHYGGSLWTLGQGTKVEV

SAb19H:
QVQLVESGGGVVQPGRSLRLSCAASGFTFSSYAIYWVRQAPGKGLEWVTVVSYDGSNTYYAD
SVKGRFTISRDNSKNTLYLQMNSLRAEDTAVYYCARAGSGNYKSWFDPWGQGTLVTVSS

SAb19L:
EIVMTQSPATLSVSPGERATLSCRASQSISSNLAWYQQKPGQAPRLLIYGASTRATGIPARFSGS
GSGTEFTLTISSLQSEDFAVYYCQQYNNWPPLTFGQGTKVEIK

SAb20H:
QVHLVQSGAEVRKPGASVKVSCKASGFNFRDFYMHWVRQAPGQGFEWMGTITSSGSNTDYA
QKFRGRVSMTRDTSTSTVYMELSSLTSDDTAVYYCARDGVFLTGYSNFEYWGQGTLVTVSS

SAb20L:
DIVMTQSPVSLPVTPGEPASMSCRSSQSLLHTNGKNNLDWYLQKPGQSPQLLIYLGSNRASG
VPDRFSGSGSGTDFTLKISRVEAEDVGIYYCMQALETPPTFGQGTKVEIK

SAb21H:
QVHLVESGGGLVKPGGSLRLSCAASGFTFSDYYMSWIRQAPGKGLEWVSYISNSGSSKNHAD
SVKGRFTISRDNAKNSLYLQMNSLRAEDTAVYYCARDWSPYDRSDYLPSWGLGTLVTVSS

SAb21L:
DIQMTQSPSSLSASVGDRVTITCRASQDISNYLAWFQQKPGKAPKSLIYAASSLQSGVPSKFSG
SGSGTDFTLSISSLQPEDFATYYCQQYKSYPLTFGGGTKVEIK

SAb22H:
QVQLVQSGAEVKKPGASVKVSCKASGYTFNSYYIHWVRQAPGQGLEWMGMINPDGGATSYA
QKFQGRVTMTSDSSTTTVYMALSSLRDEDTAFYYCARDIVLIPAATGCDVWGQGTLVTVSS

SAb22L:
EIVLTQSPATLSLSPGERATLSCRASQSVRSYLAWYQQKPGQAPRLLIYDASNRATGIPDRFSGS
GSGTDFTLTISSLEPEDFAVYYCQQRSNWPRIFTFGPGTKVDIK

SAb23H:
QVQLQESGPGLVKPSQTLSLTCTVSGDSISSGGYYWSWIRQHPGKGLEWIGYIYYSGSTYYNPS
LGSRVTISIDRSKNQFSLKLTSVTAADTAVYYCALYNWNYNDYWGQGTLVTVSS

SAb23L:
DIQMTQSPSSLSASVGDRVTITCRASLGIRNDLGWYQQKPGKAPKRLIYAASSLQSGVPSRFSG
SGSGTEFTLTISSLQPEDFATYYCLQHNSFPFTFGQGTRLEIK

SAb24H:
QVQVVQSGAEVKKPGSSVKVSCKASGGTFNSYAISWVRQAPGQGLEWMGGIIPIFHTTNYAQK
FQGRVTITADDSTGTTYMELSSLRSEDTAVYYCARNHPYDSSGYYNDDWGQGTLVTVSS

SAb24L:
EIVLTQSPATLSLSPGERATFSCRASQSVSNFLAWYQQKPGQAPRLLIYDASNRATGIPARFSGS
GSGTDFTLTISSLEPEDFAVYYCHQRSNWPPRITFGQGTRLEIK

SAb25H:
QVQLVQSGAEVKKPGASVKVSCKASGYTFIGSYIHWVRQAPGQGLEWMGWINPNSGVTKYAQ
KFQGWVTMTSDTSISTAYMELSRLRSDHTAVYYCARESVVVESDYSYGMDVWGQGTTVTVSS

SAb25L:
QSALTQPRSVSGSPGQSVTISCTGTSNDVGGYDYVSWYQQHPGKAPKLMIFDVNKRPSGVPD
RFSGSKSGNTASLTISGLQAEDEADYSCCSYAGTYTLVFGGGTKVTVL

SAb26H:
QVQLQESGPGLVKPSETLSLTCSVSGGSIRSYYWSWIRQPPGKGLEWIGFFYYSGNTNYNPSLK
SRVTISVDTSKNQFSLRLRSVTAADTAVYYCATRGDCRGGSCYSADVFDVWGQGTMVTVSS

SAb26L:
DIEMAQSPSTLSASVGDRVTITCRASQSFSTWLAWYQQKPGKAPKLLIYDVSSLESGVPSRFSG
SGSGTEFTLTISSLQPDDFATYYCQQYNGYPYTFGQGTKLEIK

SAb27H:
QITLKESGPTLVKPTQTLTLTCTFSGFSLSTRGRGVGWIRQPPGKALEWLALVFWDDDKRYSPSL
KSRLTVTKDTSKNQVVLTMTNMDPVDAATYYCAHTKGDGGYGWGENFDYWGQGALVTVSS

SAb27L:
SYELTQPPSVSVSPGQTARITCSGDAFPNQYAYWYQQMSGQAPVLVIYKDSERPSGIPERFSGS
SSGTTVTLTISGVRSEDEADYYCQSADSRGVVFGGGTKLTVL

SAb28H:
QVQLVESGGGVVQPGRSLRLSCAASGFTFNGYTIHWVRQAPGKGLEWVAVISYDGINKYYTDS
VKGRFAISRDNSKNTLYLQMNSLRAEDTAVYYCARGGGNYLNSLGYWGQGTLVTVSS

SAb28L:
SYVLTQPHSVSVAPGKTARITCGGNNIGTKSVHWYQQRPGQAPVLVVSDDSDRPSGIPERFSG
SNSGNTATLTLSRVEAGDEADYYCQVWDSSSDHPVVFGGGTKLTVL

SAb29H:
QITLKESGPTLVKPTQTLTLTCTFSEFSLSTSGVGVGWIRQPPGKALEWLALIYWDDDKRYSPSLK
SRLTITKDTSKNQVVLTMTNMDPVDTATYYCARLKSNGWWGGDTFDVWGQGTMVTVSS

SAb29L:
QSVPTQPPSASGTPGQRVTISCSGSRSNIGGNYVNWYQLFPGAAPKVLIYSNDQRPSGVPGRF
SGSKSGTSASLAISGLQSEDEAEYYCASWDDSLNGWVFGGGTKLTVL

SAb30H:
QVQLVESGGGVVQPGRSLRLSCAASGFIFSTYSMHWVRQTPGKGLEWVALISYDGMNSYYAD
SVKGRFTISRDNSKHTLYLQMNSLRGDDTAVYYCARTNGYFTPFDFWGQGTLVTVSS

SAb30L:
EIVLTQSPGTLSLSPGERATLSCRASQTVSNNYVAWYQQKPGQAPRLLIYGASSRATGIPDRFSG
SGSGTDFTVTISRLEPEDLAIYYCQQYGNPPYTFGQGTKLEIK

SAb31H:
QVQLQESGPGLVRPSQTLSLTCTVSGGSVNSGDYYWSWIRQHPGKGLEWIGYVYYSGSTYYN
PSLMGRVTISVDTSKSQFSLKLSSVTAADTAVYYCARGHFDSSGNYFNAFDIWGQGTMVTVSS

SAb31L:
DIVLTQSPDSLAVSLGERATINCKSSQSVLYTSNNKNYLAWYQQKPGQPPKLLIYWASTRESGV
PDRFSGSGSGTDFTLTISSLQAEDVAVYYCLQYYSTRTFGQGTKLEIK

SAb32H:
EVQLLESGGDLVQPGGSLRLSCAASRFAFSNYAMSWVRQAPGKGLEWVSVISSSGGSTNYAD
SVKGRFTISRDNPKNTLYLQMNFLRVEDTAVYYCAGGVGSWFPDYWGQGTLVTVSS

SAb32L:
DIQMTQSPSSLSASVGDRVTITCRASQGIRNDLGWYQQKPGKAPKRLIHAASSLQSGVPSRFS
GSGSGTEFTLTINNLQPEDFATYYCLQYNYYPQYTFGQGTKLEMK

SAb33H:
QVTLKESGPVLVKPTETLTLTCTVSGFSLINARMGVSWIRQPPGKALEWLAHIFSNDEKSYSTSLK
SRLSISKNTSKGQVVLTMTNMDPVDTATYYCARITYGDYINYWYFDLWGRGTLVTVSS

SAb33L:
SYGLTQPPSVSVSPRQTASITCSGDKLVNKFASWYQQKPGQSPVLVIYLNNKRPSGVPERFSGS
KSGNTATLTISGTQAMDEADYYCQAWDSSTMIFGGGTKLTVL

SAb34H:
EVQLLESGGGLVQPGGSLRLSCAASGFTFSNYAMHWVRQTPGKGLEWVSGISGSGGDTYYAA
SVKGRFTISRDNSKNTLYLQMNSLRAEDTAVYYCAKGERIIMLVVVTLIDYWGRGTLVTVSS

SAb34L:
QSVLTQPPSVSAAPGQKVTISCSGSSSNIGNNYVSWYQQLPGTAPKLLIYDNNKRPSGIPDRFS
GSKSGTSATLGISGLQTGDEADYYCGTWDRSLSAYVFGTGTKVTVL

SAb35H:
QMQLVQSGPEVKKPGTSVKVSCKASGFTFYYSAVQWVRQARGQGLEWIGWIVVASGNTNYE
QKFQERVTITRDMTTSTVYMELSSLTSEDTAVYYCAAPNCRGGTCYDGFDIWGQGTMVTVSS

SAb35L:
EIVLTQSPGTLSLSPGERATLSCRASQSVSSSYLAWYQQKPGQAPRLLIYGASSRATGIPDRFTG
SGSGTDFTLTISRLEPEDFAVYHCQHYGGSLWTFGQGTKVETK

SAb36H:
QITLKESGPTLVKPTQTLTLTCTFSGFSLSSSGVGVGWIRQPPGKALEWLALIYWDEDKRYIPTLK
SRLTITKDTSKNQVVLTVTNMDPVDTATYFCARRRPVDGSMLFDYWGQGTLVTVSS

SAb36L:
DIQMTQSPSTLSASVGDRVTITCRASQSISSWLAWYQQKPGKAPKLLIYKASRLESGVPSRFSG
SGSGTEFTLTISSLQPDDFATYYCQQYNSYSIFAFGPGTKVEIK

SAb41H:
QLQLQQSGPGLVKPSQTLSLTCAISGDSVSSNSIAWNWIRQSPSRGLEWLIRTYYRSKWFTDYA
PSVKSRINIYPDTSMNQLILHLHSVTPDDTAVYYCVGATGAPSSIPAAEFHSWDQGILVSVSS

SAb41L:
DIQVTQFPSSLSASVGDRVTIFCRTSQSISTYVNWYQQKPGEPPRILIDAASRLQSGVPSRFSGS
GSGTAFTLTISGLQVEDFATYYCQQCYAIPITFGQGTRLDIK

SAb42H:
EVQLVESGGGLVQPGRSLRLSCVATGFTSDDYAMHWVRQSPGKGLEWVSGISWKSDYKGYAD
SVKGRFTISRDNAKNSLYLQMNSLRPEDTAFYYCAKEGPVDYVWGRYRYVYWGQGILVTVSS

SAb42L:
EIVLTQSPGTLSLSPGERATLSCRASQSVSSSFLAWYQQRPGQVPRLLIYGASNRATGIPDRFSG
SGFGTDFTLTISRLDPEDFAVYYCQQYGSSPRWTFGQGTKVEIK

SAb49H:
EVQLVESGGGLVKPGGSLRLSCAASGFTFSTYSMNWVRQAPGKGPEWVSSISNTGSFIYYADS
VEGRFTISRDNAKNSLFLHMNSLRAEDTAVYYCARDNGGFYSTVLWYWGQGAQVTVSS

SAb49L:
EIVLTQSPDTLSLSPGERATLSCRASQSLASNYLGWYQQKPGQAPRLLIFGASIRAPGIPDRFGG
SGSGTDFTLTISRVEPEDFAVYYCQQYDSSHRTFGQGTRLDIK

SAb51H:
EVQLVQSGAEVKKPGESLKISCQTSGYSFPSYWIGWVRQMPGKGLEWMGIIYLSDSDTRYSPS
FQGQVTISADTSVSTAYLQWSSLKASDTAMYYCATGVTVQGEVHCWGQGTLVTVSS

SAb51L:
DIQMTQSPSSLSASVGDRITITCRASQGISNYLAWFQQKPGKAPKSLIYAASSLQSGVPSKFSGS
GSGTDFTLTISSLQPEDFATYYCQQYKSYPPTFGQGTKVENK

SAb53H:
QITLQESGPTLVKPTETLTLTCTFSGFSFNAGGEGVAWIRQSPGKALECLAVIFWDDDKRYSPAL
KTRLTITKDTSRNQVILAMTDMDPADTATYFCAHRRGRRKEAALFDYWGQGTLLTVSS

SAb53L:
DIQMTQSPSYLAASVGDSVTITCRAGENIQAYLHWYQQKPGKAPKVLMFAATTLQSGVPSRFSG
SGFGTDFTLTISSLQPEDFATYYCQQGFSSPPTFGQGTRLEIK

SAb55H:
EMQLLESGGGLIQPGGSLRLSCAASGFTFSDYAITWVRQAPGEGLEWVSAVSRSGGSVYYAGA
VKGRFTISRDNSKNTVFLQMDDLRGEDTAIYYCTKDQTKMAVAAPRKVAGDFDVWGQGTMVT
VS

SAb55L:
SALTQPPSASGSPGQSVTLSCTGTSGDVGGYNSVSWYQQHPGKAPKLIIYEVTKRPSGVPDRF
SGSRSGNTASLTVSGLQTEDEATYFCSSYAGFNTVIFGVGTRLTVL

SAb56H:
QVQLVESGGGVVQPGRSLRLSCEPSGFVFSNYVMHWVRQAPGKGPEWLAVISYDGSNIYYAD
SVKGRFTISRDNSNNRLHLQMNSLTTEDTAVYYCARSRAVTAVTSPFGYWGQGTQVTVSS

SAb56L:
EILLTQSPATLPVSPGDRVTLSCRASHSLSTNLAWYQQKPGQAPRLVIYGASTRATDIPARFSGS
GSGTEFTLTITSLQSEDFAIYFCQQYHNWPPTWTFGQGTRVEIK

SAb57H:
QVQLQESGPGLVRPSQTLSLTCTVSGDSISSDEYYWSWFRQPPGKGLEWIGFIYYRVTTYYNPS
LNSHFSISMDTSRNEFSLNVNSVTAADTAVYFCARARLYIEYFDHWGRGTLVTVSS

SAb57L:
VMTQSPGTLSVSPGERATLSCRASQSVYSKLAWYQQKPGQAPRLLIYDASTRATGIPARFSGSG
SGTEFTLTISSLQSEDFAVYYCQQYANWPPITFGQGTRLEIK

SAb67H:
EVQLLESGGGVVPPGGSLRLSCAASGFTFTDYAMNWVRQAPGKGLEWVSTIGGSAGSTYYAD
SVKGRVIITRDNSKNTLSLQMNSLRADDTAVYYCAKDRYVWFGRTDLTTFDVWGQGTLVTVSS

SAb67L:
DIQMTQSPSSLSASVGDRVTITCRASQSINTYLNWYQQKPGKAPKLLIYAESNLQSGVPSRFSG
SGSGTDFSLTISSLQPEDFAAYYCQQSHTIPYTFGQGTKLEI

SAb68H:
EVQLVESGGGLVQPGGSLRLSCVVSGFRFRDYWMDWVRQAPGKGLEWVANIKYDGSERYYV
DSVKGRFTISRDNNKNSVFLQMNRLRVEDTAVYYCSRQLEEDFWGQGTLVTVSS

SAb68L:
DIQLTQSPSCLSASVGDRVTITCRASQGIRNELGWYQQKSGKAPKRLIYGVSSLHSGVPSRFSG
GGSGTEFTLTISSLQPEDFATYYCLQWNSYPRTFGQGTRVEIK

SAb69H:
QVHLVQSGAELKKPGASVKVSCKTSGYIFTTYAVHWVRQAPGQRLEWIGWINAGDGATKYSQ
RFQDRVTITRDTVAATAYMEMTNLKSEDTAVYYCARDDLRAEFGGHGRGVLYRFDPWGQGTL
VSVSS

SAb69L:
SYVLTQPPSLSVAPGQTASISCGGNNIGGKGVQWYQQKAGQAPVMVIYYNNDRPSGIPERFSG
SNSGITATLTISGVEAGDEADYYCQVWDRSDDHVVFGGGTKLTVL

SAb70H:
QVHLQESGPRLVKPSGTLSLTCAVSGVSVGNIYWWSWVRQSPAKGLEWIGEIFHSGSTNYNPS
LESRVTISIDKSNNHISLRLTSVTAADTAVYYCARGRACSGGTCAPMQFDYWGPGSLVTVSS

SAb70L:
DIVMTQSPLSLSVTPGEPASISCRSSQNLLFSNGYNYLDWYLQKPGQSPQLLIYLGSTRASGVP
DRFSGSGSGTDFTLRITRVEAEDIGVYYCMQALQTPFTFGRGTKLELK

SAb71H:
QAQLQESGPGLVEPSQTLSLTCSVSGDSLSSPDYYWSWIRQQPGKGLEWIGYIFYTGSTYYNPS
LKRRVSISADKSKNQFSLKLTSVTAADTAMYYCARDQWHCGGGGCYWFDPWGPGTLVTVSS

SAb71L:
QSALTQPPSASGSPGQSVTISCTGTSTDVGGYNYVSWYQHHPGKAPKLIIFDVSRRPSGVPARF
SGSKSGNTASLTVSGLQADDEATYYCSSFEGSNKVRVFGTGTEVTVL

SAb72H:
EVQLLESGGDLVQPGGSLRLSCVASGFTFSSYAMNWVRQAPGKGLEWVSVISASGGSIYYAES
VEGRFTISRDNSKNTLYLQLNSLRADDTAVYYCAKGSRGFSIPPDYWGQGTLVSVSS

SAb72L:
QSALTQPASVSGSPGQSITISCTGTSSDVGGYNYVSWYQQSPGKAPKLIIYDVNNRPSGVSTRF
SGSKSGDTASLTISGLQTEDEADYYCSSYRASSTPVVFGGGTKLTVL

SAb76H:
QITLKESGPTLVKPTQTLTLTCTFSGFSLTTTGVGVGWIRQPPGKALEWLALIYWDDDKHYSPSLQ
SRLTITKDTSKNQVVLTMTNMDPVDAATYYCVHRTSAIIVGFDYWGQGTLVTVSS

SAb76L:
SYDLTQPPSVSVSPGQTASITCSGDDLGDKYVCWYQQRPGQPPVLVIYQDDKRPSGIPERFSG
SNSGNTATLTISGTQAMDEADYYCQAWDSLIVVFGGGTKLTVL

SAb77H:
EVQLVESGGGLVQPGRSLRLSCAASGFTFDDYAMHWVRQAPGKGLEWVSGISWNSGSIGYA
DSVKGRFTISRDNAKNSLYLQMNSLRAEDTALYYCAKDRATRHYYYGMDVWGQGTTVTVSS

SAb77L:
QSALTQPASVSGSPGQSITISCTGTSSDVGGYNYVSWYQQHPGKAPKLMIYDVSNRPSGVSNR
FSGSKSGNTASLTISGLQAEDEADYYCSSYTSSSTVVFGGGTKLTVL

SAb78H:
QVQLVQSGAEVKKPGASVKVSCKASGYTFTSYGITWVRQAPGQGLEWMGWISTYNGNTNYAQ
KLQGRVTMTTDTSTSTAYMELRSLRSDDTAVYYCARGPLWGPDYWGQGTLVTVSS

SAb78L:
NFMLTQPHSVSESPGKTVTISCTGSSGSIASNYVQWYQQRPGSAPTTVIYEDNQRPSGVPDRF
SGSIDSSSNSASLTISGLKTEDEADYYCQSYDSSNQVFGGGTKLTVL

SAb79H:
QVQLQESGPGLVKPSQTLSLTCTVSGGSISSGDYYWSWIRQPPGKGLEWIGYIYYSGSTYYNPS
LKSRVTISVDTSKNQFSLKLSSVTAADTAVYYCACYGGNSGAFDYWGQGTLVTVSS

SAb79L:
SYELTQPPSVSVSPGQTARITCSGDALPKQYAYWYQQKPGQAPVLVIYKDSERPSGIPERFSGSS
SGTTVTLTISGVQAEDEADYYCQSADSSGTYGFGGGTKLTVL

SAb80H:
QITLKESGPTLVKPTQTLTLTCTFSGFSLNTRGVGVGWIRQPPGKALEWLALIYWDDVKRYSPSLL
SRLTITKDTSKNQVVLTMTAMEPVDTATYYCIHRQPDYIWGWGQGTLVTVSS

SAb80L:
DIVMTQSPLSLPVTPGEPASISCRSSQSLLHSNGNNYLDWYLQKPGQSPQLLIYLGSNRASGV
PDRFSGSGSGTDFTLKISRVEAEDVGVYYCMQALQTPLTFGGGTKVEIK

SAb81H:
EVQLVESGGGLVQPGGSLRLSCAASGFTFSSYWMSWVRQAPGKGLEWVANIKQDGSEKYYV
DSVKGRFTISRDNAKNSLYLQMNSLRAEDTAVYYCARDLIIGNWFDPWGQGTLVTVSS

SAb81L:
SYELTQPPSVSVSPGQTARITCSGDALPKQYAYWYQQKPGQAPVLVIYKDSERPSGIPERFSGSS
SGTTVTLTISGVQAEDEADYYCQSADSSGTYRGVFGGGTKLTVL

SAb82H:
QVQLVQSGAEVKKPGASVKVSCKASGYTFTGYYMHWVRQAPGQGLEWMGWINPNSGGTNY
AQKFQGRVTMTRDTSISTAYMELSRLRSDDTAVYYCARGEGGSYSPDYFDYWGQGTLVTVSS

SAb82L:
SYELTQPPSVSVSPGQTARITCSGDALPKQYAYWYQQKPGQAPVLVIYKDSERPSGIPERFSGSS
SGTTVTLTISGVQAEDEADYYCQSADSSGTYVVFGGGTKLTVL

C.9 Gating strategy for the identification of spike specific, IgM and IgG B cells in mice

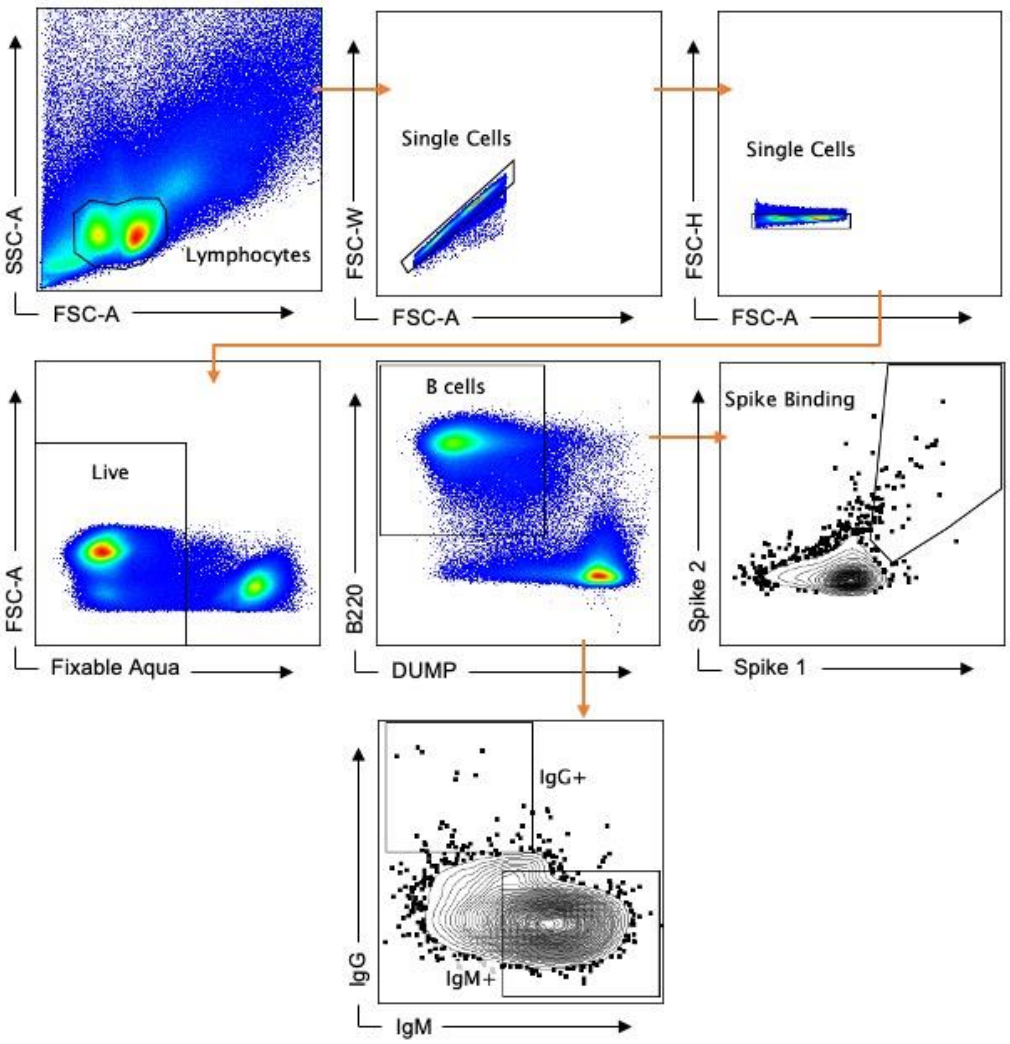

Figure 9.8. Gating strategy for spike binding, IgM, and IgG mouse B cells. Staining shown on lymph node cells of vaccinated mouse.

C.10 Quality control of three batch processing of B cells for single cell sequencing

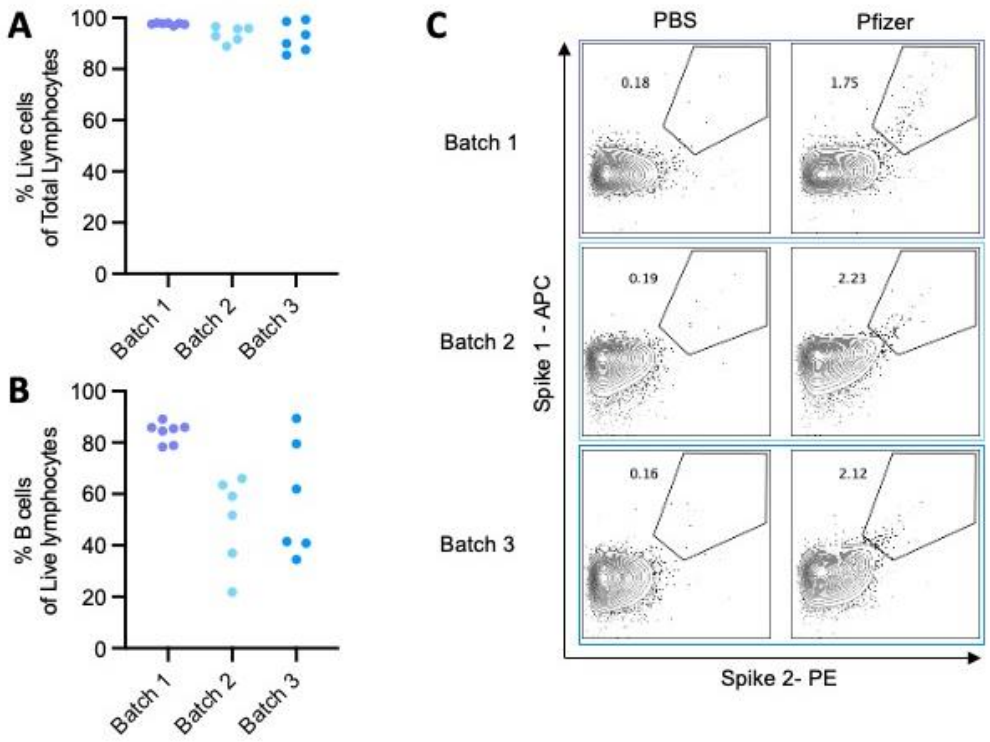

Figure 9.9. Flow cytometry to quality control batches of cells prepared for single cell sequencing. A) Viability of B cells from three batches following pan B isolation as indicated by percentage fixable live/dead stain negative indicated by flow cytometry. **B)** Proportion ($CD19^{+}CD3^{-}$) B cells of total cells following pan B isolation for each batch of cells prepared for sequencing as indicated by flow cytometry. **C)** Validation of multimer conjugation as indicated by increased dual positivity for multimer binding in splenocytes from PBS and BNT162b2 immunised mice for each batch of multimer prepared for respective batch of cells sequenced.

C.11 Anti-Spike ELISA of produced antibodies

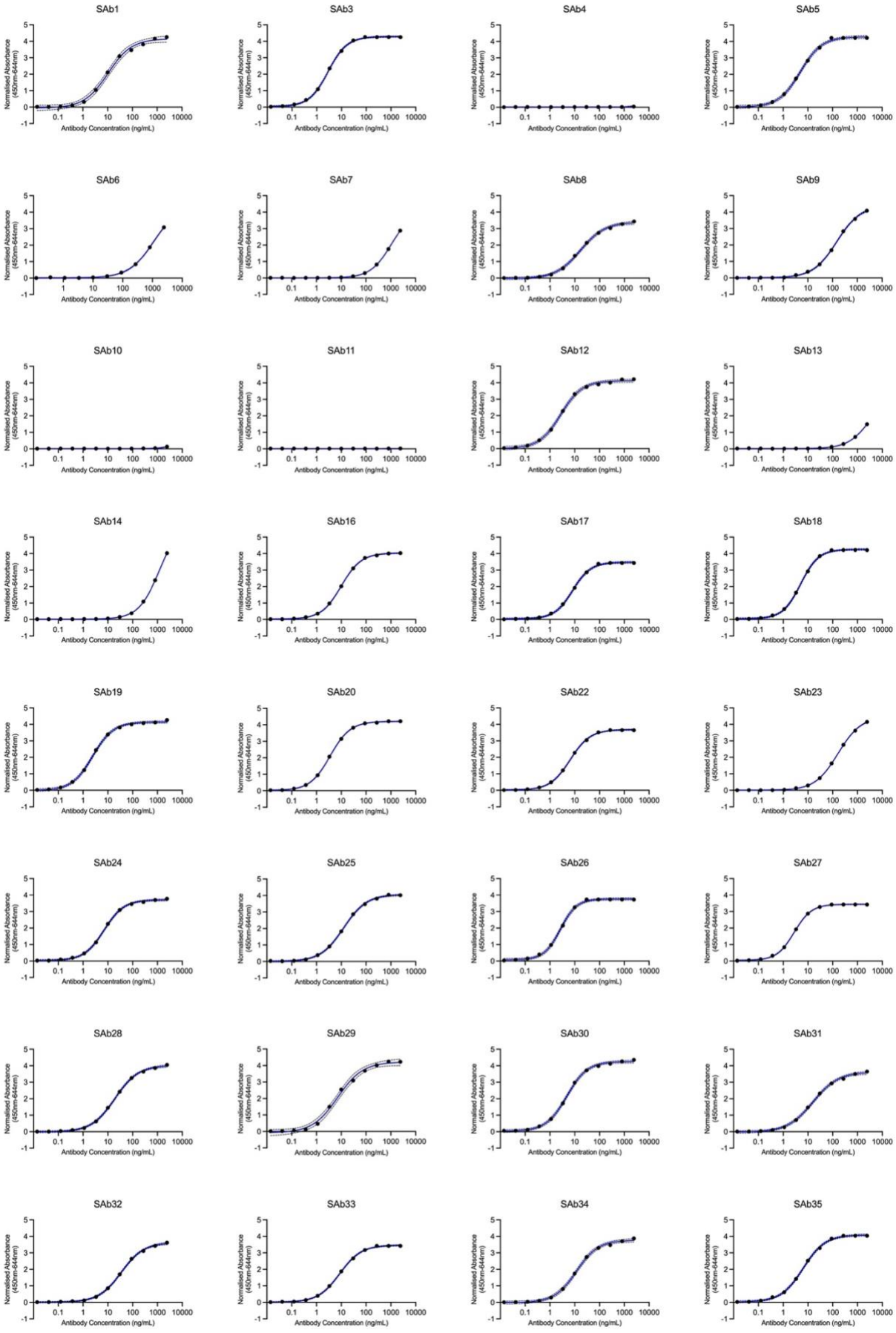

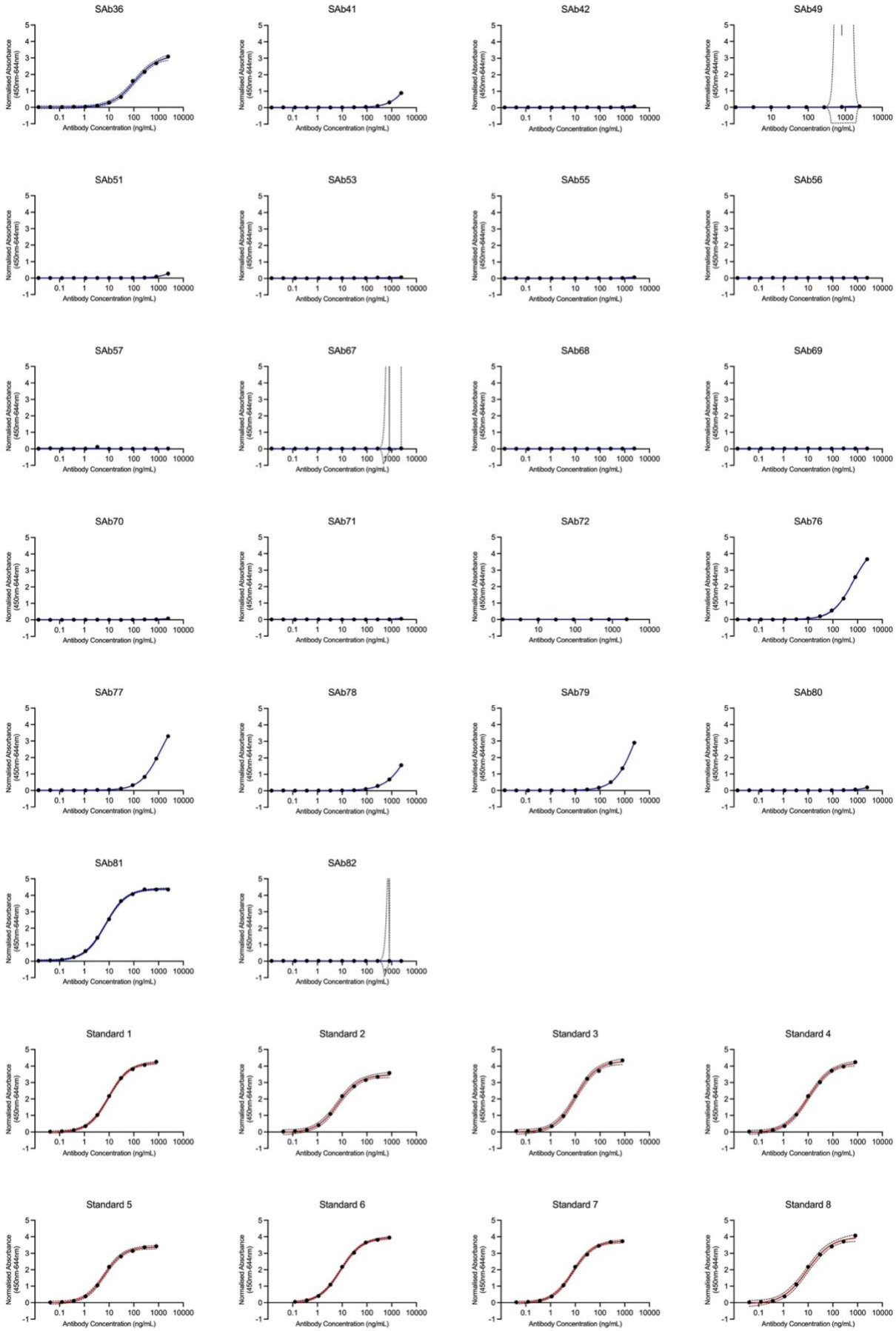
SAb36
SAb41
SAb42
SAb49
SAb51
SAb53
SAb55
SAb56
SAb57
SAb67
SAb68
SAb69
SAb70
SAb71
SAb72
SAb76
SAb77
SAb78
SAb79
SAb80
SAb81
SAb82
Standard 1
Standard 2
Standard 3
Standard 4
Standard 5
Standard 6
Standard 7
Standard 8
Normalised Absorbance (450nm-644nm)
Antibody Concentration (ng/mL)

Figure 9.10. Anti-Spike monoclonal antibody affinity ELISAs. Indirect ELISAs of antibodies produced from V(D)J sequences and monoclonal anti-RBD IgG standard. Absorbance readings at 450-644nm indicated by black points. 4PL Sigmoidal curve fitted by GraphPad prism indicated by blue (antibody) and red (standard) curves, dashed lines indicate 95% CI.

C.12 Mutational counts of spike binding naïve and memory cells

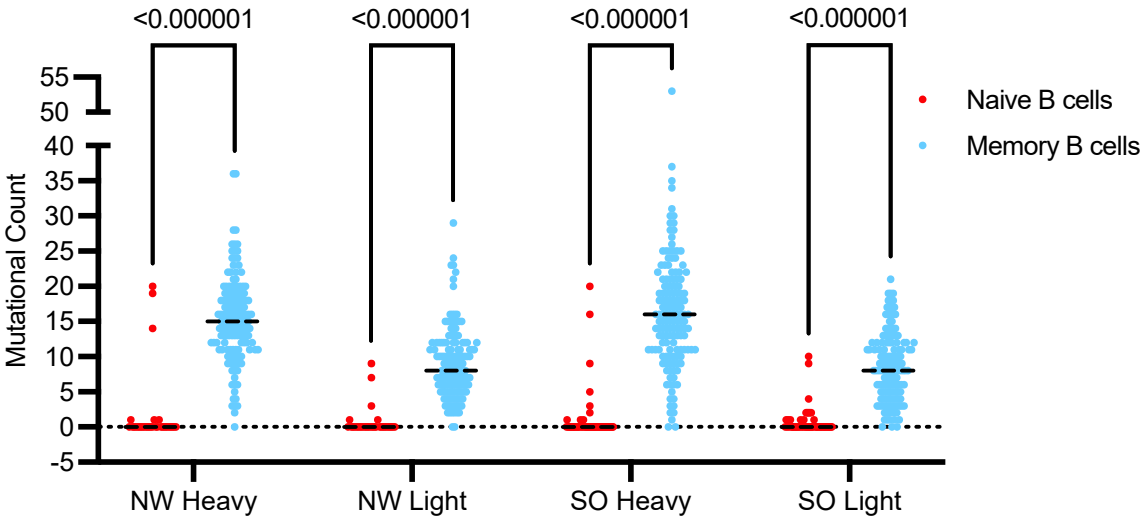

Figure 9.11. Comparison of mutational counts of spike binding naïve and memory cells. Comparison of the mutational counts in the heavy and light chains encoded by spike binding naïve (red) and memory (blue) B cells from individuals with SO and NW. Multiple Mann Whitney Tests. Horizontal bars indicate median values.

Appendix D. Supplementary Data for Chapter 6.

D.1 BNT162b2 vaccination in mouse models

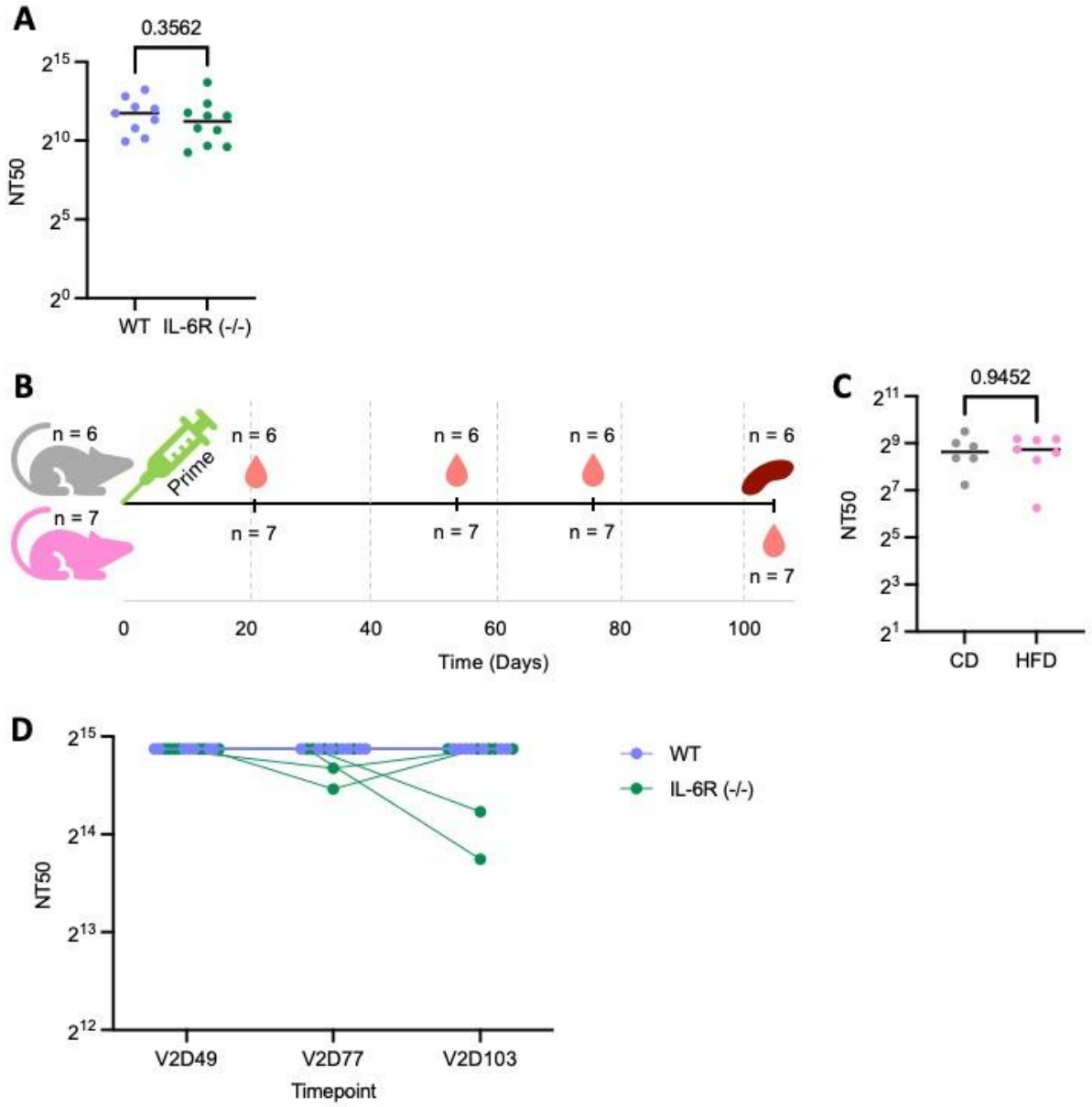

Figure 9.11. Supplementary information for BNT162b2 vaccine studies in mouse models. A) Live virus neutralising capacity of WT (purple) and *Il6ra* knockout (green) mice 21 days following single dose IM BNT162b2 vaccination. **B)** Schematic of the timings of the study of single dose BNT162b2 vaccination in mice on standard chow diet (grey) and high fat diet (pink). **C)** Live virus neutralising capacity of WT mice on standard show diet (grey) and high fat diet (pink) 21 days following single dose IM BNT162b2 vaccination. **D)** Live virus neutralising capacity of WT (purple) and *Il6ra* knockout (green) mice 49, 77, and 103 days following second dose IM BNT162b2 vaccination. Where present significance values indicate the result of a Mann-Whitney test.

D.2 Gating strategy for the identification of plasma cells in mouse bone marrow

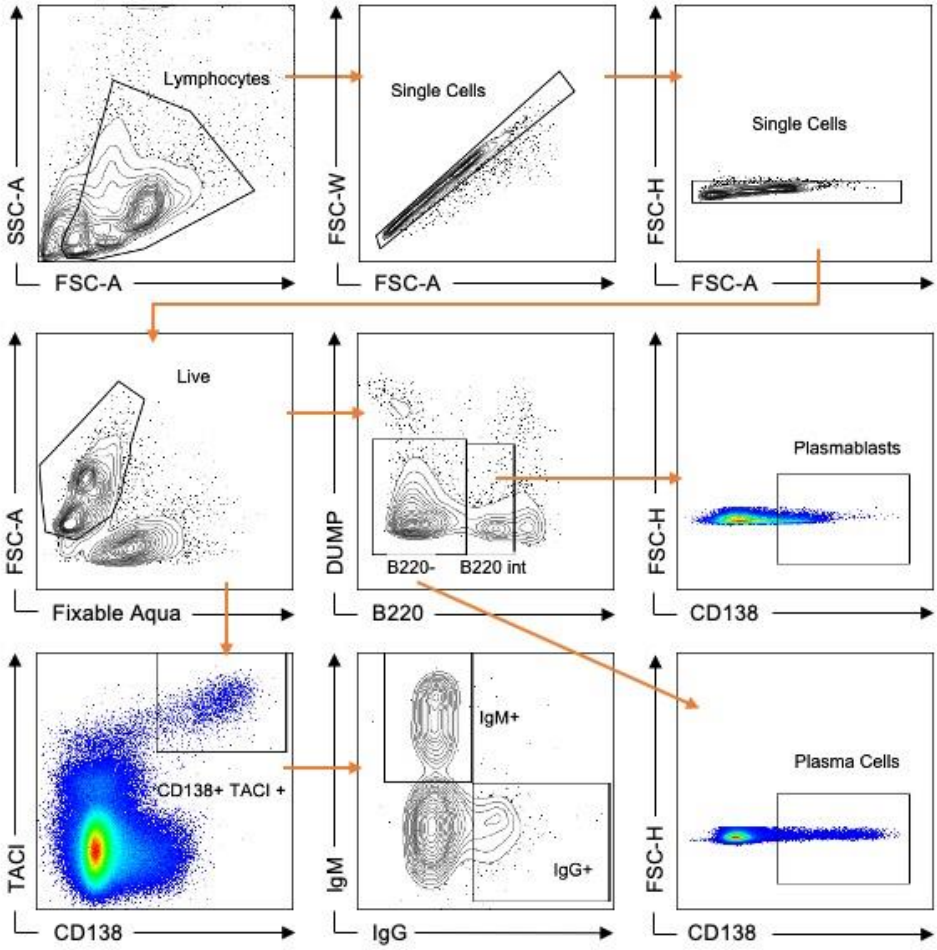

Figure 9.12. Gating strategy for plasma cell subsets from mouse bone marrow.